THE EFFECT OF TREATMENTS ON THE MECHANICAL PROPERTIES OF *STAPHYLOCOCCUS EPIDERMIDIS* BIOFILMS UNDER FLUID SHEAR AND MECHANICAL INDENTATION

by

Eric Robert Brindle

A thesis submitted in partial fulfillment
of the requirements for the degree

of

Master of Science

in

Mechanical Engineering

MONTANA STATE UNIVERSITY
Bozeman, Montana

September 2009

APPROVAL

of a thesis submitted by

Eric Robert Brindle

This thesis has been read by each member of the thesis committee and has been found to be satisfactory regarding content, English usage, format, citation, bibliographic style, and consistency, and is ready for submission to the Division of Graduate Education.

Dr. David A. Miller

Approved for the Department of Mechanical Engineering

Dr. Christopher H.M. Jenkins

Approved for the Division of Graduate Education

Dr. Carl A. Fox

STATEMENT OF PERMISSION TO USE

In presenting this thesis in partial fulfillment of the requirements for a master's degree at Montana State University, I agree that the Library shall make it available to borrowers under rules of the Library.

If I have indicated my intention to copyright this thesis by including a copyright notice page, copying is allowable only for scholarly purposes, consistent with "fair use" as prescribed in the U.S. Copyright Law. Requests for permission for extended quotation from or reproduction of this thesis in whole or in parts may be granted only by the copyright holder.

Eric Robert Brindle

September 2009

ACKNOWLEDGEMENTS

I would like to thank my lovely wife Brianna and my parents Mr. and Mrs. Richard Brindle for their love and encouragement throughout my academic career at Montana State University. Also, I would like to express my sincerest thanks to my professors, Dr. David A. Miller and Dr. Philip S. Stewart, for their time, guidance, encouragement, patience, constructive criticism, and friendship throughout the course of my masters program. This study was supported by NSF Award Number: 0728621.

TABLE OF CONTENTS

TABLE OF CONTNETS - CONTINUED

LISTS OF TABLES

Table Page

LISTS OF TABLES - CONTINUED

Table Page

LIST OF FIGURES

Figure Page

LISTS OF FIGURES - CONTINUED

Figure Page

LISTS OF FIGURES - CONTINUED

Figure Page

LISTS OF FIGURES - CONTINUED

Figure Page

LISTS OF FIGURES - CONTINUED

Figure Page

LISTS OF FIGURES - CONTINUED

Figure Page

LISTS OF FIGURES - CONTINUED

Figure Page

LISTS OF FIGURES - CONTINUED

Figure Page

LISTS OF FIGURES - CONTINUED

Figure Page

LISTS OF FIGURES - CONTINUED

Figure Page

LISTS OF FIGURES - CONTINUED

Figure Page

LISTS OF FIGURES - CONTINUED

Figure Page

LISTS OF FIGURES - CONTINUED

Figure Page

LISTS OF FIGURES - CONTINUED

Figure Page

LISTS OF FIGURES - CONTINUED

Figure Page

LISTS OF FIGURES - CONTINUED

Figure Page

LISTS OF FIGURES - CONTINUED

Figure Page

LISTS OF FIGURES - CONTINUED

Figure Page

LISTS OF FIGURES - CONTINUED

Figure Page

LISTS OF FIGURES - CONTINUED

Figure Page

LISTS OF FIGURES - CONTINUED

Figure Page

ABSTRACT

Biofilms exist on most every wetted surface both in the natural environment and in industrial and medical settings. The bacterial cells are surrounded by protective extracellular polymeric substances (EPS) which provide the mechanical stability for these biofilms. Little is known about the material properties of attached biofilms, making it difficult to predict how a biofilm will behave in response to an applied force. The work presented here measured the force–deflection characteristics of biofilm by two different techniques. The first method involved time lapse imaging of a biofilm grown in a capillary flow cell reactor under a constant fluid shear stress and the second method was based on micro-indentation using an atomic force microscope.

For the flow cell experiments *Staphylococcus epidermidis* was grown in a capillary flow cell reactor. After a day of growth the biofilms received a pretreatment fluid shear while displacements were measured. The biofilms were then treated with different agents which alter the structure of the EPS matrix and thus change the mechanical properties/response of the biofilm. The four treatments examined in these experiments were $FeCl_2$, chlorhexidine, DispersinB®, and urea. The same fluid shear was applied after the fifteen minute treatment soak and the deflections were recorded. These measurements revealed that i) biofilms behave viscoelastically ii) $FeCl_2$ and chlorhexidine made the biofilm stiffer while urea and DispersinB® reduced the viscosity of the biofilm.

For the micro-indentation experiments *Staphylococcus epidermidis* was grown in a drip-flow reactor. After four hours of growth the biofilms received a pretreatment indentation (5μm depth) in which force-displacements were measured. The biofilms were then treated with $FeCl_2$, chlorhexidine, DispersinB®, and urea. The 5μm indentation was applied after the fifteen minute treatment soak and force displacements were again measured. The measurements revealed that again i) biofilms behave viscoelastically ii) $FeCl_2$ and chlorhexidine made the biofilm stiffer while urea and DispersinB® reduced the viscosity of the biofilm.

Quantification of biofilm material properties and demonstration that their properties can be altered by chemical or enzymatic treatments opens the door to development of new technologies for controlling detrimental biofilm based on targeting biofilm cohesion rather than killing microorganisms.

INTRODUCTION

Biofilm Overview

Bacterial conglomerates of structured microorganisms encased in self produced polymeric substances found on wetted surfaces are collectively referred to as 'biofilms.' These biofilms commonly produce an extracellular polymeric substance (EPS) comprised of a hydrated matrix of polysaccharide and protein that protects them from antimicrobial agents and provides mechanical stability (Flemming, et al. 2000). Biofilms form when a single planktonic bacterial cell traveling in bulk flow attaches itself to a substratum wetted surface. This single cell multiples, connecting the new community of cells with EPS matrix. These biofilms can be very detrimental to industry where their formation can lead to increased pressure drop in piping systems (Zelver 1979) and increased drag on ship hulls, which consequently results in higher fuel consumption (Townsin 2003).

Mechanical detachment of biofilms can lead to transmission of pathogens in drinking water systems (Walker, et al. 1995) and food production facilities (Vieira, Melo and Pinheiro 1993). Bacteria that adhere to implanted medical devices and develop biofilm lead to persistent infections that are very difficult to eradicate (Costerton, Stewart and Greenberg 1999).

Biofilm bacteria are more difficult to kill than their planktonic counterparts; they have several resistance mechanisms that aid in their survival during harsh treatment conditions. First, biofilms resist antimicrobial treatments by diffusion limitations. The diffusion rate trough the EPS matrix is slower than that of water, which leads to a need

for longer exposure time to allow the antimicrobial to penetrate entirely through the biofilm. Many treatments are consumed quickly at the biofilm surface and when the rate of reaction is higher than the rate of diffusion, cells in the interior remain unexposed (Costerton, Stewart and Greenberg 1999). Second, many antimicrobials are only effective when bacterial growth is rapid. Penicillin is an example of an antimicrobial agent that requires growth of active cells to be effective. Cells on the interior of the biofilm, where there are limited nutrients, grow very slowly limiting or cancelling the effectiveness of the antimicrobial treatment (Costerton, Stewart and Greenberg 1999). A third mechanism of antibiotic resistance is that a few cells in the population of the biofilm enter a unique, resistant phenotypic state. It has been shown that after an antimicrobial treatment has been administered and most of the cells have been killed, the tolerant presister cells will be able to repopulate the biofilm community once the antibiotic has been removed (Stewart and Costerton 2001). Biofilm cells are capable of persisting in the presence of antimicrobials at concentrations that are 1,000-fold higher than those necessary to eradicate a planktonic population (Hamilton 2002).

Motivation

The purpose of studying biofilm mechanical properties is to understand better ways of removal, eradication, and accumulation of these biofilms. For instance, mechanical removal of biofilms is an everyday occurrence with routine tooth brushing. Removal of the biofilm is achieved by shear forces applied through direct contact of toothbrush bristles on the gums and teeth (Vinogradov, et al. 2004). Moreover eradication

of the biofilm can be accomplished by altering their mechanical properties to allow higher susceptibility to mechanical stresses and then treating when the bacteria are no longer in a biofilm. Overall, more is known about slowing or stopping biofilm growth or killing biofilms with antimicrobials than removing the biofilm (Chen and Stewart 2000).

There are circumstances where biofilms are beneficial and their removal by fluid shear or other mechanical forces is unwanted, such as in wastewater treatment or in bioreactors (Nicollea, Van Loosdrecht and Heihnen 2000). Understanding what fluid shear levels a particular system can operate at before detachment, or mechanical failure, of the biofilm is very important. Little is known about the mechanical properties of biofilms for two main reasons. First, there have only been a few groups to recognize the importance of viewing biofilms as a material with specific mechanical properties. Second, biofilms are very difficult to test mechanically. Unlike most engineering materials, biofilms cannot be molded into a test specimen without scraping and disrupting their original properties. They are also microscopically small which limits conventional approaches to ascertain their mechanical nature (Stoodley, et al. 2002).

Previous Work

While there are few groups that have studied the mechanical nature of biofilms, the work they have done has been pioneering. Many studies of biofilm mechanics begin with adhesion to various surfaces (Garrett, Bhakoo and Zhang 2008); while this area of research is novel there is still much that needs to be understood about the cohesive nature or overall material properties of the biofilm.

Classic approaches to understanding the mechanical nature of biofilm have been through macroscopic rheometer techniques (Vinogradov, et al. 2004), (Sutton 2008), (Towler, et al. 2003). These approaches gather insight into the viscoelastic nature of biofilm but often have disadvantages of disrupting the original biofilm structure. This process entails the use of pressuring the biofilm between the two disks of a rotating rheometer, which compromises the original structure and manipulates the EPS matrix. Rheometry testing shows that a solid viscoelastic Burger model works well to fit constitutive equations for the material properties of the biofilms.

Uniaxial compression measurements have been employed to study the mechanical stability of biofilms (Korstgens, et al. 2001). The apparent modulus of elasticity and yield strength were studied using this method, but above a certain yield point, the gel structure fails and the system behaves as highly viscous fluid. Again this method is limited in obtaining an overall material behavior for biofilm structures.

Preliminary studies into the mechanical properties of biofilms were conducted by growing mixed culture biofilm in glass flow cells and structurally deform the clusters under fluid shear (Stoodley, et al. 1999). These clusters were stained with fluorescent particles to illuminate bright dots which were used as fiducial points during the image analysis. This analysis found that the biofilms behave like elastic and viscoelastic solids. This may account for the large pressure drops observed in biofilm fouled pipes (Stoodley, et al. 1999).

Another similar approach was taken by Klapper et al. in which *Pseudomonas aeruginosa* biofilms were grown in glass capillary flow cells and tested under high fluid

shear (Klapper, et al. 2002). Displacements of biofilm streamers were measured with time lapse microscopy. Klapper's conclusions were that the biofilms behave as viscoelastic fluids, demonstrating both irreversible flow as well as elastic and viscoelastic recoil.

The experimental data from flow cell work was taken one step further by Towler et al. (2007) in which a two dimensional finite element model of a hemispherical biofilm cluster was studied under fluid shear. The premise was to use a viscoelastic Burger material model with experimentally derived material parameters in a computational fluid dynamic code. Simulations were run on the theoretical fluid-structure interactions between a biofilm cluster and its surrounding bulk flow. Constitutive Burger model material parameters were examined as well as the effects of biofilm size. Many of the finite element modeling results of this report closely followed experimental results suggesting that biofilms can be described as viscoelastic solids (Towler, et al. 2007).

While all of these flow cell approaches were novel, there are limitations inherent in their design. First, fluid-structure interactions are complicated creating a large margin for error when calculating stresses in the structure. To further complicate the matter, geometry of the biofilm cluster under flow cannot be measured precisely because of viewing a three dimensional structure in a two dimensional plane. Finally, it has been suggested that maturity and growth conditions of the biofilm play an important role in mechanical properties (Dunsmore, et al. 2002), increasing variability between experiments.

Cohesive strength investigations using a micro-cantilever method on biofilm flocs is one novel way of investigating biofilm tensile strength (Poppele and Hozalski 2003). The force required to separate an aggregate was determined directly from the deflection of a cantilevered glass micropipette. The force measurement combined with an estimate of the cross-sectional area of the aggregate at the fracture point indicates the cohesive strength or ultimate stress of the biofilm floc (Poppele and Hozalski 2003). Although this technique leads to great understanding of ultimate cohesive strength it did not address the viscoelasticity of biofilms.

Mechanical properties and failure mechanisms of biofilms using a micro-indentation apparatus in combination with a confocal microscope was used to determine the viscoelastic properties of *Streptococcus mutans* biofilms (Cense, et al. 2006). The micro-indentation device was comprised of a small glass indenter and a highly sensitive force transducer (Cense, et al. 2006). This technique offers mechanical sampling of biofilm properties at the micrometer scale and alleviates the problems with large-scale rheometry which permanently deforms the EPS structure.

BACKGROUND

The path of this project is discussed in the following chapter beginning with the bacterium used in the experiments followed by a background on viscoelastic materials. This chapter will explain mechanical analog models and the testing of materials to ascertain numerical parameters. It will also discuss problems with previous methods used for testing biofilm mechanics, and present methods which alleviate those problems. Finally, a synopsis of the chemical and enzymatic treatments will be discussed.

Staphylococcus epidermidis

S. epidermidis is a bacterium about one micrometer in diameter and present in the skin flora of humans. Most strains are not pathogenic, but can become problematic when an implanted medical device is present. Frequently *S. epidermidis* is found on the surfaces of devices such as catheters, heart valves, orthopedic prostheses and vascular grafts (Gotz 2002). *S. epidermidis* was selected for this project because it is a strong biofilm-forming bacterium that has been extensively studied. *S. epidermidis* is a biosaftey level 1 organism, so there are no special safety precautions that need to be implemented while handling it. Lastly *S. epidermidis* has been used extensively by predecessors of this project, giving rapid knowledge transfer.

Viscoelasticity

Viscoelastic materials exhibit aspects of both viscous fluids and elastic solids under deformation. Or in another sense, viscoelastic materials can both dissipate energy, a viscous property, and store energy, an elastic property. When a stress is applied, the elastic deformation is instantaneous while the viscous behavior occurs over time. Silly Putty® is a common example of a viscoelastic material. It behaves as a fluid when hung from the ceiling loaded under its own weight, but it will also bounce like a rubber ball, behaving like an elastic material at a high strain rate (Lakes 1999).

Elastic Materials (Hookean Spring Model)

Elasticity is the property of materials that, while under stress, the material deforms but when the stress is removed the material returns to its original shape. Elastic materials may follow Hooke's law of linear elasticity: stress (τ) is proportional to strain (ε) through Young's modulus (E).

$$\tau = E\varepsilon \qquad (1)$$

A simple mechanical analog of a Hookean spring can be used to represent this elastic material as shown below in Figure 1.

Figure 1) Hookean Spring

This spring element behaves as a perfect linear elastic (Hookean) material deforming under stress and returning to its original state when the load is removed. Graphically this is represented in Figure 2.

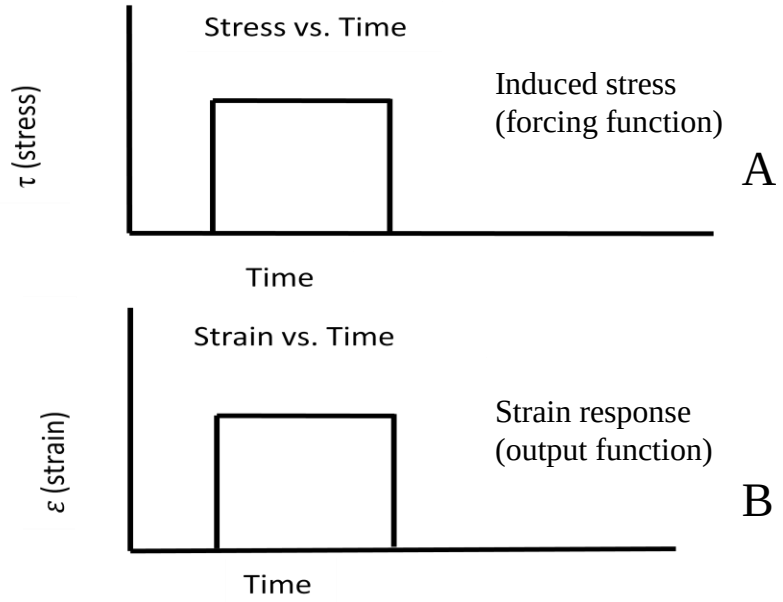

Figure 2) linear elastic material A) induced stress and B) strain response

The induced stress is shown in Figure 2A and the strain response is shown in Figure 2B. Under an instantaneous stress increase there is an instantaneous strain response, when that stress is relieved the strain returns to its initial position.

Viscous Fluids (Newtonian Dashpot Model)

Viscous fluids that have a linear stress versus strain rate and begin at the origin are called Newtonian fluids. Fluids will strain indefinitely as opposed to elastic materials whose strain is proportional to applied stress. To mathematically describe a Newtonian fluid shear stress (τ) is now linearly proportional to strain rate ($\frac{d\varepsilon}{dt}$) by viscosity (η).

$$\tau = \eta \frac{d\varepsilon}{dt} \qquad (2)$$

This fluid response can be represented using a Newtonian dashpot (Figure 3).

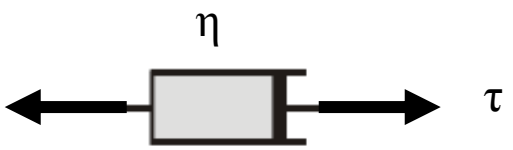

Figure 3) Newtonian Dashpot

The Newtonian dashpot strains linearly, under an applied stress, which can be seen in Figure 4:

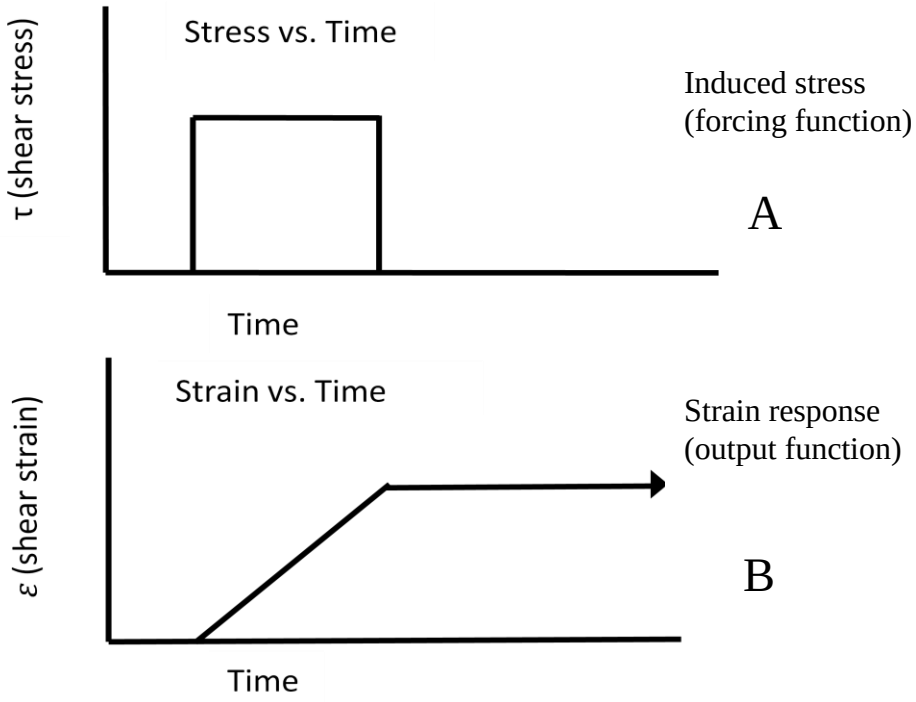

Figure 4) Newtonian fluid dashpot model A) induced stress and B) strain response

For an instantaneous stress applied over a finite time (Figure 4A) the strain response or output function (Figure 4B) creeps then does not return when the stress is released.

Maxwell Model

A Maxwell model consists of a linear spring and a linear dashpot in series Figure 5:

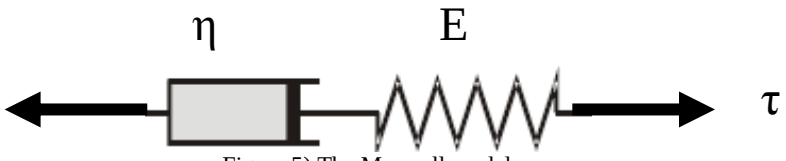

Figure 5) The Maxwell model

Total stress in the Maxwell model is the amount of stress acting through the entirety of the spring and dashpot in series. Total strain is the change in length of both the spring and dashpot in series. To differentiate stress/strain between the, spring/dashpots and the Maxwell element, subscripts of S and D are used respectively. Because the spring and dashpot are connected in series, the stresses for the model are equal while the associated strains are additive:

$$\tau = \tau_s = \tau_D \quad (3)$$

$$\varepsilon = \varepsilon_S + \varepsilon_D \quad (4)$$

It is known that:

$$\varepsilon_S = \frac{\tau_S}{E} \quad (5)$$

$$\dot{\varepsilon_S} = \frac{\dot{\tau_S}}{E} \quad (6)$$

$$\dot{\varepsilon_D} = \frac{\dot{\tau_D}}{\eta} \quad (7)$$

In equations (6) and (7) the dots are used to represent the partial time derivative (∂/∂t) but for one dimension there is no variation in the space coordinate and the differential reduces to an ordinary time derivative (d/dt). When (3) and (4) are combined with (5), (6) and (7) we obtain:

$$\dot{\varepsilon} = \dot{\varepsilon_S} + \dot{\varepsilon_D} = \frac{\dot{\tau}}{E} + \frac{\tau}{\eta} \qquad (8)$$

The most common tensile test procedure for a viscoelastic solid is known as a creep test, where an instantaneous stress is applied at time zero (t=0), and this constant stress is maintained thereafter. Solving equation (8) for the special case of a creep test with a constant stress (τ_o) from t=0:

$$\varepsilon = \frac{\tau_o}{E} + \frac{\tau_o}{\eta} t \qquad (9)$$

Graphically this is shown in Figure 6:

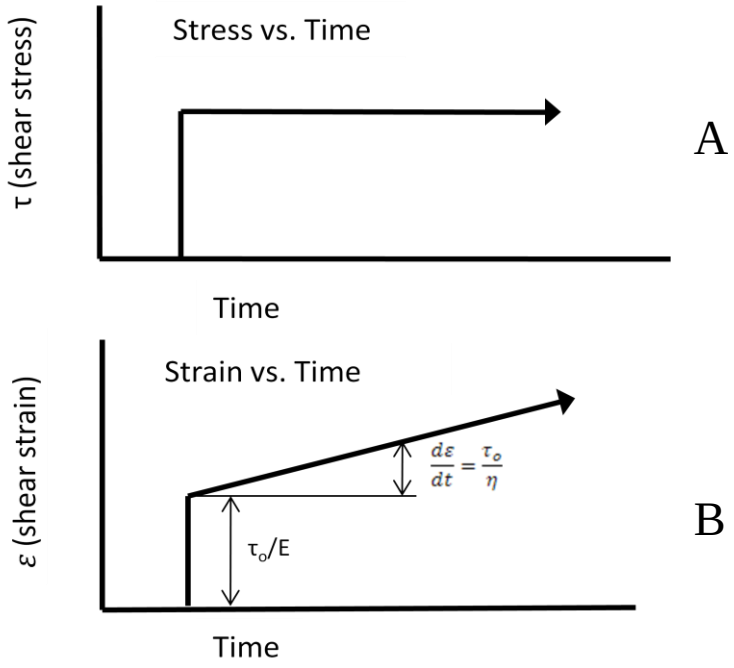

Figure 6) Creep test procedure for a Maxwell model for A) induced stress and B) strain response

Notice in Figure 6 the instantaneous strain response (τ_o/E), due to the elastic spring of the Maxwell model, which is followed by the viscous creep from the Newtonian dashpot.

Kelvin Model

Next consider a Kelvin model consisting of a spring and dashpot in parallel Figure 7:

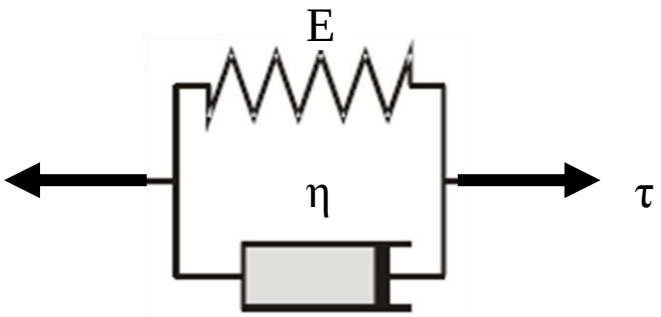

Figure 7) The Kelvin model

This parallel arrangement leads to equal strains in both elements, whereas the stresses in this model are additive. Again total stress/strain is differentiated between stress/strain in spring and dashpot elements by subscripts S and D respectively. So mathematically:

$$\tau = \tau_S + \tau_D \qquad (10)$$

$$\varepsilon = \varepsilon_S = \varepsilon_D \qquad (11)$$

Again using the equations for spring and dashpot descriptions:

$$\varepsilon_S = \frac{\tau_S}{E} \quad (12)$$

$$\dot{\varepsilon}_D = \frac{\tau_D}{\eta} \quad (13)$$

Combining (9) and (10) with (11) and (12) we obtain the stress equation for a Kelvin model:

$$\tau = \eta\dot{\varepsilon} + E\varepsilon \quad (14)$$

Solving the differential equation (8) for the special case of a creep test where an instantaneous stress is applied at a zero time (t=0), to the Kelvin model with a constant stress (τ_o):

$$\varepsilon = \frac{\tau_o}{E}\left(1 - e^{-E\frac{t}{\eta}}\right) \quad (15)$$

And graphically in Figure 8:

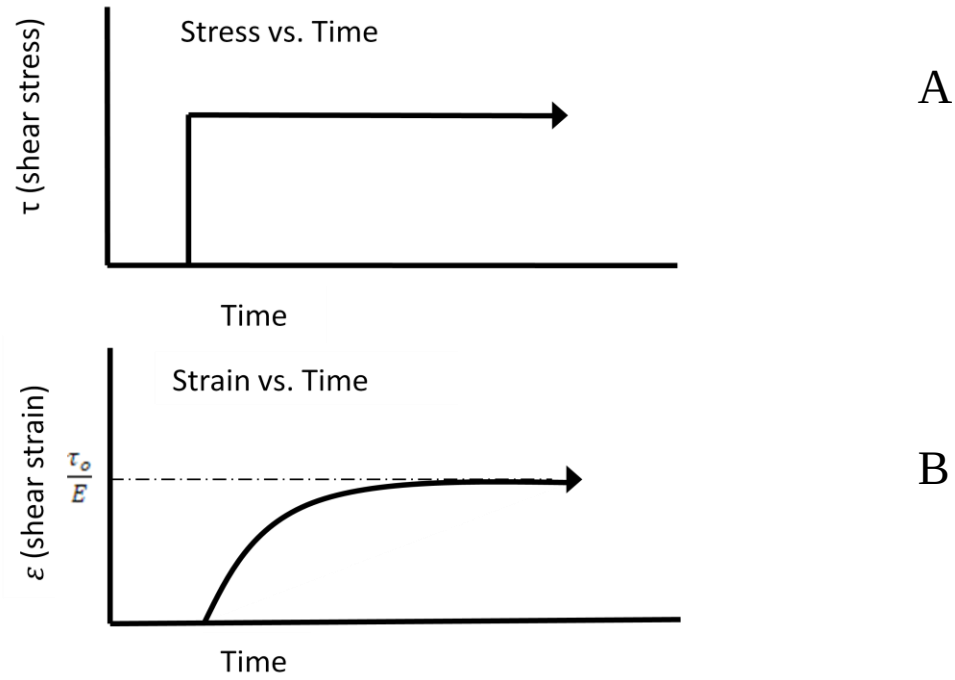

Figure 8) Creep test procedure for a Kelvin model for A) induced stress and B) strain response

Burger Model

When a Kelvin model and Maxwell model are linked in series, a new four-parameter element known as a Burger model is formed which is shown in Figure 9.

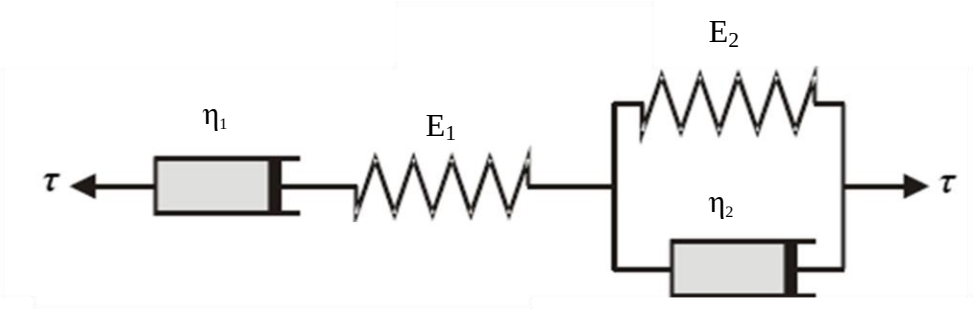

Figure 9) Four parameter fluid or Burger model

Because the elements are in series, the stresses through each element are the same and the strains are additive. Just as before using the subscript M for Maxwell and K for Kelvin:

$$\tau = \tau_M = \tau_K \qquad (16)$$

$$\varepsilon = \varepsilon_M + \varepsilon_K \qquad (17)$$

Combining (8) and (14) to develop a governing differential equation for the Burger model:

$$E_1\eta_1\eta_2\ddot{\varepsilon} + E_1E_2\eta_1\dot{\varepsilon} = \eta_1\eta_2\ddot{\tau} + (E_1\eta_2 + E_2\eta_1 + E_1\eta_1)\dot{\tau} + E_1E_2\tau \qquad (18)$$

Again solving the differential (18) for the special case of a creep test with a constant stress (τ_o) from t=0:

$$\varepsilon(t) = \tau_o[\frac{1}{E_1} + \frac{t}{\eta_1} + \frac{1}{E_2}\left(1 - e^{\frac{-E_2 t}{\eta_2}}\right)] \qquad (19)$$

And graphically Figure 10:

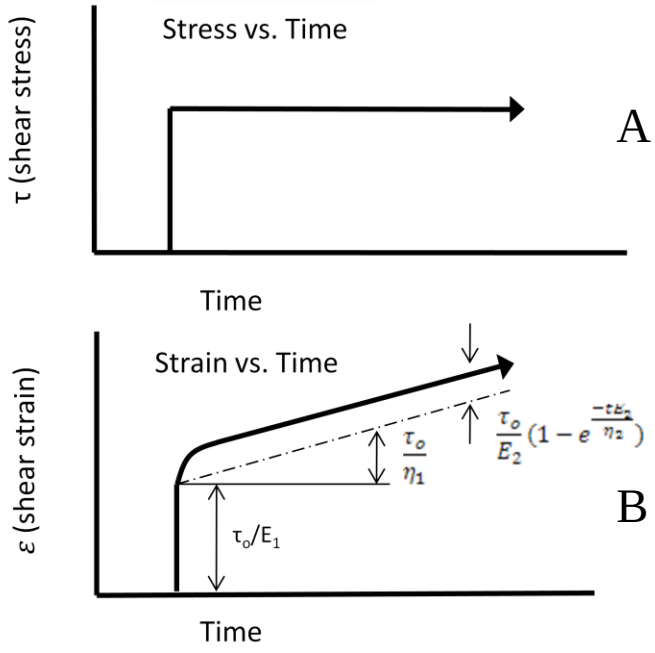

Figure 10) Creep test procedure for a Burger model for A) induced stress and B) strain response

The strain response to a creep test applied to a Burger's model is shown in Figure 10. Notice that there is an instantaneous strain response due to the Maxwell spring followed by viscous creep due to both the Maxwell dashpot along with the entire Kelvin element.

Linearly Viscoelastic Materials

For a material to be linear then it must satisfy both superposition and homogeneity. For example when stress and strain are taken as the input and response, the following equations for superposition and homogeneity are utilized, respectively:

$$\varepsilon(\tau + \tau_1) = \varepsilon(\tau) + \varepsilon(\tau_1) \qquad (20)$$

$$\varepsilon(\beta\tau) = \beta\varepsilon(\tau) \qquad (21)$$

If both of these equations are satisfied then the material is said to be linearly viscoelastic. Another important key is that the strain in linearly viscoelastic materials depends upon

the stress path, not just the instantaneous values of stress; in other words, strain is a function of stress history.

A common experiment to verify linearity, using the superposition property, is by conducting a creep recovery test on the material. A creep recovery test consists of applying a constant stress to a material while recording the strain for a set amount of time and then removing that stress and recording the relaxation in the material. The creep-recovery test for a Burger model is shown in Figure 11:

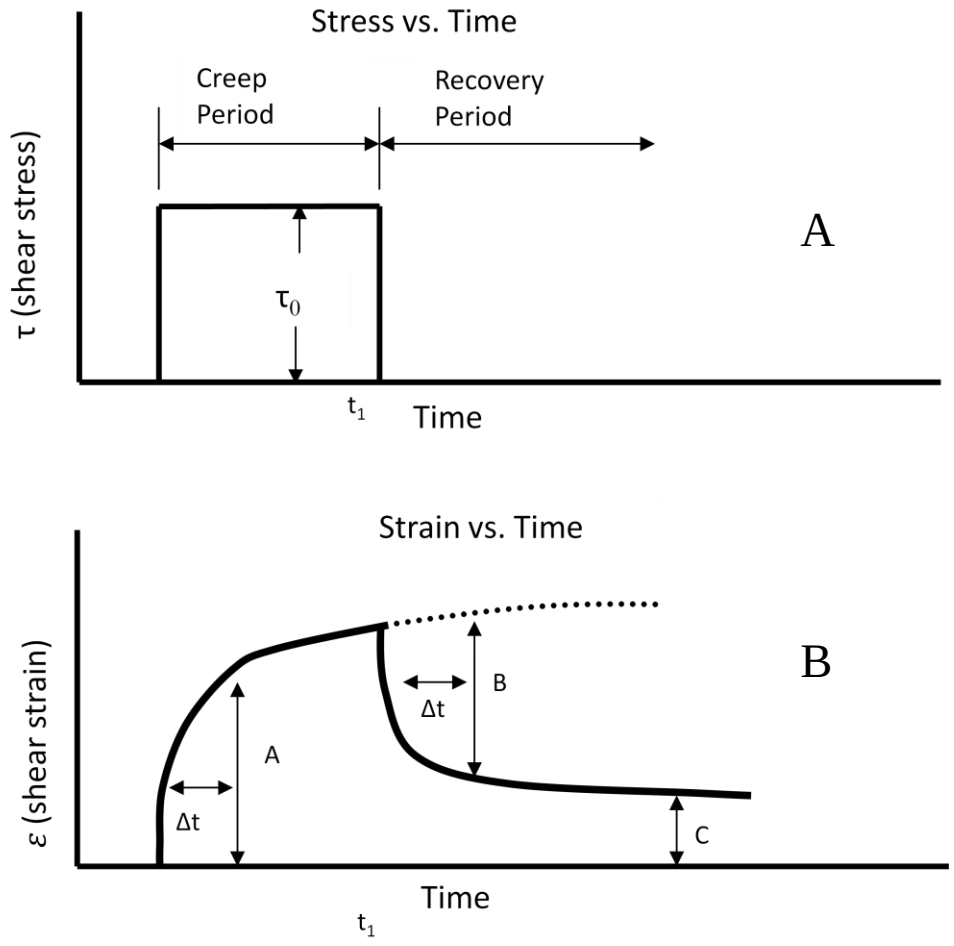

Figure 11) Creep and recovery test for a Burger model for A) induced stress and B) strain response

The creep and recovery graph in Figure 11 displays a linearly viscoelastic Burger model induced stress from t_0 to t_1 and the strain response to that stress. In general, a linearly viscoelastic material behaves the same in creep as it does in relaxation. In Figure 11, A and B are equal for the same Δt, only if the material is linearly viscoelastic. The height of C is the irreversible viscous creep due to the dashpot (η_1) on the Maxwell portion of the Burger model. For times greater than t_1, the solution to the linear elastic Burger model becomes:

$$\varepsilon(t) = \tau_o \left[\frac{t_1}{\eta_1} + \frac{1}{E_2}\left(1 - e^{\frac{-E_2(t-t_1)}{\eta_2}}\right)\right] \qquad for \quad t > t_1 \qquad (22)$$

where t_1 is the time at which stress returns to the zero condition.

Stress-Strain and Structure Response

It is important to note that there is a difference between stress-strain relationships and structural responses under an applied force. For example in the simplest case a 1cm bar that strains 10% has an elongation of 0.1cm where as a 1m bar that strains 10% has a elongation of 10cm. Viscoelastic stress and strain are characterized by Burger model and other constitutive equations. The structural response of viscoelastic materials incorporates overall geometry of the object in question. Instead of strain responses of a single Burger model element there are now multiple elements linked together undergoing deformation. This geometry effect creates problems when trying to solve for constitutive equation parameters.

Testing Direction

Previous work determined that biofilm structures behave in a viscoelastic manner and that there are large variations in mechanical properties of these films (Stoodley, et al. 1999) (Shaw, et al. 2004) (Shaw, et al. 2004) (Vinogradov, et al. 2004) (Sutton 2008). In this thesis project, to eliminate large variations of mechanical properties a new approach was taken, in which the change of mechanical properties is measured, in response to chemical and enzymatic treatments. Testing a biofilm structure before and after treatments eliminates problems with diverse geometries.

Previous Testing Problems

Much of the previous mechanical characterizations of biofilm utilized several methods of inducing a load and measuring displacements on the biofilm structure. Many biofilm material properties found in literature are listed in Table 1.

Table 1) Previous studies conducted on mechanical characterizations of biofilms (Cense, et al. 2006)

Authors	Species	Method	G(Pa)	E(Pa)	η(Pa s)
Stoodley et al. (1999)	Mixed	Visual	27±1	40±8	
Klapper et al. (2002)	*P. aeruginosa*	Visual	65±21		
Shaw et al. (2004)	*S. mutans*	Rheometer	10-1000		10^4-10^6
Towler et al. (2003)	Mixed	Rheometer	0.3-45		10-7000
Vinogradov et al. (2004)	*S. mutans*	Rheometer	1900±3800		(2.8±6.4) 10^5
Korstgens et al. (2001)	*P. aeruginosa*	Compression		6500±500	

Notice that there is not only a large range of methods and bacteria used but there are large deviations within experiments. For example in Shaw et al. 2004 there are two orders of magnitude of difference with the viscosity coefficient (η). Ultimately, the large variation of mechanical properties between species of biofilms, methods of obtaining properties,

and within single experiments, show that understanding the mechanical properties of biofilm is still in its infancy.

Measuring Changes

With the large variations in biofilm properties shown in earlier research, another approach was developed to investigate these biofilm structures. This approach follows similar concepts as Sutton's work in which biofilm was tested and treated to detect alterations in mechanical properties. One problem with these experimental results was that there were extensive variations in mechanical properties between individual biofilms within treatments and the control. Each biofilm showed broad differences in mechanical properties even though they had the same growth conditions. These differences in mechanical properties make it difficult to compare treatments to each other and to the control sets.

To minimize this problem we used a procedure that mechanically tested an untreated biofilm as a control then treated that same biofilm with chemicals or enzymes and mechanically tested it again. This way each biofilm had its own control in which the growth conditions, biofilm structures, and loading conditions were the same. Two procedures using this test treat test method were used; first a flow cell technique using fluid shear to mechanically deform the biofilm structure and second an indentation system using an atomic force microscope. Each of these methods can be found in the next two chapters.

Treatments

The treatments that were used in this research were chosen based on effects on *S. epidermidis* biofilm reported by Sutton, 2008. The four treatments used in this research were iron chloride, chlorhexidine, urea and DispersinB®. Each of these treatments has been shown to affect the mechanical properties of the *S. epidermidis* biofilm. Iron chloride ($FeCl_2$) has been shown to increase the apparent viscosity of certain biofilms (Sutton 2008) (Chen and Stewart 2002). When put into solution, iron chloride forms the cation Fe^{2+} which is capable of binding or cross linking two negatively charged sites in the EPS. Iron chloride at a concentration of 0.1 molar was used in this testing.

Chlorhexidine is a chemical antiseptic commonly used in low concentrations in contact lens solutions and in dental mouth wash. Chlorhexidine at a concentration of 0.1% was used in this study.

Urea is theorized to disrupt the hydrogen-bonding interactions which are thought to be important for EPS mechanical stability. Disrupting the hydrogen bonds should disrupt the EPS matrix resulting in a weaker biofilm (Chen and Stewart 2000). Urea at a concentration of 0.5 molar was used in this testing.

DispersinB® catalyzes the hydrolysis of poly-N-acetylglucosamine, a sticky extracellular polysaccharide produced by various bacteria including *Staphylococcus aureus* and *Staphylococcus epidermidis* (Kaplan, et al. 2003). DispersinB® has been shown to effectively disrupt *S. epidermidis* creating a softer, less consolidated biofilm cluster (Chaignon, et al. 2007). DispersinB® at a concentration of 40 μg/ml was used in this testing.

Objectives

The three main objectives in this project are to develop and apply techniques to characterize the viscoelastic nature of *S. epidermidis* biofilms. Two, demonstrate change in biofilm material properties in response to chemical and enzymatic treatments. And three, develop methods to characterize viscoelastic changes in mechanical properties through the use of constitutive equations and basic modeling.

METHOD 1: FLOW CELL

Materials and Methods

Utilizing the flow cell technique, a version of the standard creep-recovery mechanical test is performed on the biofilm. A creep-recovery test involves applying a constant force to a structure and measuring the time dependent deformation, or creep. The test is completed by removing the force and measuring the time dependent recovery of the deformation toward the original configuration. The time dependant deformation, and recovery, of the biofilm is related to the viscoelastic nature of the biofilm. In a perfectly elastic structure, the deformation will directly follow the application and removal of the applied force. The flow cell technique of the creep-recovery test utilizes the constant velocity of the flow cell medium to apply a stress to the biofilm structure through the fluid-structure interaction.

An initial culture was started for inoculation using full strength tryptic soy broth (TSB) with *Staphylococcus epidermis* (ATCC 35984). The *S. epidermidis* inoculum incubated for 24 hours on a shaker plate at 37^{o}C. The 24 hour culture was then used to inoculate a square glass capillary flow cell reactor 0.9 I.D. 170μm thickness (Friedrich & Dimmock) in which 2 hours was allowed for attachment before the flow of nutrients was initiated. The reactor then had 10 percent TSB pumped through the glass capillaries at a flow rate of 1ml/min for 24 hours at 37^{o}C. Refer to Figure 12 for a diagram of the setup of the flow cell reactor.

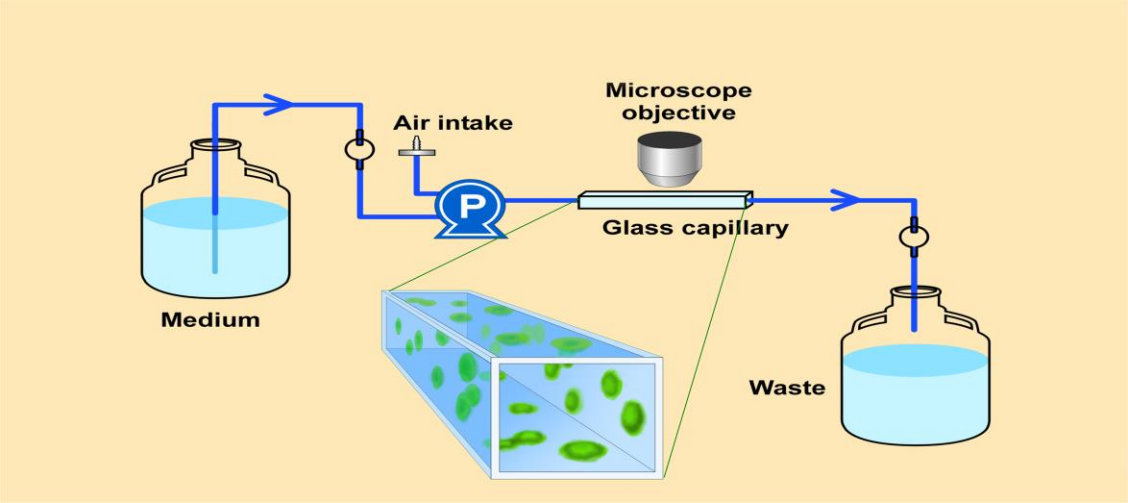

Figure 12) Setup for capillary flow cell reactor during growth of *S. epidermidis* biofilm

The glass capillary reactor which now contained the mature biofilm was removed and viewed using a Nikon Eclipse E800 microscope, Hamamatsu C2400-75AH camera and MetaVue software. Using a Cole Palmer continuous cycle syringe pump (R-74901-50) a 10ml/min (Reynolds number 230) shear test using 10 percent TSB was applied to the biofilm for 15 seconds while recording one frame every 0.3 seconds for 30 seconds to capture both elongation and relaxation of a particular biofilm cluster. A schematic of the creep recovery test is shown in Figure 13.

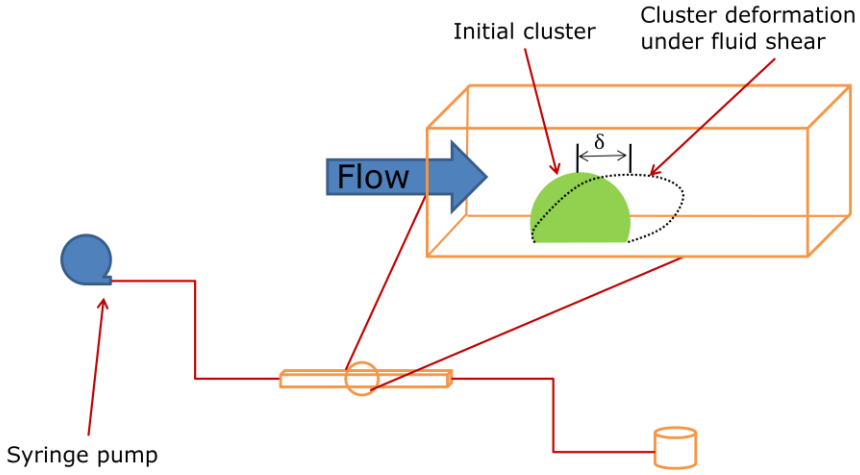

Figure 13) Setup for inducing a fluid shear stress creep and recovery test onto a biofilm cluster

Figure 14 displays the ideal fluid flow rate for the duration of the fluid shear test on the biofilm in the capillary tube.

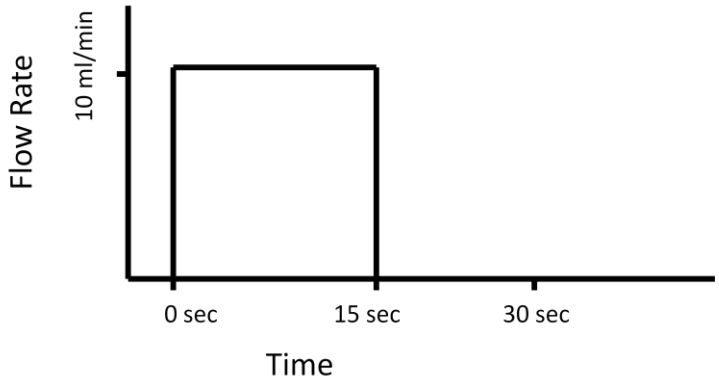

Figure 14) Hypothetical flow rate input over time through the capillary tube with mature biofilm

The syringe pump was then used to inject a treatment into the capillary tube at a flow rate of 0.25ml/min. Treatments shown in Table 2:

Table 2) Treatment schedule for capillary fluid shear creep recovery test of *S. epidermidis* biofilm

Control	$FeCl_2$	Chlorhexidine	Urea	Dispersin B ®
	0.1 Molar	0.1% Concentration	0.5 Molar	40 μg/mL
No treatment applied (10% TSB)	Thought to bind two negatively charged sites on EPS matrix	Chemical antiseptic	Thought to disrupt hydrogen bonding in EPS matrix	Catalyzes the hydrolysis of EPS

The treatment was allowed a 15 minute soak period recording time-lapse images every 30 seconds throughout. After the soak period, another shear test was conducted, with the same parameters of the initial shear test, recording time-lapse imaging of the biofilm cluster creep and recovery. Specific points were recorded with time giving displacement magnitudes through the entire creep test of the biofilm structure. The points monitored throughout the data collection were positions that remained identifiable

throughout the creep and recovery of both the pre and post-treatment fluid shear tests. An animation of data collection can be seen in Figure 15.

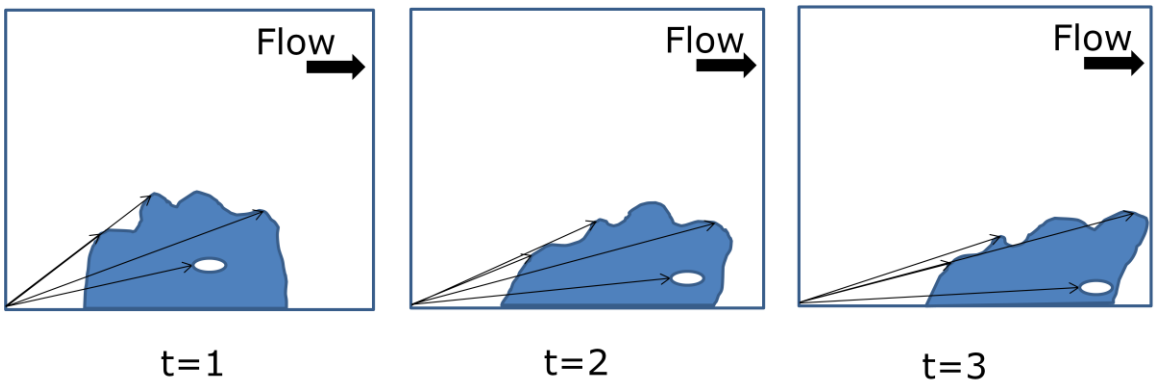

Figure 15) Time series of a biofilm cluster with recognizable points and vectors to these points shown with deformation as fluid shear moves over biofilm structure

Each vector in Figure 15 tracks a point on the biofilm in which a set amount of time passes between images. For each vector shown in Figure 15, a displacement vector can be created by subtracting the initial vector from the next vector in time, thus giving a displacement measurement for time step which is shown in Figure 16 below.

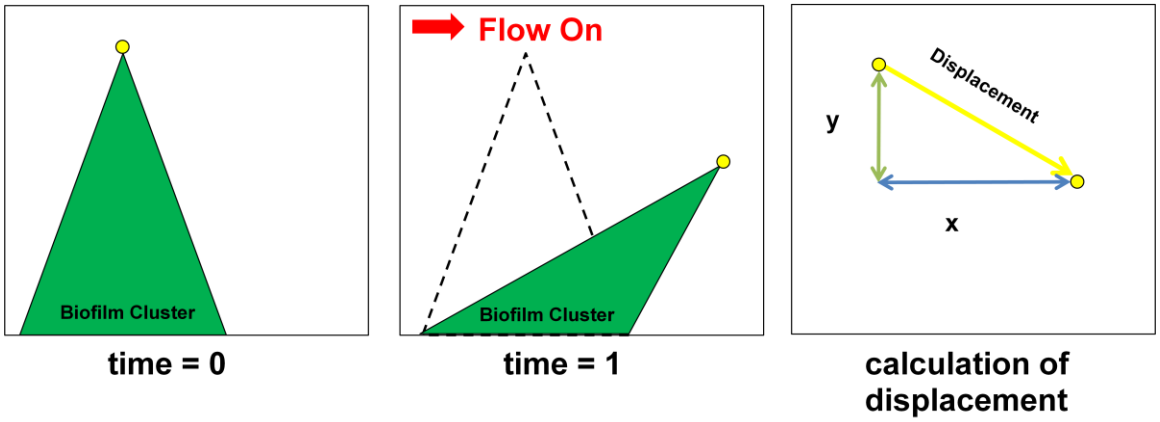

Figure 16) Displacement calculation representation of a point on a biofilm cluster for a single time increment

Each flow cell experiment had three fiducial points analyzed from initial flow to final relaxation. These points were manually tracked throughout the images manually using

MetaMorph image analysis software. The change in fiducal point displacement vectors were then averaged together to form a general displacement of the biofilm cluster with time. The raw data is plotted in these average vector displacements with time.

To illustrate one example of the creep recovery testing, the six images in Figure 17 below are flow cell screen captures illustrating the deformation and the recovery of the biofilm.

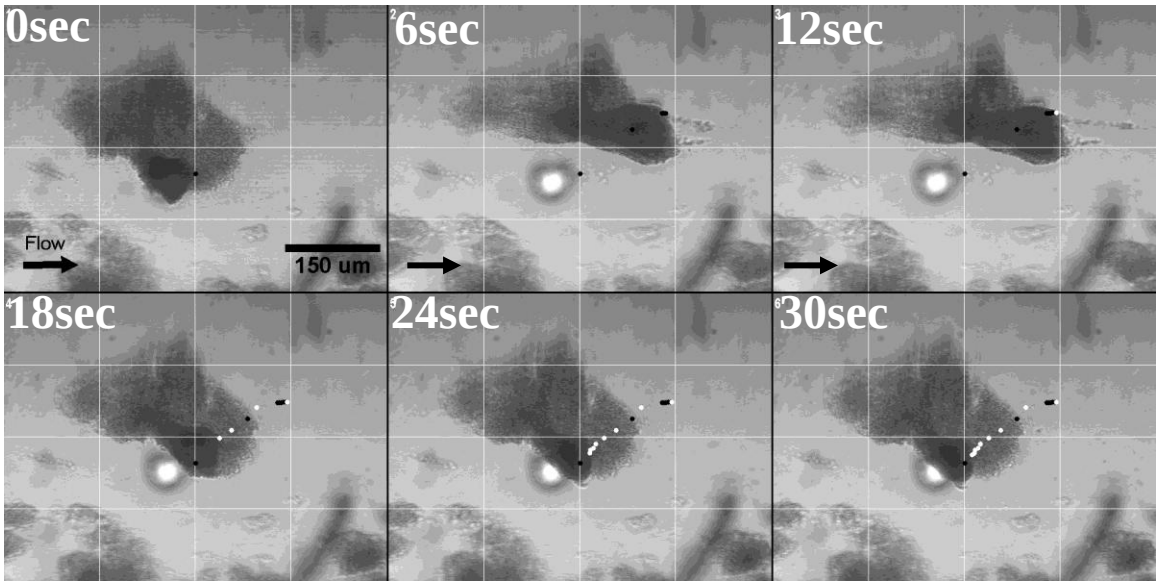

Figure 17) Flow cell time lapse images of *S. epidermidis* biofilm with 15sec fluid shear and 15 sec relaxation period. 0sec frame is the initial configuration of the biofilm and 30sec is the final configuration after the fluid shear test. (Black dots follow displacement through elongation of a single point and white dots follow displacement through relaxation of that single point)

The first image, 0sec, in Figure 17 is the original configuration of the biofilm prior to loading. The biofilm consists of the large dark mass in the center of image 0sec. The biomass is attached to the upper surface of the capillary flow cell in which the image is taken looking down upon the cluster. Images 6sec and 12sec illustrate the motion of the biofilm under a constant fluid flow at time intervals of approximately 6 seconds. The black dots follow displacements of a single point through elongation. The white dots

track the same point on the biofilm structure after the flow is removed. Each dot represents two seconds that have passed. When the flow is initiated, or shut off, the dots initially have large displacements but as the elongation reaches steady-state or maximum elongation the dots are closer together showing less displacement for the same time interval.

Results

The results for the capillary flow cell creep and recovery testing data are broken down between treatments; first the stiffening agents iron chloride and chlorhexidine then urea and DispersinB®, shown to create a more viscous biofilm, and finally the untreated control. Each treatment has three separate trials. Only the data from the first trial is shown here, the remaining two trials for each treatment can be found in Appendix A.

Iron Chloride Treatment

Iron chloride is thought to bind two negatively charged spots on the EPS matrix, ultimately creating a cross-linked, stiffer biofilm. The following sequences are of the same cluster both before and after treatment under the same fluid shear.

$FeCl_2$ Pre-treatment fluid shear test

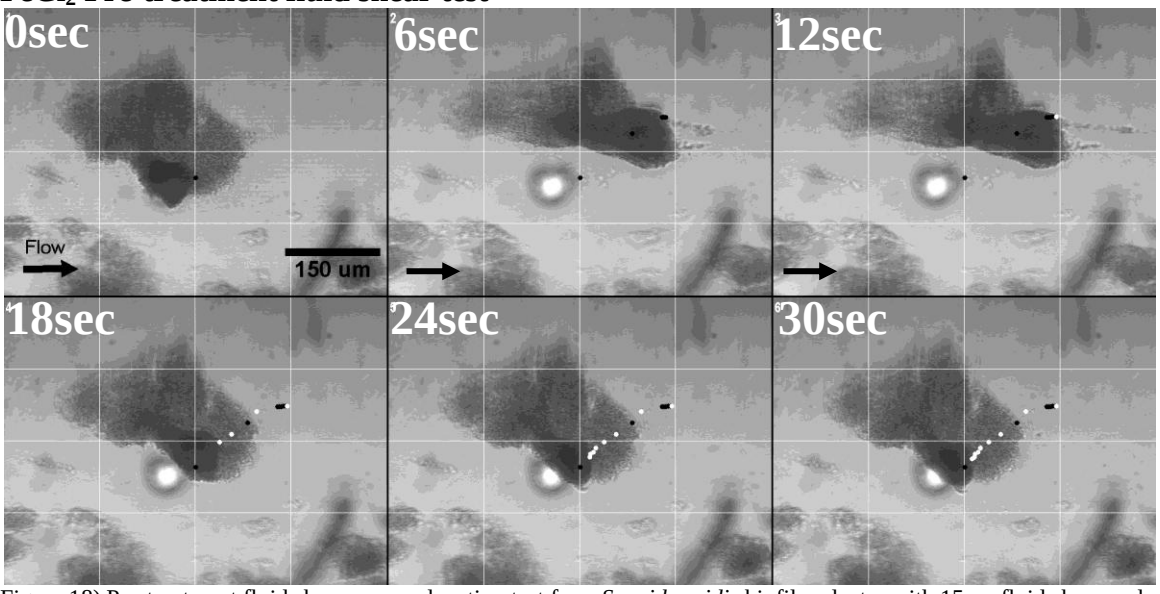

Figure 18) Pre-treatment fluid shear creep relaxation test for a *S. epidermidis* biofilm cluster with 15sec fluid shear and 15 sec relaxation period. 0sec frame is the initial configuration of the biofilm and 30sec is the final configuration after the fluid shear test. (Black dots follow displacement through elongation of a single point and white dots follow displacement through relaxation of that single point)

$FeCl_2$ Post-treatment fluid shear test

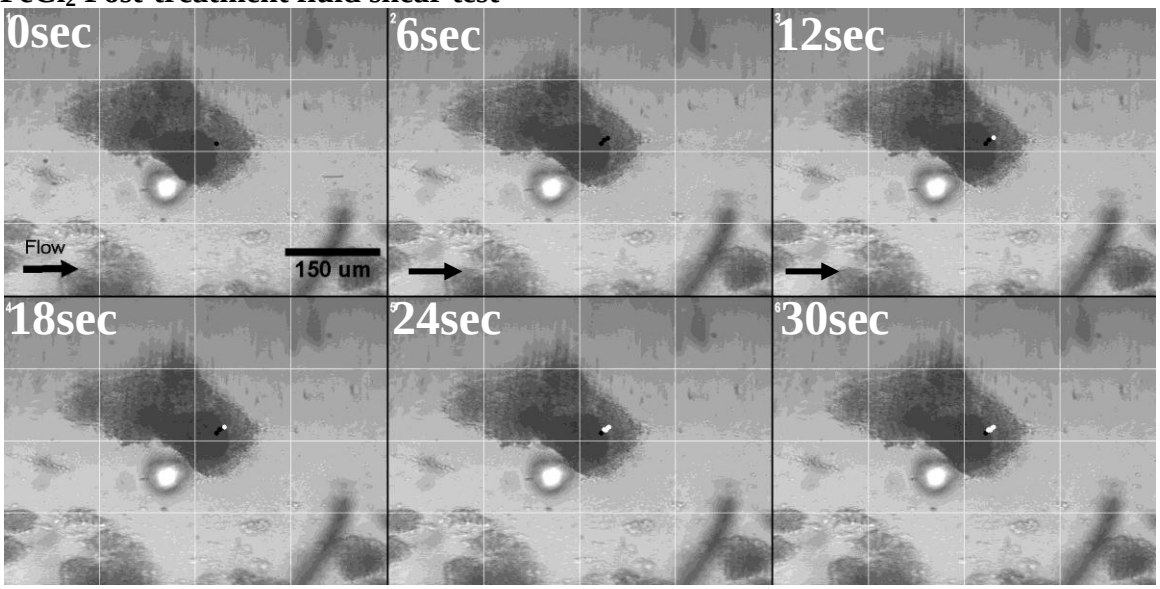

Figure 19) Post-treatment fluid shear creep relaxation test for a *S. epidermidis* biofilm cluster treated with 0.5M $FeCl_2$ and 15sec fluid shear and 15 sec relaxation period. 0sec frame is the initial configuration of the biofilm and 30sec is the final configuration after the fluid shear test. (Black dots follow displacement through elongation of a single point and white dots follow displacement through relaxation of that single point)

Notice the large deformation under the fluid shear before the biofilm was treated with iron chloride in Figure 18. Using the time-lapse images, three particular points on the structure were measured for displacement throughout the fluid shear. The average of these vectors was plotted with time to produce a displacement time graph for both the pre-treatment and post-treatment displacement magnitudes shown in Figure 20:

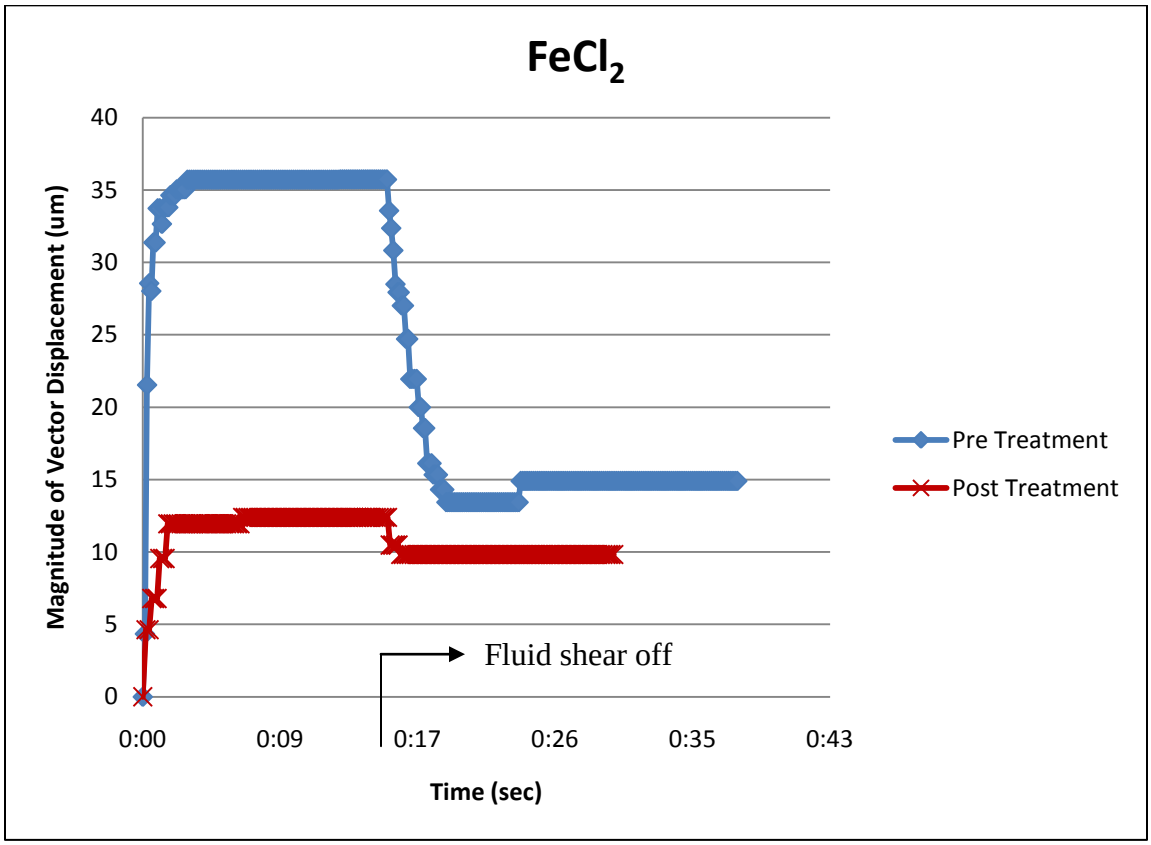

Figure 20) $FeCl_2$ treatment of average of vector displacements for specified spots on the biofilm cluster (Post-treatment displacements much lower than initial displacements)

Notice that the post-treatment biofilm has a much smaller maximum displacement than that of the pre-treated biofilm. There was still a relaxation contraction in the after-treatment biofilm, but it was not as large as the total relaxation contraction of the initial biofilm.

Another piece of information that can be obtained from the plots of the magnitude of displacement vectors is the instantaneous elastic region, which corresponds to the E_1 of the Burger model. Only the initial seven displacement points are plotted on the same graph as seen in Figure 21:

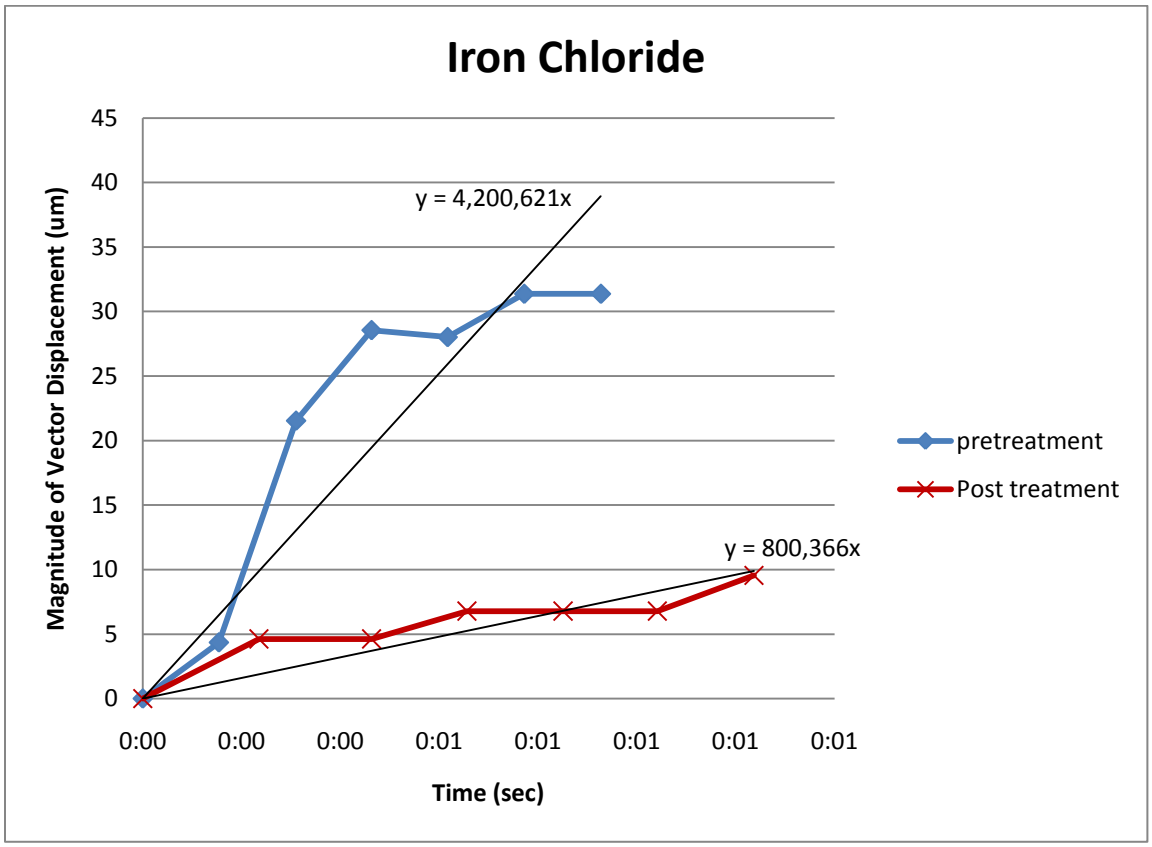

Figure 21) Initial elastic response of $FeCl_2$ treated and untreated biofilm

Notice that before the biofilm was treated there was a much steeper slope, or the biofilm moves farther, under a constant force, lending to a smaller elastic modulus, E_1 of the Burger model. In other words, the E_1 of the untreated biofilm was smaller than that of the treated biofilm or the treated biofilm was stiffer than the untreated biofilm. The ratio of slopes was 0.36 (Post-treatment/Pre-treatment).

Another piece of information obtained from the creep recovery graph was the ability the biofilm to recover after a shear test. Using the Burger model analogy, this gives insight to the dashpots or the ability of the biofilm to dissipate energy. Three recovery percentages were calculated.

Table 3) $FeCl_2$ percent recovery table

% Recovery Pre-treatment	22.8
% Recovery Post-treatment	15.4
Post-treatment max deformation (as % of pre-treatment)	42.2

Table 3 summarizes the effect of the $FeCl_2$ treatment on the percentage of recovery seen during the flow cell reactor creep-recovery test. The first two rows contain the percent recovery of the untreated and after-treated biofilm. This was found by taking the maximum value of displacement reached during the fluid shear and subtracting the final position; this defines the amount of unrecoverable strain, which is then divided by the maximum value of displacement. The post-treatment maximum deformation was found by dividing the maximum post-treatment displacement by the maximum pre-treatment displacement. These results show that although a permanent deformation is seen (100% recovery would be no permanent deformation), the treatment reduces the amount of recovery from the pre-treatment condition. A reduction in the amount of recovery implies that the treatment reduces the energy stored in the biofilm structure, or in the Burger model more dominate values for the viscous dashpot representing η_1. The post-treatment deformation is also shown as a percentage of the pre-treatment deformation. Therefore less than 100% showed smaller deformation than the pre-treatment. The iron chloride treatment is shown to significantly reduce the deformation of the biofilm

Next, by recording biomass area throughout the initial shear test and the post-treatment shear test insights about the density and failures of the biofilm can be observed. This property was measured using MetaVue software, which assigns each pixel an intensity value, black to white, with 255 variations of gray in-between. A limit was set so that each dark pixel below a certain value was considered biomass. Each image had the percent area recorded so ultimately a graph of normalized percent of biomass with time was made.

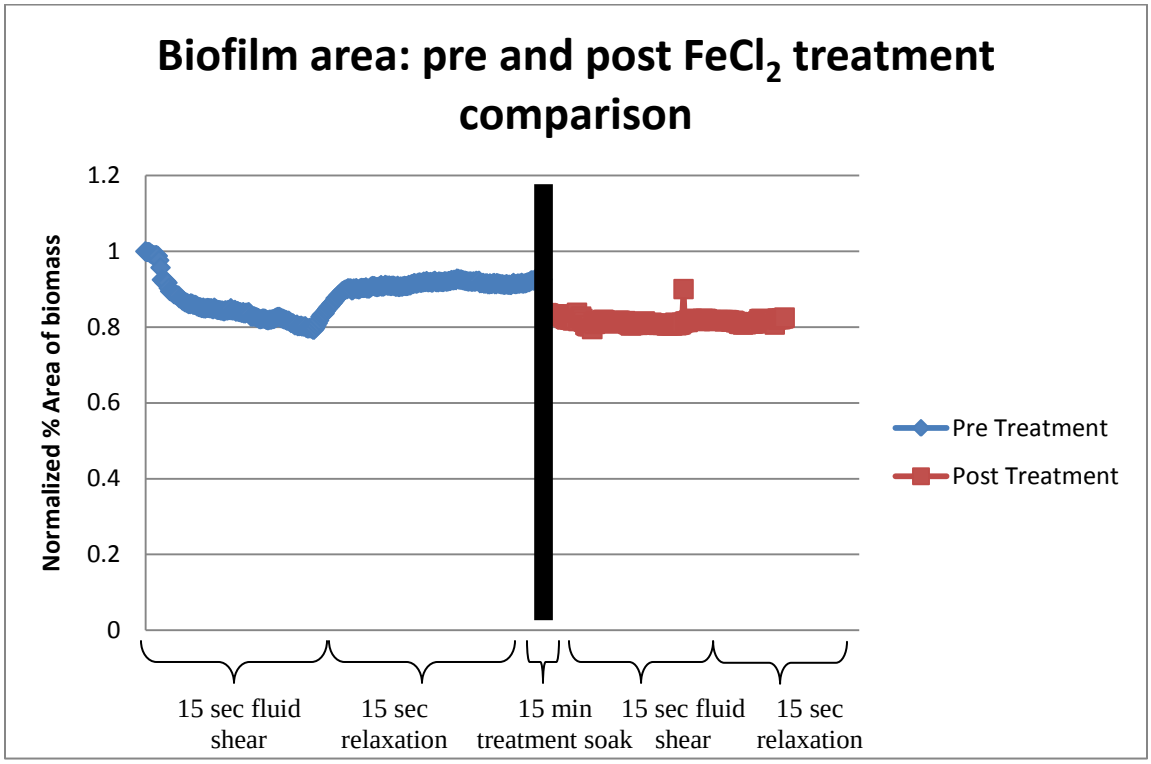

Figure 22) Pre and post-treatment measurement of biomass % area during fluid shear test for $FeCl_2$

Notice in Figure 22 that in the pre-treatment fluid shear test there was a large change in covered area. This is due stretching of biofilm in the downstream direction of flow. Notice also that when the flow is shut off in the pre-treatment relaxation phase much of

that area returns as the biofilm restores to its original structure. The black line in the center of the graph represents the fifteen minute treatment soak in which iron chloride was added to the biofilm. The post-treatment in this case made a large decline in area showing that biofilm shrunk during the treatment. There was little change in area in the post-treatment due to stretching of the biofilm in the downstream direction, which shows a stiffer biofilm. It is important to note that this is a two dimensional image of a three dimensional biofilm thus loss of area could be from out of plane deformations. Results from trials 2 and 3 for iron chloride that show similar results can be found in Appendix A.

Chlorhexidine Treatment

Chlorhexidine, a common antiseptic in mouth wash and contact lens solutions, was used at a concentration of 0.1% in this study. The same procedure is repeated and shown in Figure 23 and Figure 24:

Chlorhexidine pre-treatment fluid shear test

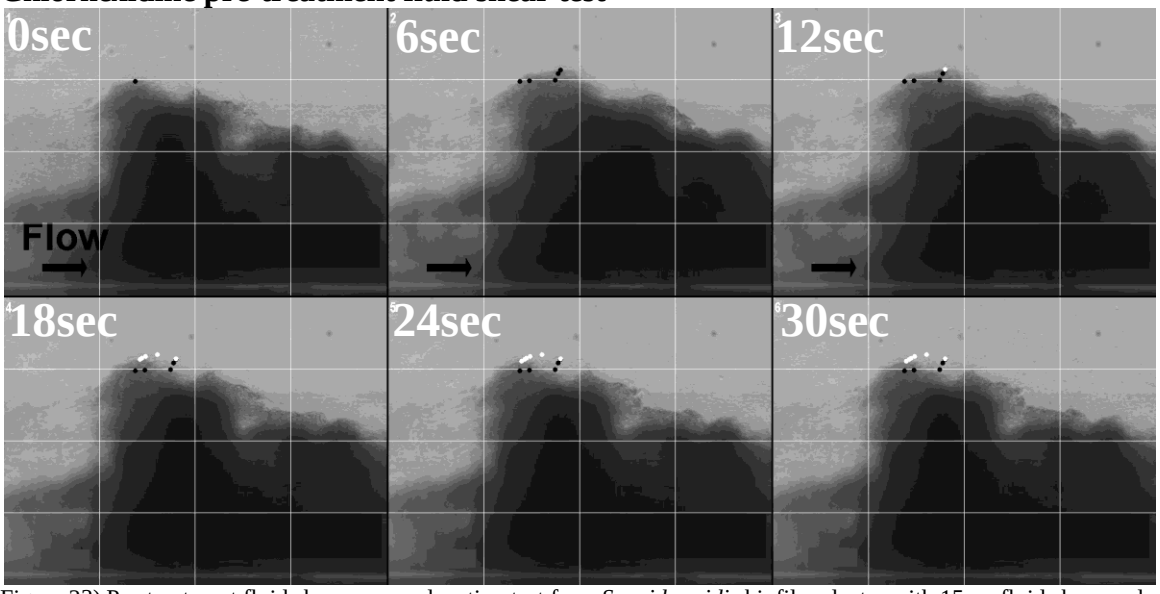

Figure 23) Pre-treatment fluid shear creep relaxation test for a *S. epidermidis* biofilm cluster with 15sec fluid shear and 15 sec relaxation period. 0sec frame is the initial configuration of the biofilm and 30sec is the final configuration after the fluid shear test. (Black dots follow displacement through elongation of a single point and white dots follow displacement through relaxation of that single point)

Chlorhexidine post-treatment fluid shear test

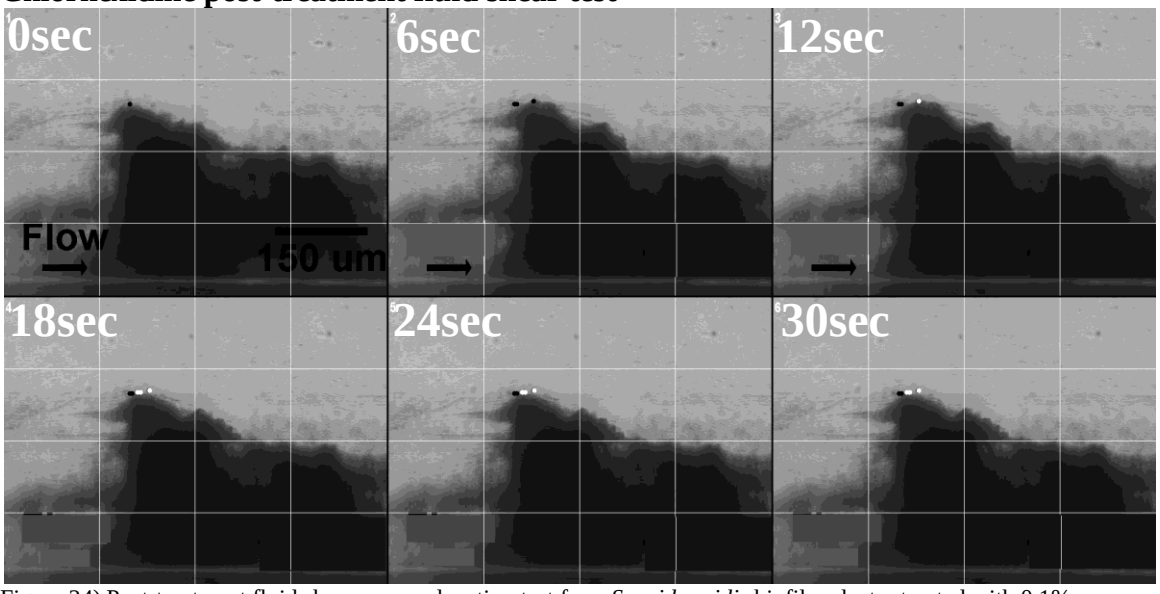

Figure 24) Post-treatment fluid shear creep relaxation test for a *S. epidermidis* biofilm cluster treated with 0.1% chlorhexidine and 15sec fluid shear and 15 sec relaxation period. 0sec frame is the initial configuration of the biofilm and 30sec is the final configuration after the fluid shear test. (Black dots follow displacement through elongation of a single point and white dots follow displacement through relaxation of that single point)

Notice the large deformation under the fluid shear before the biofilm is treated with chlorhexidine, Figure 23, compared to the post-treatment Figure 24. Repeating the same procedure the average displacement vector is plotted with time to produce a displacement time graph for both the pre-treatment and post-treatment displacement magnitudes.

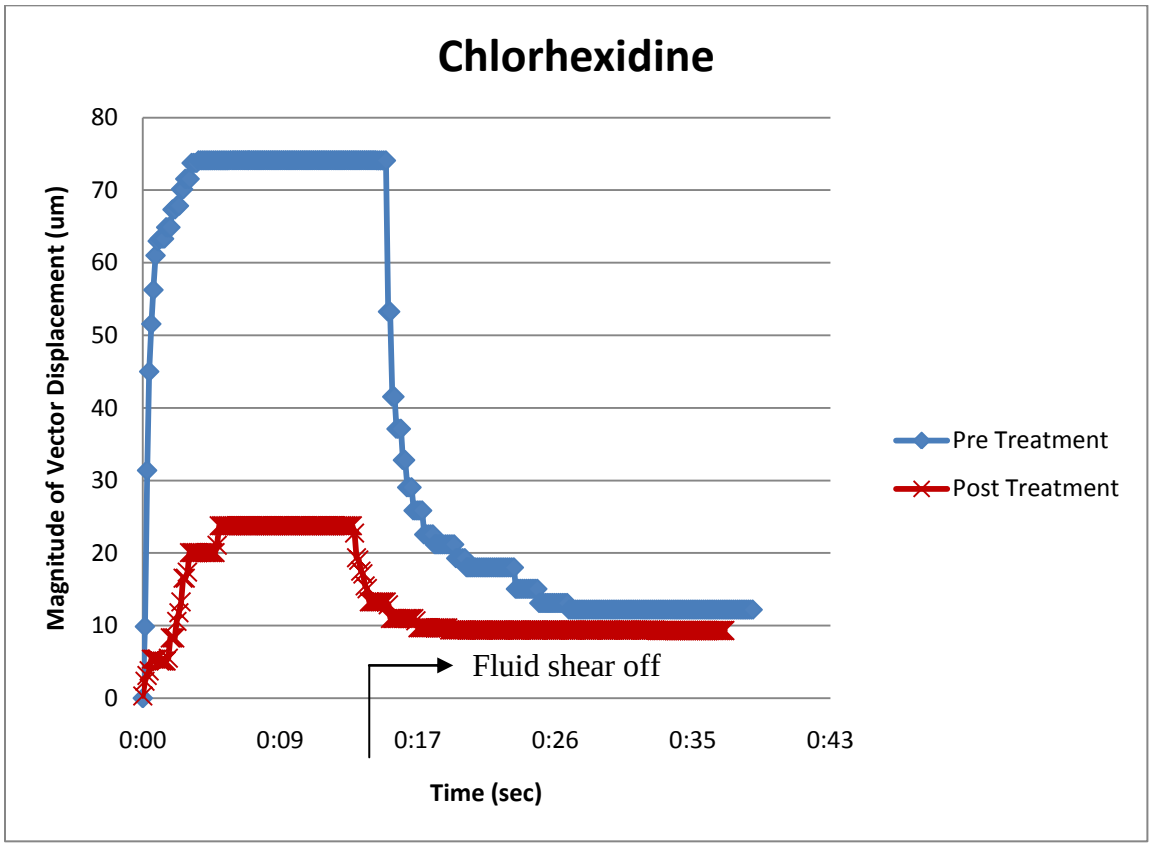

Figure 25) Chlorhexidine treatment of average of vector displacements for specified spots on the biofilm cluster (Post-treatment displacements much lower than initial displacements)

Notice in Figure 25 that the post-treatment had a much smaller maximum displacement than that of the pretreated biofilm. There were still large amounts of relaxation contraction in the post-treatment biofilm showing viscoelastic characteristics even after the chlorhexidine treatment. Unfortunately in this particular trial for chlorhexidine the

fluid shear was shut off before the 15sec time allotment. The results are still valid however because the displacements had reached a steady state.

The instantaneous elastic region corresponding to the E_1 of the Burger model was examined using the initial displacements under the fluid shear. Just the initial seven points are plotted on the same graph as shown in Figure 26.

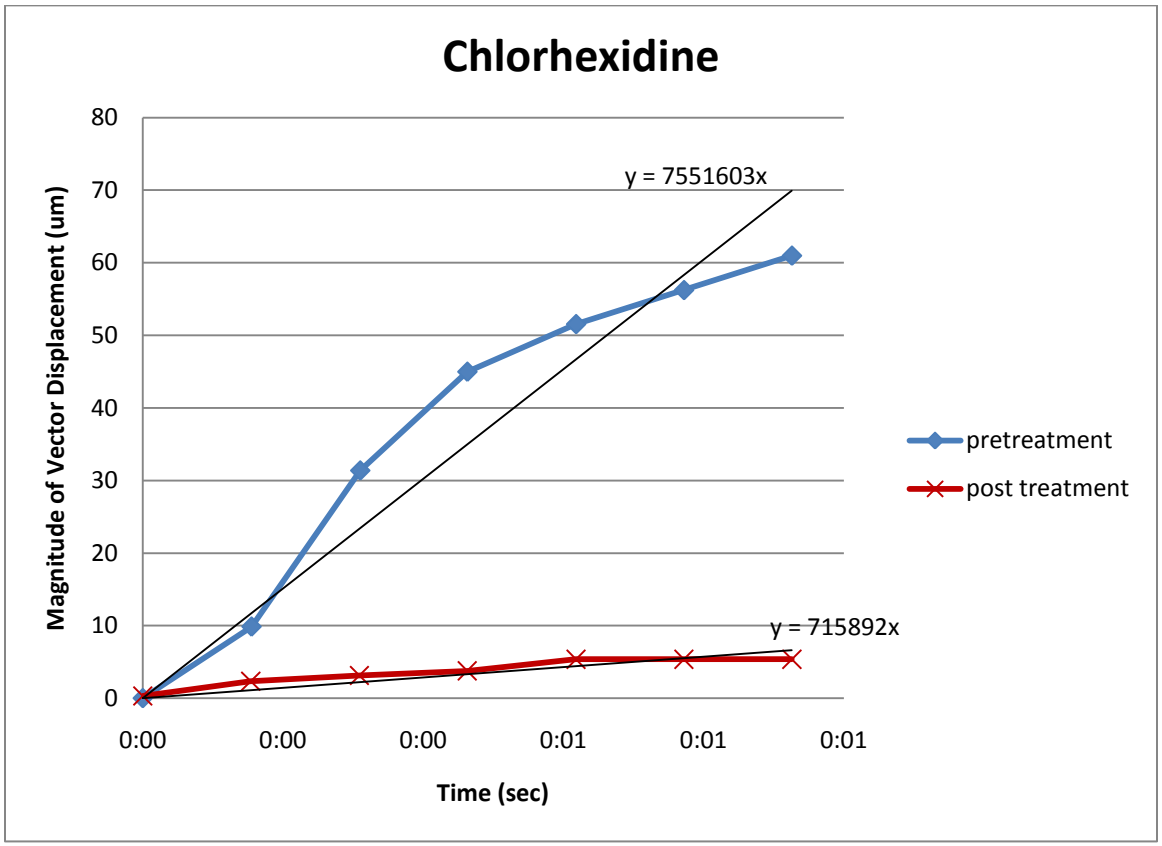

Figure 26) Initial elastic response of chlorhexidine treated and untreated biofilm

Notice that before the biofilm was treated there was a much steeper slope. The biofilm moves farther under a constant force thus lending way to a smaller elastic modulus dominated by E_1 of the Burger model then that of the treated biofilm. So the treated

biofilm was stiffer than the untreated biofilm. The ratio of slopes for chlorhexidine was 0.09 (Post-treatment/Pre-treatment).

Information from the creep recovery graph that was obtained is the ability the biofilm to recover after a shear test. Using the Burger model analogy this gives insight to the viscous dashpots or the ability of the biofilm to dissipate energy. Again three recovery percentages were calculated.

Table 4) Chlorhexidine percent recovery table

% Recovery Pre-treatment	85.4
% Recovery Post-treatment	60.4
Post-treatment max deformation (as % of pre-treatment)	38.8

Table 4 summarizes the effect of the chlorhexidine treatment on the percentage of recovery seen during the flow cell reactor creep-recovery test. The chlorhexidine treatment is shown to significantly reduce the deformation and recovery of the biofilm.

Next by monitoring biomass area throughout the initial shear test and the post-treatment shear test conclusions about the density and failures of the biofilm were made.

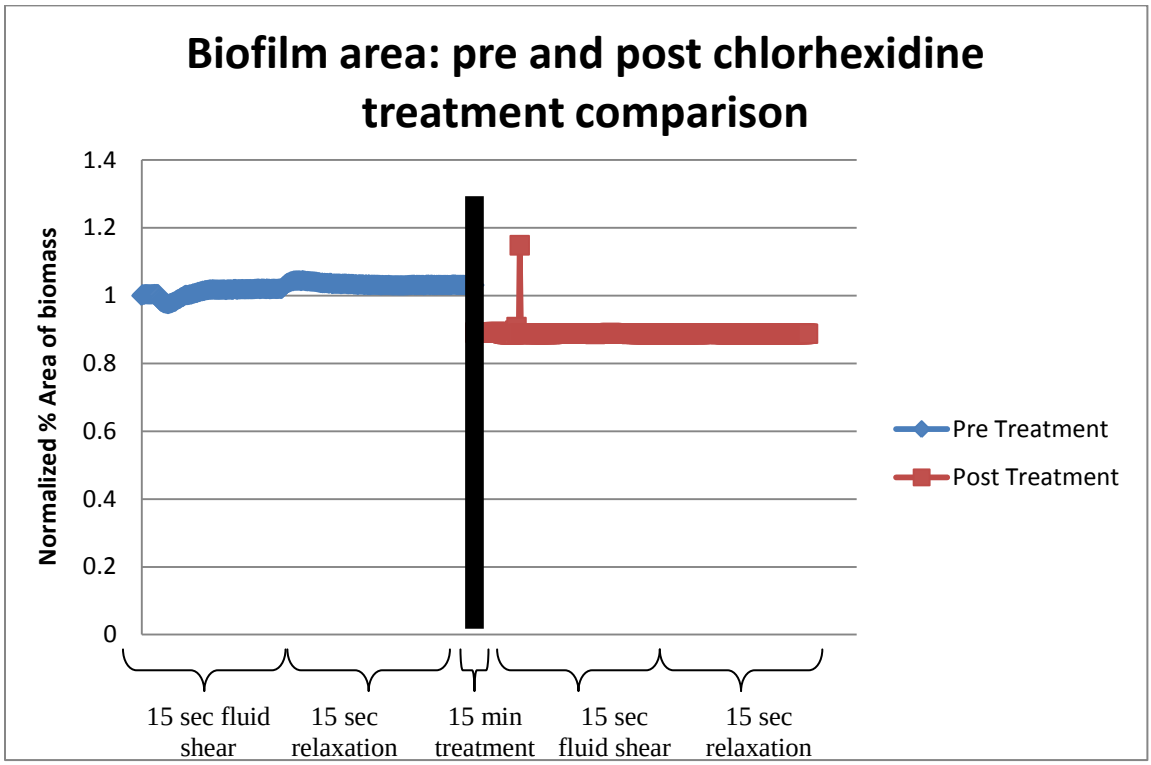

Figure 27) Pre and post-treatment measurement of biomass % area during fluid shear test for chlorhexidine

Notice in Figure 27 that the post-treatment in this case made a large decline in area showing that biofilm shrunk during the treatment. Notice also that there was little change in area during the post-treatment which relates to a stiffer biofilm. Similar results from trials 2 and 3 for chlorhexidine can be found in Appendix A.

Urea Treatment

Urea is theorized to disrupt hydrogen-bonding interactions which are thought to be important for EPS mechanical stability. Urea at a concentration of 0.5 molar was used in this testing. The previous methodologies were repeated for this treatment and shown in Figure 28 and Figure 29:

Urea Pre-treatment fluid shear test

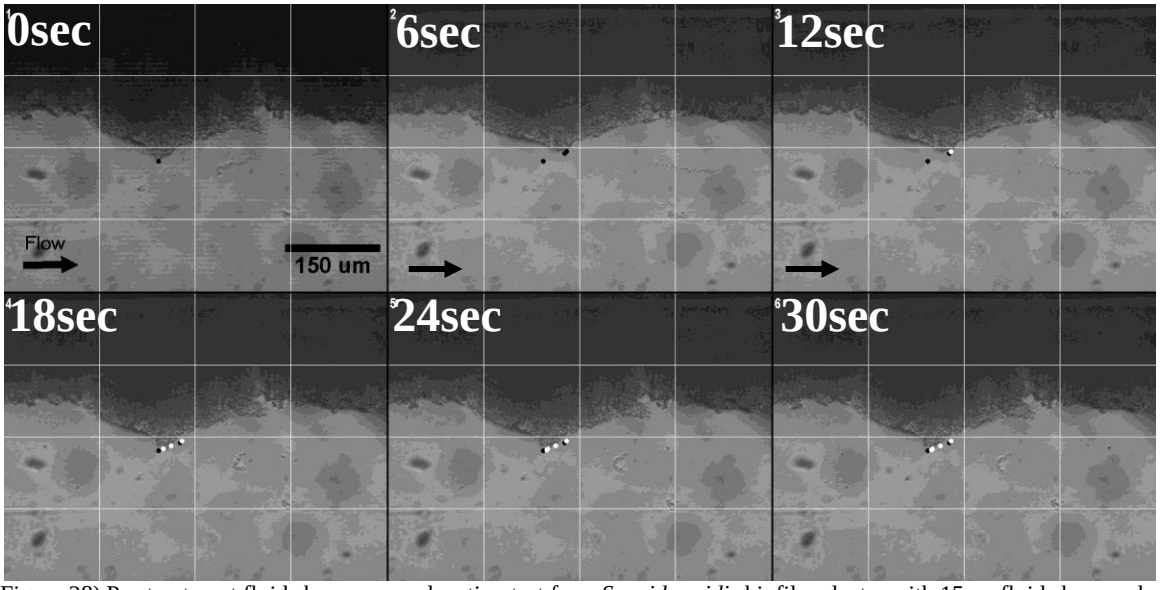

Figure 28) Pre-treatment fluid shear creep relaxation test for a *S. epidermidis* biofilm cluster with 15sec fluid shear and 15 sec relaxation period. 0sec frame is the initial configuration of the biofilm and 30sec is the final configuration after the fluid shear test. (Black dots follow displacement through elongation of a single point and white dots follow displacement through relaxation of that single point)

Urea Post-treatment fluid shear test

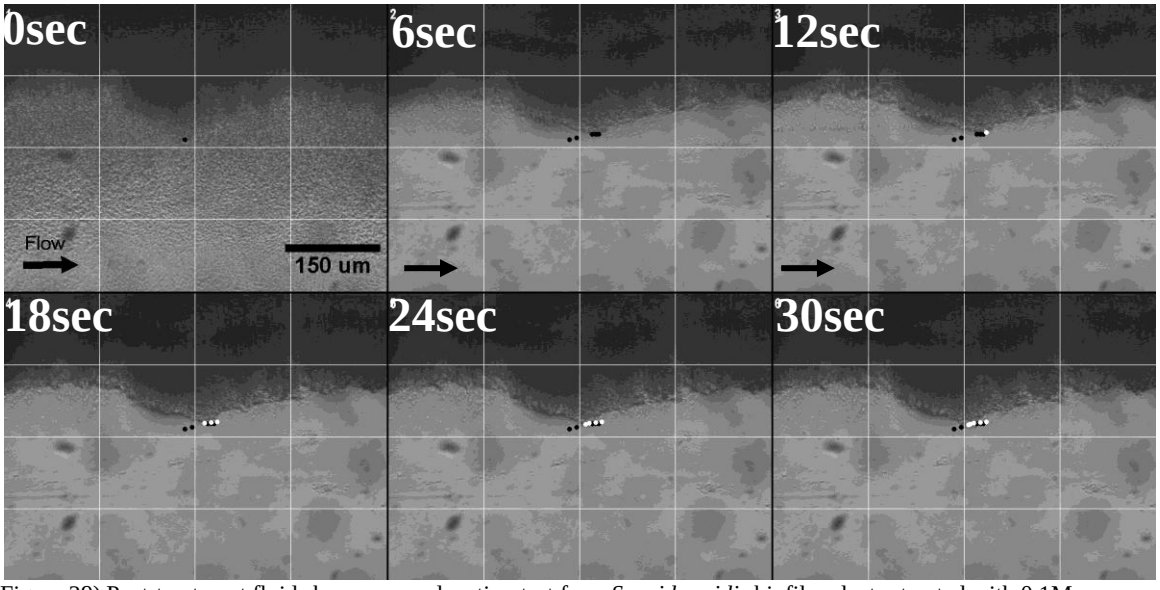

Figure 29) Post-treatment fluid shear creep relaxation test for a *S. epidermidis* biofilm cluster treated with 0.1M urea and 15sec fluid shear and 15 sec relaxation period. 0sec frame is the initial configuration of the biofilm and 30sec is the final configuration after the fluid shear test. (Black dots follow displacement through elongation of a single point and white dots follow displacement through relaxation of that single point)

Notice the larger deformations under the fluid shear after the biofilm is treated with urea.

Also notice that there is in a large number of scattered cells in the first frame of post-

treatment (Figure 29, 0sec) before fluid shear is induced. Again using the time lapse images displacements of points on the biofilm throughout the fluid shear are averaged and plotted with time to produce a displacement time graph for both the pre-treatment and post-treatment displacement magnitudes.

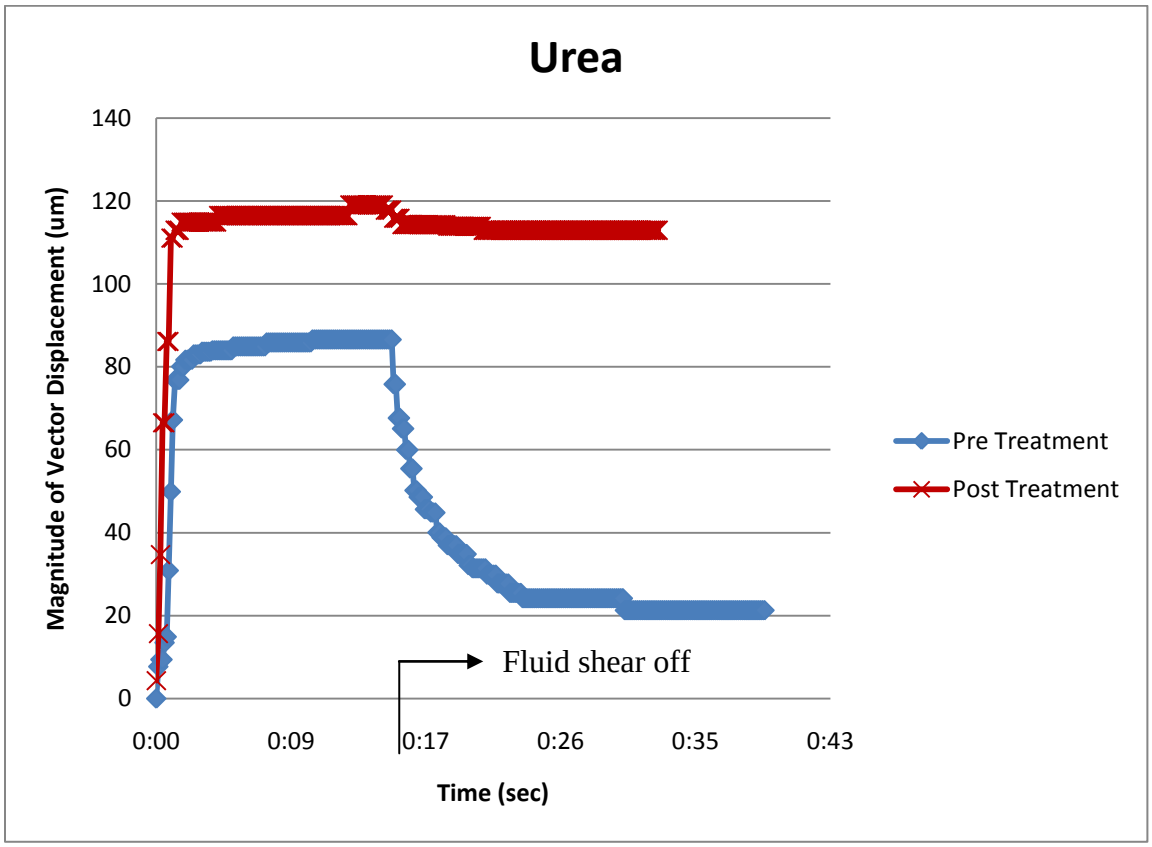

Figure 30) Urea treatment of average of vector displacements for specified spots on the biofilm cluster (Post-treatment displacements much higher than initial displacements)

In Figure 30, the post-treatment had a larger maximum displacement than that of the pre-treated biofilm. There was only a small amount of relaxation contraction in the post-treatment biofilm.

Plots of the magnitude of displacement vectors for the instantaneous elastic region correspond to the E_1 of the Burger model. Only the initial seven points are plotted on the same figure as seen below in Figure 31.

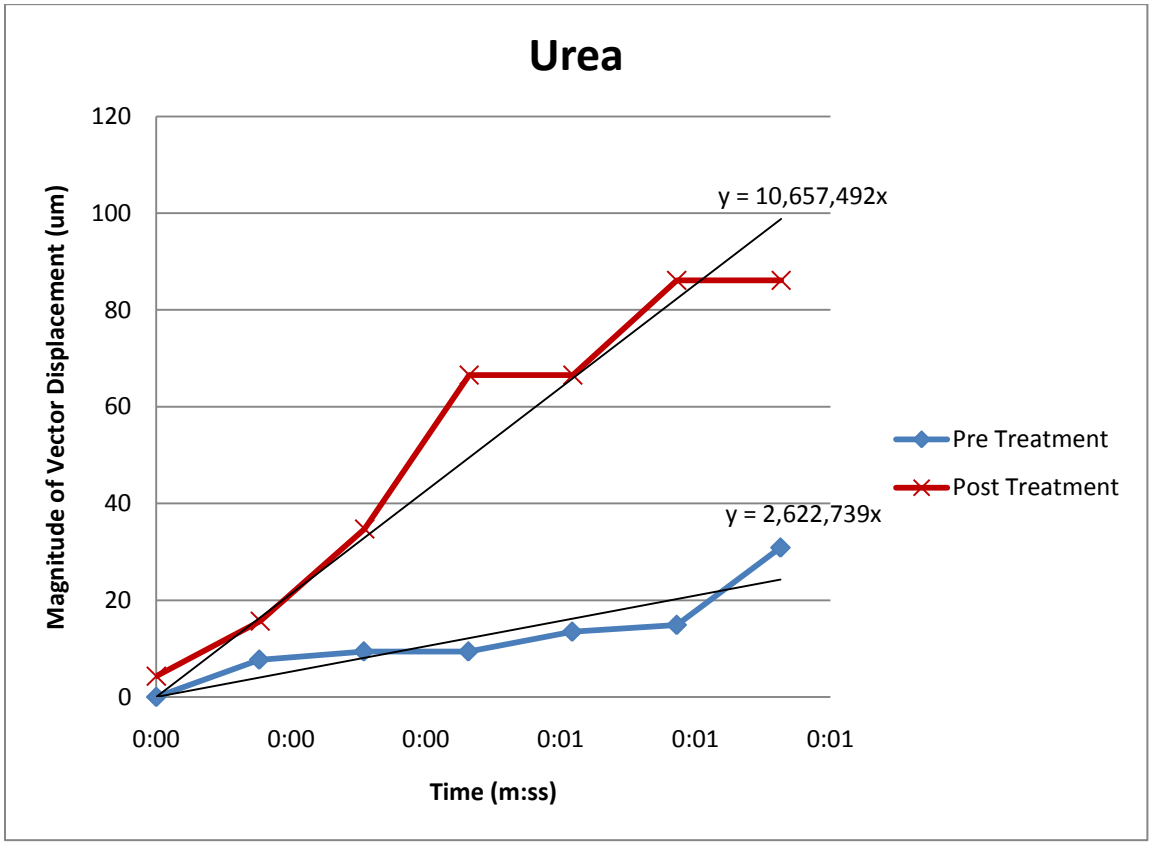

Figure 31) Initial elastic response of urea treated and untreated biofilm

Notice that after the biofilm was treated there was a much steeper slope or the biofilm moves farther under a constant force. The treated biofilm had a lower elastic modulus dominated by E_1 of the Burger model. In other words the E_1 of the untreated biofilm was larger than that of the treated biofilm or the treated biofilm is more viscous than the untreated biofilm. The ratio of slopes for urea was 4.06 (Post-treatment/Pre-treatment).

Again information from the creep recovery graph was obtained to examine ability the biofilm to recover after a shear test.

Table 5) Urea percent recovery table

% Recovery Pre-treatment	68.5
% Recovery Post-treatment	10.2
Post-treatment max deformation (as % of pre-treatment)	209

Table 5 summarizes the effect of the urea treatment on the percentage of recovery seen during the flow cell reactor creep-recovery test. The urea treatment is shown to significantly increase the deformation but not the recovery of the biofilm.

As before by monitoring biomass area throughout the initial shear test and the post-treatment shear test, conclusions about the density and failures of the biofilm could be made.

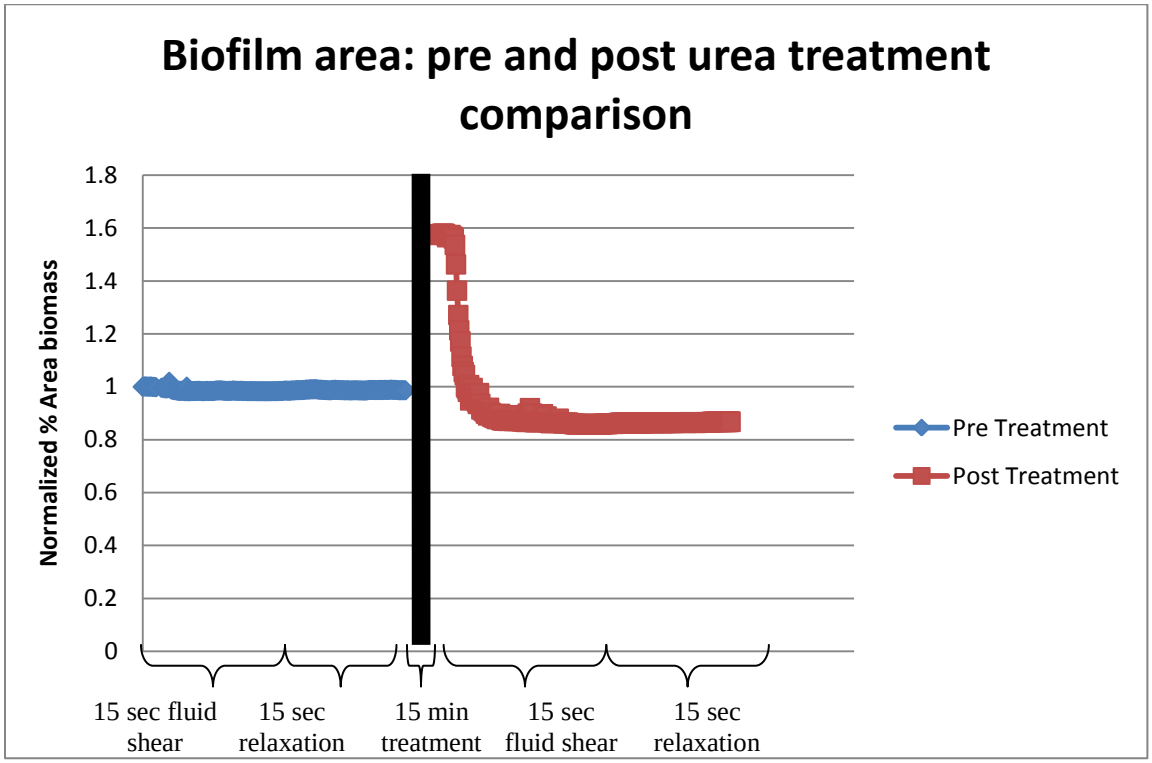

Figure 32) Pre and post-treatment measurement of biomass % area during fluid shear test for urea

Notice in Figure 32 that there is a large amount of biomass area at the beginning of the post-treatment fluid shear. This increase in area is due to the dispersion of cells during the fifteen minute treatment soak. These cells are however unconsolidated and wash down stream as soon as the fluid shear test is started. The final area of biomass is around 15% less than of the original biofilm that was tested before the treatment. Similar results from trials 2 and 3 for urea can be found in Appendix A. These results show urea creating a more viscous biofilm.

DispersinB® Treatment

DispersinB® catalyzes the hydrolysis extracellular polysaccharide produced by *Staphylococcus epidermidis*. DispersinB® at a concentration of 40μg/ml was used in this testing. The procedure was repeated and results are shown in Figure 33 and Figure 34

Dispersin B ® pre-treatment fluid shear test

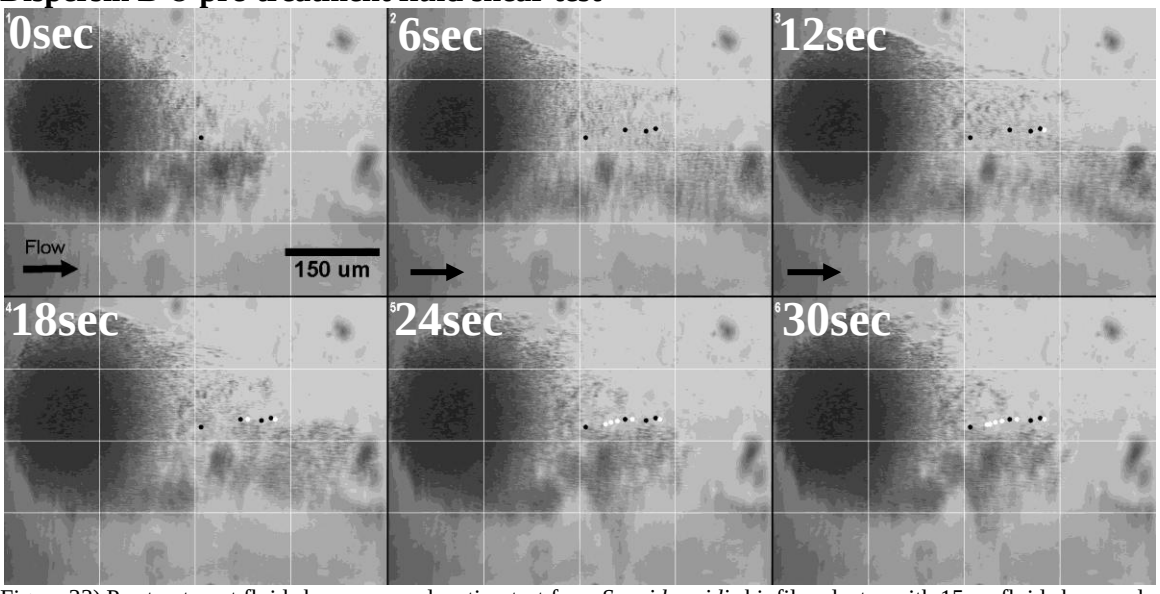

Figure 33) Pre-treatment fluid shear creep relaxation test for a *S. epidermidis* biofilm cluster with 15sec fluid shear and 15 sec relaxation period. 0sec frame is the initial configuration of the biofilm and 30sec is the final configuration after the fluid shear test. (Black dots follow displacement through elongation of a single point and white dots follow displacement through relaxation of that single point)

Dispersin B ® post-treatment fluid shear test

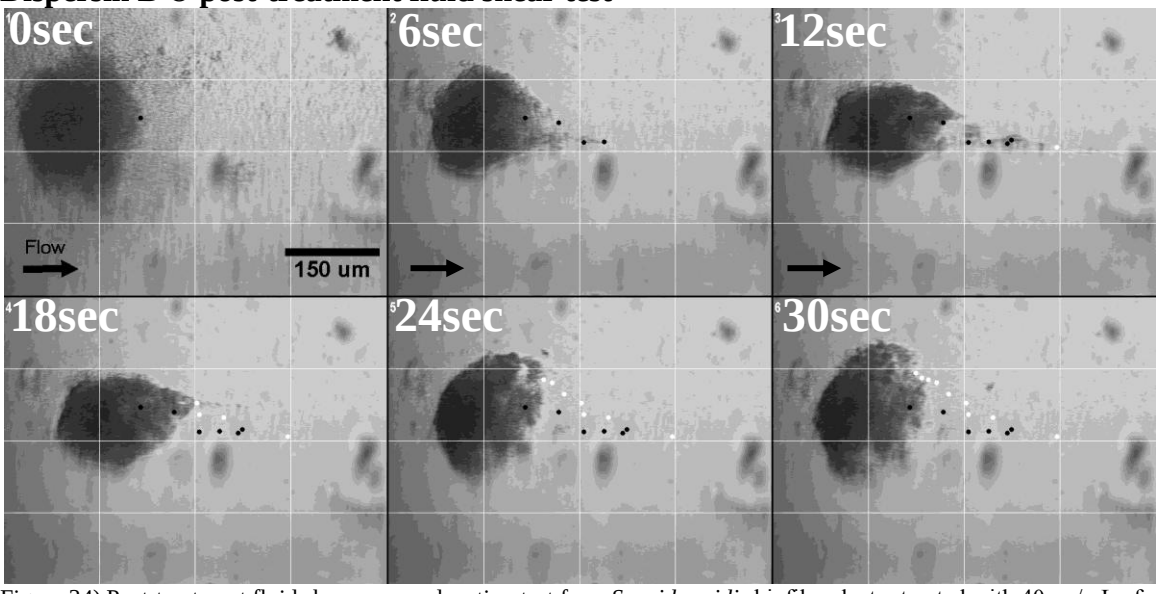

Figure 34) Post-treatment fluid shear creep relaxation test for a *S. epidermidis* biofilm cluster treated with 40 µg/mL of Dispersin B ® and 15sec fluid shear and 15 sec relaxation period. 0sec frame is the initial configuration of the biofilm and 30sec is the final configuration after the fluid shear test. (Black dots follow displacement through elongation of a single point and white dots follow displacement through relaxation of that single point)

Notice the larger deformations under the fluid shear after the biofilm is treated with Dispersin B ®. Also notice that there is in a large number of scattered cells in the

first frame of the post-treated (Figure 34 image 1) before fluid shear is induced. Again using the time lapse images three points on the structure are measured for displacement throughout the fluid shear. The average of these vectors is plotted with time to produce a displacement time graph for both the pre-treatment and post-treatment displacement magnitudes shown in Figure 35.

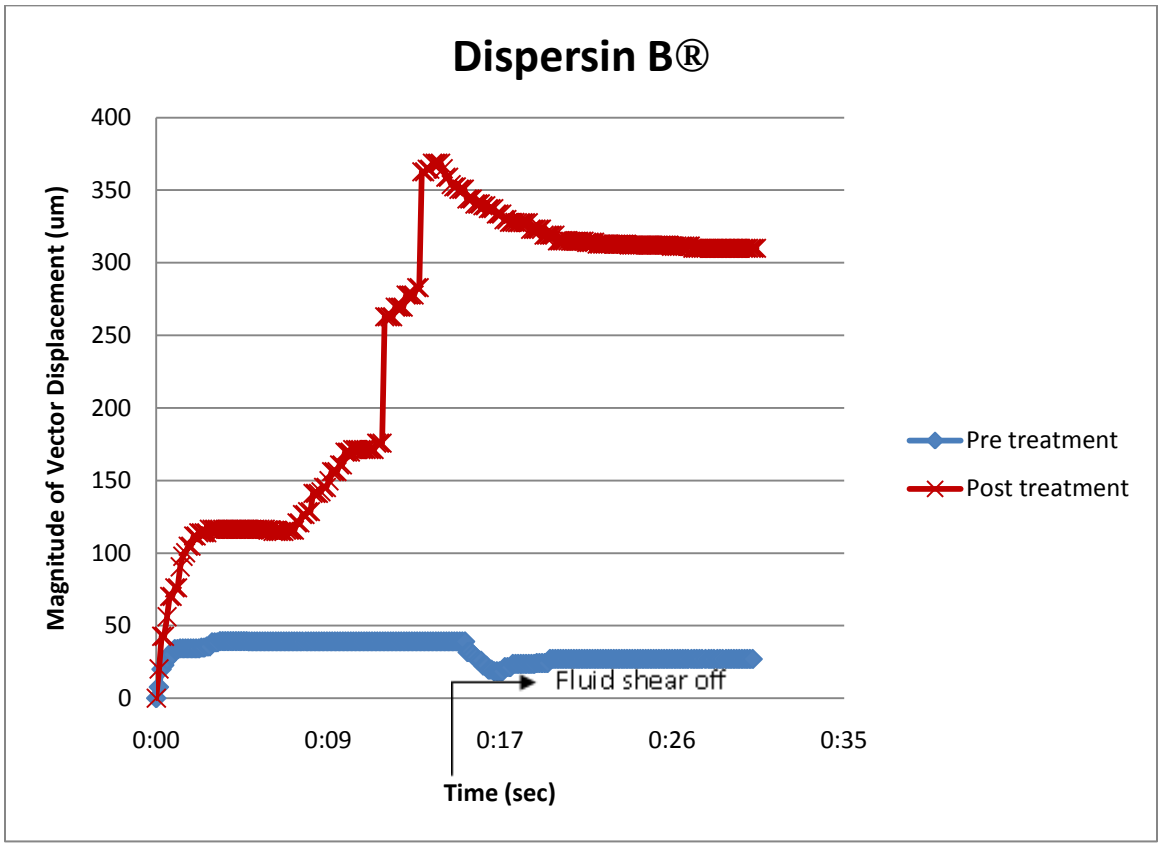

Figure 35) Dispersin B ® treatment of average of vector displacements for specified spots on the biofilm cluster (Post-treatment displacements much higher than initial displacements)

Notice that the post-treatment has a much larger maximum displacement than that of the pre-treated biofilm. There is only a small amount of relaxation contraction in the post-treatment biofilm.

Just the initial seven points of the displacement with time are plotted in Figure 36.

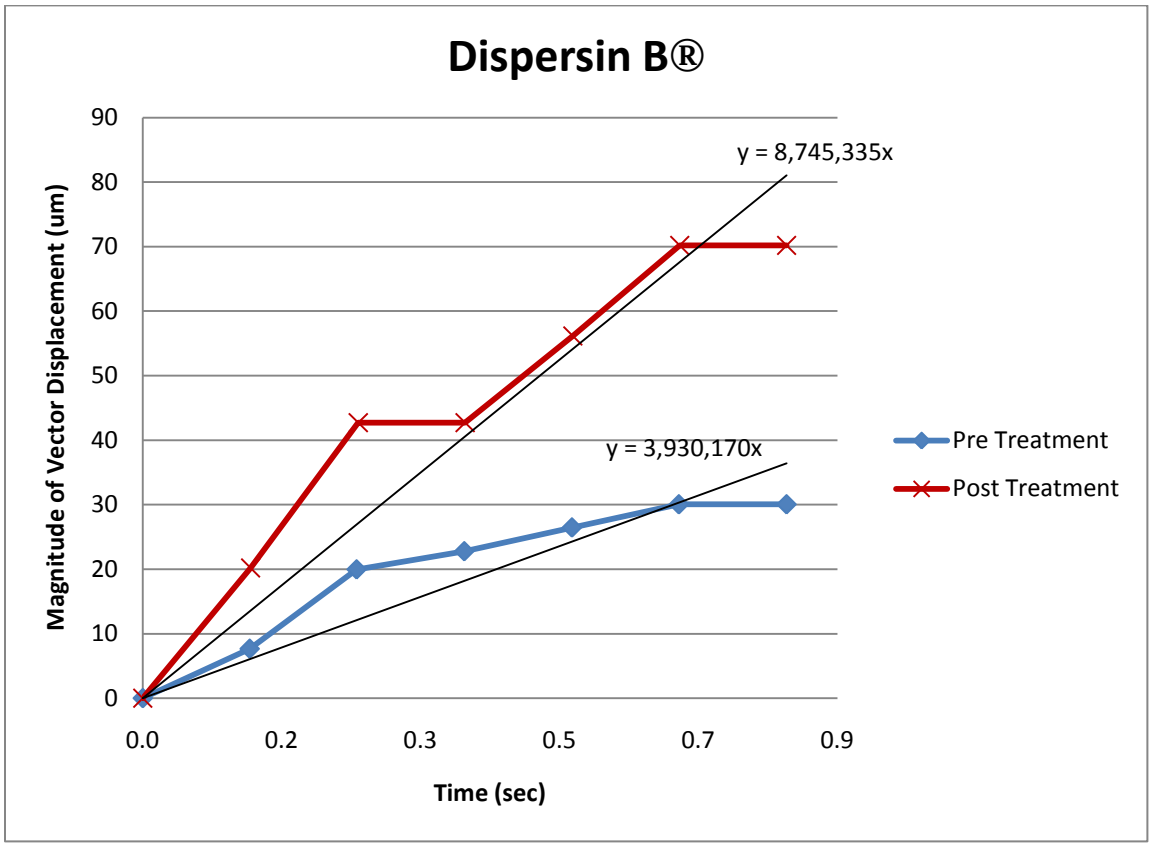

Figure 36) Initial elastic response of Dispersin B ® treated and untreated biofilm

Notice that after the biofilm is treated there is a much steeper slope or the biofilm moves further under a constant force. The treated biofilm has a lower elastic modulus dominated by E_1 of the Burger model. In other words the E_1 of the untreated biofilm is larger than that of the treated biofilm or the treated biofilm is more viscous than the untreated biofilm. The ratio of slopes for this trial of DispersinB® was 2.23 (Post-treatment/Pre-treatment).

Information from the creep recovery graph was obtained to examine ability the biofilm to recover after a shear test.

Table 6) Dispersin B ® percent recovery table

% Recovery Pre-treatment	28.0
% Recovery Post-treatment	27.0
Post-treatment max deformation (as % of pre-treatment)	1030

Table 6 summarizes the effect of the Dispersin B ® treatment on the percentage of recovery seen during the flow cell reactor creep-recovery test. The treatment reduces the amount of recovery from the pre-treatment condition. A reduction in the amount of recovery implies that the treatment reduces the energy stored in the biofilm structure; or in the Burger model more dominate viscous dashpots. The DispersinB® treatment is shown to significantly increase the deformation of the biofilm.

Next, by monitoring biomass area throughout the initial shear test and the post-treatment shear test, conclusions about the density and failures of the biofilm could be made.

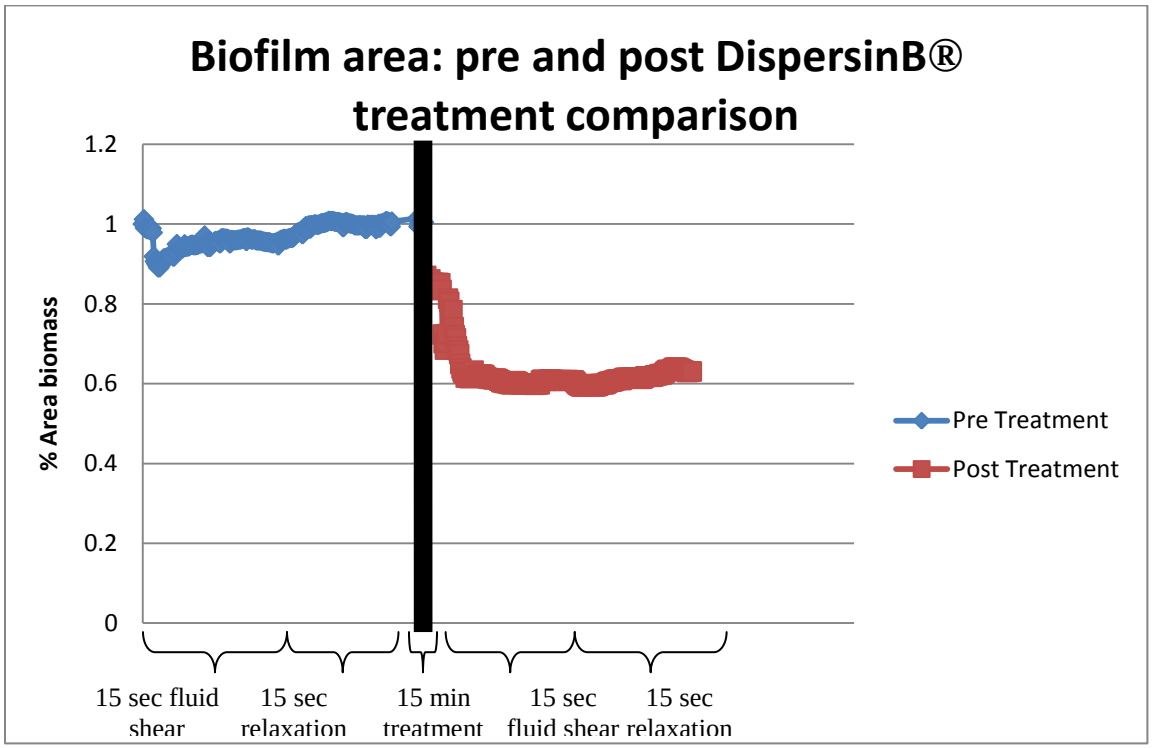

Figure 37) Pre and post-treatment measurement of biomass % area during fluid shear test for DispersinB®

Notice in Figure 37 that there is a large removal of biomass area at the beginning of the post-treatment fluid shear. These cells are unconsolidated and wash down stream as soon as the fluid shear test is started. The final area of biomass is around 40% less than the original biofilm that was tested before the treatment. Similar results from trials 2 and 3 for DispersinB® can be found in Appendix A.

Control Trial

An experiment was conducted to examine permanent strain in the biofilm structure. The procedure was repeated without any treatment, only a buffer solution applied during the fifteen minute soak. Results are shown in Figure 38 and Figure 39

Control pre-treatment fluid shear test

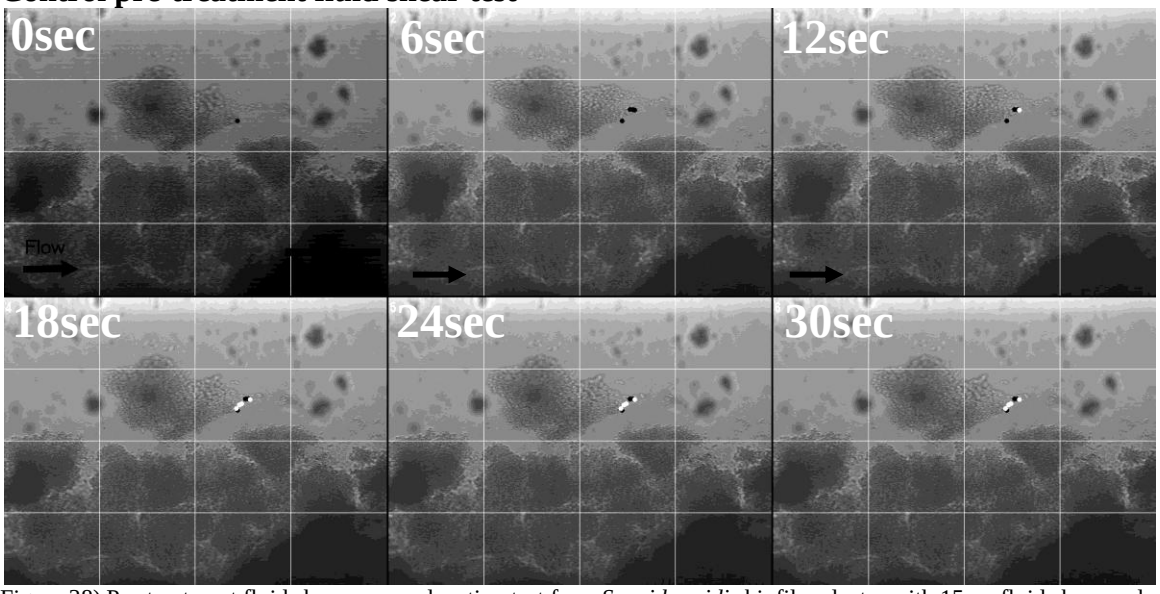

Figure 38) Pre-treatment fluid shear creep relaxation test for a *S. epidermidis* biofilm cluster with 15sec fluid shear and 15 sec relaxation period. 0sec frame is the initial configuration of the biofilm and 30sec is the final configuration after the fluid shear test. (Black dots follow displacement through elongation of a single point and white dots follow displacement through relaxation of that single point)

Control post-buffer treatment fluid shear test

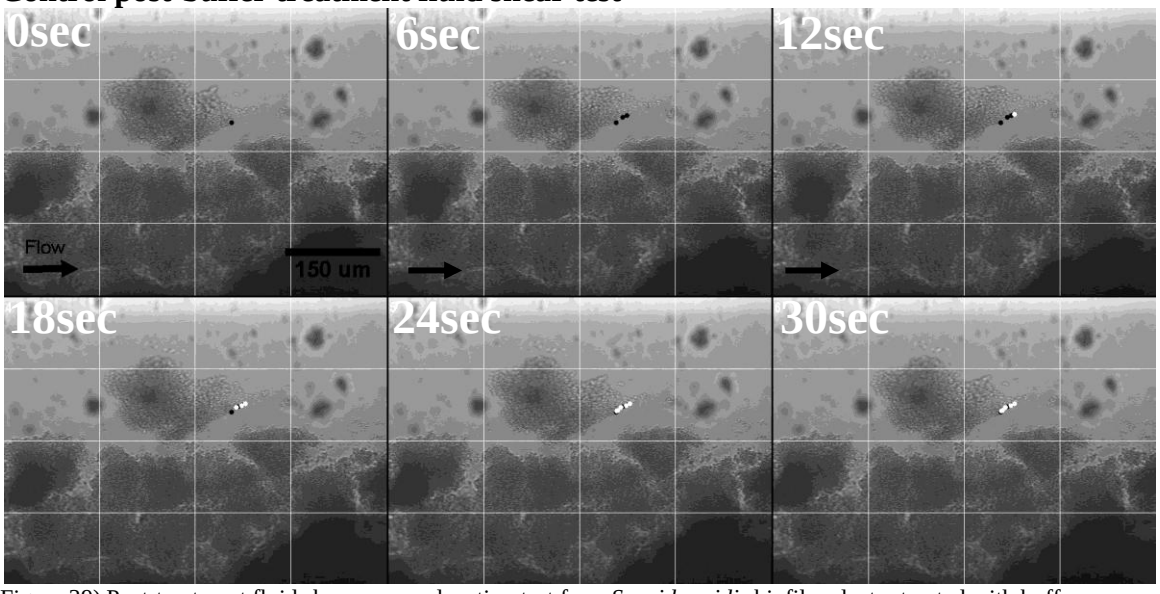

Figure 39) Post-treatment fluid shear creep relaxation test for a *S. epidermidis* biofilm cluster treated with buffer solution and 15sec fluid shear and 15 sec relaxation period. 0sec frame is the initial configuration of the biofilm and 30sec is the final configuration after the fluid shear test. (Black dots follow displacement through elongation of a single point and white dots follow displacement through relaxation of that single point)

Notice that throughout the creep and relaxation for both the before and after buffer treatment there is little difference in displacements. Also notice that the biofilm

structure remains for the most part intact after undergoing a 10-fold increase of fluid shear stress from that of growth conditions showing how resilient these structures were.

Again using the time-lapse images, three continually indefinable points on the structure are measured for displacement throughout the fluid shear. The average of these vectors is plotted with time to produce a displacement time graph for both the pre-treatment and post-treatment displacement magnitudes shown in Figure 40.

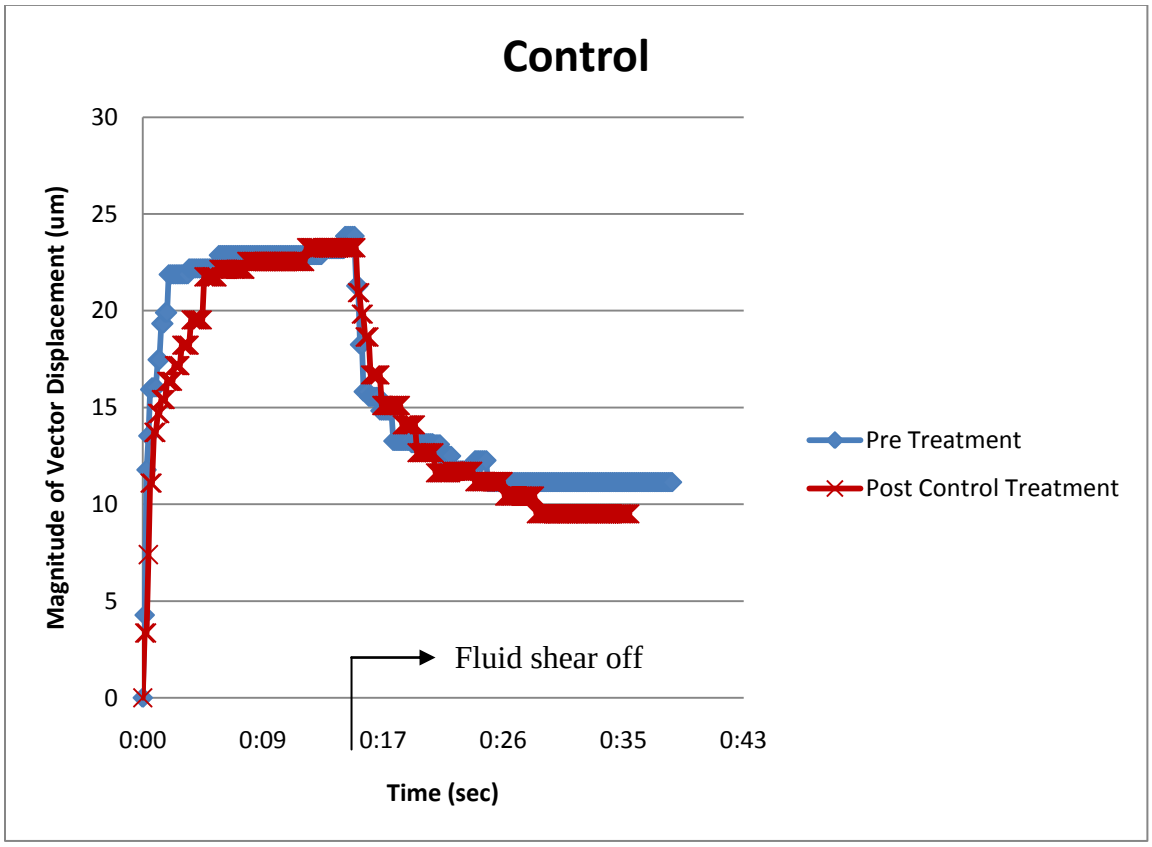

Figure 40) Control treatment of average of vector displacements for specified spots on the biofilm cluster (Post-treatment displacements about the same as initial displacements)

Notice in Figure 40 that the post-treatment has roughly the same displacement as the pretreated biofilm. The amount of relaxation contraction in both the pre-treated trial and control treated biofilm are also very similar.

The magnitude of displacement vectors for the instantaneous elastic region is shown in Figure 41. This corresponds to the E_1 of the Burger model. Just the initial seven points are plotted on the same graph shown in Figure 41.

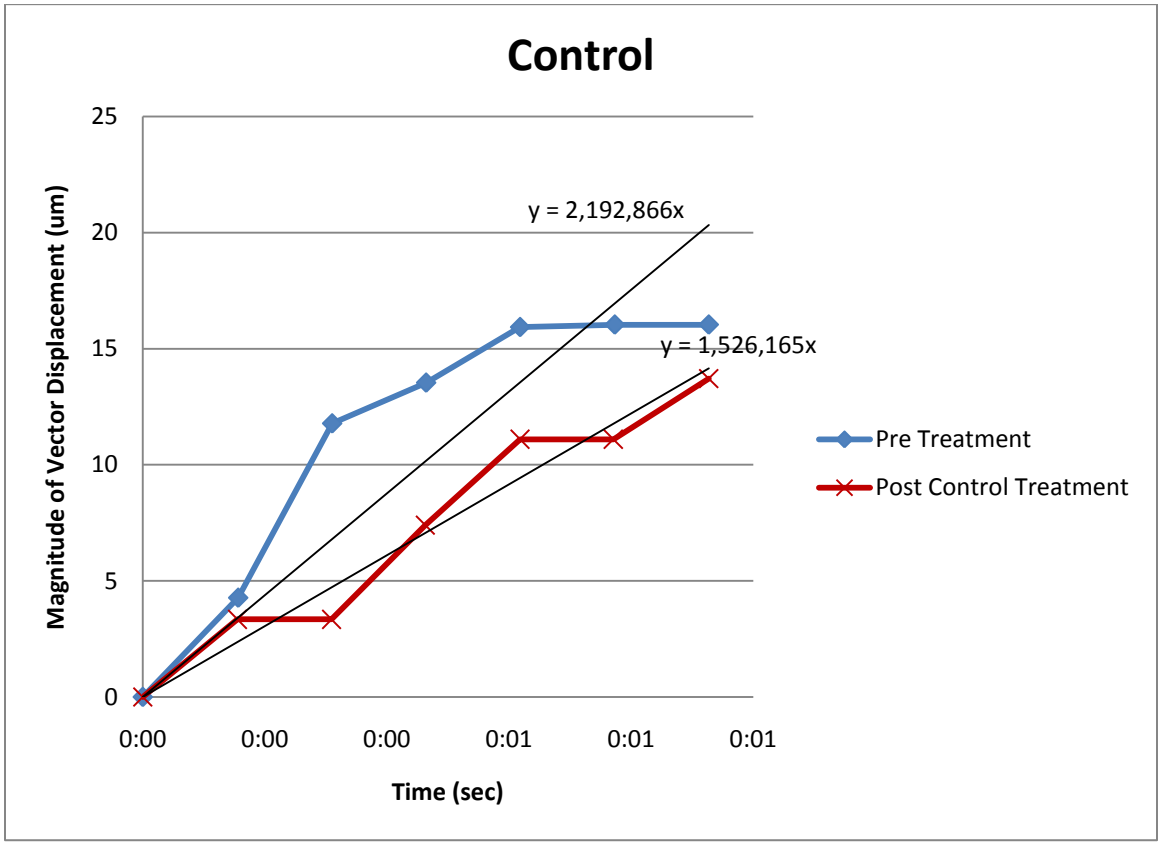

Figure 41) elastic response control treated and untreated biofilm

Notice that after the biofilm has been treated with buffer there is a slight decrease in slope or the biofilm moves less under a constant force. The treated biofilm has undergone some sort of strain or work hardening after the initial fluid shear test.

Information from the creep recovery graph was obtained to examine ability the biofilm to recover after a shear test. Using the Burger model analogy this gives insight to

the dashpots, η_1, or the ability of the biofilm to dissipate energy. Three recovery percentages were calculated.

Table 7) Control percent recovery table

% Recovery pre-treatment	61.0
% Recovery control treatment	52.0
Post-treatment max deformation (as % of pre-treatment)	91.6

Table 7 summarizes the effect of the control treatment on the percentage of recovery seen during the flow cell reactor creep-recovery test. The control treatment has about the same deformation of the pre-treated biofilm.

Next by monitoring biomass throughout the initial shear test and the post-treatment shear test conclusions about the density and failures of the biofilm could be made.

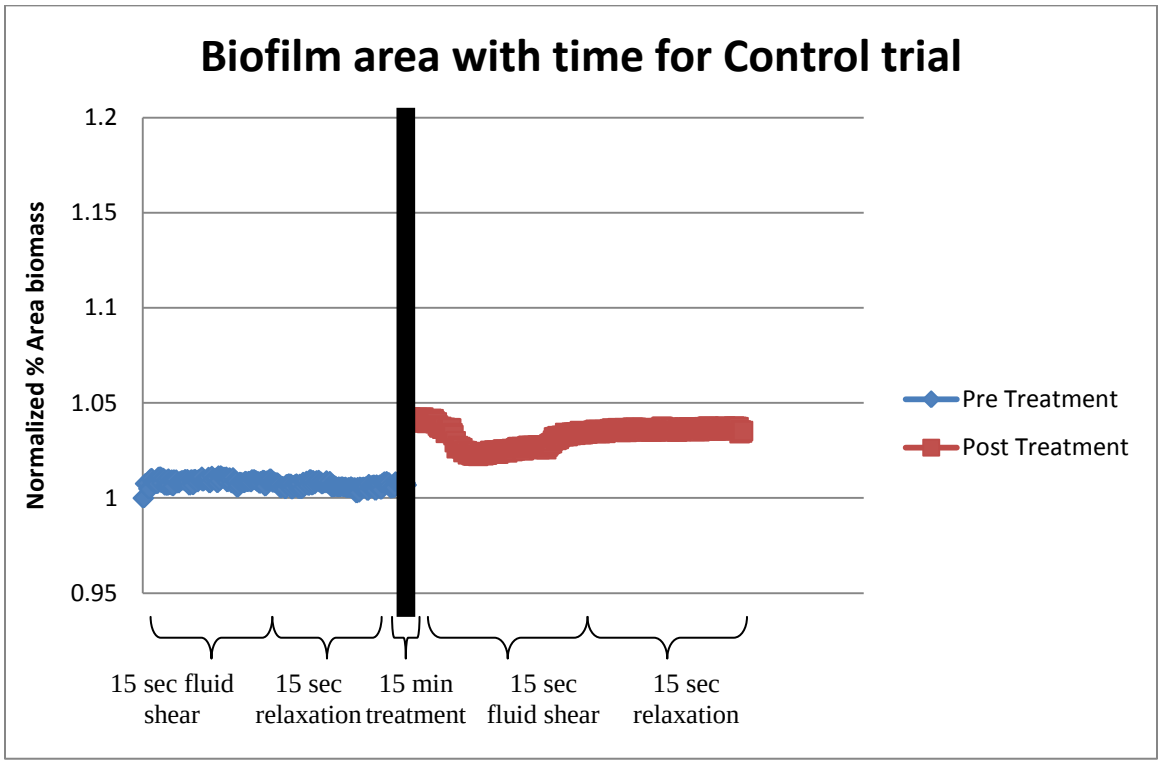

Figure 42) Pre and control treatment measurement of biomass % area during fluid shear test for the no treatment or control

Notice that in Figure 42 there were relatively consistent amounts of biomass before and after the control treatment trials. There were no major sloughing events or major failures of the biofilm in the capillary flow cell. There was a slight increase in size after the treatment representing some swelling but overall negligible amounts (less than 5%).

Burger Model Fit

Fluid structure interactions make it nearly impossible to determine the exact shear stresses acting on the biofilm structure. Without knowing the shear stress acting on the structure, constitutive parameters to the Burger model cannot be evaluated, however

changes in the parameters before treatment and after treatment can be determined. To do this we must set up the creep compliance of a viscoelastic material:

$$D(t) = \frac{\varepsilon}{\tau_o} = \frac{1}{E_1} + \frac{t}{\eta_1} + \frac{1}{E_2}\left(1 - e^{\frac{-E_2 t}{\eta_2}}\right) \quad (23)$$

This states that the creep compliance D(t) is a function of the Burger model elements which were used to compare treatment creep compliances for both before, $D(t)_{pre}$ and after, $D(t)_{post}$. Assuming that the shear stresses are nearly the same on a particular cluster the ratio of $D(t)_{pre}$/ $D(t)_{post}$ does not depend on a calculated shear stress. Assuming that the initial position of each tracking point on the biofilm is relatively at the same point both before and after treatments the strain for $D(t)_{pre}$/ $D(t)_{post}$ reduces to the changes in length with time. Thus we can say that there is change in the Burger model parameters before and after treatment or for each treatment there is an E_{1post}/E_{1pre}, E_{2post}/E_{2pre}, η_{1post}/η_{1pre}, and η_{2post}/η_{2pre}. Thus a non-dimensional comparison of linearly elastic Burger model parameters can be obtained.

To find the four Burger model parameters that best fit the data a MATLAB program was created. The program finds the minimum of a scalar function of several variables, starting at an initial estimate, and is generally referred to as unconstrained nonlinear optimization (MATLAB). The data fit was an average of all three trials of displacement magnitudes. This averaging was done to minimize the discrepancies associated with fluid structure interactions. Curves were fit to the elongation or creep of the biofilm then parameters were compared with the after treatment parameters to obtain

the dimensionless E_{1post}/E_{1pre}, E_{2post}/E_{2pre}, η_{1post}/η_{1pre}, and η_{2post}/η_{2pre}. Again these are not true Burger model parameters but rather they are changes in parameters from treatments.

The E_{1post}/E_{1pre}, E_{2post}/E_{2pre}, η_{1post}/η_{1pre}, and η_{2post}/η_{2pre} are the changes from pre-treatment to post-treatment. The E_{1post}/E_{1pre}, E_{2post}/E_{2pre}, η_{1post}/η_{1pre}, and η_{2post}/η_{2pre} were found from an average of all the displacement vectors which were normalized to the largest displacement of the pre-treatment trial. Each chart and corresponding table contain the plot of normalized average displacements with Burger model fit and the average dimensionless E_{1post}/E_{1pre}, E_{2post}/E_{2pre}, η_{1post}/η_{1pre}, and η_{2post}/η_{2pre} for each treatment.

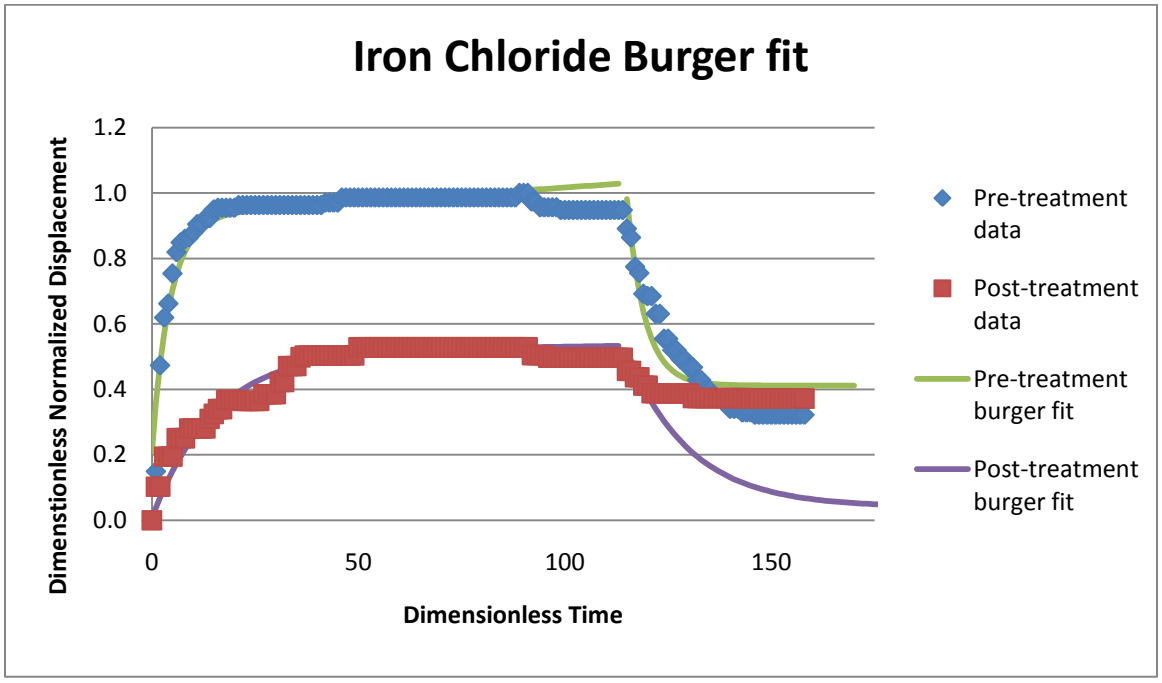

Figure 43) Iron chloride average Burger model fit for three trials

Table 8) Iron chloride treatment change in Burger model parameters

E_{1post}/E_{1pre}	E_{2post}/E_{2pre}	η_{1post}/η_{1pre}	η_{2post}/η_{2pre}
0.48	1.14	5.82	4.89

The iron chloride has a stiffening effect on the biofilm which is seen in the videos and data. The model shows that the post-treatment is stiffer then the pre-treatment in Figure 43. In Table 8 the changes in Burger model parameters is shown. $E_{2post}/E_{2pre,}$ η_{1post}/η_{1pre}, and η_{2post}/η_{2pre} are greater than one so there is a decrease in parameter value from pre to post-treatment.

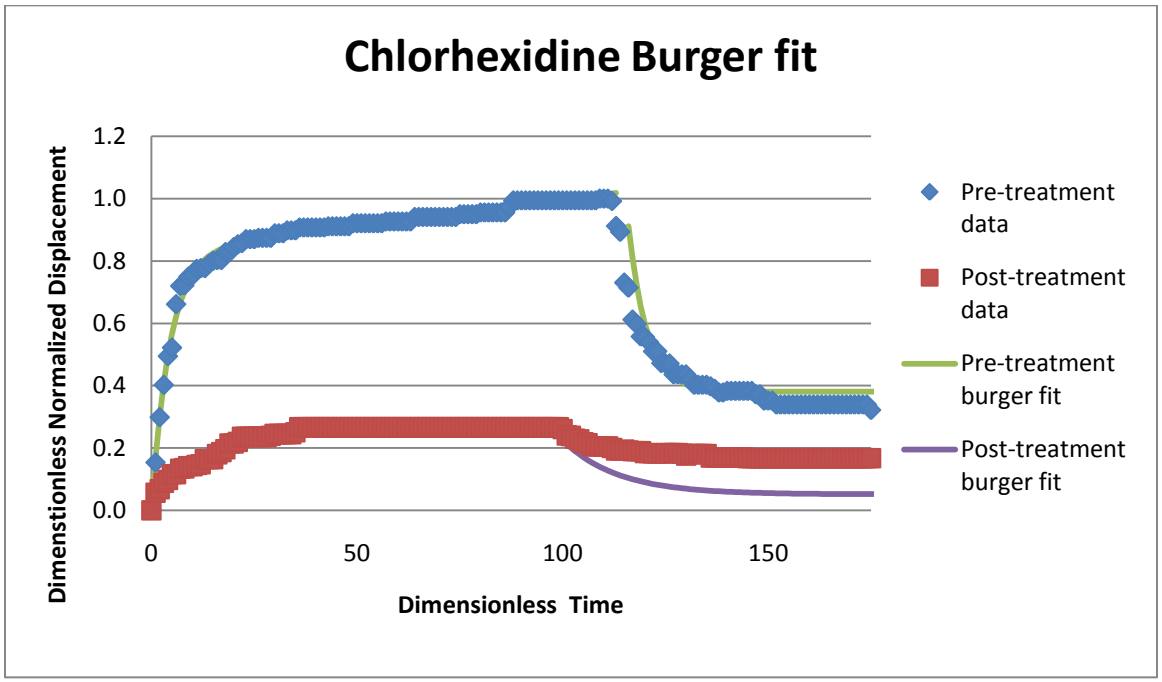

Figure 44) Chlorhexidine average Burger model fit for three trials

Table 9) Chlorhexidine treatment change in Burger model parameters

E_{1post}/E_{1pre}	E_{2post}/E_{2pre}	η_{1post}/η_{1pre}	η_{2post}/η_{2pre}
0.14	3.51	17.15	10.35

The chlorhexidine has a stiffening effect on the biofilm which is seen in the videos and data. The model shows that the post-treatment is stiffer then the pre-treatment in Figure 44. In Table 9 the changes in Burger model parameters is shown. $E_{2post}/E_{2pre,}$ η_{1post}/η_{1pre}, and η_{2post}/η_{2pre} are greater than one so there is a decrease in parameter value from pre to post-treatment.

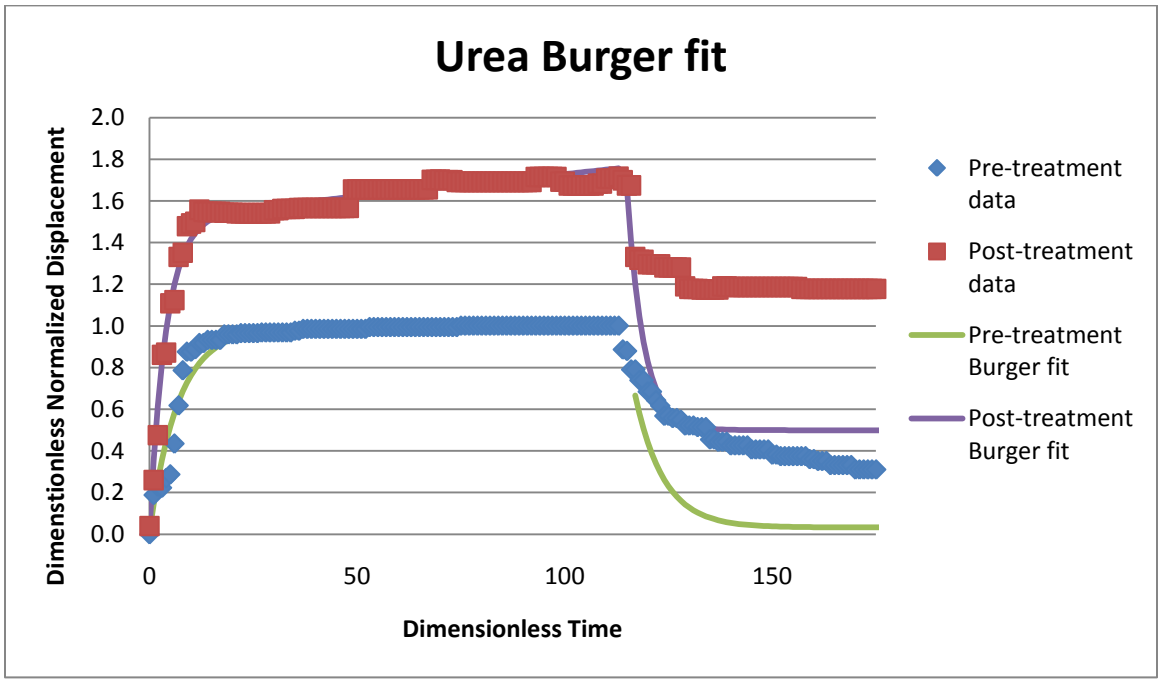

Figure 45) Urea average Burger model fit for three trials

Table 10) Urea treatment change in Burger model parameters

E_{1post}/E_{1pre}	E_{2post}/E_{2pre}	η_{1post}/η_{1pre}	η_{2post}/η_{2pre}
0.56	0.65	0.05	0.38

The urea has a softening effect on the biofilm which is seen in the videos and data. The model shows that the post-treatment is more viscous then the pre-treatment Figure 45. In Table 10 the changes in Burger model parameters is shown. E_{1post}/E_{1pre} is less than one so there is a decrease in parameter value from pre to post-treatment.

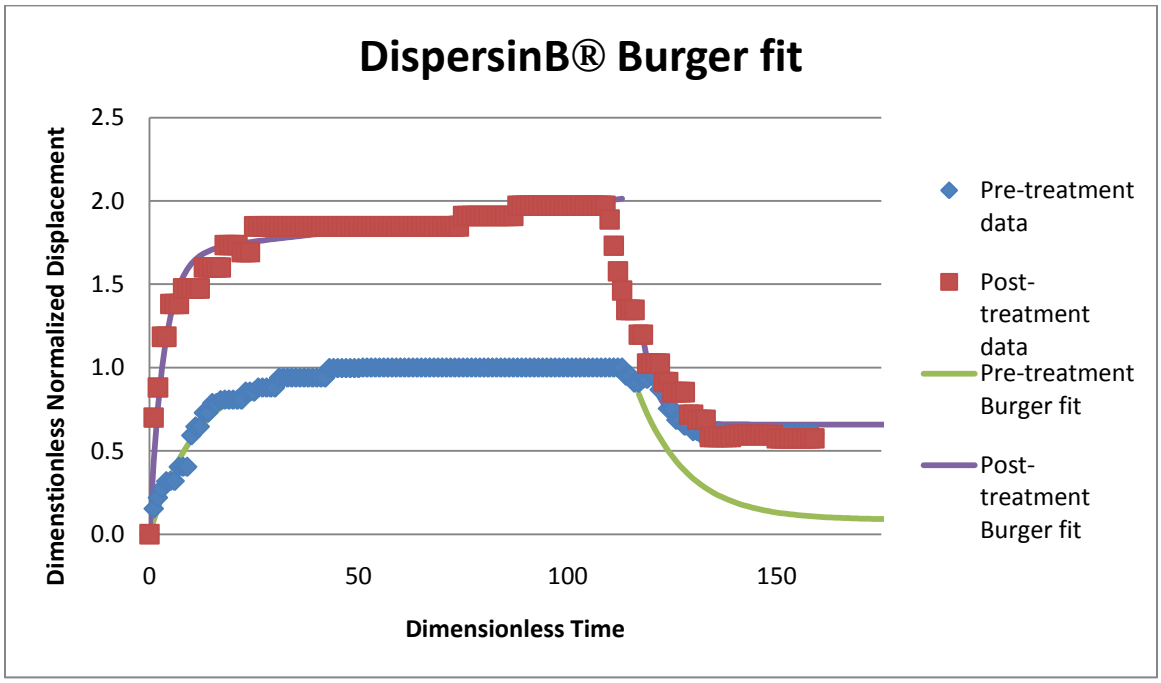

Figure 46) DispersinB ® average Burger model fit for three trials

Table 11) DispersinB ® treatment change in Burger model parameters

E_{1post}/E_{1pre}	E_{2post}/E_{2pre}	η_{1post}/η_{1pre}	η_{2post}/η_{2pre}
0.51	0.58	0.13	0.17

The DispersinB® has a softening effect on the biofilm which is seen in the videos and data. The model also shows this softening effect in Figure 46. Much like the urea treatment, the DispersinB® treatment has E_{1post}/E_{1pre} that is less than one so there is a decrease in parameter value from pre to post-treatment shown in Table 11.

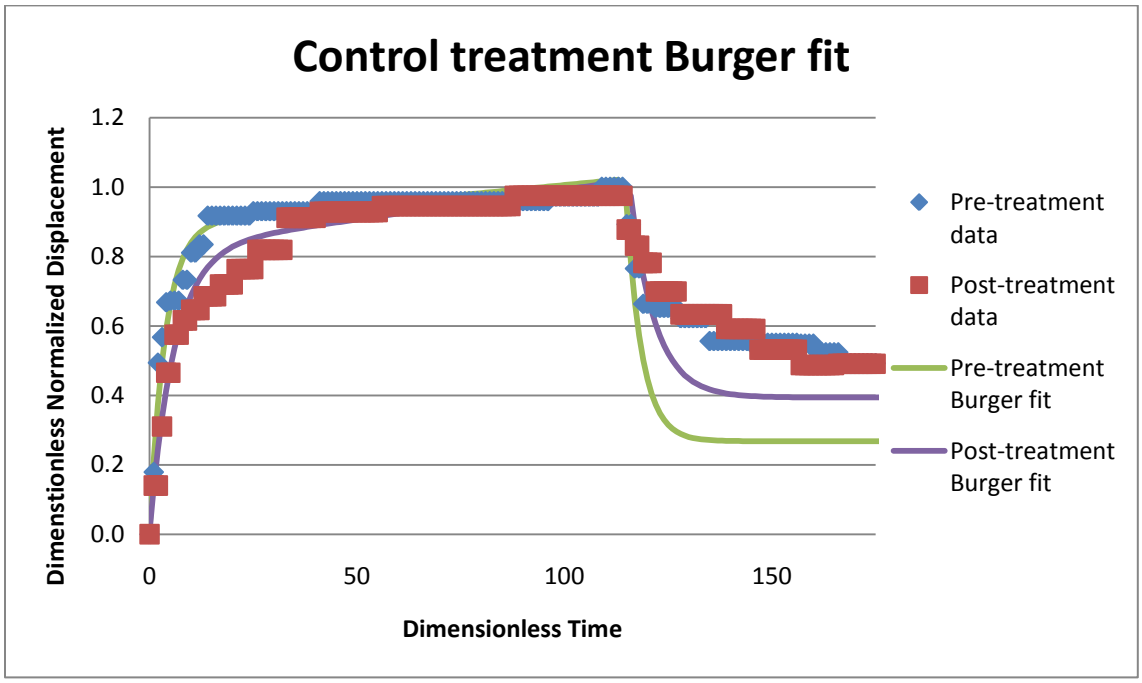

Figure 47) Control treatment average Burger model fit for three trials

Table 12) Control treatment change in Burger model parameters

E_{1post}/E_{1pre}	E_{2post}/E_{2pre}	η_{1post}/η_{1pre}	η_{2post}/η_{2pre}
0.91	1.09	0.68	1.71

The control treatment shows displacement curves similar to the results seen with experimental data shown in Figure 47. Notice that in Table 12, there is little change in the Burger model parameters from pre-treatment to post-treatment.

Discussion

One problem with this experiment is that repeatability between trials of the same treatment was difficult to maintain. The main cause of this lack of replication between trials was a result of the large variability in biological systems, which has been common in previous studies (Table 1). The repeatability discrepancies can be seen in Table 13, which contains results from each of the trials conducted.

Table 13) Results from all treatments and trials for %recovery before and after treatment along with post-treatment max deformation (greater than 100% represents more displacement then pre-treated biofilm)

Iron Chloride Treatment		% Recovery Pre-treatment	% Recovery Post-treatment	Post-treatment max deformation (as % of pre-treatment)
	Trial#1	22.7	15.3	42.2
	Trial #2	74.6	0.0	45.7
	Trial #3	53.7	36.1	128.1
	Average ±SD	**50.4**±26	**17.2**±18	**72.0**±48
Chlorhexidine Treatment		% Recovery Pre-treatment	% Recovery Post-treatment	Post-treatment max deformation (as % of pre-treatment)
	Trial#1	85.3	60.4	38.7
	Trial #2	63.3	12.9	17.5
	Trial #3	48.4	23.6	75.7
	Average ±SD	**65.7**±19	**32.3**±25	**44.1**±29
Urea Treatment		% Recovery Pre-treatment	% Recovery Post-treatment	Post-treatment max deformation (as % of pre-treatment)
	Trial#1	68.5	10.2	209.2
	Trial #2	53.9	71.4	479.3
	Trial #3	69.8	0.0	734.0
	Average ±SD	**64.1**±9	**27.2**±38	**474.1**±262
DispersinB® Treatment		% Recovery Pre-treatment	% Recovery Post-treatment	Post-treatment max deformation (as % of pre-treatment)
	Trial#1	27.9	26.6	1029.0
	Trial #2	31.3	21.4	106.6
	Trial #3	53.6	0.0	488.1
	Average ±SD	**37.6**±14	**16.0**±14	**541.3**±463
Control Treatment		% Recovery Pre-treatment	% Recovery Post-treatment	Post-treatment max deformation (as % of pre-treatment)
	Trial#1	60.8	51.6	91.7
	Trial #2	57.8	12.3	121.0
	Trial #3	63.2	69.9	72.9
	Average ±SD	**60.6**±2	**44.6**±29	**95.4**±25

It is important to remember that this experiment is measuring displacement of the biofilm structure. Although every effort was made to ensure that biofilms of similar size and geometry were utilized, the inherent geometric differences will also contribute to the

scatter of this data. Although there were large variations in data between trials, trends between treatments remained the same. Notice for iron chloride and chlorhexidine that the post-treatment max deformation was consistently below 100% which shows that these post-treatment biofilms consistently displaced less than their pre-treatment counter parts. The opposite is true for the urea and DispersinB® which always displaced more than the pre-treatment counterpart and substantially more than the control trial.

Failure events during the pre and post-treatment trials can be seen during the percent area of biomass as discussed earlier. Graphical results can be found in Appendix A. Trends are shown by monitoring changes in area during the pre-treatment flush, treatment soak and post-treatment flush displayed in Table 14.

Table 14) Percent biomass area loss during 15 second pre and post-treatment fluid shear and during treatment soak (negative numbers correspond to increases in area)

Iron Chloride Treatment		% Loss During Pre-treatment	% Loss During Post-treatment	%Loss During Treatment
	Trial#1	7.4	2.7	8.9
	Trial #2	1.3	10.9	9.6
	Trial #3	6.1	-0.1	6.4
	Average ±SD	**4.9**±3.2	**4.4**±5.7	**8.3**±1.7
Chlorhexidine Treatment		% Loss During Pre-treatment	% Loss During Post-treatment	%Loss During Treatment
	Trial#1	-3.1	0.4	14.0
	Trial #2	-0.2	0.5	-6.4
	Trial #3	-0.6	6.0	-70.8
	Average ±SD	**-1.3**±1.6	**2.3**±3.2	**-21.1**±44
Urea Treatment		% Loss During Pre-treatment	% Loss During Post-treatment	%Loss During Treatment
	Trial#1	1.3	70.7	-58.8
	Trial #2	-0.5	62.0	-48.1
	Trial #3	14.4	81.4	-53.5
	Average ±SD	**5.1**±8.1	**71.4**±9.7	**-53.4**±5.3
DispersinB® Treatment		% Loss During Pre-treatment	% Loss During Post-treatment	%Loss During Treatment
	Trial#1	-0.4	24.3	14.2
	Trial #2	-10.0	56.2	28.5
	Trial #3	-4.9	38.9	25.5
	Average ±SD	**-5.1**±4.7	**39.8**±15	**22.7**±7.5
Control Treatment		% Loss During Pre-treatment	% Loss During Post-treatment	%Loss During Treatment
	Trial#1	1.0	2.7	-2.3
	Trial #2	-0.9	0.5	-3.1
	Trial #3	6.9	-0.1	0.9
	Average ±SD	**2.3**±4.1	**1.0**±1.5	**-1.5**±2.1

The percent biomass area loss data has large standard deviations between trials but there are general trends from the various treatments. Iron chloride has about the loss of area during the post-treatment fluid shear and the pre-treatment fluid shear representing few failure events. The chlorhexidine has little loss during the post-treatment flush corresponding with few failure events. The chlorhexidine also has a phenomenon during the treatment period which shows a negative loss during treatment. Chlorhexidine

typically contracts the biofilm into a smaller volume but during Trial #3 (see Appendix A) much of the thin translucent biofilm condensed and gave the appearance that more biofilm was in the capillary than before.

Both the Urea and DispersinB® show large amounts of post-treatment fluid shear loss, which correlates to more failure events caused by weaker bonding. The urea also had a negative loss during the treatment, which is a gain in biomass area. This gain is due to the dispersion of cells from the cluster associated with cells drifting without a strong EPS matrix to hold them together. Notice in all the graphs for urea biomass area with time (Figure 32) there was large removal when the post-treatment shear was applied. This large removal event was also associated with the DispersinB® treatment (Figure 37).

The slope found from the first several points when the fluid shear is initiated gives insight to the instantaneous elastic composition of the biofilm, mainly E_1 of the Burger model. Results are found in Table 15:

Table 15) Instantaneous elastic slope comparison for post-treatment/pre-treatment

Instantaneous elastic slope comparison (Post/Pre)					
	Iron Chloride	**Chlorhexidine**	**Urea**	**DispersinB®**	**Control**
Trial #1	0.36	0.09	4.06	12.1	0.70
Trial #2	0.19	0.17	2.07	2.2	0.27
Trial #3	0.21	0.87	6.92	1.4	0.46
Average ±SD	0.25±0.1	0.38±0.42	4.35±2.4	5.25±6.0	0.44±0.2

Notice that both the iron chloride and chlorhexidine have values less than one which implies that the post treatment is stiffer then the pre-treatment. This is also true, to a lesser extent, for the control which implies there was some amount of strain hardening occurring during the initial pre-treatment fluid shear. Both the urea and DispersinB®

show an increase in post treatment instantaneous elastic slope which implies they become less elastic.

Using displacement results from the capillary flow cell experiment, changes in the four Burger model parameters were calculated which are shown in Table 16:

Table 16) Summary of changes in Burger model parameters for various treatments

Calculated Burger model parameter comparison (post/pre)					
	Iron Chloride	**Chlorhexidine**	**Urea**	**DispersinB®**	**Control**
E_{1post}/E_{1pre}	0.48	0.14	0.56	0.51	0.91
E_{2post}/E_{2pre}	1.14	3.51	0.65	0.58	1.09
η_{1post}/η_{1pre}	5.82	17.15	0.05	0.13	0.68
η_{2post}/η_{2pre}	4.89	10.35	0.38	0.17	1.71

In general, the iron chloride and chlorhexidine showed to stiffen the biofilm or alter E_1 and E_2, while decreasing the viscous parameters, η_1 and η_2. Urea and DispersinB® showed a softening of the biofilm creating a viscously dominated biofilm. This correlates to the large change in the η parameters for these two treatments. Notice in Table 16 that compared to the control there is a significant change in both η_{1post}/η_{1pre} and $\eta_{2post}/\eta_{2pre.}$ This large change in the viscous parameters shows what effect these treatments have on the model. Both the iron chloride and chlorhexidine have large increases in η parameters which correspond to an increase in viscosity which would relate to a stiffer biofilm. The urea and DispersinB® have a large decrease in η parameters or decrease in viscosity elements which lead to a softer more fluid like biofilm.

As discussed in the Burger model section there was typically seen a divergence in displacements from the Burger model to that of the actual data collected after the stress was removed. One explanation to this divergence could be due to the syringe pump being

incapable of a complete, instantaneous stop. Another possibility is the pressure in the silicone tubing causing expansion, ultimately acting like a bladder or a balloon. This slow shut-down of fluid shear leads to a more gradual instantaneous relaxation curve. A third possible reason for this change in relaxation creep is from permanent plastic deformation.

$$\varepsilon^T = \varepsilon^P + \varepsilon^V \qquad (24)$$

Total strain (ε^T) in a material is the addition of both the plastic strain (ε^P) and the viscoelastic strain (ε^v). The Burger model cannot capture irreversible plastic strain. A recommendation for further mathematical models is to add a plastic slider element in series with the Burger model.

One variable that must be mentioned that alters the true change in mechanical properties is that of volumetric changes in the biofilm cluster from pre to post-treatment. The change in Burger model parameters is valid if the same fluid shear forces are applied to a biofilm cluster before and after treatment. The flow rate was controlled precisely but alterations in the biofilm volume could not be held constant. In the average iron chloride had about an 8% reduction in biomass area from when the treatment was applied to the end of the fifteen minute soak period (Table 14). For example a sphere that has 8% reduction in cross-sectional area would have close to a 12% change in volume. This volumetric change affects the hydrodynamics on the biofilm cluster and alters the amount of stress applied to the cluster. Although there was some variability with cross-sectional area changes, the overall effect was minimal compared to the magnitude of change in mechanical properties derived.

Recommendations for Future Work

The flow cell work investigated the mechanical response and properties of the biofilm under a combination of mechanical stresses and chemical treatment. Typically in industrial settings biofilm control is usually maintained by one or both of these techniques. Future work of biofilm mechanics could involve examining properties over an extended period of time with a chemical treatment.

To illustrate additional mechanical removal coupled with chemical treatment one experiment was run in the capillary flow cell. *S. epidermidis* was grown for twenty four hours on ten percent tryptic soy broth until a mature biofilm developed. The growth flow rate was again 1 mL/min. Next, an extended time treatment was applied to the biofilm as 0.1 molar concentration urea was pumped through the capillary with a flow rate of 10mL/min (10x the growth conditions) for one hour. The result was a dramatic increase in biofilm removal due to the high combination of mechanical shear stress and chemical treatment.

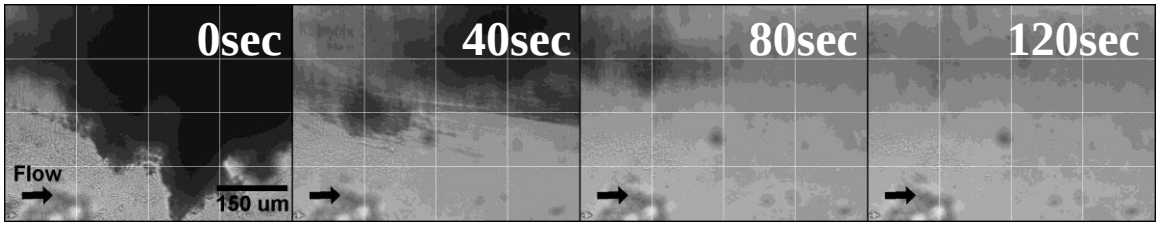

Figure 48) Time lapse of *S. epidermidis* removal using increased fluid shear and 0.1 molar urea treatment (each picture has 40sec separation)

The initial biofilm cluster before fluid shear was initiated is shown in Figure 48 of the time lapse imaging. Each frame represents forty seconds of increased fluid shear and urea treatment. Most of the biofilm is removed within the first few minutes of treatment.

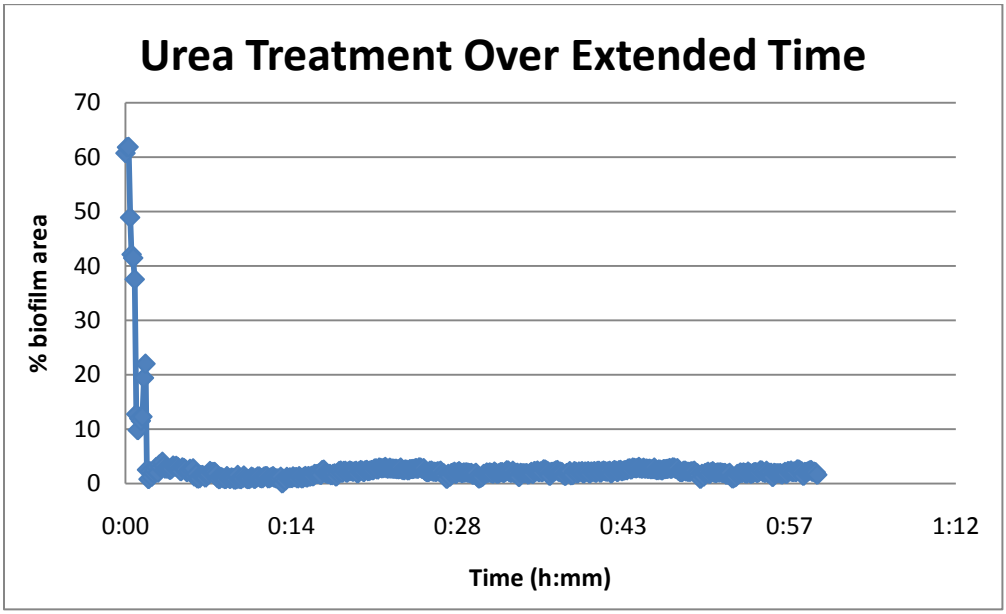

Figure 49) Percent area of biomass with time for the extended urea treatment

Notice that, in Figure 49, most of the removal occurs during the first five minutes of treatment and fluid shear stress. This experiment could be altered to discover which treatments and what fluid shear rates work best for a particular biofilm. This could also be performed as optimization of shear stress and chemical treatment capabilities.

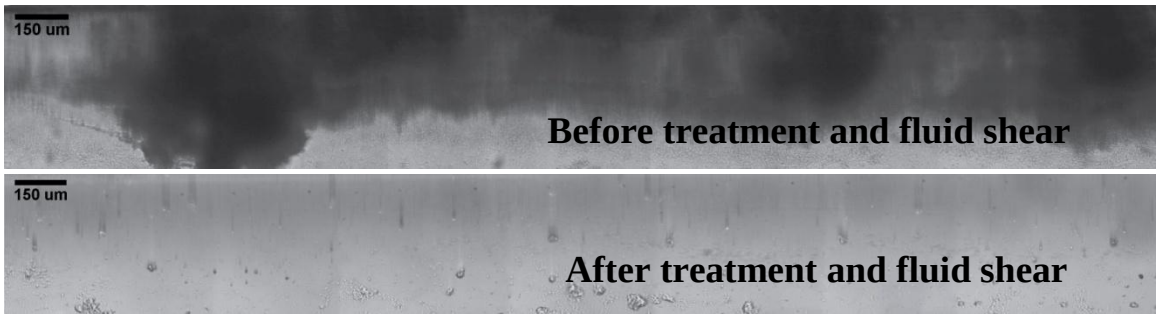

Figure 50) *S. epidermidis* biofilm pictured along the length of the capillary flow cell reactor before and after induced with fluid shear and 0.1 molar urea treatment

Figure 50 is the same section panorama of the glass capillary flow cell reactor before and after the urea and fluid shear treatment. Notice in the after treatment and fluid shear there are no large biofilm masses along the side of the capillary. Most of the specks in the after treatment picture are from dust on the outside of the tube that is making dark areas in the image.

This experiment shows that there are many possibilities to biofilm removal with a combined mechanical force and chemical treatment. Granted there was a large increase in fluid shear from the growth conditions and a large chemical treatment but that was done to illustrate the dramatic removal of biofilm along the capillary.

METHOD 2: ATOMIC FORCE MICROSCOPY MICRO INDENTATION

An atomic force microscope (AFM) in an imaging mode works by scanning a sharp tip over a surface while simultaneously recording deflection of the tip. The deflection time course is then converted into an image of the surface profile (Binnig, Quate and Gerber 1986). To obtain the mechanical properties of a material surface one can use the AFM tip to exert precisely controlled displacements in a selected location and record the corresponding sample forces. The limitation of this technique is that the manipulation can only occur through the accessible surface of the biofilm and cannot measure properties well inside the biofilm without an influence of boundary conditions (Janmey and Schmidt 2006).

Materials and Methods

The second experimental technique utilizes an atomic force microscope (AFM) to interrogate the biofilm structure and material properties through micro-indentation. Micro-indentation utilizes a tip of known geometry to indent the biofilm at the micrometer scale and generates a complex force-displacement measurement related to the mechanical properties of the biofilm. However, other factors can also influence the measured force-displacement relationship, such as geometry of the tip and biofilm, and indentation depth. The influence of these variations can be diminished by good experimental technique and repeated measurements.

An initial culture was started for inoculation using full strength TSB with *Staphylococcus epidermidis* (ATCC 35984). The *Staphylococcus epidermidis* inoculum incubated for 24hours on a shaker plate at 37^{o}C. The 24 hour culture was then used to inoculate a drip flow cell reactor (Bio Surface Technologies shown in Figure 51) placed in a horizontal position with 1ml of overnight culture and 9ml of full strength TSB in each well.

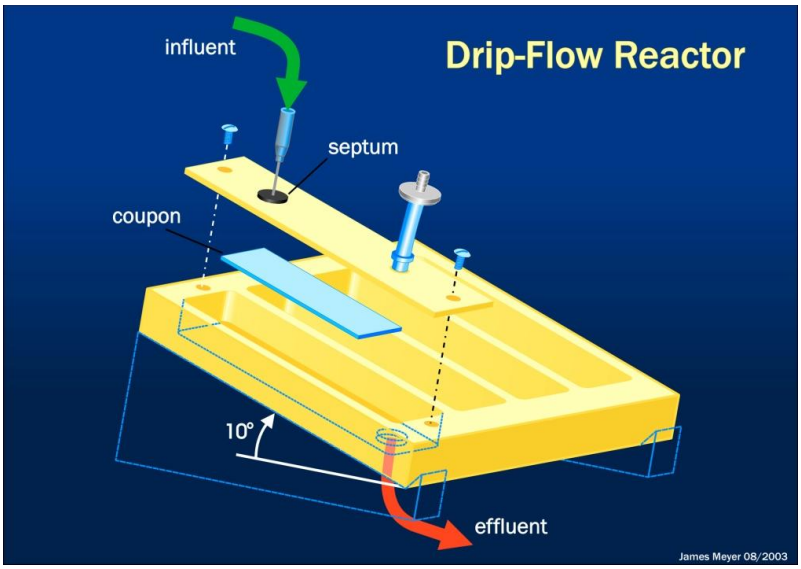

Figure 51) Drip flow reactor from Bio Surfaces Technologies influent nutrients run across inoculated coupon developing biofilm

A small piece of autoclave tape was placed on the metal slide in the drip flow reactor to support a 1 x 1 cm silicon wafer with a thin silicon dioxide surface shown in Figure 52.

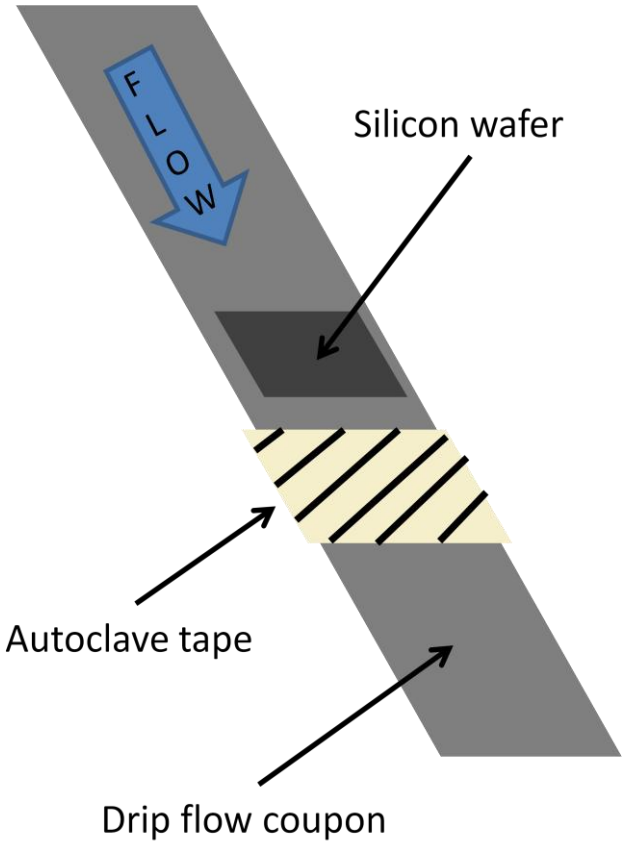

Figure 52) Drip flow reactor slide with silicon wafer for testing of biofilm in atomic force microscope

Two hours were allowed for attachment of cells, after which the inoculum bath was drained and the reactor was moved to an inclined position in which nutrient flow began. Nutrient flow consisted of 10 percent TSB dripped through each well at a flow rate of 1ml/min for 4 hours in an incubator set to 37^{o}C. Once a thin layer of biofilm had grown on the wafer it was removed and tested using a Veeco MultiMode PicoForce atomic force microscope in conjunction with diNanoScope Software version 7.0.

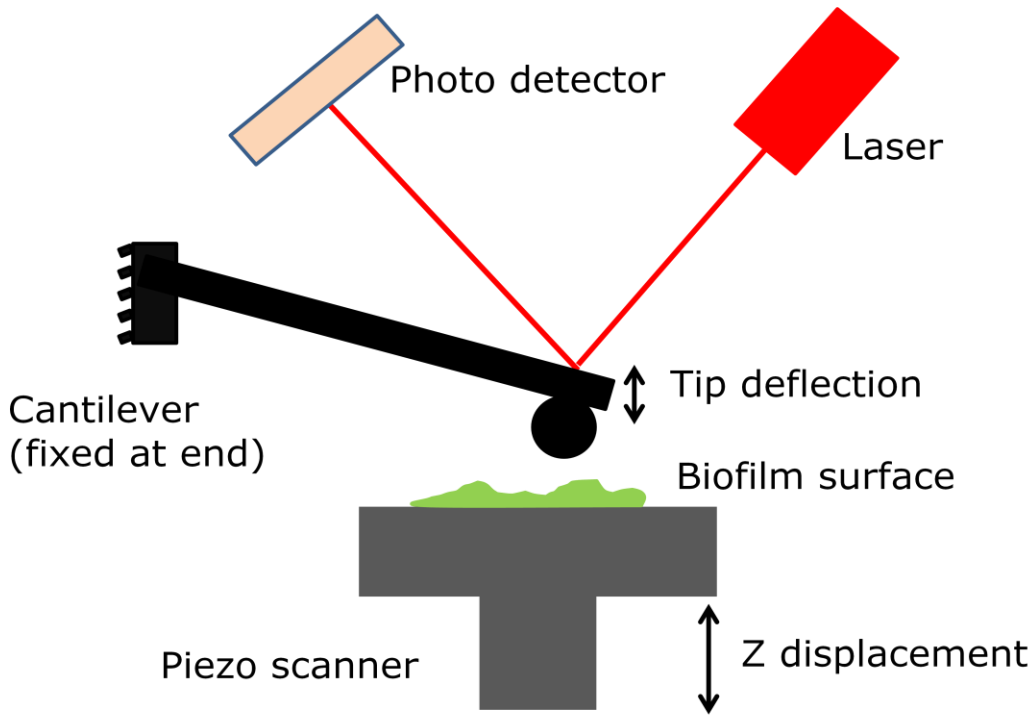

Figure 53) Basic components of AFM indentation

The basic function of the AFM is shown in the cartoon in Figure 53. A cantilever was fixed in space with a laser reflected off the tip to a photo sensing detector. The biofilm was placed on a piezoelectric scanner capable of moving with small, regulated increments on the nanometer scale. The biofilm was raised into the cantilever beam causing the beam to deflect. The deflection was measured by the change in position of the laser on the photo detector. The spring constant of the beam was used to calculate the amount of force exerted on the biofilm, allowing for force displacement curves to be generated.

The biofilm was tested at various loading rates using the micro cantilever beam with a 30um diameter glass sphere as the indenter. The loading rates covered of a range from 1μm/sec to 100μm/sec. The silicon wafer surface containing the biofilm was treated

and allowed to soak for 15 minutes. The same loading rates and indentation depths were then applied to the same point on the biofilm.

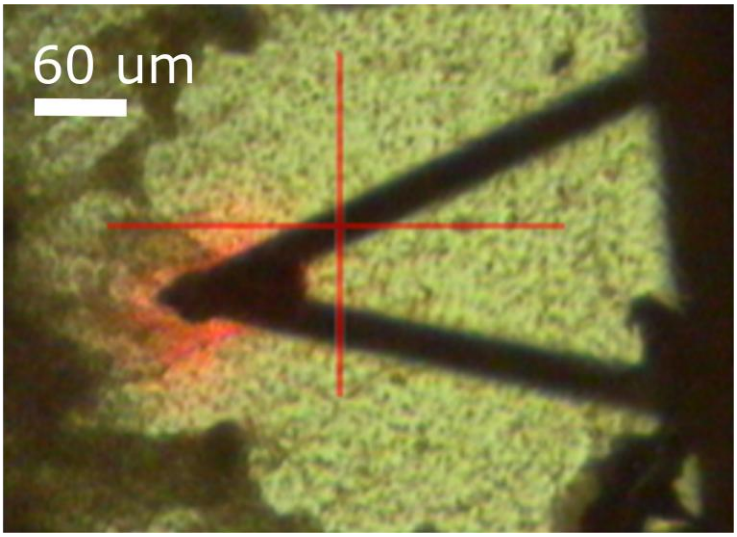

Figure 54) Picture of triangular cantilever beam with 30um spherical indentation tip

An image of one particular biofilm test looking down on the cantilever beam is shown in Figure 54. The darker areas are biofilm, and the small specks are individual cells or small groups of cells. At the end of the tip a 30 um spherical glass bead is attached as the indenter.

Each test was run at the same location of the biofilm. Testing the same spot before and after treatment is critical to comparing mechanical properties before and after a particular treatment. To accomplish this task, extra care was taken when adding the treatment not to disrupt the location of the cantilever beam or the silicon wafer which held the biofilm. Three trials for each treatment were conducted.

Indentation results were collected in the form of force displacement curves. A force displacement curve is generated by measuring the force on both the loading and the unloading of the biofilm structure. Sample force displacement curves are shown below in

Figure 55 for a purely elastic (no dissipation) material and a viscoelastic material. The shape of the curve explains much about the material properties of the testing material.

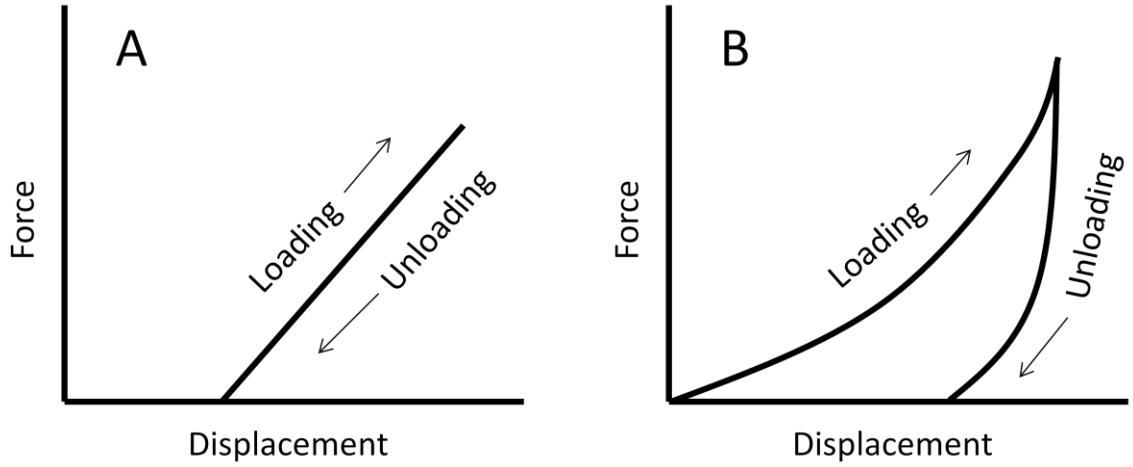

Figure 55) Sample force displacement curves for indentation test of A) elastic material and B) viscoelastic material

Results

The results for the indentation tests are broken down into the following five sections. These five sections consist of: 1) the untreated biofilm to show the viscoelastic nature of these materials, 2) iron chloride treatment, 3) chlorhexidine treatment, 4) the urea treatment, and 5) the DispersinB® treatment.

Untreated Biofilm Indentation

To show the viscoelastic nature of *S. epidermidis* biofilm, tests were conducted at various loading rates. These rates were 1μm/sec, 10μm/sec, and 97.7μm/sec. These variable loading rates are shown the Figure 56 below.

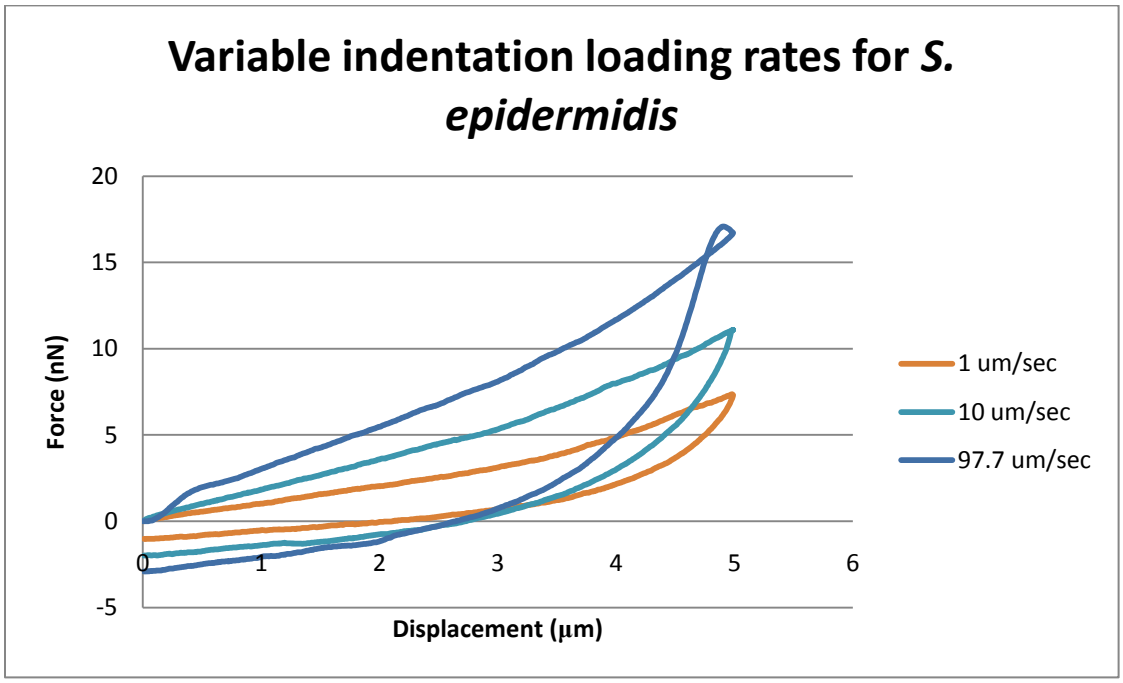

Figure 56) Variable indentation loading rates for *S. epidermidis* biofilm with atomic force microscopy

Each test is repeated on the same location of the biofilm as to avoid discontinuities associated with a rough surface. Notice that the higher the loading rates the larger force that is required to displace the indenter five microns into the surface of the biofilm. From the Burger model the larger the strain rate, the larger the elastic dominance of the material and conversely, the smaller the strain rate the more the viscous dominance of the material.

Another approach to showing the linear viscoelasticity of *S. epidermidis* biofilm was to plunge the indenter 5µm into the biofilm and hold it at that point for various time intervals. The hold allows for the biofilm to viscously deform around the indenter. Each trial was run at the same loading rate while varying the hold time.

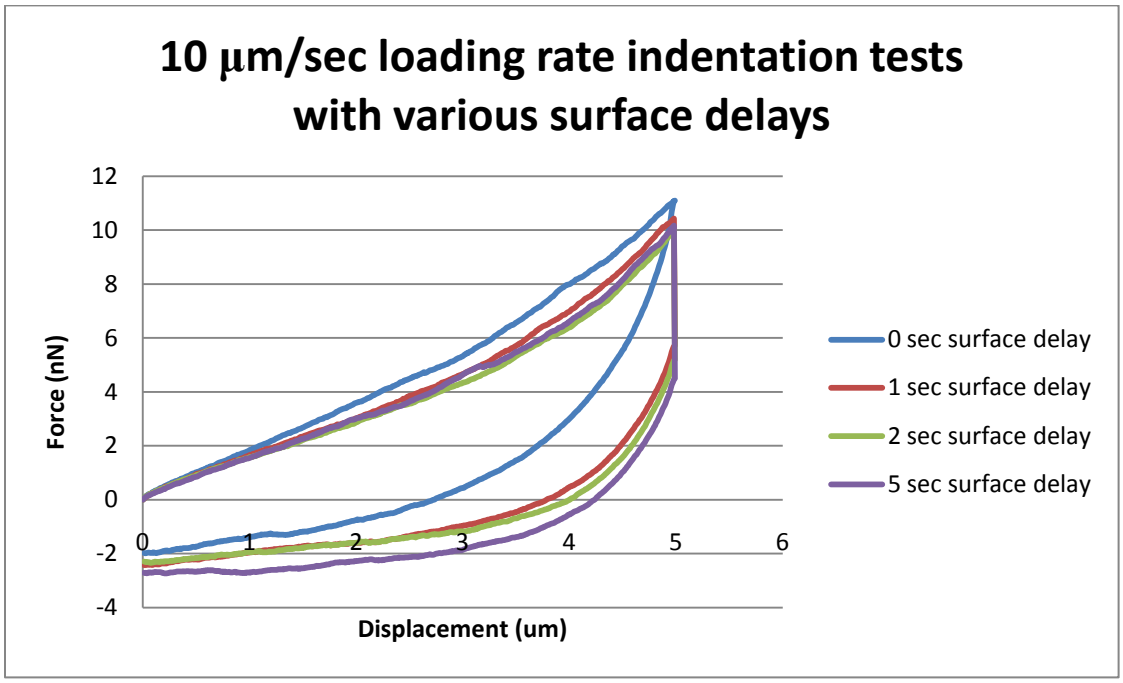

Figure 57) 10µm/sec loading rate indentation test for *S. epidermidis* biofilm with various surface delays

The force displacement curves for various indentation tests with a pause at peak loading are shown in Figure 57. The indenter travels 5µm into the surface of the biofilm and either returns immediately or holds for 1, 2, or 5 sec. Notice the loading curves are relatively similar for a specific spot on the biofilm surface. The unloading curves vary in magnitude due to viscous deformation relaxation in the biofilm while the indenter was in the biofilm surface.

For comparison, a blank silicon wafer was tested using the same soft cantilever beam used for the biofilm with the 30µm diameter sphere attached to the end. Each test was done with a varied rate or speed of indentation.

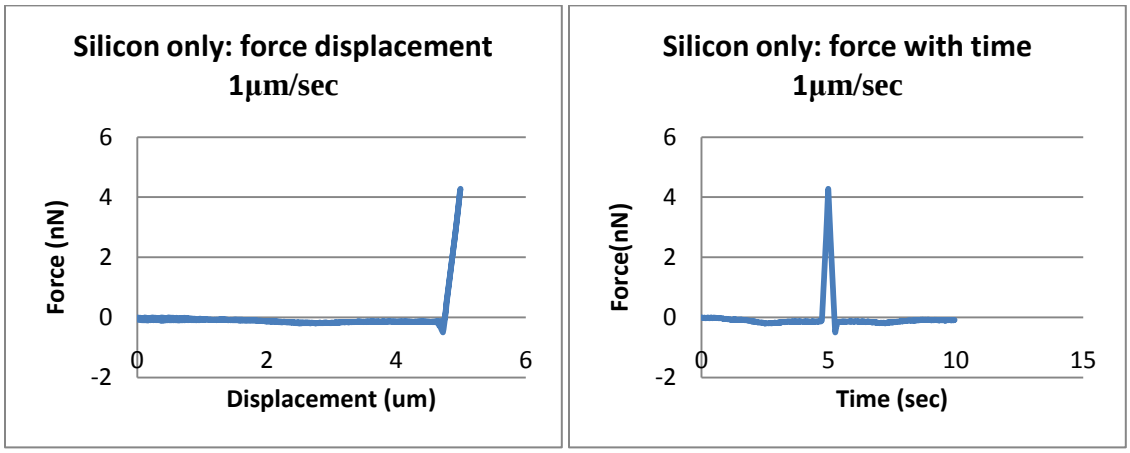

Figure 58) Silicon wafer without biofilm contamination for 1µm/sec indentation

Notice that in Figure 58 the loading and unloading follow the same curve for the empty silicon wafer condition. The slope of the line is the stiffness or the spring constant of the cantilever beam in bending. The silicon wafer is considered to be a perfectly rigid object when compared to the stiffness of the cantilever beam.

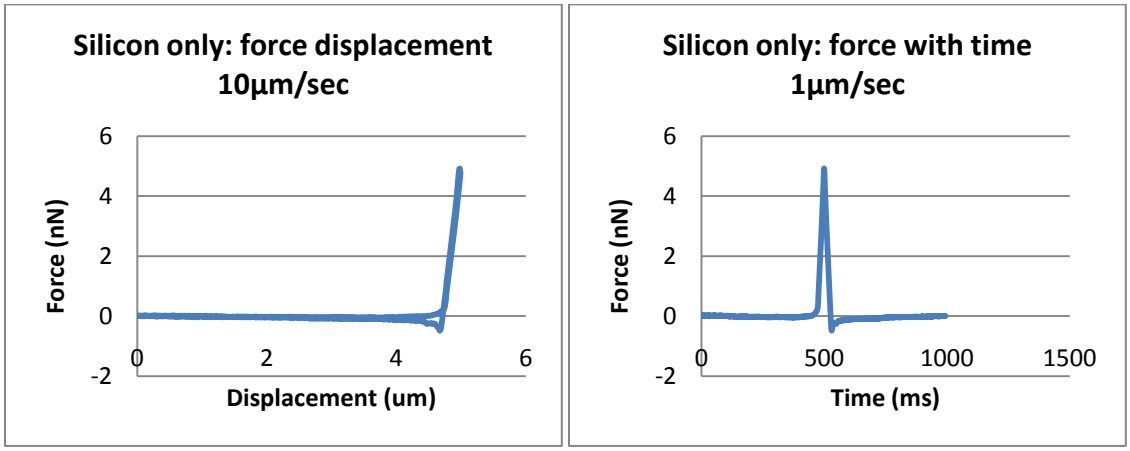

Figure 59) Silicon wafer without biofilm contamination for 10µm/sec indentation

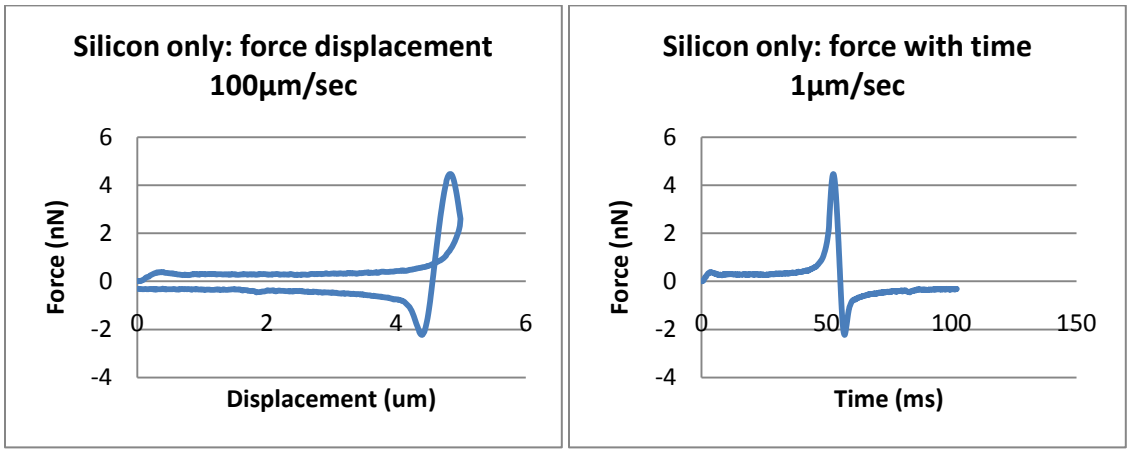

Figure 60) Silicon wafer without biofilm contamination for 100µm/sec indentation

Notice that for the higher rates (Figure 59 and Figure 60) there are inertial effects due to the large mass of the spherical tip attached to the end of the cantilever beam. This inertial effect on the blank slide is reduced in the biofilm samples because of the damping capabilities of the viscoelastic biofilm.

Iron Chloride Treatment

Iron chloride, $FeCl_2$, is thought to bind two negatively charged spots on the EPS matrix, which ultimately creates a cross-linked and stiffer biofilm. The following are force displacement curves and force time curves before and after $FeCl_2$ treatment. There are three sets of indentation rates consisting of 1µm/sec (Figure 61 and Figure 62), 10µm/sec (Figure 63 and Figure 64), and 100µm/sec (Figure 65 and Figure 66).

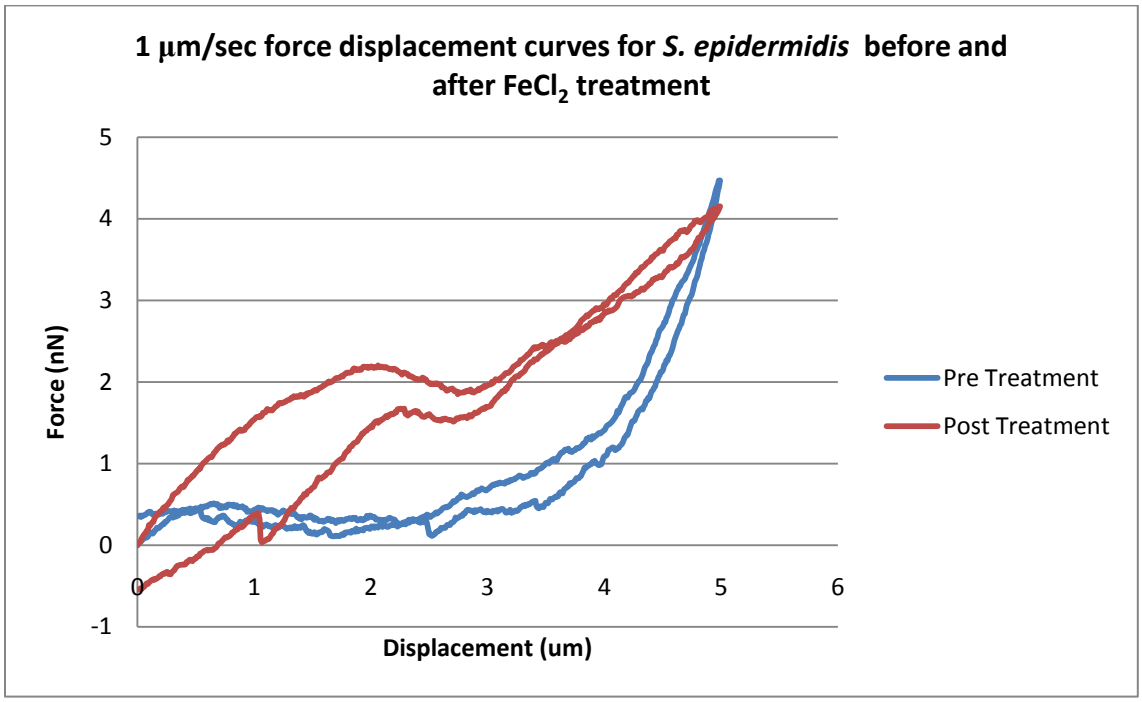

Figure 61) Force displacement curves for 1µm/sec loading rate for pre and post-treatment of iron chloride on *S. epidermidis* biofilm

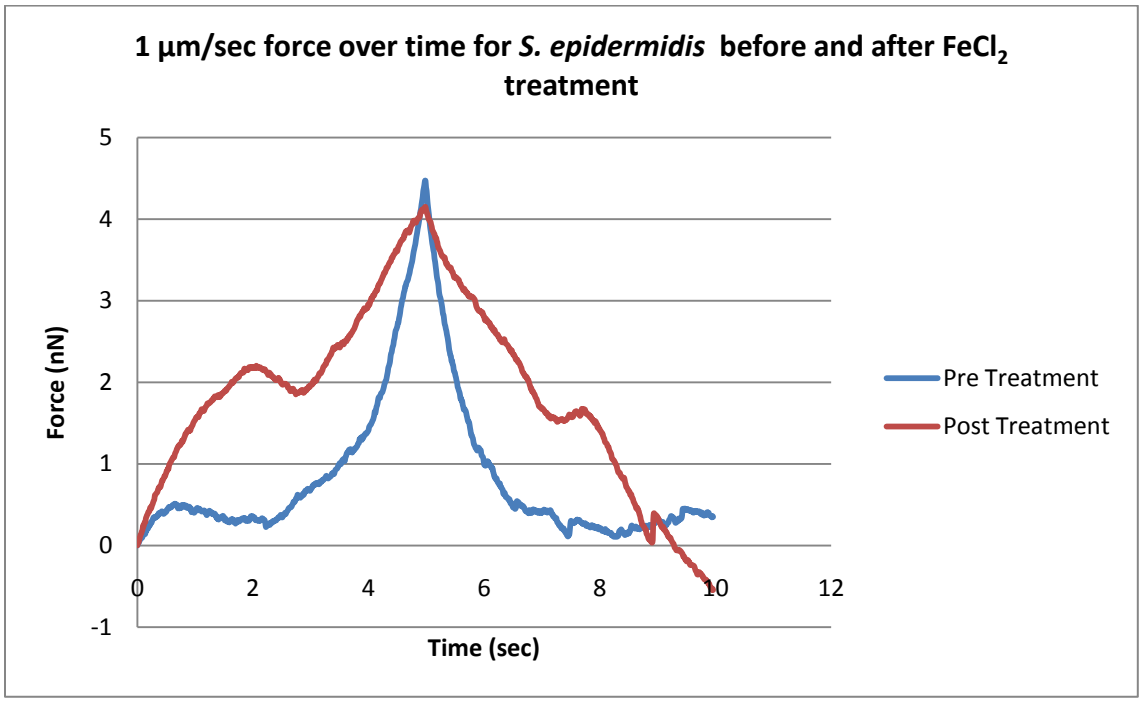

Figure 62) Force applied to *S. epidermidis* biofilm over loading time for pre and post-treatment of iron chloride using 1µm/sec loading rate

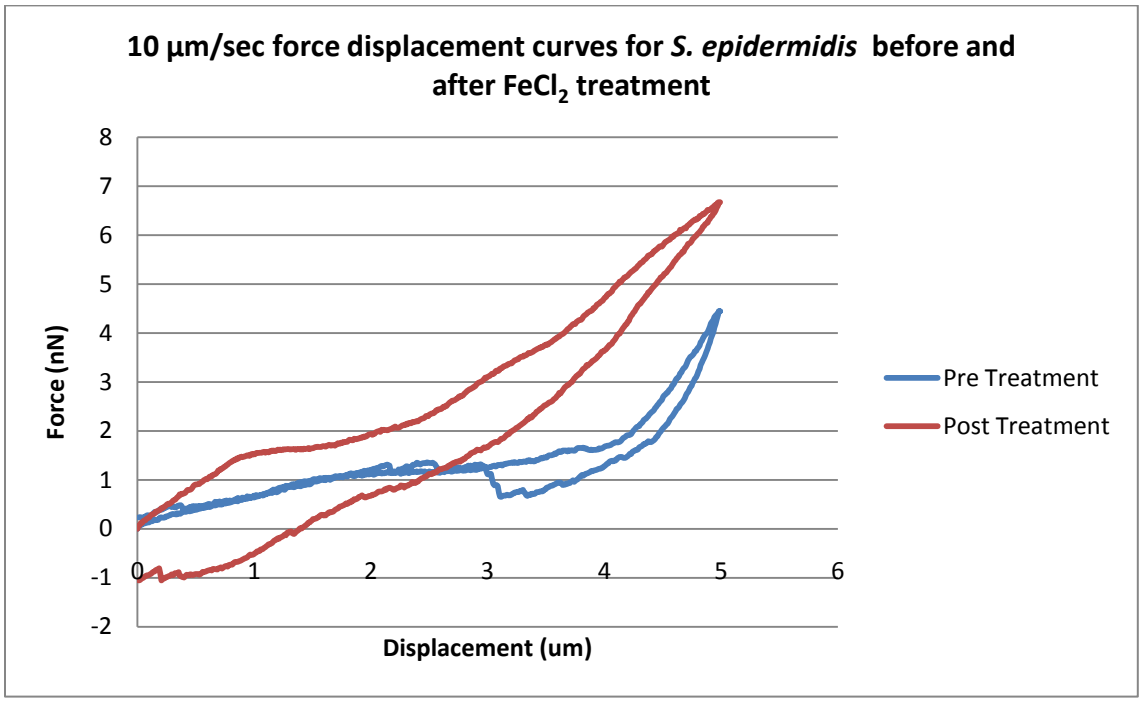

Figure 63) Force displacement curves for 10µm/sec loading rate for pre and post-treatment of iron chloride on *S. epidermidis* biofilm

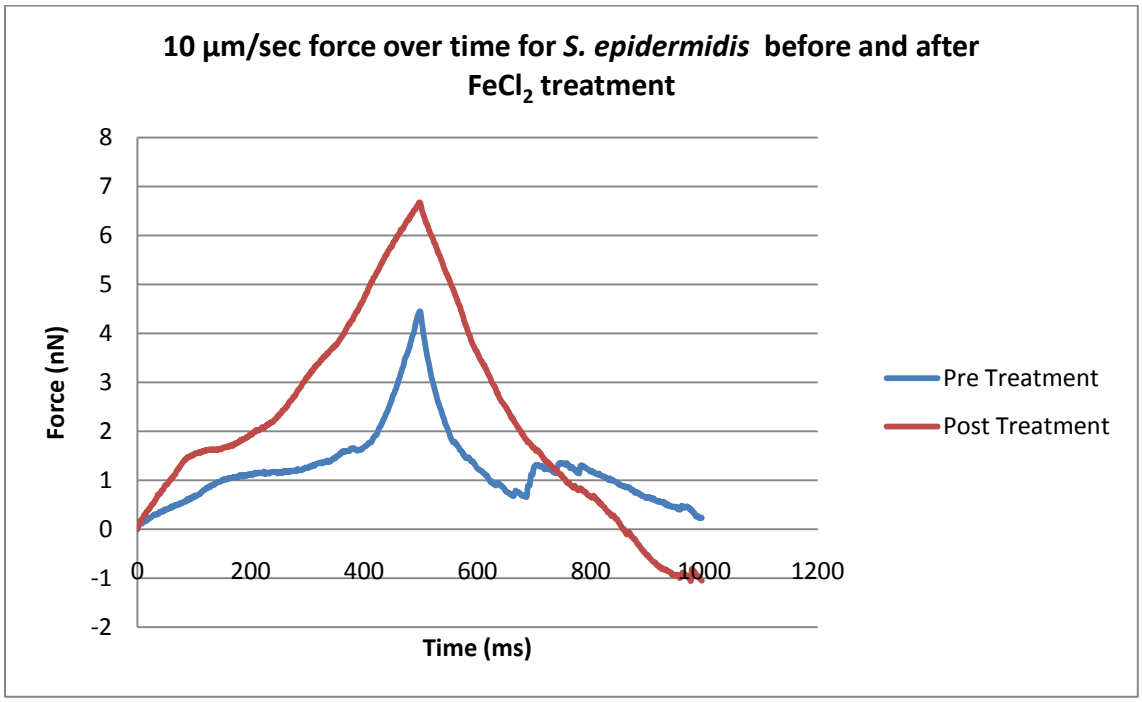

Figure 64) Force applied to *S. epidermidis* biofilm over loading time for pre and post-treatment of iron chloride using 10µm/sec loading rate

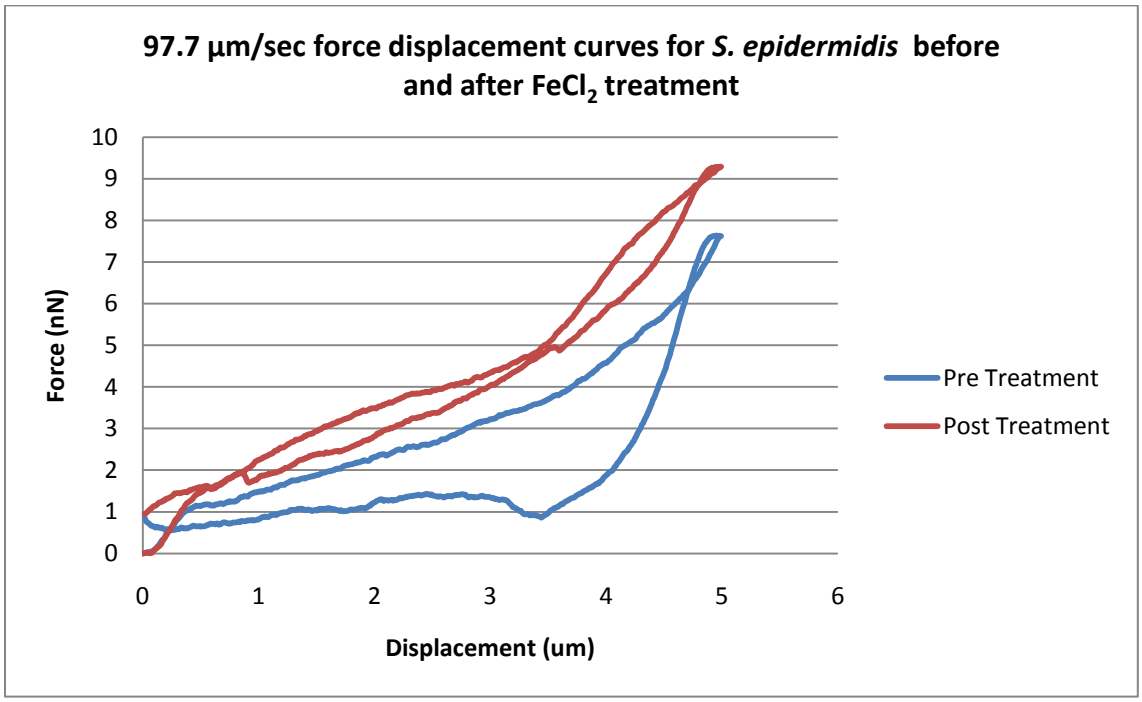

Figure 65) Force displacement curves for 97.7µm/sec loading rate for pre and post-treatment of iron chloride on *S. epidermidis* biofilm

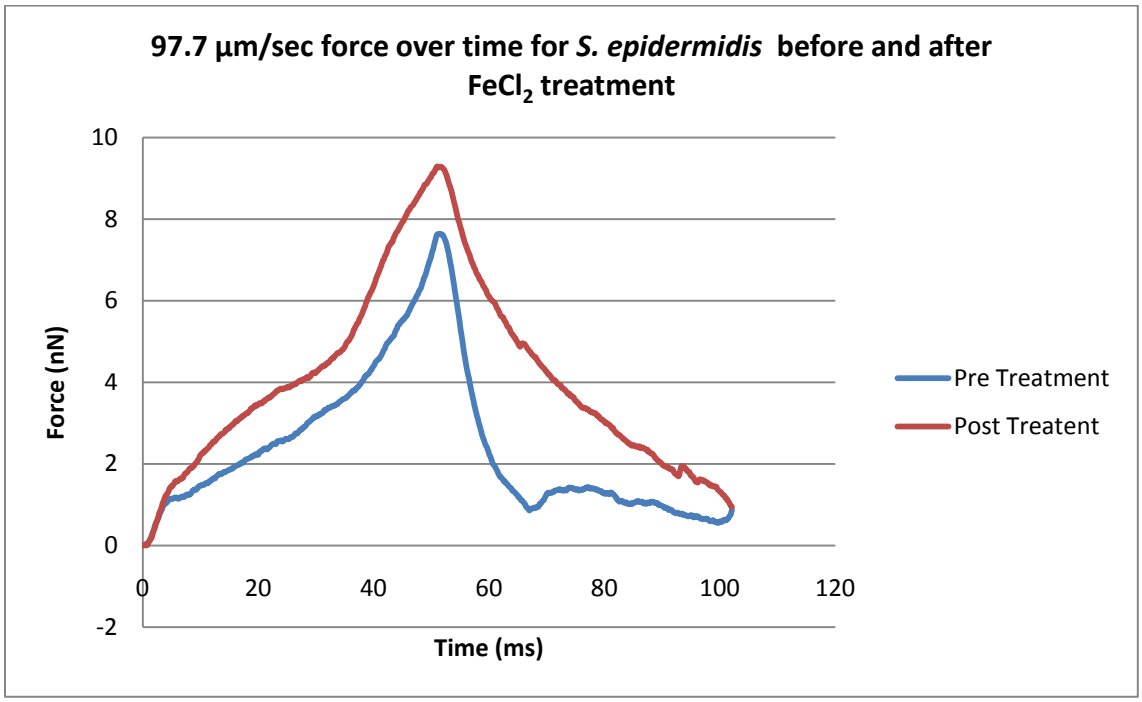

Figure 66) Force applied to *S. epidermidis* biofilm over loading time for pre and post-treatment of iron chloride using 97.7µm/sec loading rate

The iron chloride results show a stiffer post-treatment biofilm where the maximum force input is higher than that of its pre-treatment counterpart. This was most noticeable in Figure 63 under the 10μm/sec loading of the biofilm. The maximum force needed to obtain a 5μm displacement into the biofilm after the treatment is 2 ½ nN higher than the pre-treatment maximum force. The 1μm/sec test showed similar max loads for the pre and post-treated biofilm; however the non monotonic loading implies that an event occurred in the post-treatment trial to reduce the load, such as the biofilm buckling under the cantilever. Results from trials 2 and 3 can be found in Appendix B.

Chlorhexidine Treatment

Chlorhexidine a common chemical antiseptic used in contact lens solutions and mouthwash was used at a concentration of 0.1% in this study. The flow cell has shown chlorhexidine to stiffen biofilm. As before, there are three sets of indentation rates consisting of 1μm/sec (Figure 67 and Figure 68), 10μm/sec (Figure 69 and Figure 70), and 100μm/sec (Figure 71 and Figure).

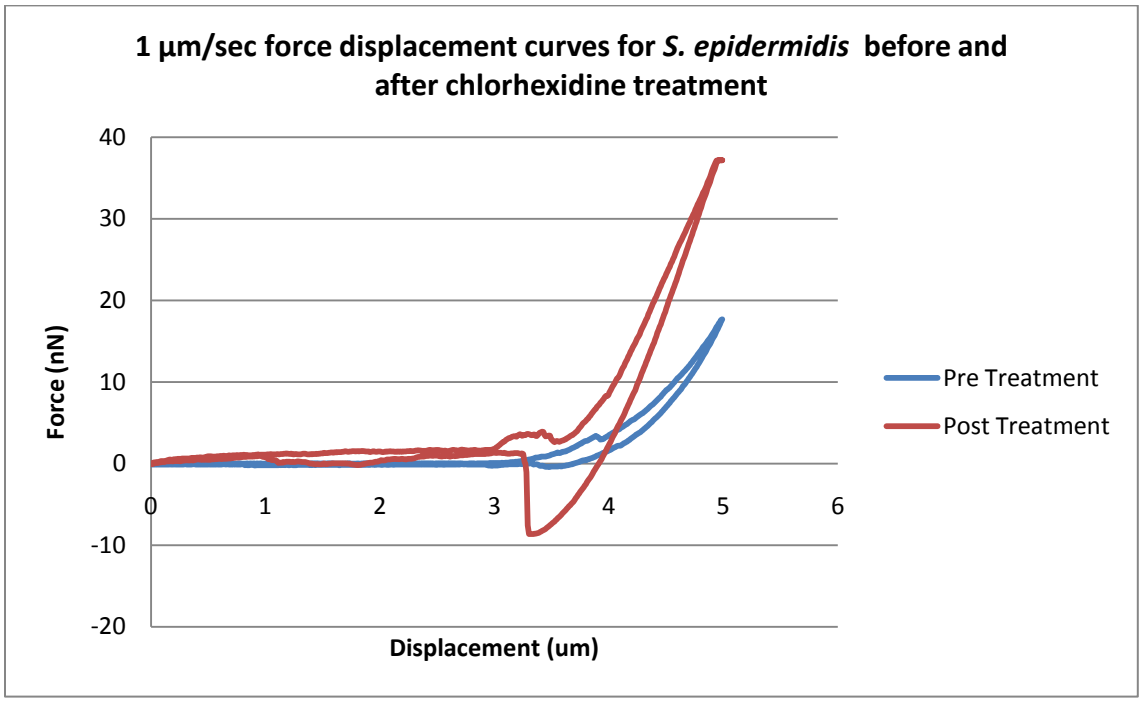

Figure 67) Force displacement curves for 1µm/sec loading rate for pre and post-treatment of chlorhexidine on *S. epidermidis* biofilm

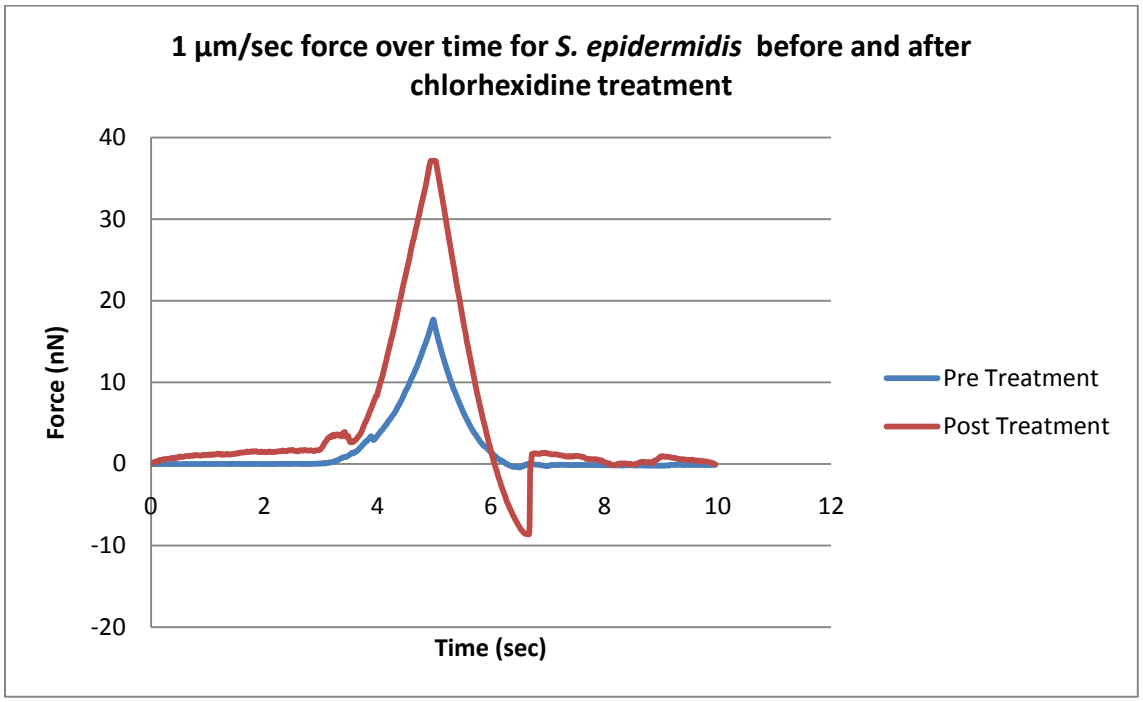

Figure 68) Force applied to *S. epidermidis* biofilm over loading time for pre and post-treatment of chlorhexidine using 1µm/sec loading rate

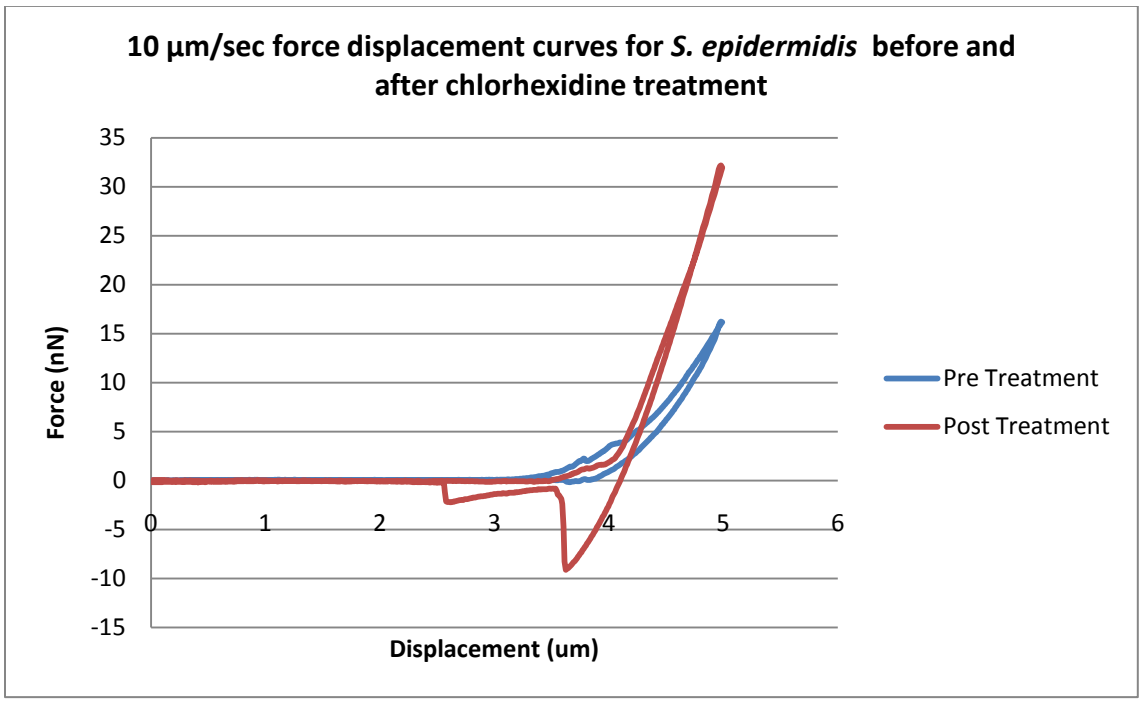

Figure 69) Force displacement curves for 10µm/sec loading rate for pre and post-treatment of chlorhexidine on *S. epidermidis* biofilm

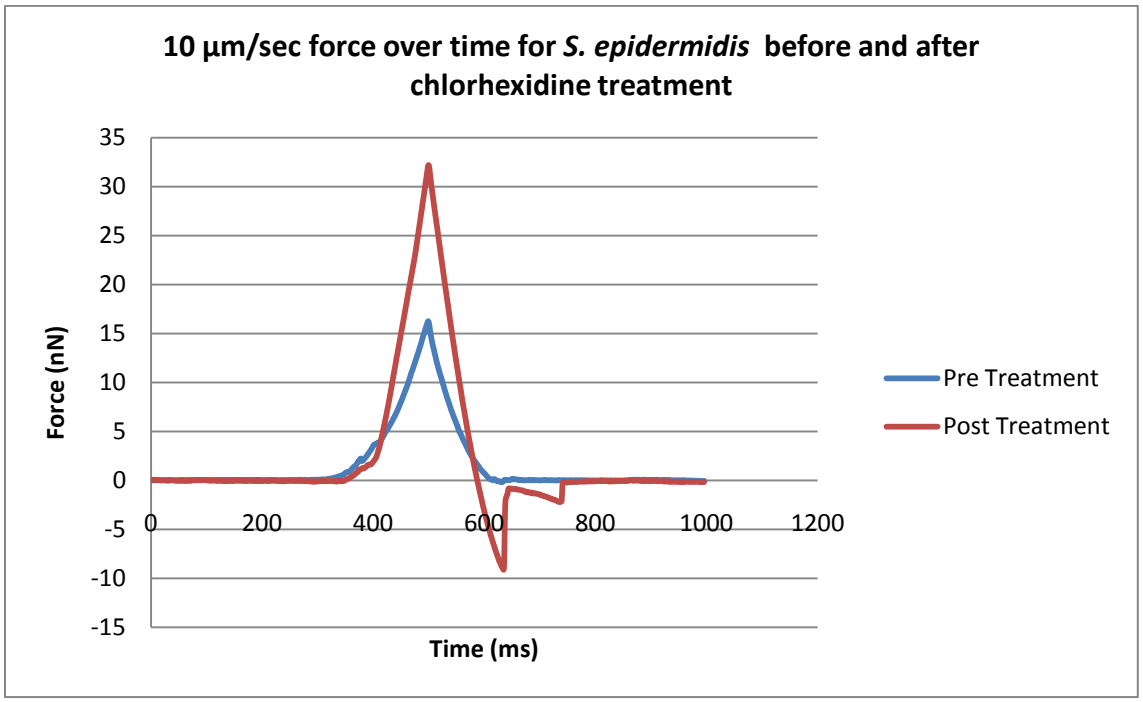

Figure 70) Force applied to *S. epidermidis* biofilm over loading time for pre and post-treatment of chlorhexidine using 10µm/sec loading rate

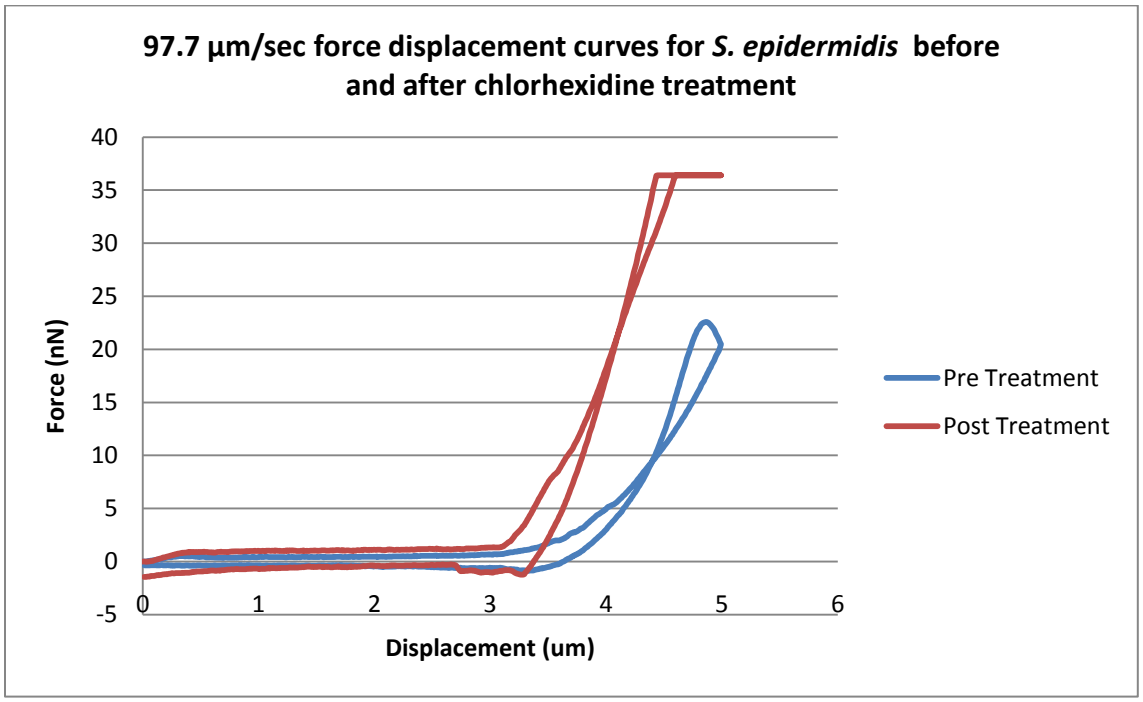

Figure 71) Force displacement curves for 97.7µm/sec loading rate for pre and post-treatment of chlorhexidine on *S. epidermidis* biofilm

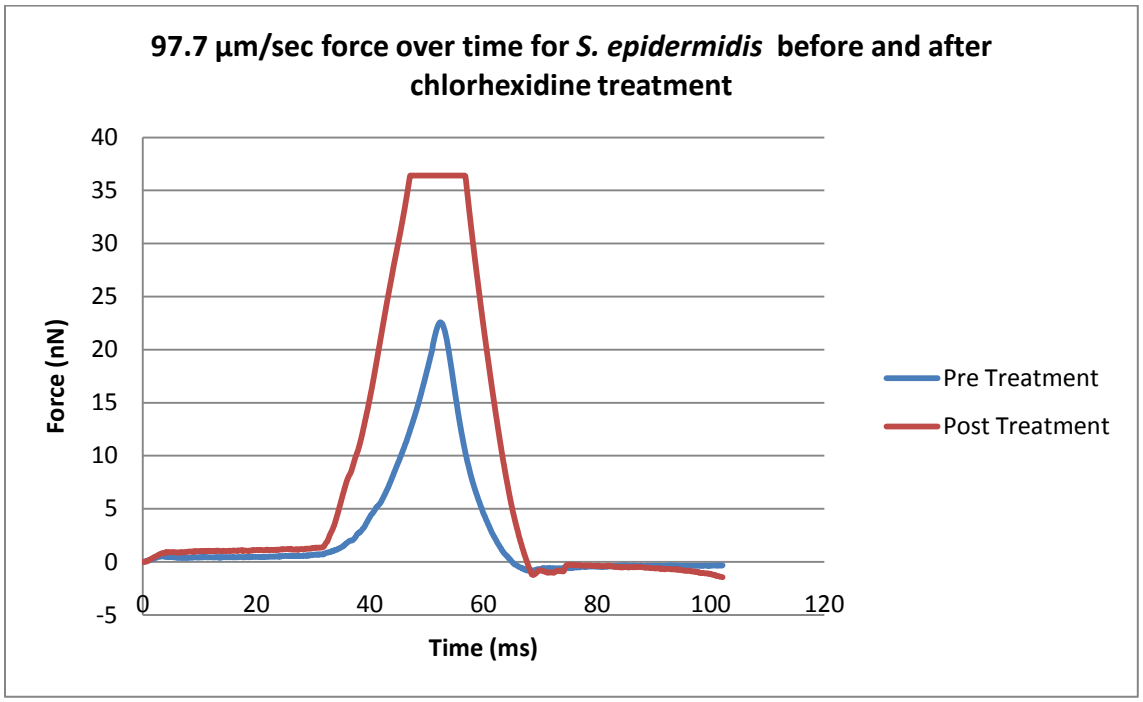

Figure 72) Force applied to *S. epidermidis* biofilm over loading time for pre and post-treatment of chlorhexidine using 97.7µm/sec loading rate

The chlorhexidine treatment in the capillary flow cell experiments have shown to stiffen the biofilm much the same way the AFM indentation shows a stiffer biofilm. Notice for every trial there was a significant increase in maximum force needed to reach a 5μm displacement. Figure 71 and Figure 72 are from the trial using the highest loading rate resulting in large forces. The deflection of the cantilever probe was enough to go beyond the maximum resolution of the AFM laser sensing diode. This is the explanation for the flattening of the force curve at 36 nN.

Another interesting phenomenon of the chlorhexidine treatment is that the biofilm becomes more adhesive to the cantilever tip. Notice that at low rates during the unloading of the biofilm there was large negative forces depicting the cantilever pulling the biofilm in tension. Once fracture or separation from the tip occurs the force returned to zero. Results from trials 2 and 3 can be found in Appendix B.

Urea Treatment

Urea is theorized to disrupt hydrogen-bonding interactions which are thought to be important for EPS mechanical stability. Urea at a concentration of 0.5 molar was used in this testing. As before, there are three sets of indentation rates consisting of 1μm/sec (Figure 73 and Figure 74), 10μm/sec (Figure 75 and Figure 76), and 100μm/sec (Figure 77 and Figure 78).

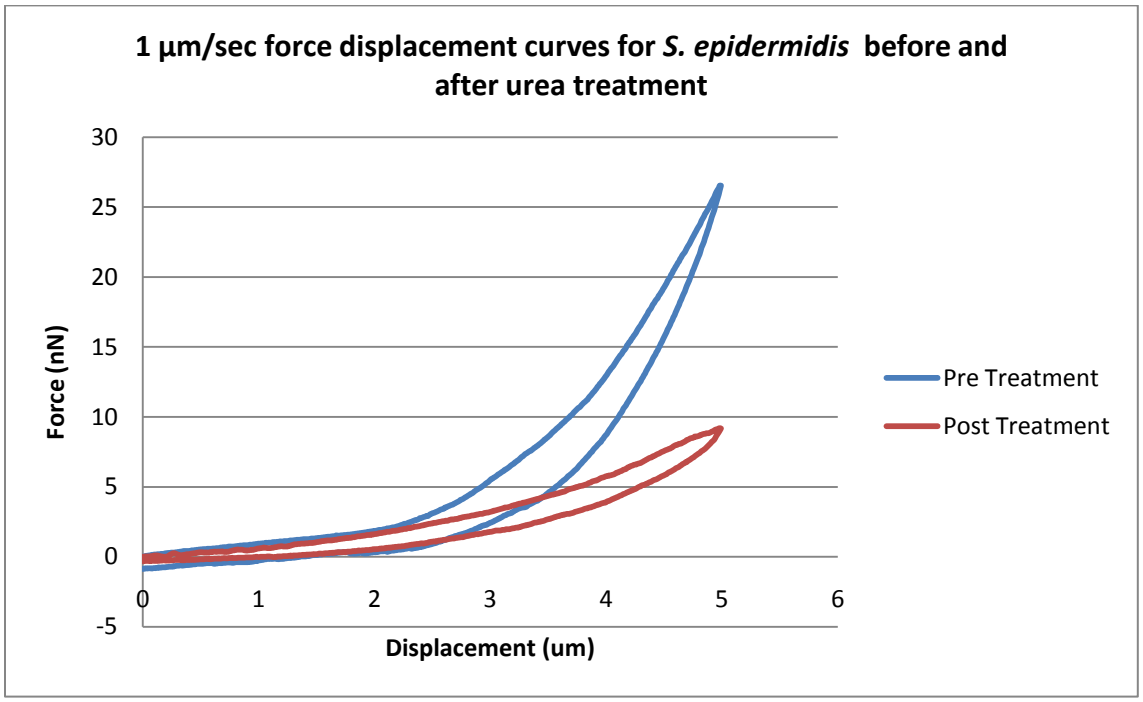

Figure 73) Force displacement curves for 1µm/sec loading rate for pre and post-treatment of urea on *S. epidermidis* biofilm

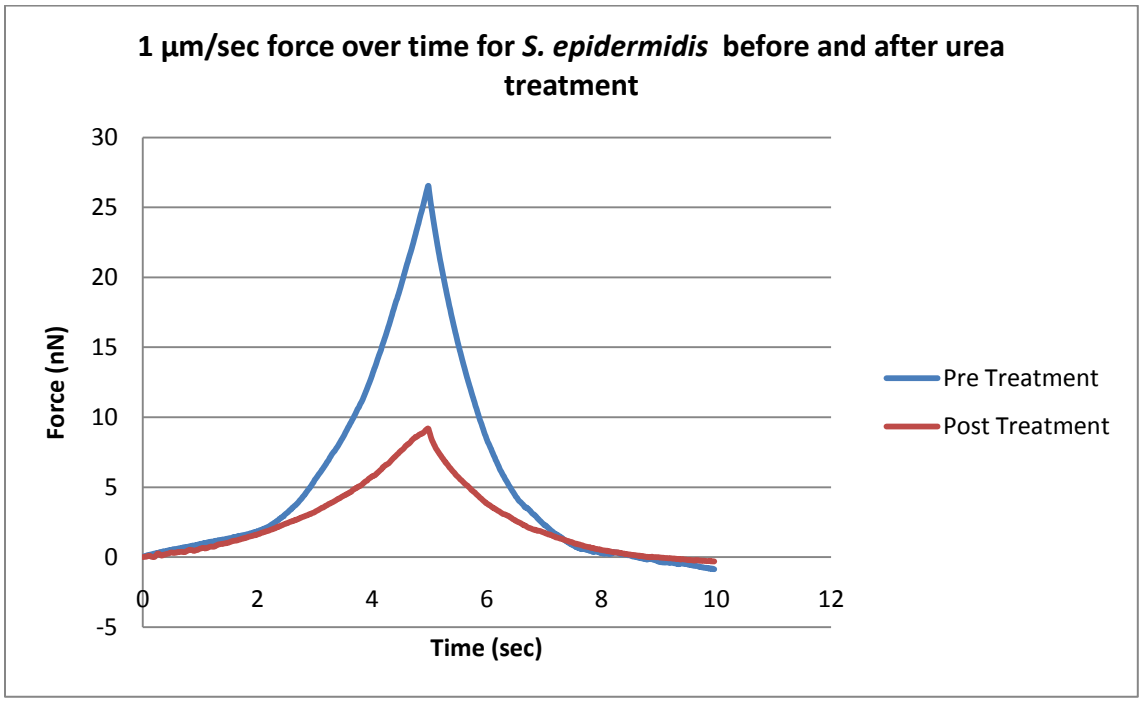

Figure 74) Force applied to *S. epidermidis* biofilm over loading time for pre and post-treatment of urea using 1µm/sec loading rate

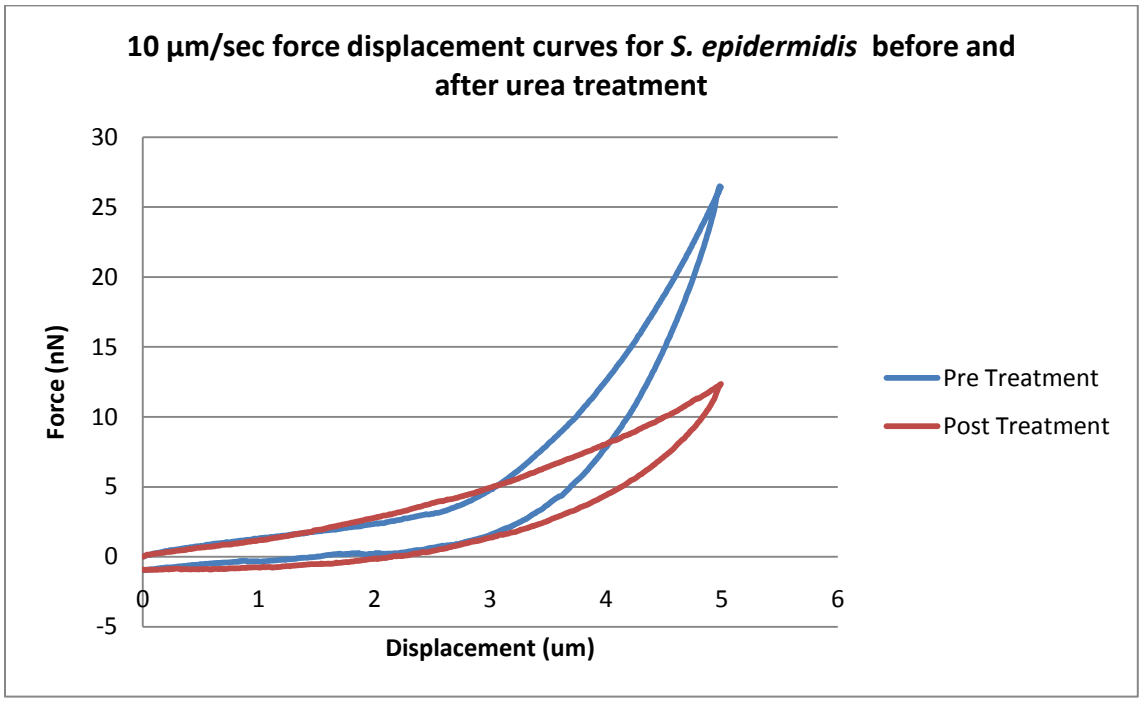

Figure 75) Force displacement curves for 10µm/sec loading rate for pre and post-treatment of urea on *S. epidermidis* biofilm

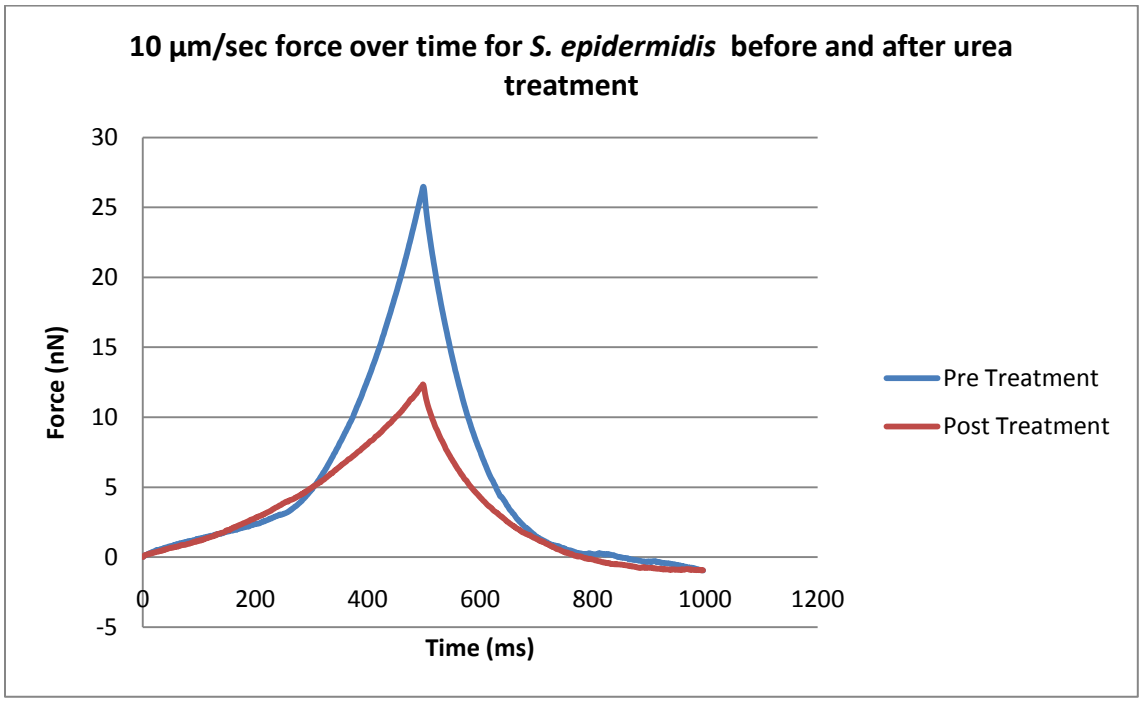

Figure 76) Force applied to *S. epidermidis* biofilm over loading time for pre and post-treatment of urea using 10µm/sec loading rate

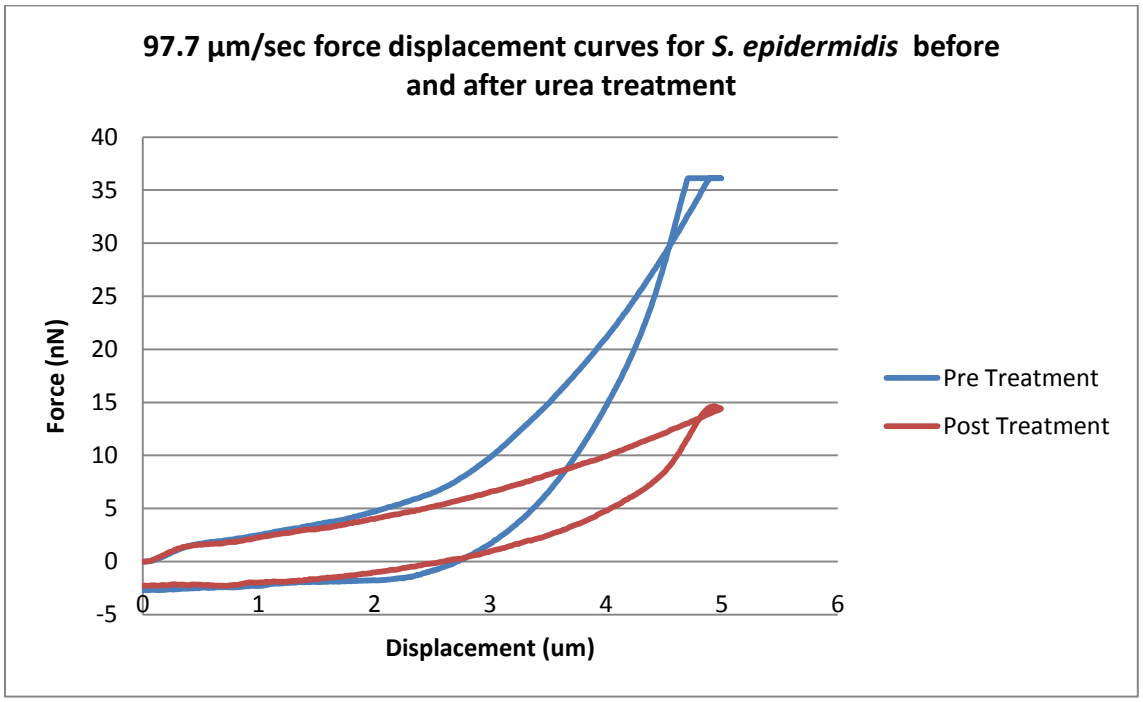

Figure 77) Force displacement curves for 97.7µm/sec loading rate for pre and post-treatment of urea on *S. epidermidis* biofilm

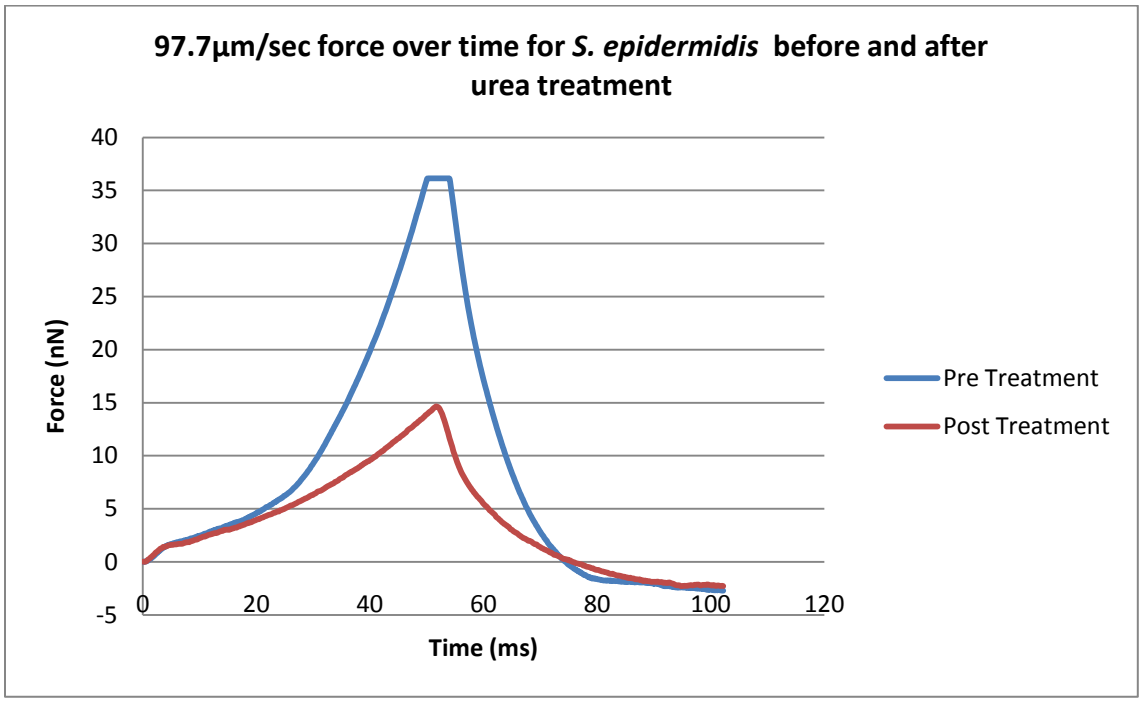

Figure 78) Force applied to *S. epidermidis* biofilm over loading time for pre and post-treatment of urea using 97.7µm/sec loading rate

The urea treatment in the capillary flow cell experiments have shown to soften the biofilm much the same way the AFM indentation shows a softer biofilm. Notice that each of the trials there was less force required after the treatment to obtain the 5μm indentation compared to the untreated biofilm. One problem with testing the urea treatment is that much of the biofilm becomes too soft for the cantilever to obtain a substantial deflection. The lack of bending in the cantilever leads to little or no force obtained in the force displacement diagram. Results from trials 2 and 3 can be found in Appendix B.

DispersinB® Treatment

DispersinB® catalyzes the hydrolysis extracellular polysaccharide produced by *S. epidermidis* which was shown to soften the biofilm in the capillary flow cell. DispersinB® at a concentration of 40μg/ml was used in this testing. As before, there are three sets of indentation rates consisting of 1μm/sec (Figure 79 and Figure 74), 10μm/sec (Figure 81 and Figure 82), and 100μm/sec (Figure 83 and Figure 84).

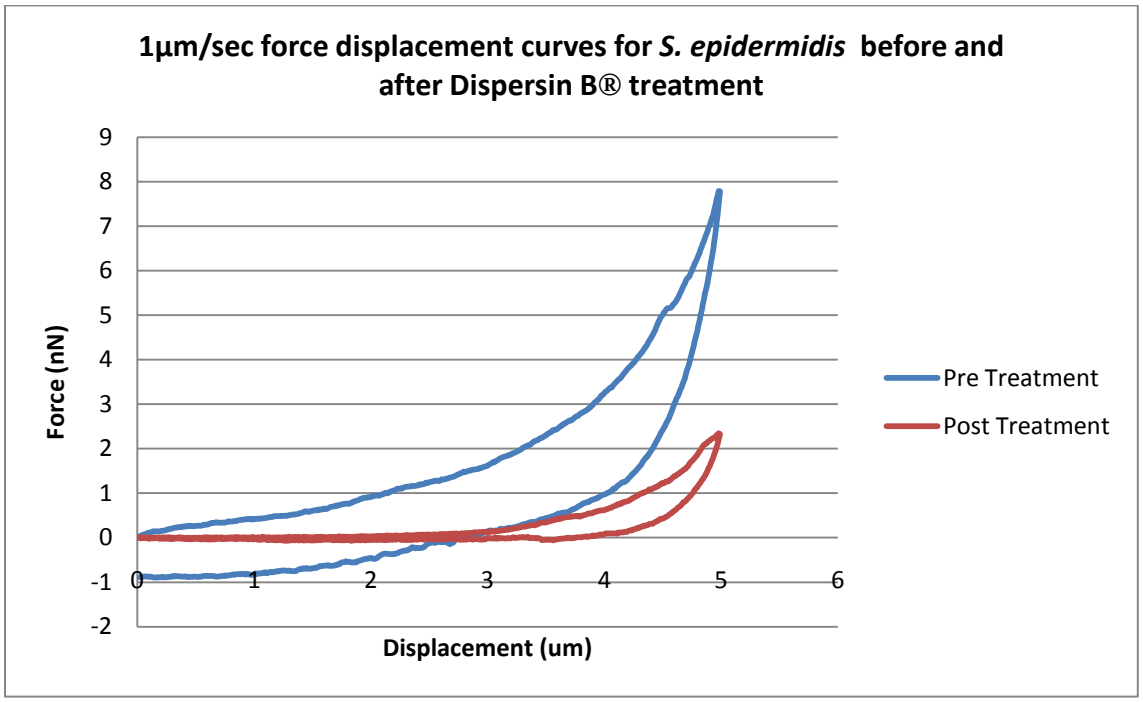

Figure 79) Force displacement curves for 1µm/sec loading rate for pre and post-treatment of DispersinB® on *S. epidermidis* biofilm

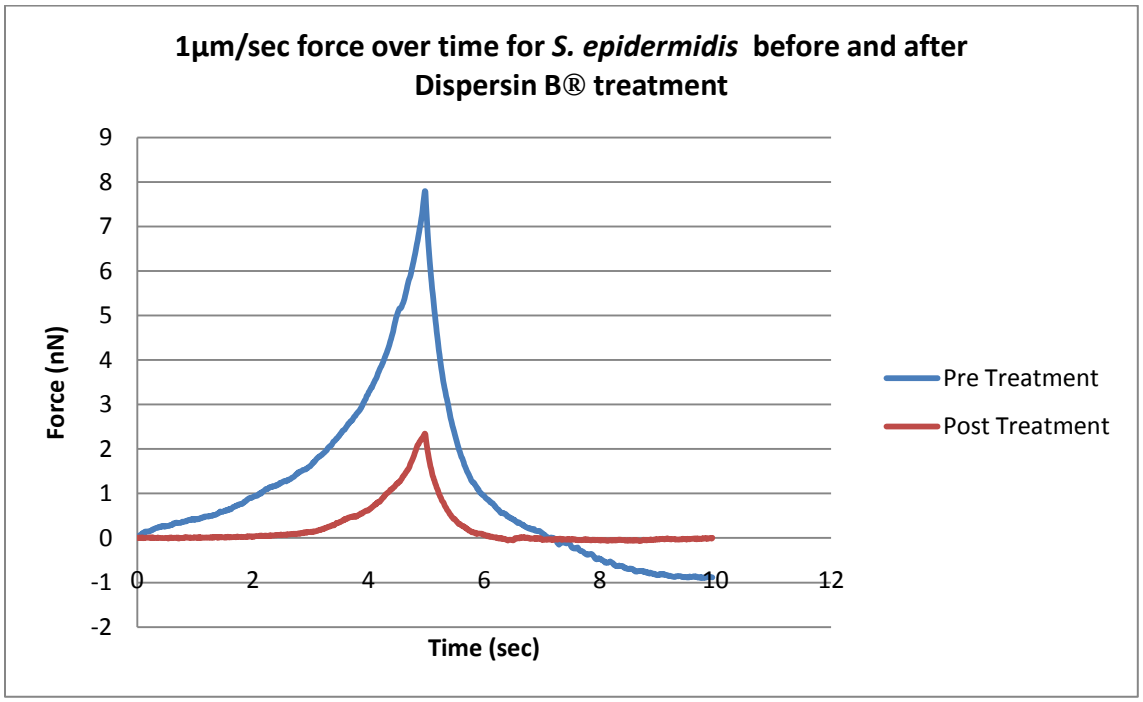

Figure 80) Force applied to *S. epidermidis* biofilm over loading time for pre and post-treatment of DispersinB® using 1µm/sec loading rate

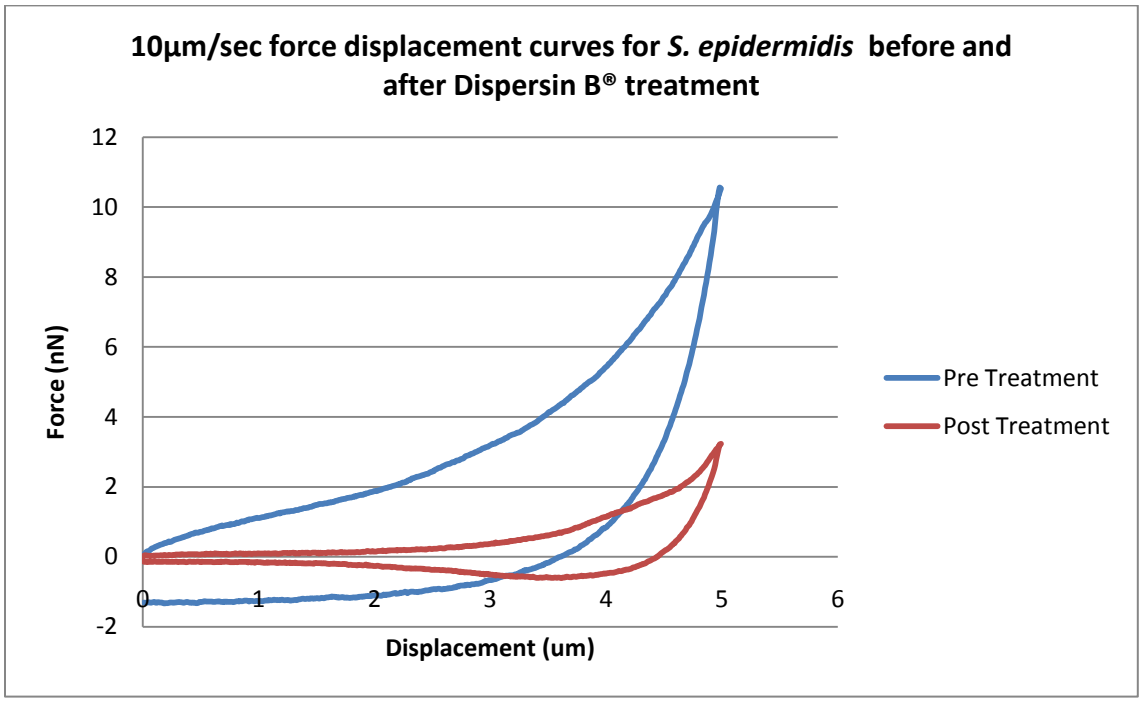

Figure 81) Force displacement curves for 10µm/sec loading rate for pre and post-treatment of DispersinB® on *S. epidermidis* biofilm

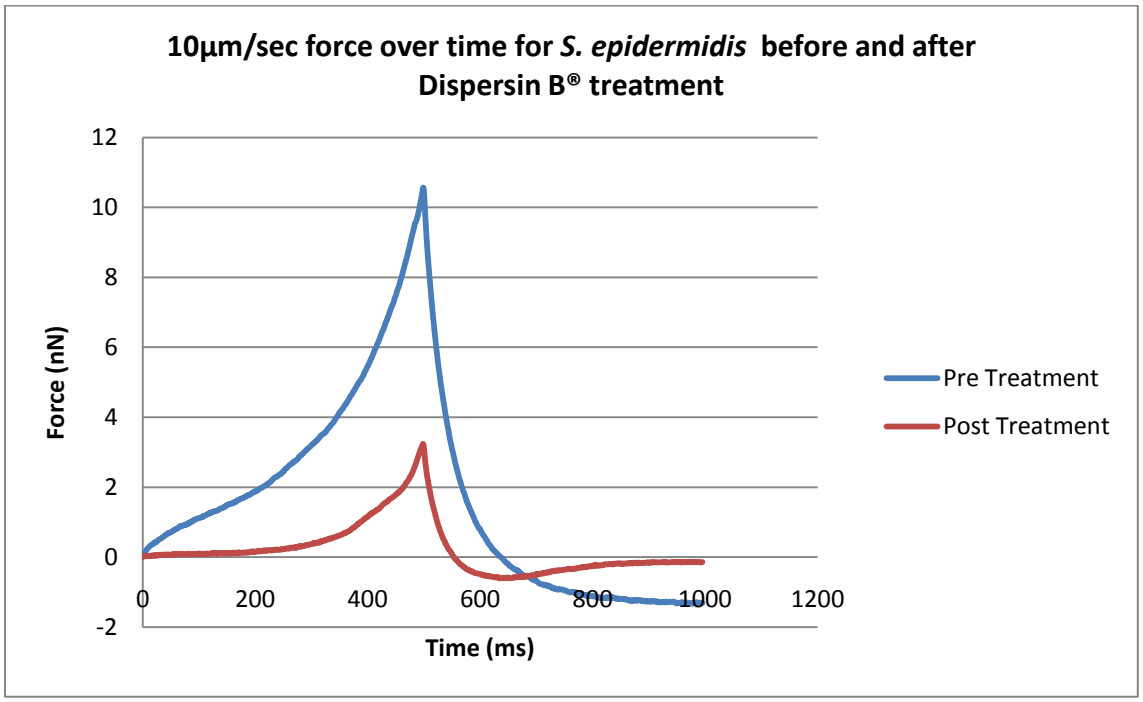

Figure 82) Force applied to *S. epidermidis* biofilm over loading time for pre and post-treatment of DispersinB® using 10µm/sec loading rate

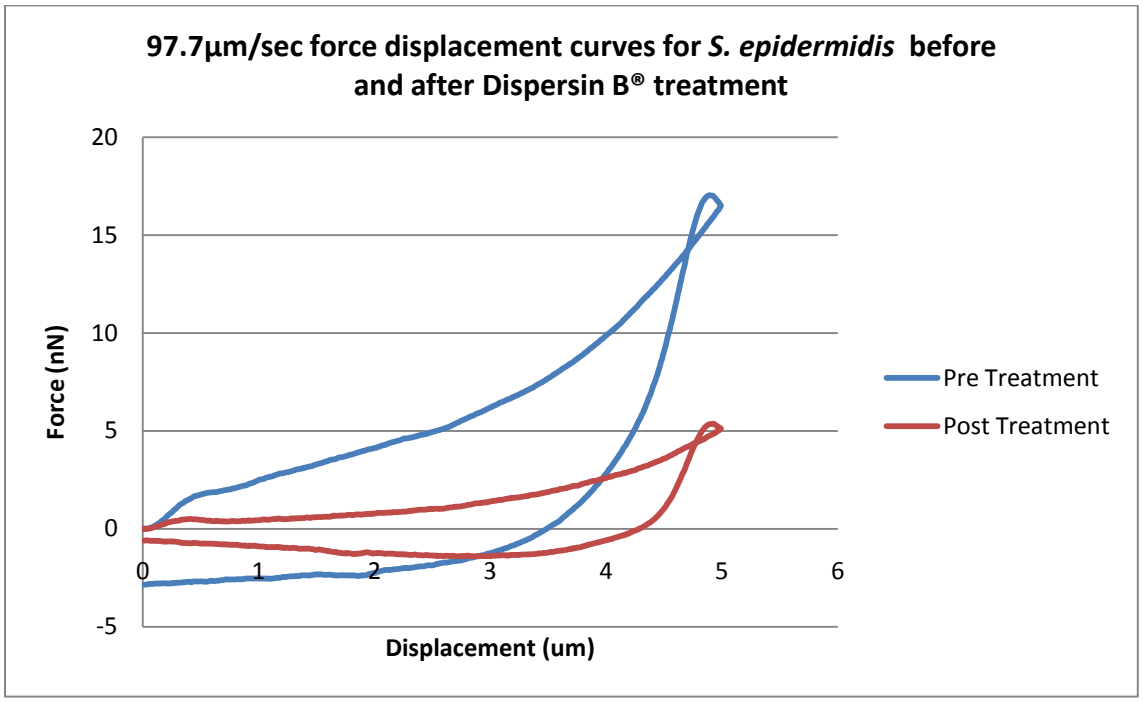

Figure 83) Force displacement curves for 97.7µm/sec loading rate for pre and post-treatment of DispersinB® on *S. epidermidis* biofilm

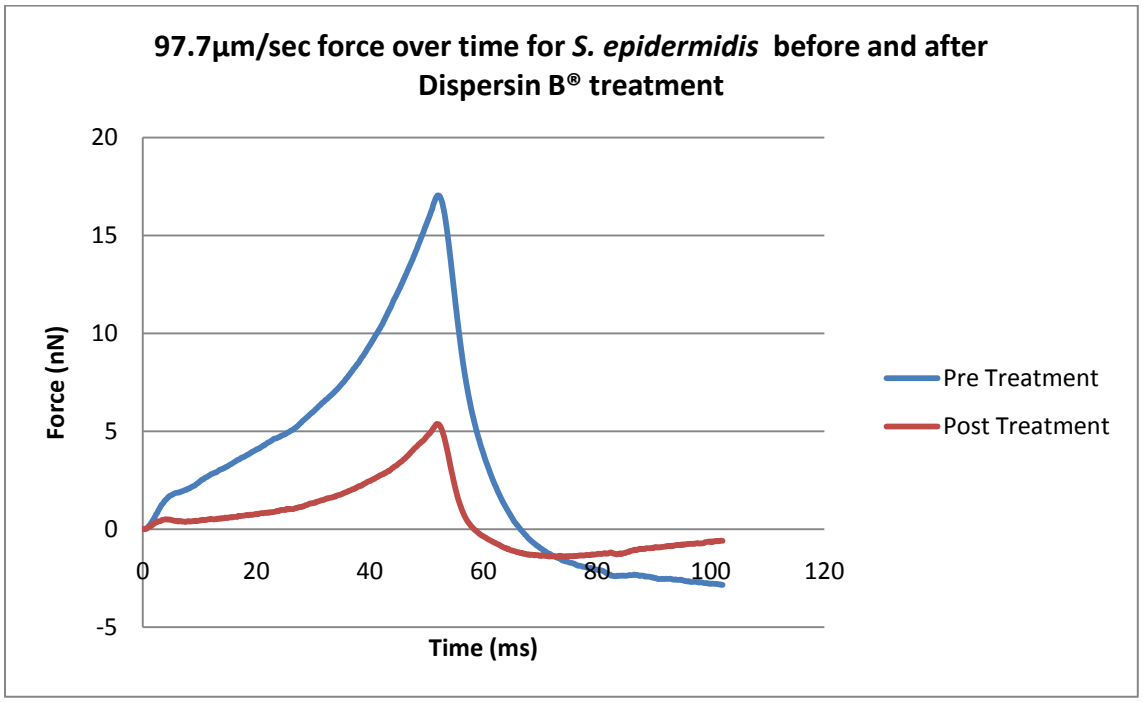

Figure 84) Force applied to *S. epidermidis* biofilm over loading time for pre and post-treatment of DispersinB® using 97.7µm/sec loading rate

The DispersinB® treatment in the capillary flow cell experiments have shown to soften the biofilm much the same way the AFM indentation shows this effect. Notice that in each one of the trials there was less force required during the post-treatment to obtain the 5μm indentation compared to the pre-treated biofilm. One problem with testing the DispersinB® (much like the urea) was that much of the biofilm becomes too soft for the cantilever to obtain a substantial deflection. Results from trials 2 and 3 can be found in Appendix B.

Discussion

Data from the force-displacement curves was analyzed focusing on two concepts. First the maximum force required to reach 5μm indent into the biofilm. For each trial the maximum post-treatment force was divided by the pre-treatment force to normalize and compare between trials. Second the area between the force-displacement curves was analyzed in much the same way, the post-treatment area was divided by the pre-treatment area. The results of these calculations are shown in Table 17.

Table 17) Maximum force of each trial with post-treatment maximum displacement divided by pre-treatment maximum displacement for all three trials. Area between indentation and retraction shown post-treatment area divided by pre-treatment area for all three trials.

		Max Force (post-treatment/pre-treatment)			Area Between Curves (post-treatment/pre-treatment)		
Iron Chloride Treatment		**1µm/sec**	**10µm/sec**	**100µm/sec**	**1µm/sec**	**10µm/sec**	**100µm/sec**
	Trial#1	0.929	1.502	1.217	1.210	3.158	0.381
	Trial #2	0.981	1.428	1.015	0.736	1.129	0.735
	Trial #3	0.801	0.925	0.782	0.757	0.739	0.857
	Average ±SD	**0.904** ±0.093	**1.285** ±0.314	**1.004** ±0.218	**0.901** ±0.268	**1.675** ±1.299	**0.657** ±0.247
		Max Force (post-treatment/pre-treatment)			Area Between Curves (post-treatment/pre-treatment)		
Chlorhexidine Treatment		**1µm/sec**	**10µm/sec**	**100µm/sec**	**1µm/sec**	**10µm/sec**	**100µm/sec**
	Trial#1	2.102	1.981	1.611	3.963	1.694	0.089
	Trial #2	2.167	4.815	2.901	1.747	1.005	0.155
	Trial #3	1.542	1.230	1.214	6.899	2.168	0.037
	Average ±SD	**1.937** ±0.343	**2.675** ±1.891	**1.908** ±0.882	**4.203** ±2.584	**1.622** ±0.585	**0.094** ±0.059
		Max Force (post-treatment/pre-treatment)			Area Between Curves (post-treatment/pre-treatment)		
Urea Treatment		**1µm/sec**	**10µm/sec**	**100µm/sec**	**1µm/sec**	**10µm/sec**	**100µm/sec**
	Trial#1	0.346	0.466	0.405	0.475	0.901	0.822
	Trial #2	0.461	0.963	0.472	0.407	0.774	0.553
	Trial #3	1.046	1.027	1.148	1.958	0.949	2.406
	Average ±SD	**0.617** ±0.375	**0.819** ±0.307	**0.675** ±0.411	**0.947** ±0.867	**0.875** ±0.090	**1.260** ±1.001
		Max Force (post-treatment/pre-treatment)			Area Between Curves (post-treatment/pre-treatment)		
DispersinB® Treatment		**1µm/sec**	**10µm/sec**	**100µm/sec**	**1µm/sec**	**10µm/sec**	**100µm/sec**
	Trial#1	0.301	0.306	0.315	0.220	0.287	0.408
	Trial #2	0.636	0.676	0.837	0.714	0.666	0.921
	Trial #3	1.283	1.150	0.834	0.990	1.313	1.060
	Average ±SD	**0.740** ±0.499	**0.711** ±0.423	**0.662** ±0.300	**0.642** ±0.390	**0.755** ±0.519	**0.796** ±0.343

Notice in Table 17 that the average maximum force for both the urea and the DisperisnB® is less than one. This shows that on average these treatments have a smaller post-treatment maximum force required to reach the 5µm depth. The less force required, the softer the material has become. The opposite is true on average for both the iron

chloride and the chlorhexidine, showing that these agents become stiffer after the treatment. Notice that chlorhexidine has larger average values for the maximum force ratio. This implies that the chlorhexidine is a stronger stiffening agent than the iron chloride. Generally the iron chloride stiffens the biofilm, but there was little conclusive proof with the micro indentation testing. This is most likely due to a combination of factors including efficiency of iron chloride which oxidizes quickly and suspended particles interfering with the laser optics of the AFM. Both the urea and DispersinB® have relatively the same amount of change from pre to post-treatment implying that they have relatively the same softening effect.

The area between the force-displacement curves data (Table 17) can be generalized as energy dissipation, or viscous dashpots, in the Burger model. One piece of information that is interesting to note that for the stiffing agents (iron chloride/ chlorhexidine) there is a general trend of decrease in the area ratio as the rate of indentation increases. Thus, at the low indentation rates the treated biofilm is more viscous and at the higher rates the treated biofilm is more elastic dissipating little energy. For the agents that create a more viscous biofilm (urea/DispersinB®) there is little overall change in area ratios which implies that they are viscously dominated at any rate. But for the most part this data is difficult to interpret and offers little conclusive proof on damping effects of the treatments.

Force-displacement curves obtained using an AFM are very useful in obtaining true forces but there are limitations to their capabilities. The biggest limitation to this particular experimental set up using the AFM is that there is no accurate method for

obtaining the thickness of the biofilm being tested. Manipulation can only occur through the accessible surface of the biofilm and cannot measure properties well inside the biofilm without an influence of boundary conditions (Janmey and Schmidt 2006). Without having an accurate biofilm thickness it becomes nearly impossible to model these biofilms accurately. Because of the scale of indentation (30μm diameter sphere) and the scale of the biofilm (10~150μm) geometrical issues dominate modeling criteria. For example, a 5μm thick biofilm will behave much differently than a 150μm biofilm. A 5μm thick biofilm will appear much stiffer because of the solid silicon wafer the biofilm is attached to will affect the measured response of the biofilm. Although modeling is not possible for these indentation tests, a comparison can be made with the capillary flow cell results.

Utilizing the changes in Burger model parameters found from the capillary flow cell results, a comparison study was conducted on the indentation results. Dimensionless force displacement curves were created using the E_{1post}/E_{1pre}, E_{2post}/E_{2pre}, η_{1post}/η_{1pre}, and η_{2post}/η_{2pre} found from the capillary flow cell results (see METHOD 1: Discussion). Unlike the flow cell experiment where a constant stress was applied to the biofilm, the indentation provides a ramped displacement loading. The Burger model equation now has stress as a function of time as well as a strain as a function of time component. Since true stresses and true strains are not measured, a comparison between pre and post-treatment displacements and forces must be made. This assumption is applicable when the biofilm being tested has not changed in geometry and the same forces are applied before and after

the treatment. At this point the force can be directly related to stress and the displacement directly related to strain. Our Burger model equation becomes:

$$\tau(t) = \varepsilon(t) / \left(\frac{1}{E_1} + \frac{t}{\eta_1} + \frac{1}{E_2}\left(1 - e^{\frac{-E_2 t}{\eta_2}}\right)\right) \qquad (25)$$

This states that the stress τ(t) is a function of the Burger model elements and the input strain with time. Assuming that geometries are nearly the same on a particular cluster and the ε(t) function is consistent from pre to post-treatment, we can say that there is change in the Burger model parameters before and after treatment or for each treatment there is E_{1post}/E_{1pre}, E_{2post}/E_{2pre}, η_{1post}/η_{1pre}, and η_{2post}/η_{2pre}. Using these non-dimensional Burger model parameters a comparison of force displacement curves was made between actual obtained data and Burger model fit data.

Curves were created using a rate of 10μm/sec to compare with normalized data collected from the AFM micro indentation. The normalization of the data was done to the largest force in the pre-treatment trial, so that a post-treatment biofilm that was stiffer than the untreated version had a larger value than one. Each treatment has two graphs, a force-displacement curve and a force with time curve. Each graph has four sets of data, the pre and post-treatment data obtained from the experiment and the pre and post-treatment Burger model fit from the values obtained in the capillary flow cell experiment. Also, the model data is assuming a constant area of contact. In reality, the contact rate will vary with the geometry of the biofilm and create highly non-linear responses in the force displacement curves not captured in the model.

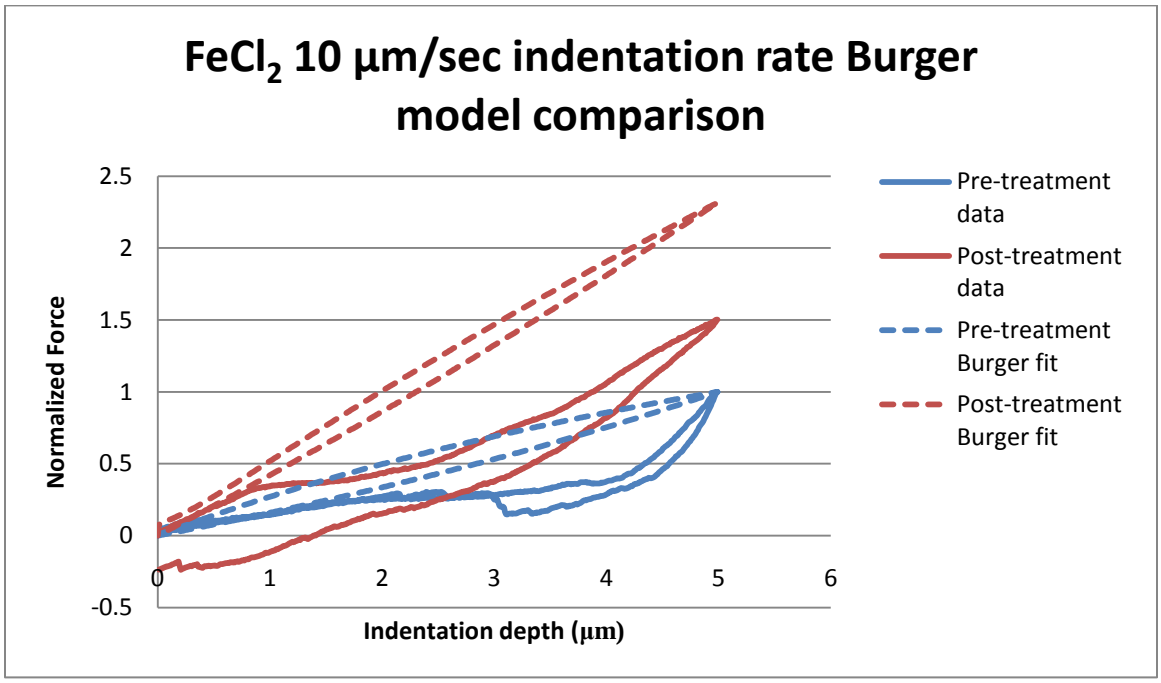

Figure 85) Force displacement curves for before and after iron chloride treated biofilms with Burger model predicted results from capillary flow cell experiments

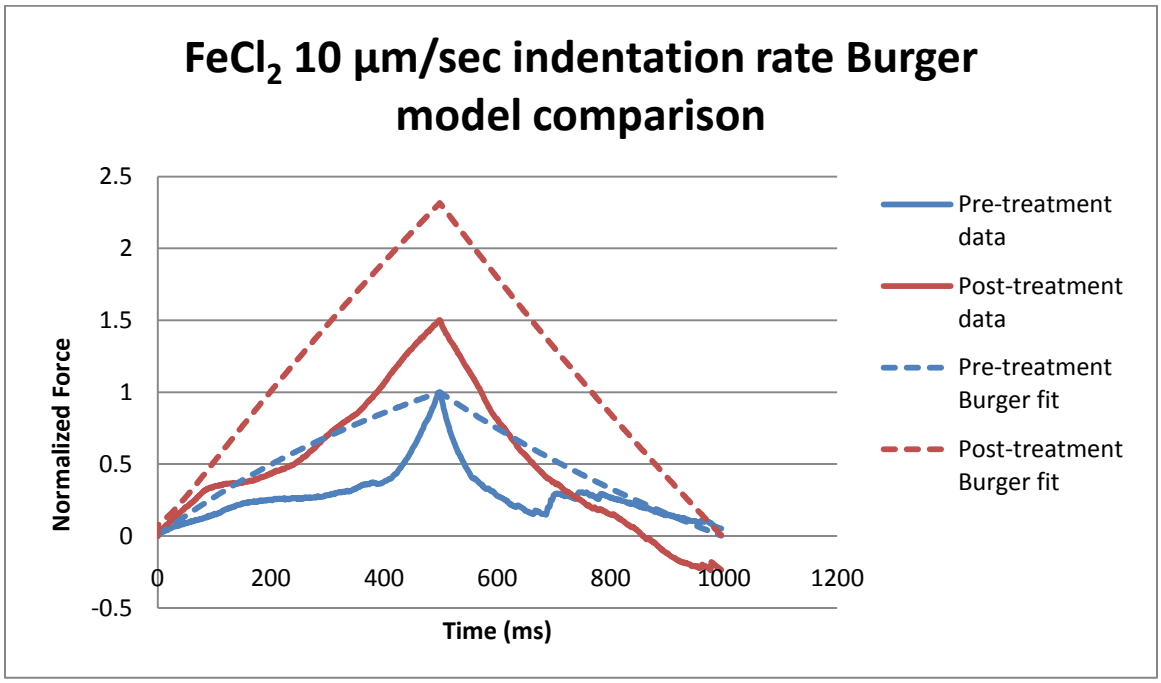

Figure 86) Force-time curves for before and after treated iron chloride biofilms plotted with changes in Burger model parameters found from capillary flow cell experiments

As discussed earlier iron chloride has a stiffing effect on the biofilm. Here the Burger model fit obtained by using values from the capillary flow cell experiment show this same stiffing effect (Figure 85 and Figure 86). The before and after treatment Burger model fit has a substantial increase in force required to displace 5µm. Notice also that the post-treatment Burger fit was nearly linear in Figure 85, representing the elastic properties of the Burger model. The pre-treatment Burger model had a larger hysteresis loop in Figure 86 showing more viscous properties. Most importantly there was an increase in force to obtain the five micron indentation depth in both the Burger model parameters and from the actual data obtained from the AFM.

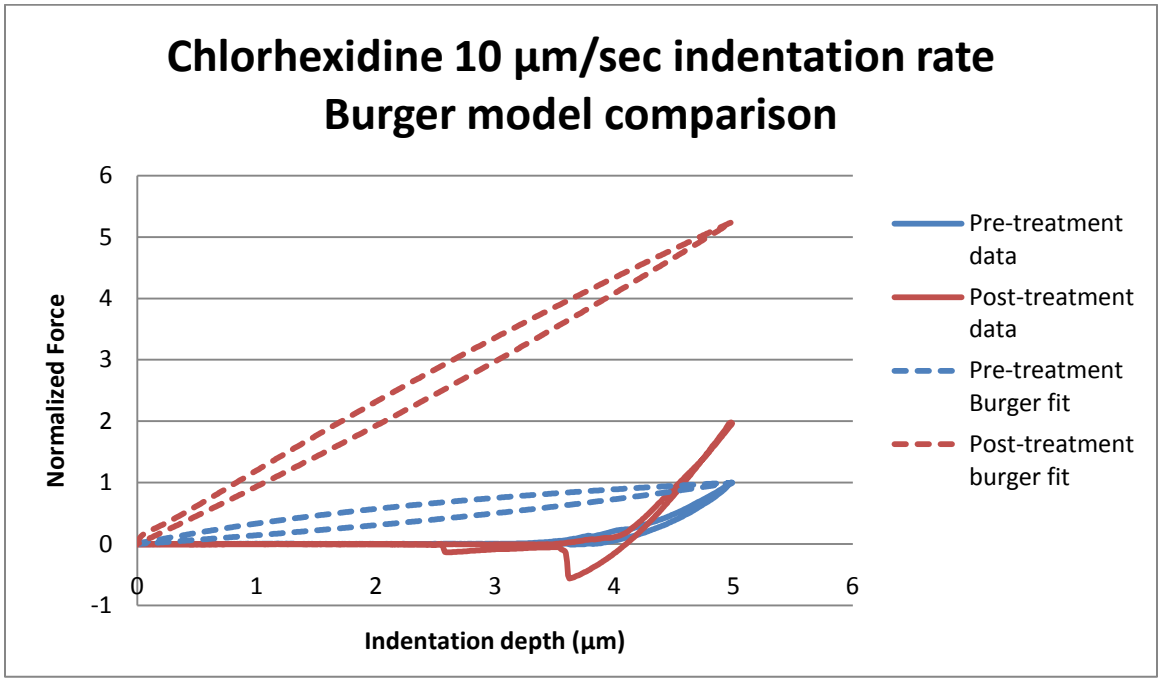

Figure 87) Force displacement curves for before and after chlorhexidine treated biofilms with Burger model predicted results from capillary flow cell experiments

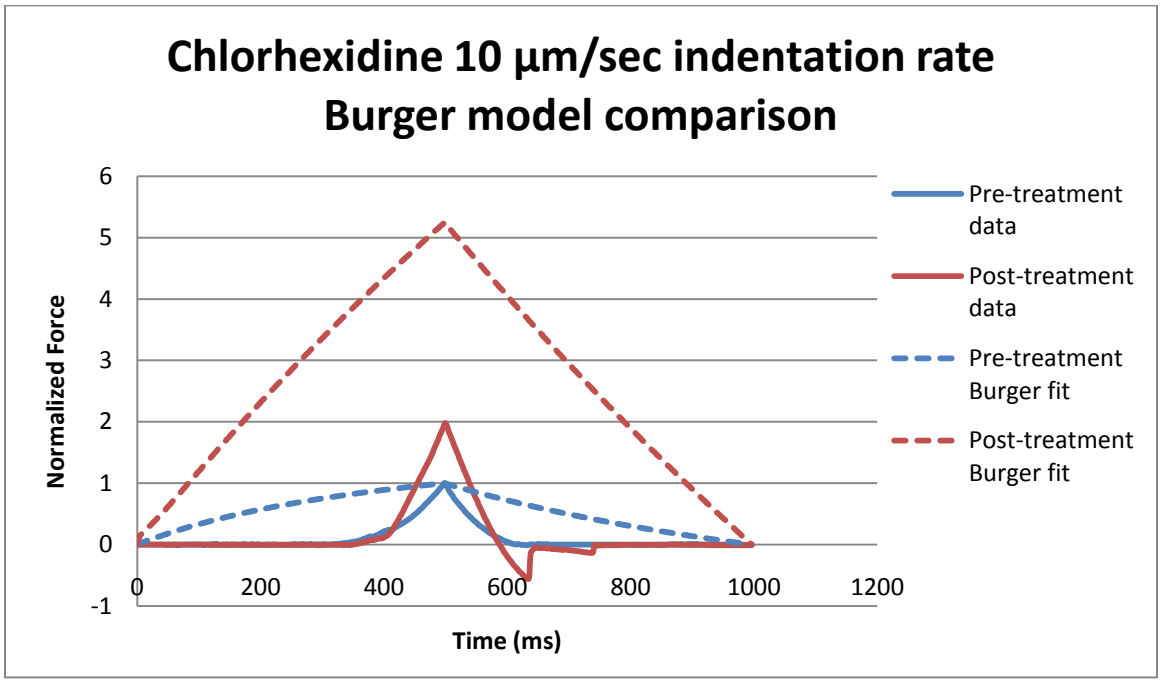

Figure 88) Force-time curves for before and after treated chlorhexidine biofilms plotted with changes in Burger model parameters found from capillary flow cell experiments

Chlorhexidine as discussed earlier also has a stiffing effect on the biofilm. Here the Burger model fit obtained by using values from the capillary flow cell experiment show this same stiffing effect. The post-treatment Burger model fit has a substantial increase in force required to obtain a 5µm displacement (Figure 87 and Figure 88). The pre and post-treatment Burger model hysterias loops, representing viscous properties, are nearly the same (Figure 87). The lack of change in the hysterias loops shows that the fitted parameters were both stiffer and still slightly viscous. Most importantly there was an increase in force to obtain the 5µm indentation depth in both the Burger model parameters and from the actual data obtained from the AFM. The large amount of difference in pre to post-treatment normalized force to that of the data collected was due to issues with contact length of the indenter and thin biofilm. Because of the soft

cantilever tip with the indentation sphere on the end there can be problems with locating the exact surface. The actual contact of the biofilm was not until nearly 4µm into displacement. This creates less material to exhibit changes in properties from pre to post-treatment. There was, however, a significant increase in stiffness in both the Burger model fit and the actual data collected.

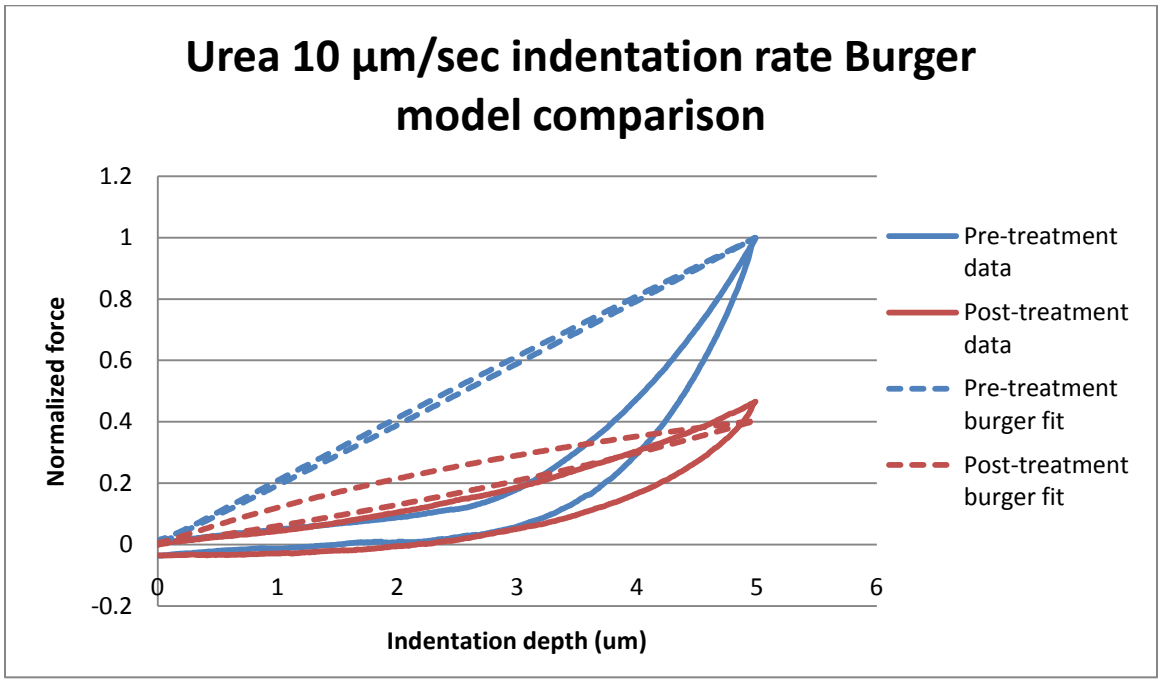

Figure 89) Force displacement curves for before and after urea treated biofilms with Burger model predicted results from capillary flow cell experiments

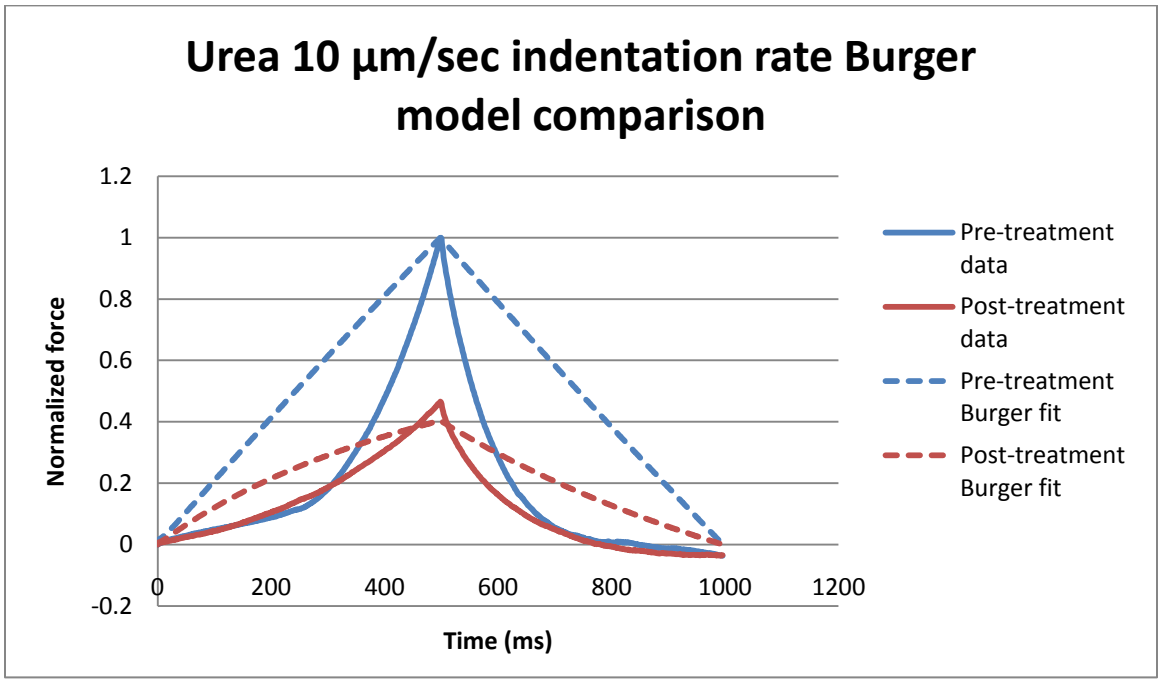

Figure 90) Force-time curves for before and after treated urea biofilms plotted with changes in Burger model parameters found from capillary flow cell experiments

The Urea treatment has been shown to soften the biofilm in both the capillary flow cell experiments and in the indentation experiment. The change in Burger model parameters found from the capillary flow cell experiment were used to model indentation of the urea treated biofilm as seen in Figure 89and Figure 90. Here the post-treatment Burger model fit had a smaller force required to obtain a 5µm indentation depth which was seen in the data. Not only was the post-treatment maximum force less, but the hysteresis loop was wider than the pre-treatment indentation. The wider hysteresis loop represents a viscous dominated biofilm after treatment.

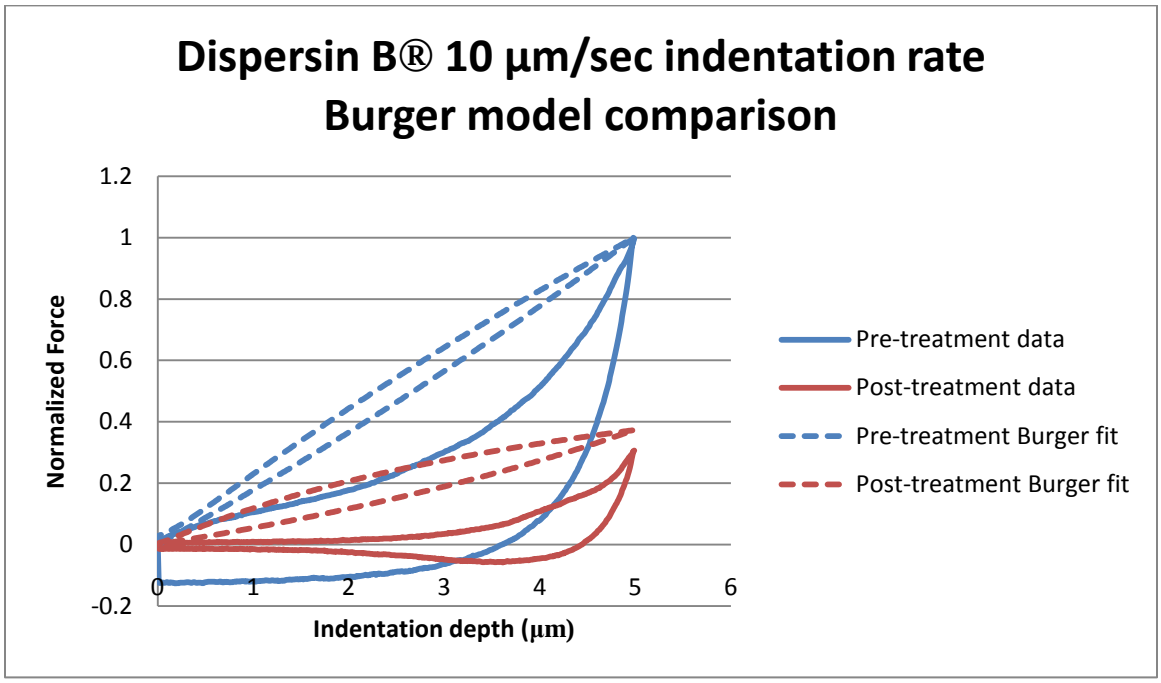

Figure 91) Force displacement curves for before and after DispersinB® treated biofilms with Burger model predicted results from capillary flow cell experiments

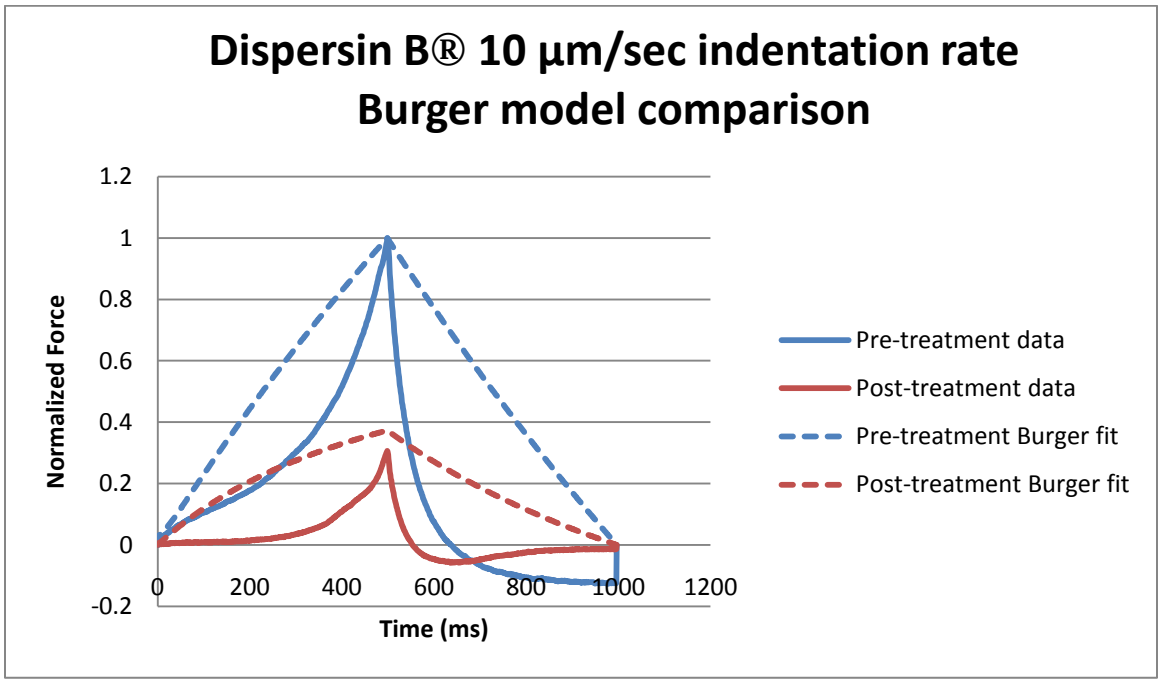

Figure 92) Force-time curves for before and after treated DispersinB® biofilms plotted with changes in Burger model parameters found from capillary flow cell experiments

The DispersinB® treatment has been shown to soften the biofilm in both the capillary flow cell experiments and in the indentation experiment. The change in Burger model parameters found from the capillary flow cell experiment were used to model indentation of the urea treated biofilm as seen in Figure 91 and Figure 92. . Here the post-treatment Burger model fit had a smaller force required to obtain a 5μm indentation depth which was seen in the data. Not only was the post-treatment maximum force less, but the hysteresis loop was wider than the pre-treatment indentation. The wider hysteresis loop represents a viscous dominated biofilm after treatment.

Recommendations for Future Work

One typical approach to measuring viscoelastic properties is to utilize its damping capabilities. Damping is the conversion of mechanical energy of a structure into thermal energy. This is also an energy dissipation element over each cycle of motion. The amount of energy dissipated is a measure of the structure's damping level (Macioce n.d.) (Attard 2007). Two trial experiments were conducted using chlorhexidine and DispersinB®. The two trials repeated the same growth procedure for the simple indentation test. During the AFM testing a cyclic indentation displacement was applied to a specific point on the biofilm. The biofilm was treated and then cyclically loaded again.

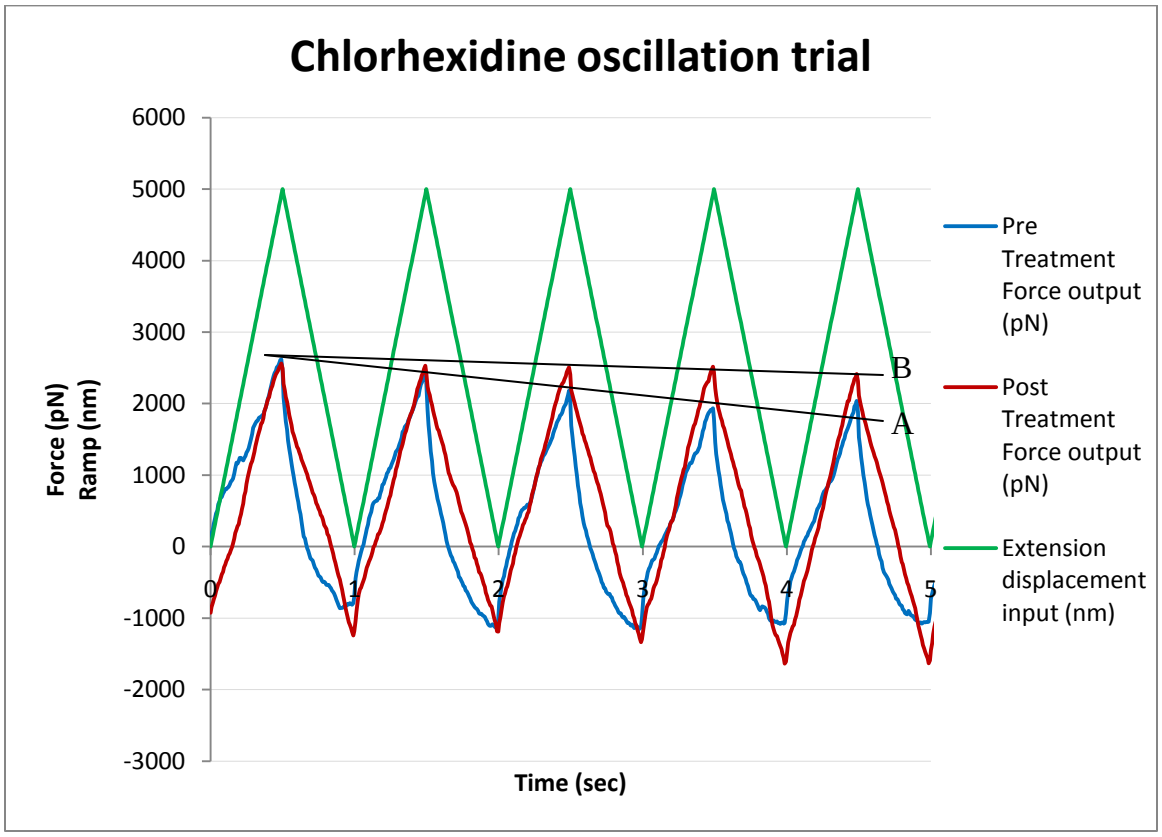

Figure 93) Chlorhexidine oscillation trial with displacement input plotted with pre and post chlorhexidine treated biofilm responses A) pre-treatment damping B) post-treatment damping

The chlorhexidine has been shown to stiffen the biofilm in both the flow cell experimentations and AFM indentation experiments. The triangular wave labeled extension displacement represents the input or extension of the cantilever beam into the biofilm. The force outputs are plotted both before and after the chlorhexidine treatment. Notice in Figure 93 both the pre and post-treatment peaks have a line labeled A and B consecutively. During the pre-treatment oscillations there is considerable damping thus a steeper slope of line A. After the biofilm has been treated the slope of line B is nearly flat, representing little damping.

Another difference in the before and after treatments was the shape of the response forces. During the pre-treatment the shape of the force response was nonlinear opposed to the post-treatment where the force response mirrored that of the displacement input. This represents a more elastic biofilm in the post-treatment or the post-treatment biofilm had less damping capabilities. In the Burger model this is represented by small values for the viscous dashpots.

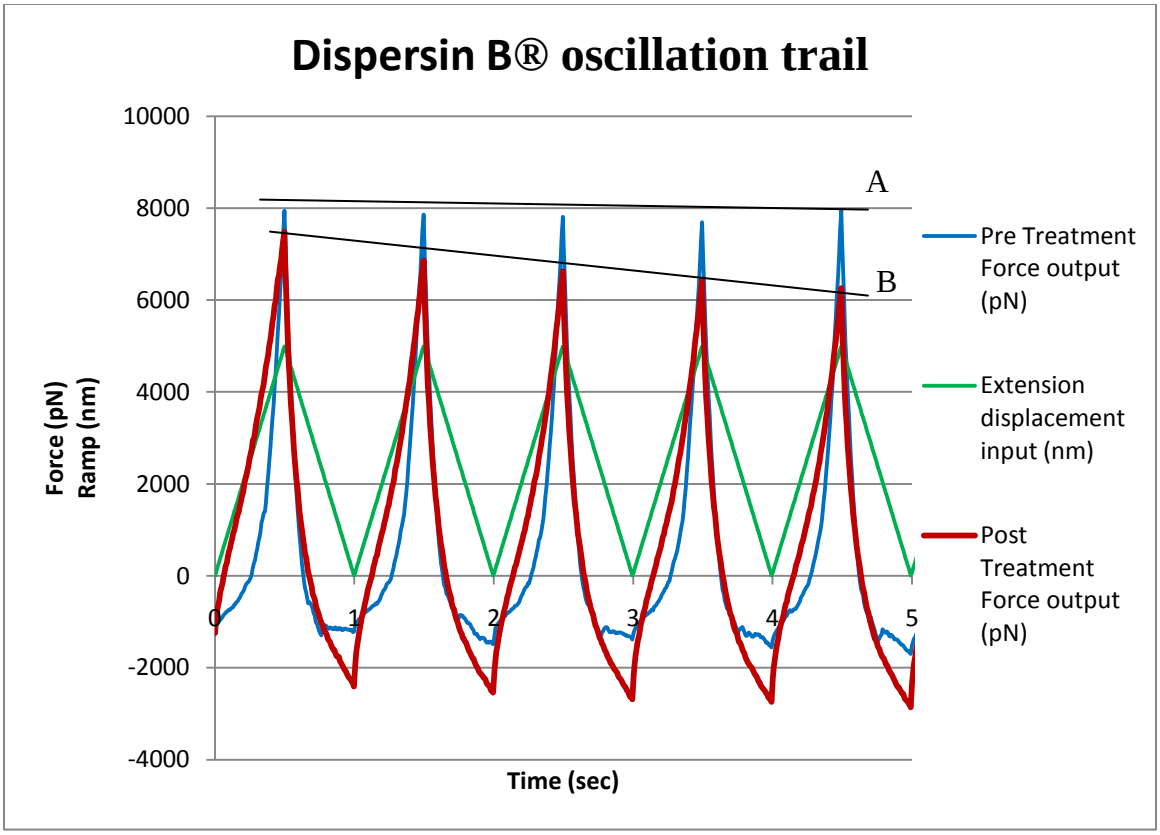

Figure 94) Dispersin B ® oscillation trial with displacement input plotted with pre and post DispersinB® treated biofilm responses A) pre-treatment damping B) post-treatment damping

The DispersinB® has been shown to soften the biofilm in both the flow cell experimentations and AFM indentation experiments. The triangular wave labeled extension displacement, in Figure 94, represents the input or extension of the cantilever

beam into the biofilm. The force outputs are plotted both before and after the DispersinB® treatment. Notice both the pre and post-treatment peaks have a line labeled A and B consecutively. During the pre-treatment oscillations there was a small amount of damping resulting in a less steep slope of line A. After the biofilm has been treated, the slope of line B is much steeper, representing significant damping after the DispersinB® treatment. The DispersinB® treatment created a more viscous biofilm with larger damping capabilities.

GENERAL DISCUSSION

The three main objectives in this project were to develop and apply techniques to characterize the viscoelastic nature of *S. epidermidis* biofilms, demonstrate change in biofilm material properties in response to chemical and enzymatic treatments, and develop methods to characterize viscoelastic changes in mechanical properties through the use of constitutive equations and basic modeling.

There were two techniques developed to characterize the viscoelastic nature of biofilms. The first technique, a fluid shear technique, was developed in which *S. epidermidis* biofilm was grown in a capillary flow cell. The biofilm had a fluid shear stress applied for a set interval of fifteen seconds, while displacements were recorded. The biofilm was treated then, another fluid shear stress was applied while recording displacements. This method has limitations, the biggest of which is the inherent complexity of fluid-structure interactions. These interactions can be considered negligible if the biofilm structure remains intact throughout the testing. This technique is powerful in visualizing the treatments effect on the biofilm. In addition, failure events and removal of the biofilm can be observed with this capillary flow cell technique. It is also possible to determine structural displacements and compare them to post-treatment displacements to gather insight into material properties.

The second technique developed used an AFM to mechanically interrogate the biofilm by indenting a tip of known geometry into the biofilm surface. *S. epidermidis* biofilm was grown on silicon wafers which were placed under the AFM. The biofilm

then was indented to a depth of 5μm, the biofilm was treated, and then indented to a depth of 5μm at the same location. Indentions were run at various loading rates to observe rate dependency. The major limitation to this technique was the variability in biofilm thickness. Without knowing the thickness of the biofilm on the silicon wafer it becomes difficult to model or determine constitutive equations. The advantage to the AFM approach is that rate dependencies can be observed which is not possible with the capillary flow cell approach.

The capillary flow cell and micro-indentation experiments on *S. epidermidis* biofilms have shown that these films behave viscoelastically, having both elastic and viscous components. Both approaches also show that iron chloride and chlorhexidine have a stiffening effect on the biofilm. Both techniques also have shown that the urea and DispersinB® create a more viscous biofilm. In the capillary flow cell technique these treatments appeared to create a weaker bonding EPS which allowed for more failure or erosion of the biofilm.

It was also shown that the use of a four parameter Burger model can be used to model the structural response of these biofilms. Using the capillary flow cell experiment, changes in the Burger model parameters were calculated between pre-treatment and post treatment. Since the measured response is structural, and not constitutive, only the change in model parameters can be compared. One limitation to the Burger model is that the model will strain infinitely under even a low stress. The biofilms however, under a low fluid shear stress do not deform viscously down the capillary flow cell. Future work might include adding plastic sliders to the model to capture the plasticity seen in many of

the untreated samples. The Burger model does not restrict irreversible viscous flow which is not seen in the biofilm structures. If the biofilm structures behaved as a true Burger model biofilm it would continually creep along the capillary under normal growth conditions.

While previous studies have quantified material parameters of biofilms with considerable variability, this study concentrated on the change in material properties from pre-treatment to post-treatment. Sutton's work (Sutton 2008) showed the same stiffing effect of the iron chloride on the biofilm. The urea created a more viscous biofilm in Sutton's study as well.

Table 18) Comparison of results from Sutton's work

		E_{1post}/E_{1pre}	E_{2post}/E_{2pre}	η_{1post}/η_{1pre}	η_{2post}/η_{2pre}
$FeCl_2$	Sutton	0.932	0.543	0.664	1.327
	This study	0.48	1.14	5.82	4.89
urea	Sutton	0.225	0.162	0.219	0.453
	This study	0.56	0.65	0.05	0.38

For comparing results from this study and Sutton's work Table 18 was created. It is difficult to compare change in parameters between the two studies because different concentrations of treatment were used and vastly different techniques were used. A possibility for this variation could result from the rheometry approach used by Sutton where the scale of testing was greater than a hundred times larger than this study. Another possibility for the large numerical differences could be due to the growth procedures between the two studies. Sutton's biofilm grew on agar, in a shear stress free environment where as in both techniques outlined here the biofilm grew in fluid shear

conditions. Typically, a biofilm grown under fluid shear conditions have shown to be stiffer than a biofilm grown in static conditions.

Future work was proposed to increase fluid shear rates in conjunction with presenting a treatment for efficient biofilm removal. One trial study was conducted using a urea treatment in the capillary flow cell for an extended fluid shear. Much of the biofilm was removed within the first few minutes of the trial showing the potential of a combined treatment and mechanical stress removal method. Another proposed method for examining these biofilms was to use the AFM to apply cyclic loading onto the biofilm structure. Utilizing this approach, more knowledge could be gained about the energy absorbance or viscous aspects of biofilms. In conclusion, quantification of biofilm material properties and demonstration that their properties can be altered by chemical or enzymatic treatments has been shown. This opens the door to development of new technologies for controlling detrimental biofilm based on targeting biofilm cohesion rather than killing microorganisms.

REFERENCES CITED

[1] Attard, Phil. "Measurement and interpretation of elastic and viscoelastic properites withatomic force microscope." *Journal of Physics: Condensed Matter,* 2007: 33pp.

[2] Binnig, G, CF Quate, and C Gerber. "Atomic Force Microscope." *Phys. Rev. Lett,* 1986: 56(9):930-933.

[3] Cense, AW, EAG Peeters, B Gottenbos, FPT Baaijens, AM Nuijs, and MEH van Dongen. "Mechanical properties and failure of Streptococcus mutans biofilms, studied using a microindentation device." *Journal of Microbiological Methods,* 2006: 67: 463-472.

[4] Chaignon, P, I Sadovskaya, Ch Ragunah, N Ramasubbu, JB Kaplan, and S Jabbouri. "Susceptibility of staphylococcal biofilms to enzymatic treatments depends on thier chemical compostion." *Applied Microbial and Cell Physiology*, 2007: 75: 125-132.

[5] Chen, X, and P.S. Stewart. "Role of electrostatic interactions in cohsion of bacterial biofilms." *Appl Microbiol Biotechnol*, 2002: 59:718-720.

[6] Chen, X., and P. Stewart. "Biofilm removal caused by chemical treatments." *Wat. Res.*, 2000: Vol. 34, No 17, pp. 4229-4233.

[7] Costerton, J.W., P.S. Stewart, and E.P. Greenberg. "Bacterial Biofilms: A Common Cause of Persistent Infections." *Science*, 1999: Vol. 284 no. 5418, pp.1318-1322.

[8] Costerton, JW, PS Stewart, and EP Greenberg. "Bacterial Biofilms a common cause of persistent infections." *Science,* 1999: 284:1318-1322.

[9] Dunsmore, BC, A Jacobsen, L Hall-Stoodley, CJ Bass, HM Lappin-Scott, and P Stoodley. "The influence of fluid shear on the structure and material properties of sulphate-reducing bacterail biofilms." *Journal of Industrial Microbiology & Biotechnology*, 2002: 29:347-353.

[10] Flemming, HC, J Wingender, C Mayer, V Koerstgens, and W Borchard. "Cohesiveness in biofilim matrix polymers." *Allison D, Gilmpert P, Lappin-Scott HM, Wilson M, editors. Cambridge: SGM Symposium Series 59.* Cambridge Universtiy Press. p 87-105, 2000. 87-59.

[11] Garrett, TR, M Bhakoo, and Z Zhang. "Bacterial adhesion and biofilms on surfaces." *Progress in Natural Science*, 2008: 19: 1049-1056.

[12] Gotz, F. "Staphylococcus and biofilms." *Mol Microbiol*, 2002: 43:1367-1378.

[13] Hamilton, MA. "Tesstin antimicrobials against biorilm bacteria." *J AOAC Int*, 2002: 85:479-485.

[14] Janmey, Paul, and Christoph Schmidt. "Experimental measurements of intracellular mechanics." In *Cytoskeletal Mechanics*, by Mohammad RK Mofrad and Roger D Kamm, 18-49. New York: Cambridge University Press, 2006.

[15] Kaplan, JB, R Chandran, N Ramasubbu, and DH Fine. "Detachment of Actinobacillus actinomycetemcomitans biofilm cells by an endogenous b-hexosaminidase activity." *Journal of Bacteriology*, 2003: 185: 4693-4698.

[16] Klapper, I, C.J. Rupp, R Cargo, B Purvedorj, and P Stoodley. "Viscoelastic Fluid Description of Bacterial Bioflm Material Properties." *Biotechnology and Bioenineering*, 2002: 80: 289-296.

[17] Korstgens, V, HC Flemming, J Wingender, and W Borchard. "Uniaxial compression measurement device for investigation of the mechanical stability of biofilms." *Journal of Microbiological Methods*, 2001: 46:9-17.

[18] Lakes, Roderic S. *Viscoelastic Solids.* Boca Raton, Florida: CRC Press LLC, 1999.

[19] Macioce, Paul. "Viscoelastic Damping 101." Roush Industries, Inc.

[20] Nicollea, C., M. Van Loosdrecht, and J. Heihnen. "Wastewater treatment with particulate biofilm reactors." *J. Biotechnol.*, 2000: 80: 1-33.

[21] Poppele, EH, and RM Hozalski. "Micro-cantilever method for measuring the tensile strength of biofims and microbial flocs." *Journal of Microbiological Methods*, 2003: 55: 607-615.

[22] Shaw, T, M Winston, C Rupp, I Klapper, and P Stoodley. "Commonality of elastic relaxation times in biofilms." *Phys. Rev. Lett.*, 2004: 93: 1-4.

[23] Stewart, PS, and JW Costerton. "Antibiotic resistance of bacteria in biofilms." *Lancet*, 2001: 358: 135-128.

[24] Stoodley, P, Z Lewandowski, JD Boyle, and HM Lappin-Scott. "Structural Deformation of Bacterial Biofilms Caused by Short-Term Fluctuations in Fluid Shear: An In Situ Investigation of Biofilm Rheology." *Biotechnology and Bioengineering*, 1999: 65:83-92.

[25] Stoodley, P., R. Cargo, C.J. Rupp, S. Wilson, and I. Klapper. "Biofilm material properties as related to shear-induced deformation and detachment phenomena." *Journal of Industrial Microbiology and Biotechnology*, 2002: 29:361-367.

[26] Sutton, Michael. "Quantifying the Viscoelastic Properties of Treated and Untreated Pseudomonas aeruginosa and Staphylococcus epidermidis Biofilms Using a Rheological Creep Anaylsis." *Masters Thesis: Montana State University*, 2008.

[27] Towler, B, A Cunningham, P Stoodley, and L McKittrick. "A model fo Fluid-Bioflim Interactions Using a Burger Material Law." *Biotechnology and Bioenineering*, 2007: 96:259-271.

[28] Towler, BW, CJ Rupp, AB Cunningham, and P Soodley. "Viscoelastic Properties of a Mixed Culture Biofilm from Rheometer Creep Analysis." *Biofouling*, 2003: 19:279-285.

[29] Townsin, L R. "The ship hull fouling penalty." *Biofouling*, 2003: 19 (Suppl): 9-15.

[30] Vieira, MJ, LF Melo, and MM Pinheiro. "Biofilm formation: hydrodynamic effects on internal diffusion and structure." *Biofoulding*, 1993: 7:67-80.

[31] Vinogradov, AM, M Winston, CJ Rupp, and P Stoodley. "Rheology of biofilms formed from the dental plaque pathogen Streptococcus mutans." *Biofilms*, 2004: 1:49-56.

[32] Walker, JT, CW Mackerness, D Mallon, T Makin, T Williets, and CW Kevil. "Control of legionella-pneumophila in a hospital water-system by chlorine dioxide." *J Indust Microbiol*, 1995: 15:384-390.

[33] Zelver, N. *Biofilm development and associated energy losses in water conduits. M.S. Thesis.* Houston, TX.: Rice Universtiy, 1979.

APPENDICES

APPENDIX A

CAPTURED IMAGES AND GRAPHS FOR ALL CREEP RECOVERY DATA

Iron Chloride Trial #2

$FeCl_2$ Pre-treatment fluid shear test trial 2

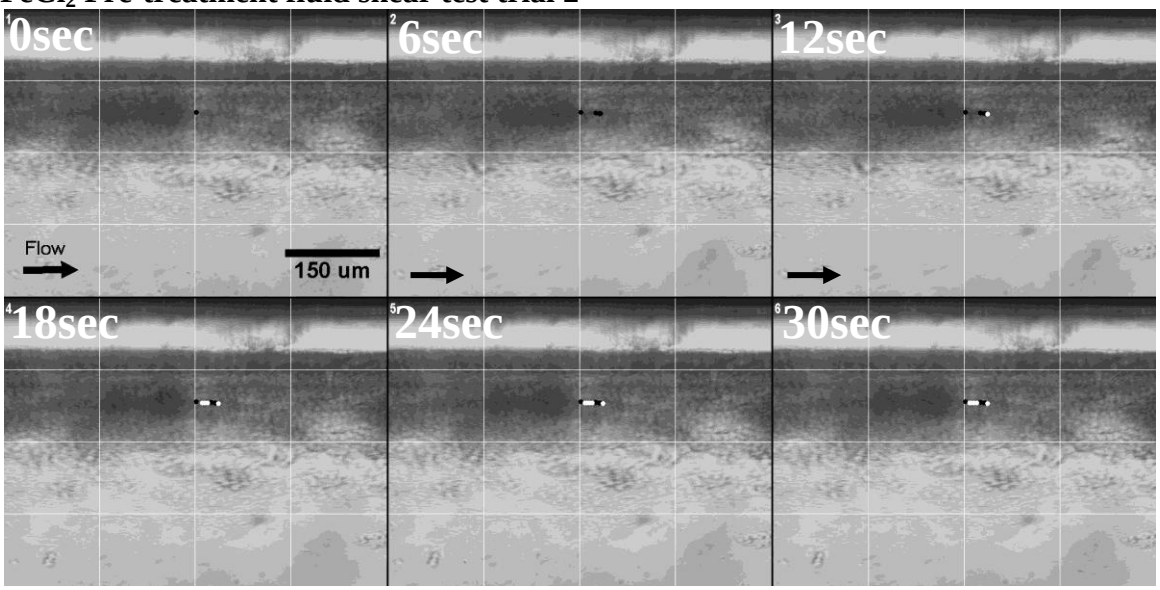

Figure 95) Pre-treatment fluid shear creep relaxation test for a *S. epidermidis* biofilm cluster with 15sec fluid shear and 15 sec relaxation period. 0sec frame is the initial configuration of the biofilm and 30sec is the final configuration after the fluid shear test. (Black dots follow displacement through elongation of a single point and white dots follow displacement through relaxation of that single point)

$FeCl_2$ Post-treatment fluid shear test trial 2

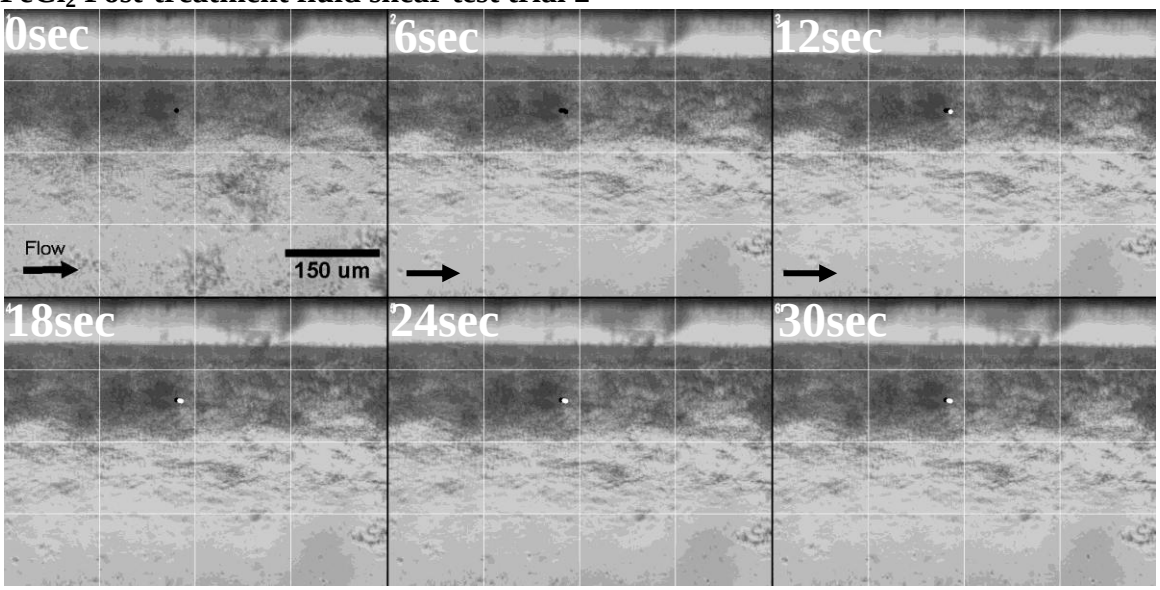

Figure 96) Post-treatment fluid shear creep relaxation test for a *S. epidermidis* biofilm cluster treated with 0.5M $FeCl_2$ and 15sec fluid shear and 15 sec relaxation period. 0sec frame is the initial configuration of the biofilm and 30sec is the final configuration after the fluid shear test. (Black dots follow displacement through elongation of a single point and white dots follow displacement through relaxation of that single point)

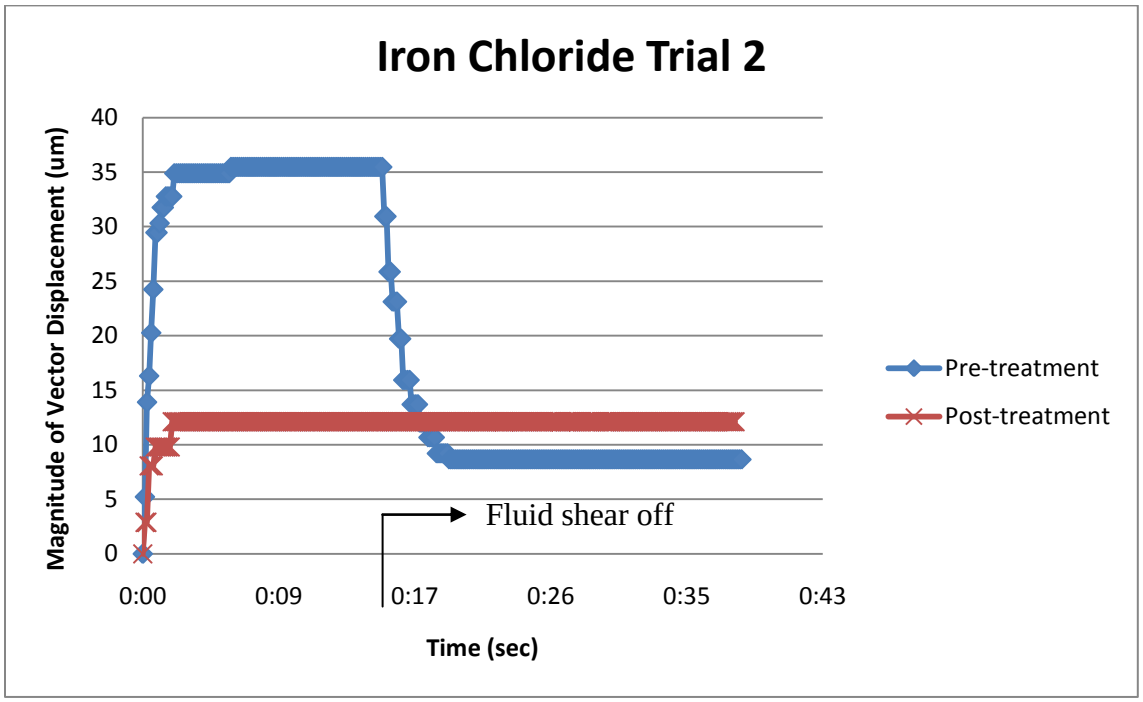

Figure 97) Iron chloride treatment of average of vector displacements for specified spots on the biofilm cluster

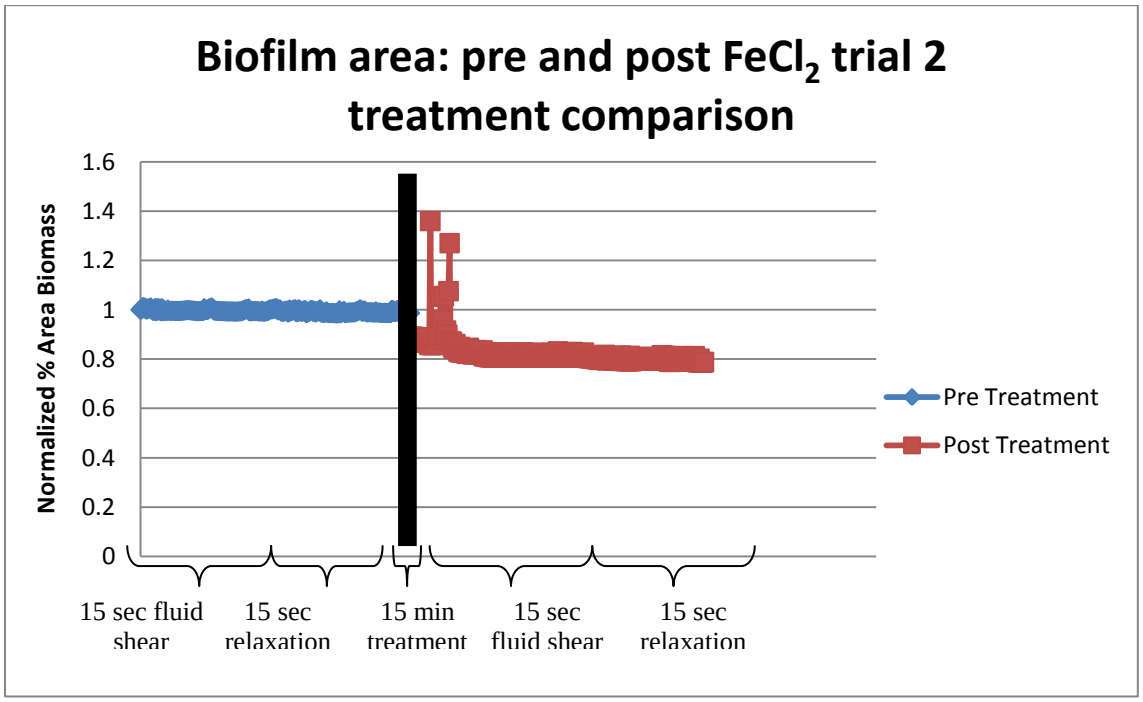

Figure 98) Pre and post-treatment measurement of biomass % area during fluid shear test for iron chloride

Iron Chloride Trial 3

$FeCl_2$ Pre-treatment fluid shear test trial 3

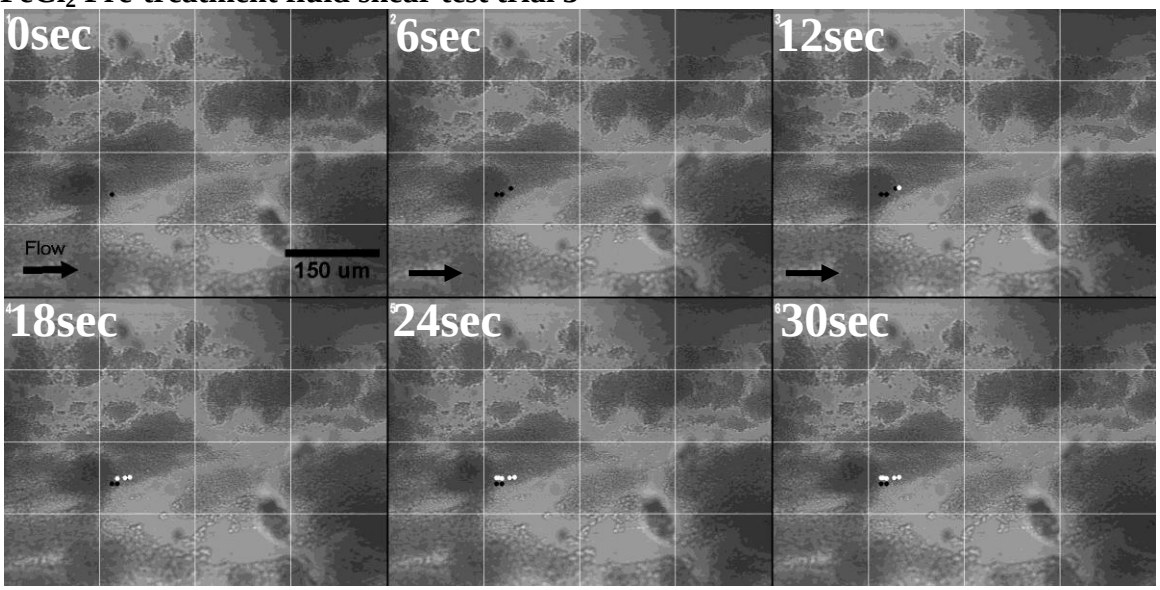

Figure 99) Pre-treatment fluid shear creep relaxation test for a *S. epidermidis* biofilm cluster with 15sec fluid shear and 15 sec relaxation period. 0sec frame is the initial configuration of the biofilm and 30sec is the final configuration after the fluid shear test. (Black dots follow displacement through elongation of a single point and white dots follow displacement through relaxation of that single point)

$FeCl_2$ Post-treatment fluid shear test trial 3

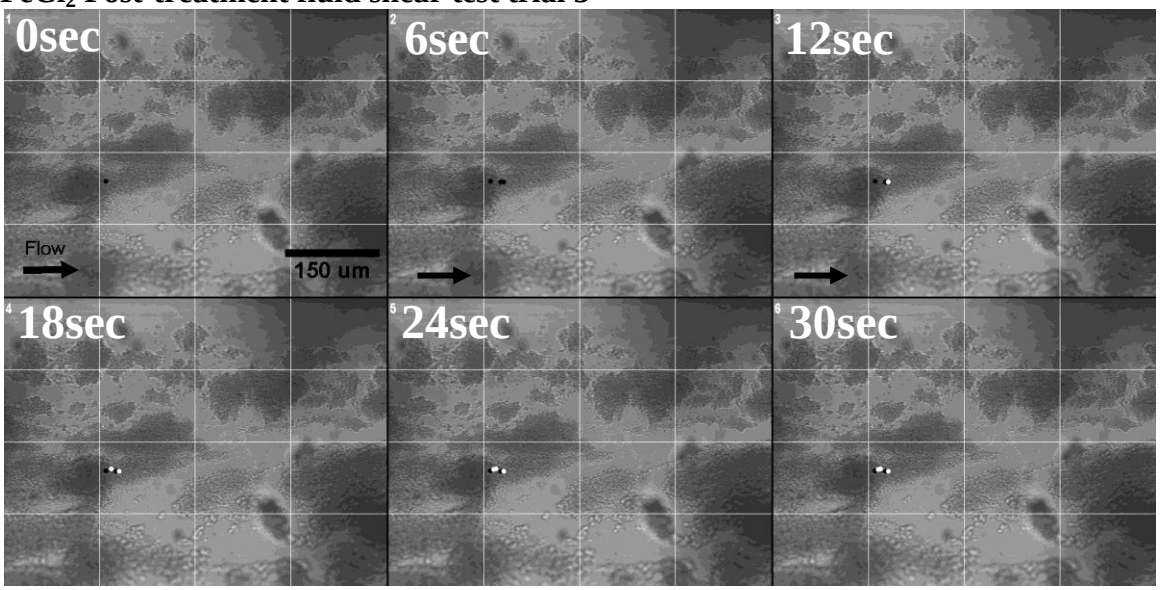

Figure 100) Post-treatment fluid shear creep relaxation test for a *S. epidermidis* biofilm cluster treated with 0.5M $FeCl_2$ and 15sec fluid shear and 15 sec relaxation period. 0sec frame is the initial configuration of the biofilm and 30sec is the final configuration after the fluid shear test. (Black dots follow displacement through elongation of a single point and white dots follow displacement through relaxation of that single point)

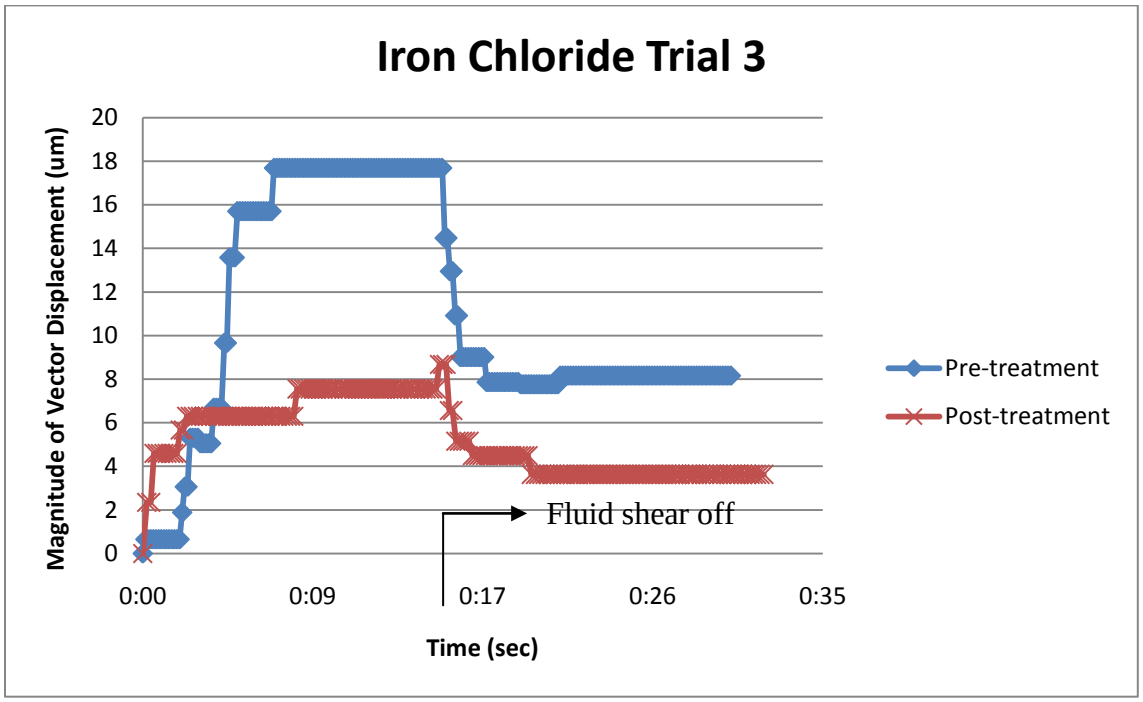

Figure 101) Iron chloride treatment of average of vector displacements for specified spots on the biofilm cluster

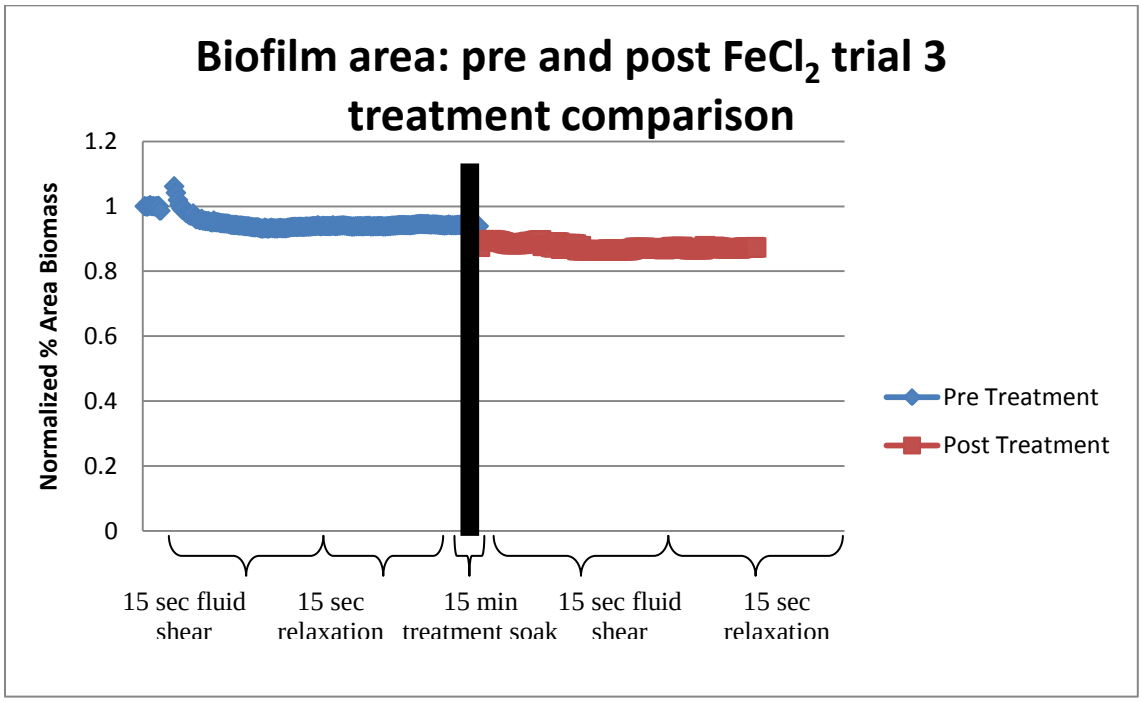

Figure 102) Pre and post-treatment measurement of biomass % area during fluid shear test for iron chloride

Chlorhexidine Trial 2

Chlorhexidine Pre-treatment fluid shear test trial 2

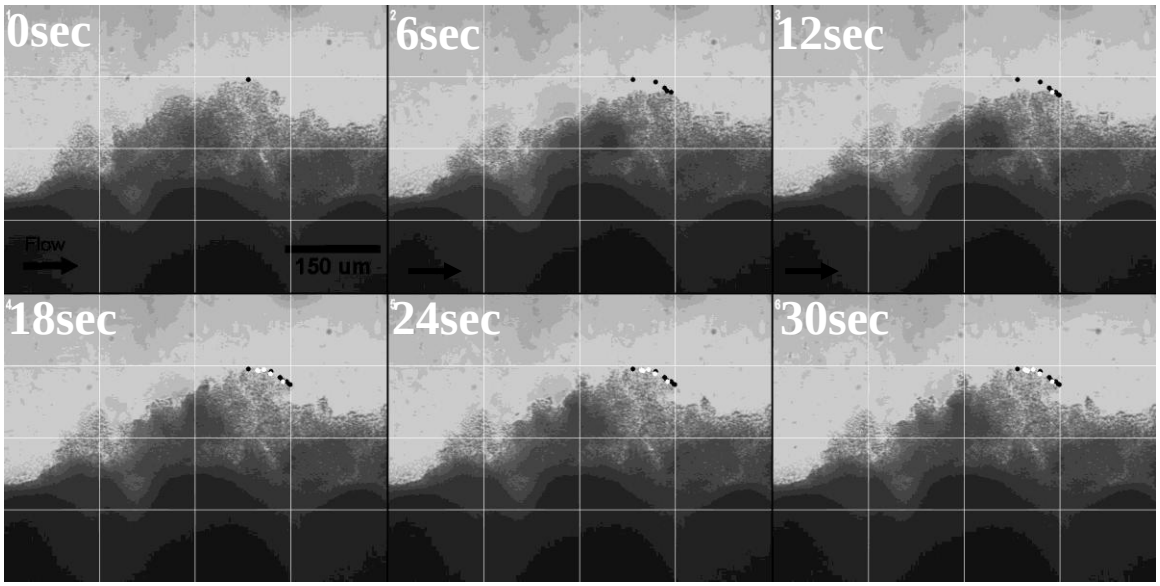

Figure 103) Pre-treatment fluid shear creep relaxation test for a *S. epidermidis* biofilm cluster with 15sec fluid shear and 15 sec relaxation period. 0sec frame is the initial configuration of the biofilm and 30sec is the final configuration after the fluid shear test. (Black dots follow displacement through elongation of a single point and white dots follow displacement through relaxation of that single point)**Chlorhexidine Post-treatment fluid shear test trial 2**

Chlorhexidine Post-treatment fluid shear test trial 2

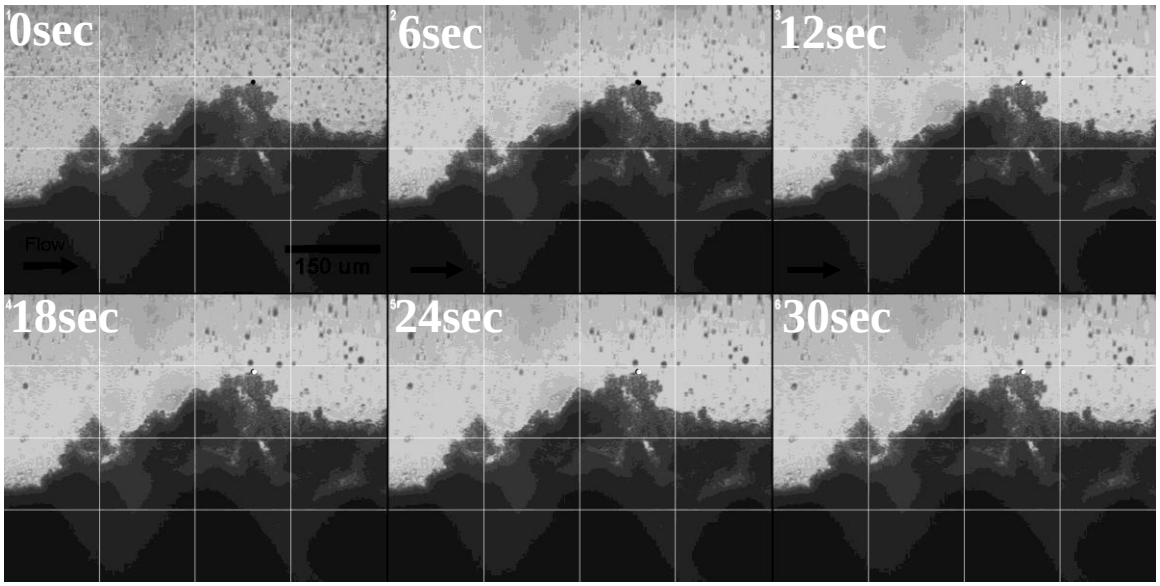

Figure 104) Post-treatment fluid shear creep relaxation test for a *S. epidermidis* biofilm cluster treated with 0.1% chlorhexidine and 15sec fluid shear and 15 sec relaxation period. 0sec frame is the initial configuration of the biofilm and 30sec is the final configuration after the fluid shear test. (Black dots follow displacement through elongation of a single point and white dots follow displacement through relaxation of that single point)

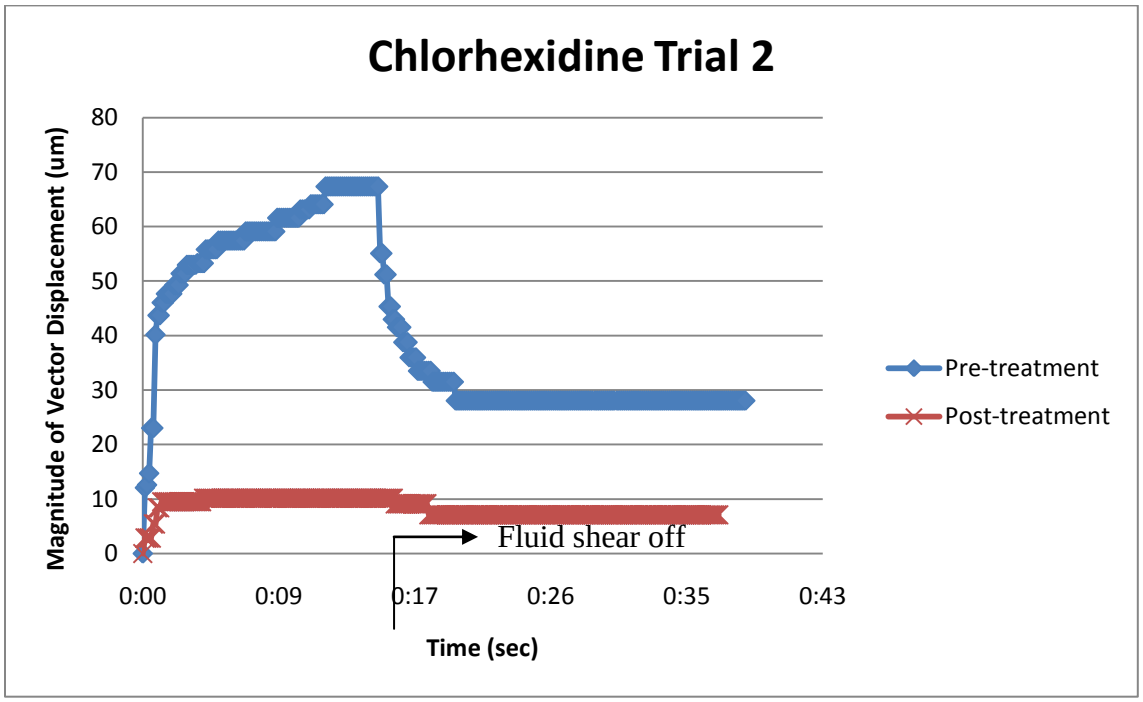

Figure 105) Chlorhexidine treatment of average of vector displacements for specified spots on the biofilm cluster

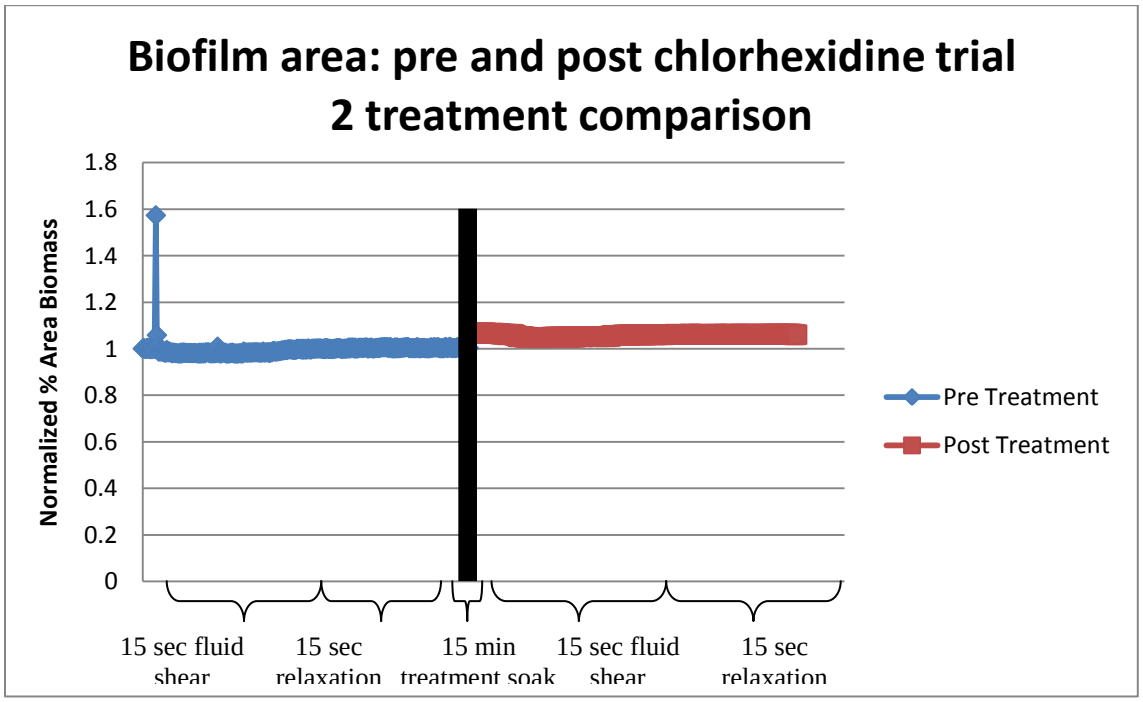

Figure 106) Pre and post-treatment measurement of biomass % area during fluid shear test for chlorhexidine

Chlorhexidine Trial 3

Chlorhexidine Pre-treatment fluid shear test trial 3

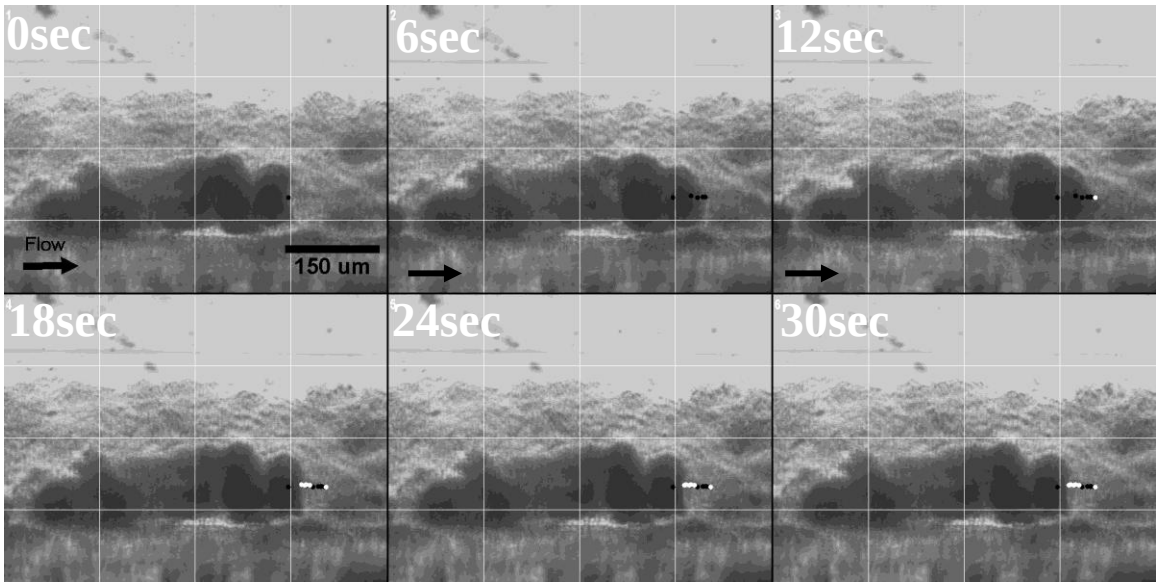

Figure 107) Pre-treatment fluid shear creep relaxation test for a *S. epidermidis* biofilm cluster with 15sec fluid shear and 15 sec relaxation period. 0sec frame is the initial configuration of the biofilm and 30sec is the final configuration after the fluid shear test. (Black dots follow displacement through elongation of a single point and white dots follow displacement through relaxation of that single point)

Chlorhexidine Post-treatment fluid shear test trial 3

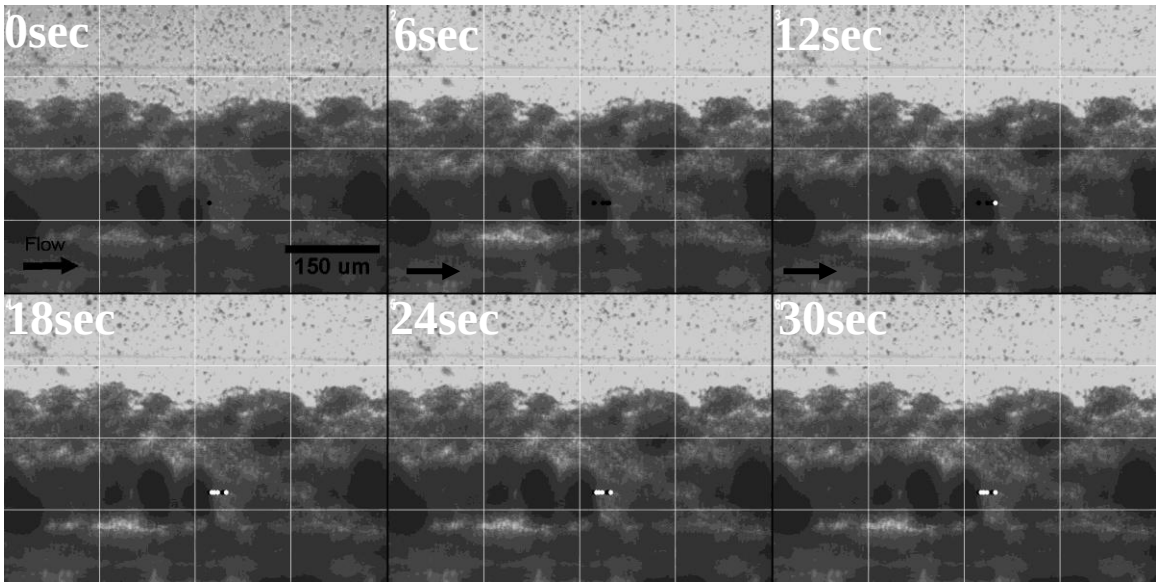

Figure 108) Post-treatment fluid shear creep relaxation test for a *S. epidermidis* biofilm cluster treated with 0.1% chlorhexidine and 15sec fluid shear and 15 sec relaxation period. 0sec frame is the initial configuration of the biofilm and 30sec is the final configuration after the fluid shear test. (Black dots follow displacement through elongation of a single point and white dots follow displacement through relaxation of that single point)

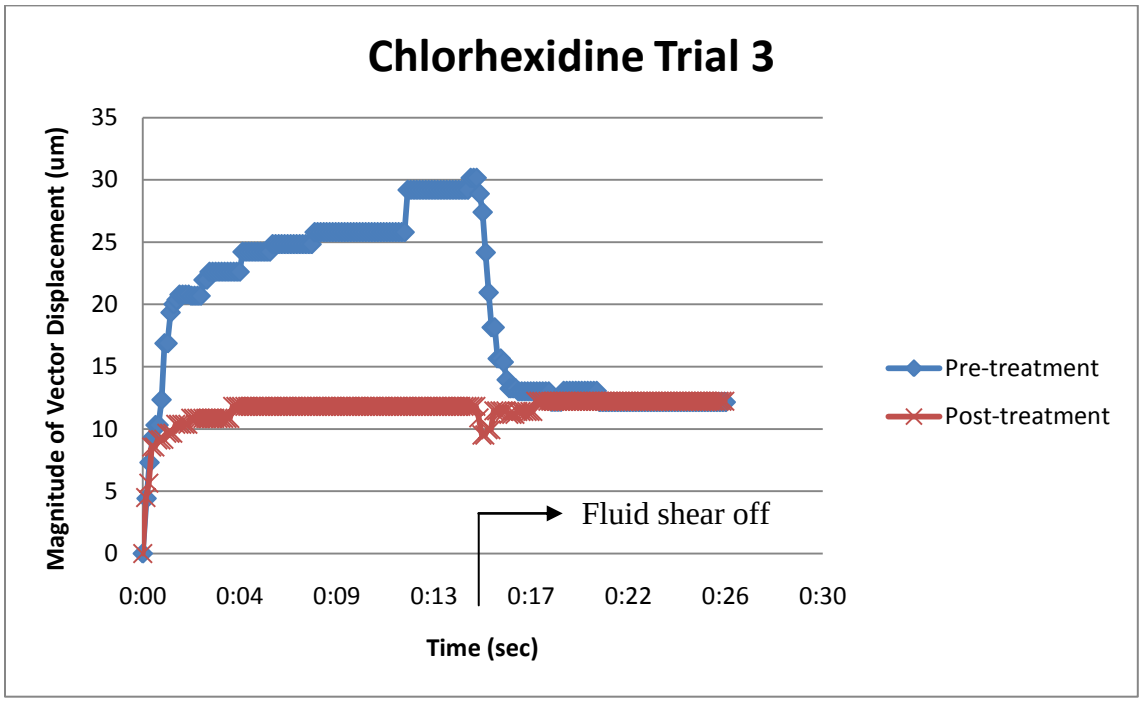

Figure 109) Chlorhexidine treatment of average of vector displacements for specified spots on the biofilm cluster

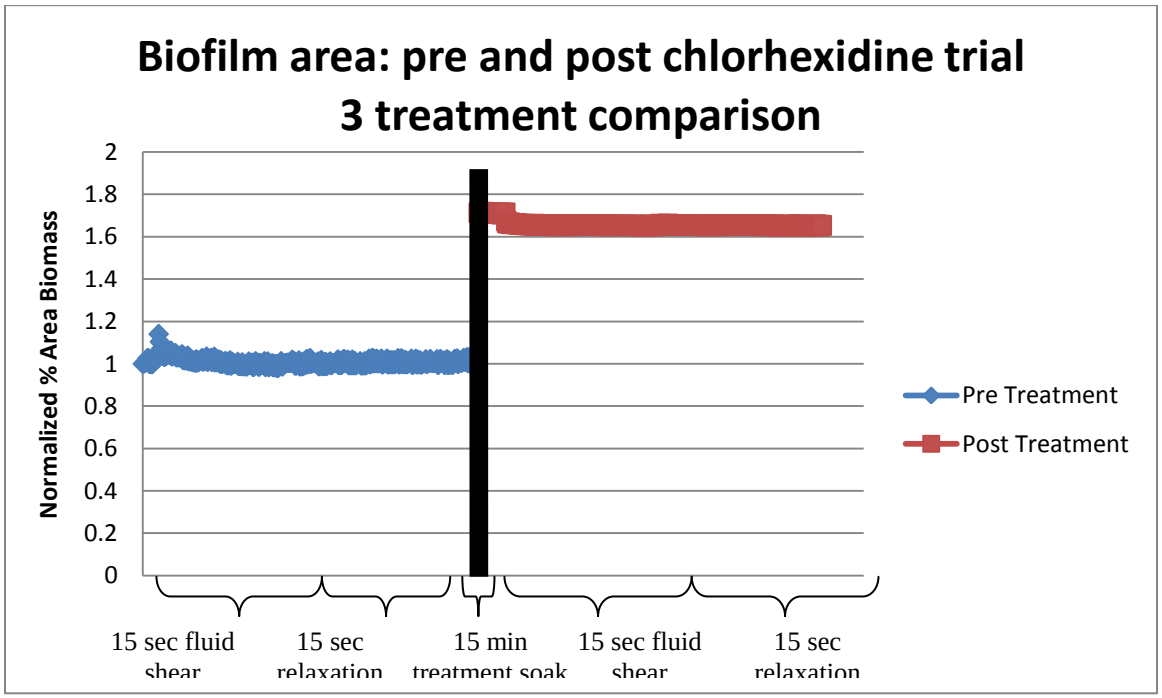

Figure 110) Pre and post-treatment measurement of biomass % area during fluid shear test for chlorhexidine

Urea Trial 2

Urea Pre-treatment fluid shear test trial 2

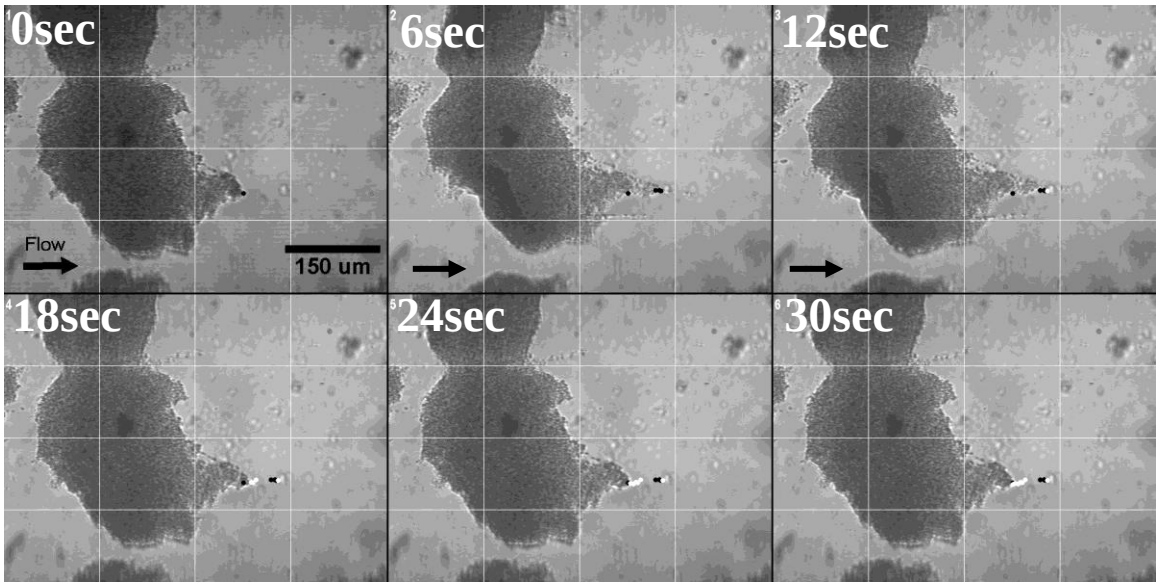

Figure 111) Pre-treatment fluid shear creep relaxation test for a *S. epidermidis* biofilm cluster with 15sec fluid shear and 15 sec relaxation period. 0sec frame is the initial configuration of the biofilm and 30sec is the final configuration after the fluid shear test. (Black dots follow displacement through elongation of a single point and white dots follow displacement through relaxation of that single point)

Urea Post-treatment fluid shear test trial 2

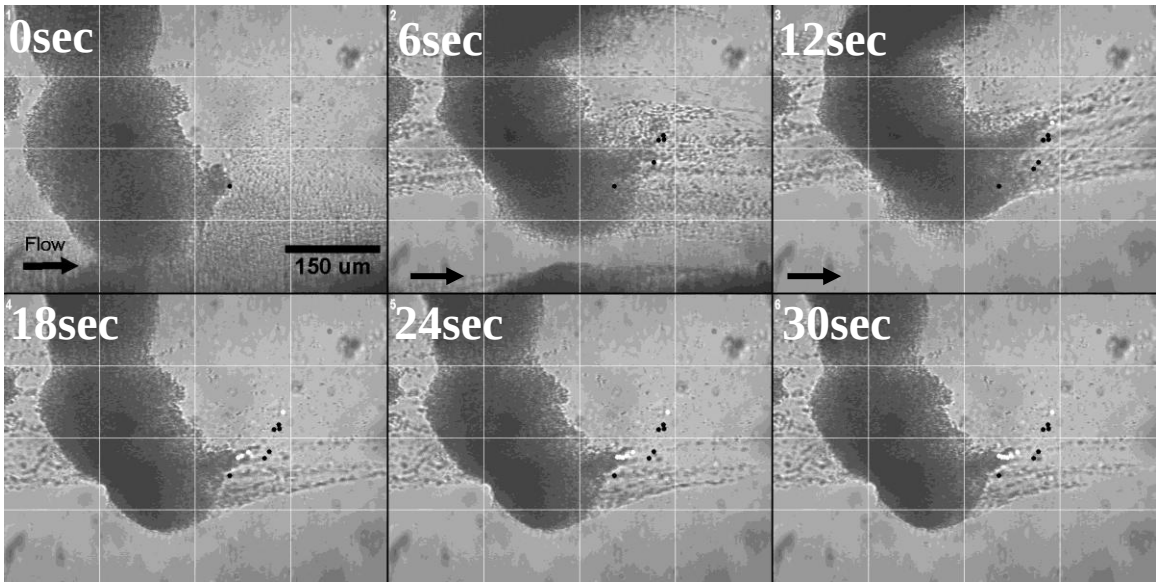

Figure 112) Post-treatment fluid shear creep relaxation test for a *S. epidermidis* biofilm cluster treated with 0.1M urea and 15sec fluid shear and 15 sec relaxation period. 0sec frame is the initial configuration of the biofilm and 30sec is the final configuration after the fluid shear test. (Black dots follow displacement through elongation of a single point and white dots follow displacement through relaxation of that single point)

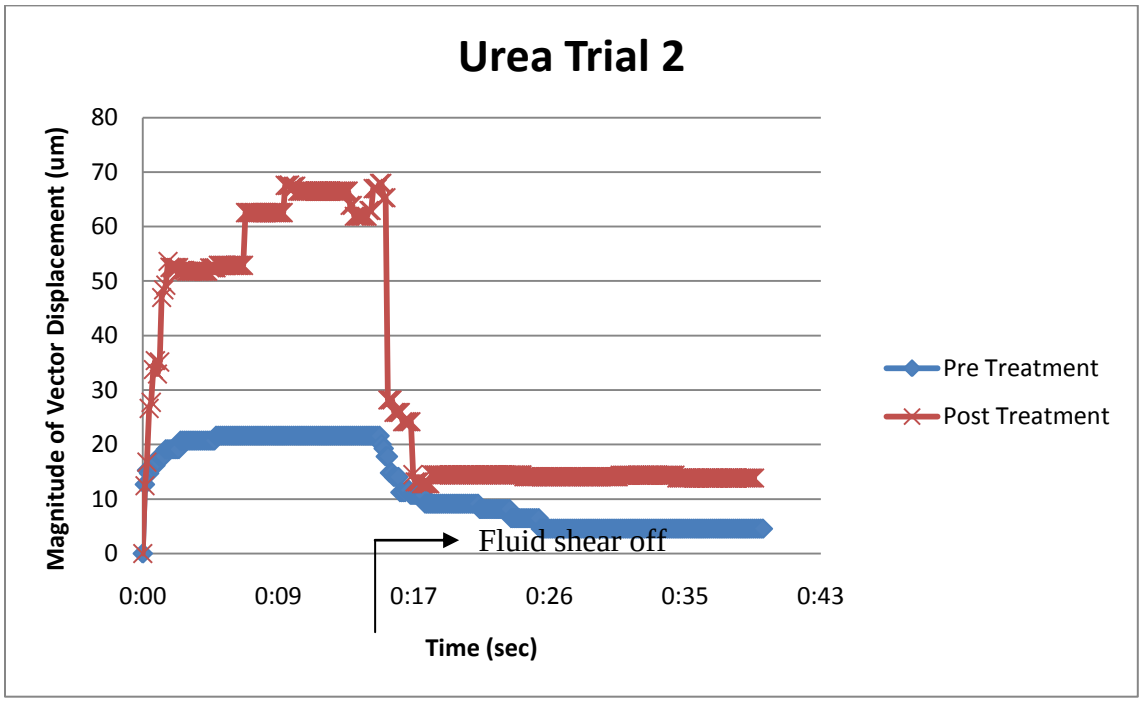

Figure 113) Urea treatment of average of vector displacements for specified spots on the biofilm cluster

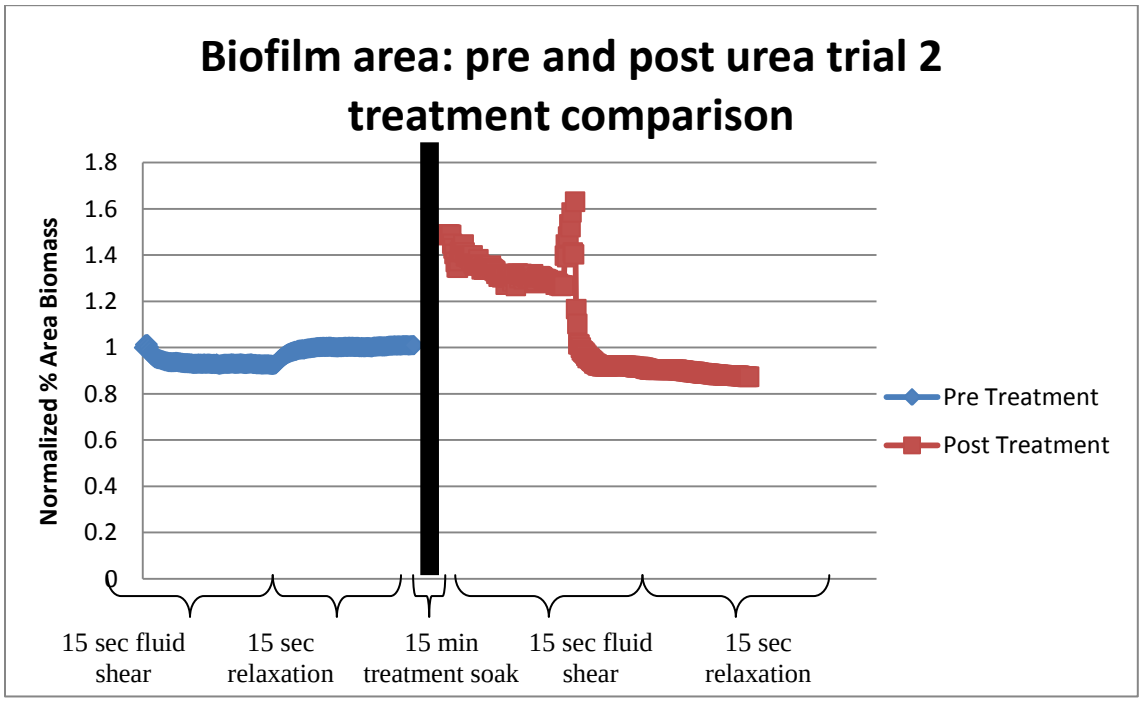

Figure 114) Pre and post-treatment measurement of biomass % area during fluid shear test for urea

Urea Trial 3

Urea Pre-treatment fluid shear test trial 3

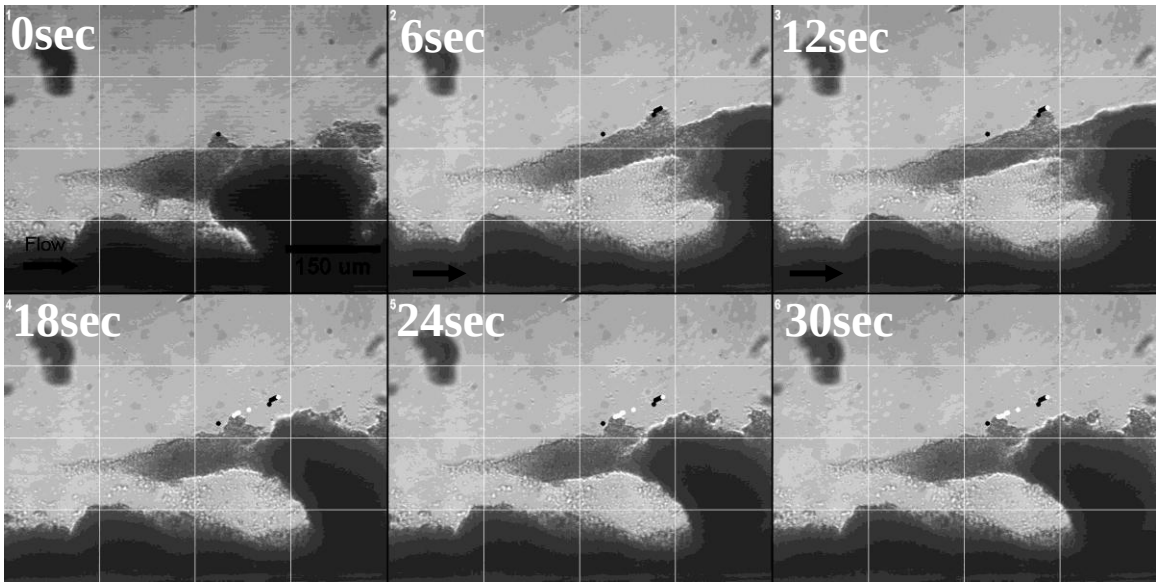

Figure 115) Pre-treatment fluid shear creep relaxation test for a *S. epidermidis* biofilm cluster with 15sec fluid shear and 15 sec relaxation period. 0sec frame is the initial configuration of the biofilm and 30sec is the final configuration after the fluid shear test. (Black dots follow displacement through elongation of a single point and white dots follow displacement through relaxation of that single point)

Urea Post-treatment fluid shear test trial 3

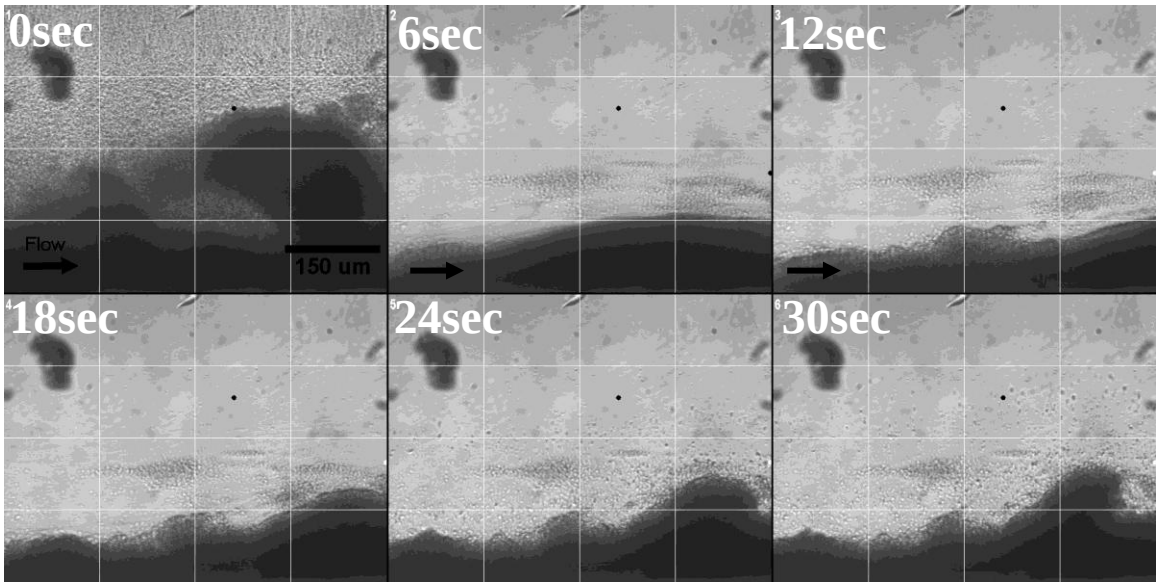

Figure 116) Post-treatment fluid shear creep relaxation test for a *S. epidermidis* biofilm cluster treated with 0.1M urea and 15sec fluid shear and 15 sec relaxation period. 0sec frame is the initial configuration of the biofilm and 30sec is the final configuration after the fluid shear test. (Black dots follow displacement through elongation of a single point and white dots follow displacement through relaxation of that single point)

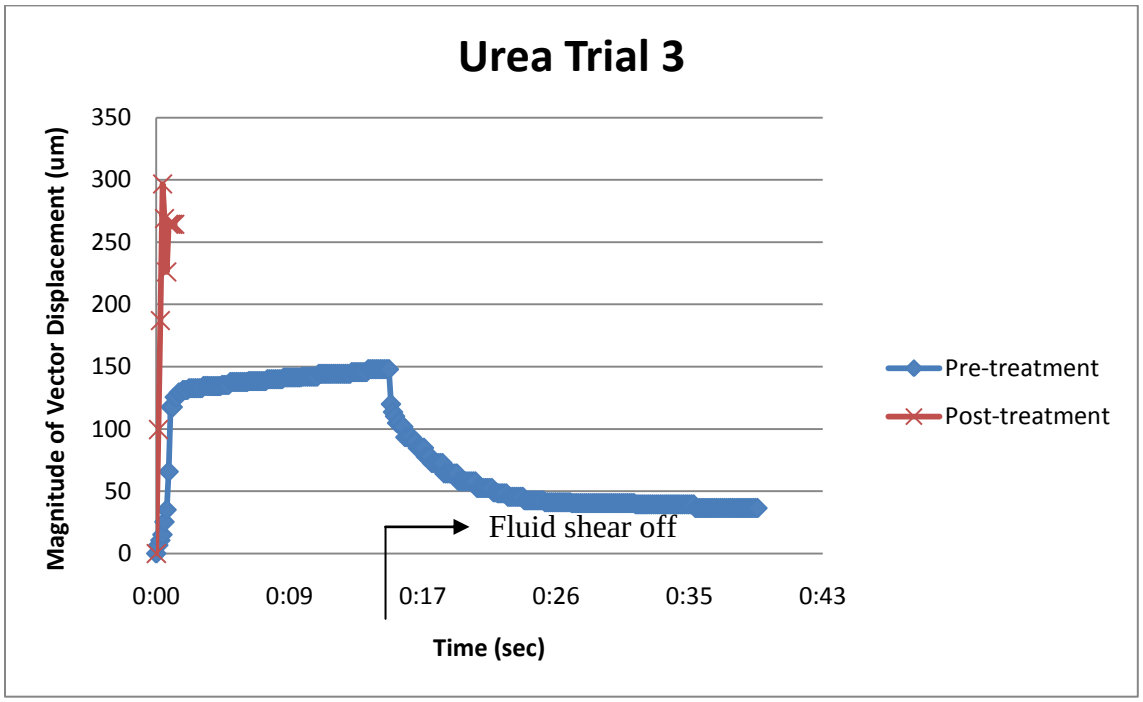

Figure 117) Urea treatment of average of vector displacements for specified spots on the biofilm cluster (Post-treatment reference points removed during fluid shear)

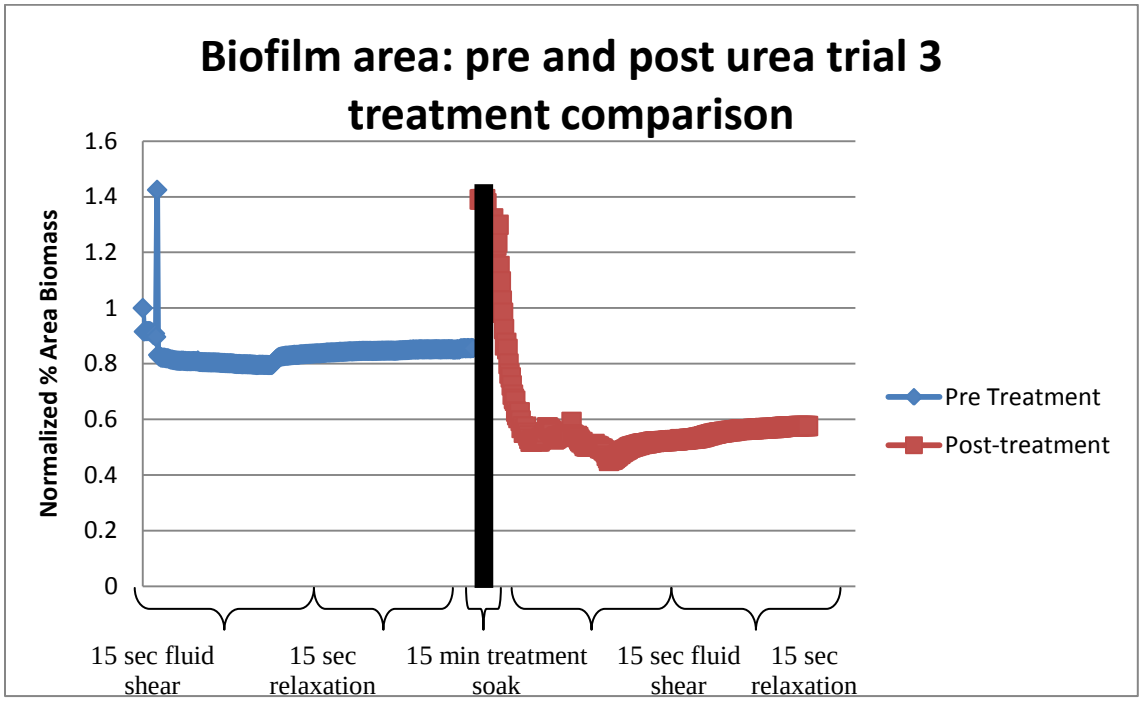

Figure 118) Pre and post-treatment measurement of biomass % area during fluid shear test for urea

DispersinB® Trial 2

DispersinB® Pre-treatment fluid shear test trial 2

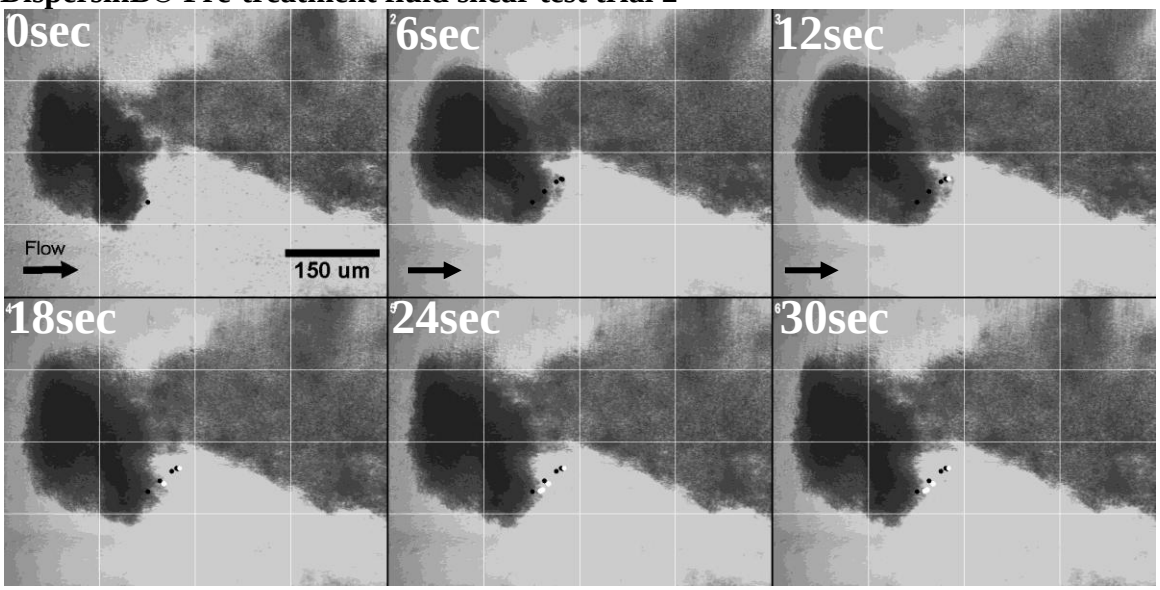

Figure 119) Pre-treatment fluid shear creep relaxation test for a *S. epidermidis* biofilm cluster with 15sec fluid shear and 15 sec relaxation period. 0sec frame is the initial configuration of the biofilm and 30sec is the final configuration after the fluid shear test. (Black dots follow displacement through elongation of a single point and white dots follow displacement through relaxation of that single point)

DispersinB® Post-treatment fluid shear test trial 2

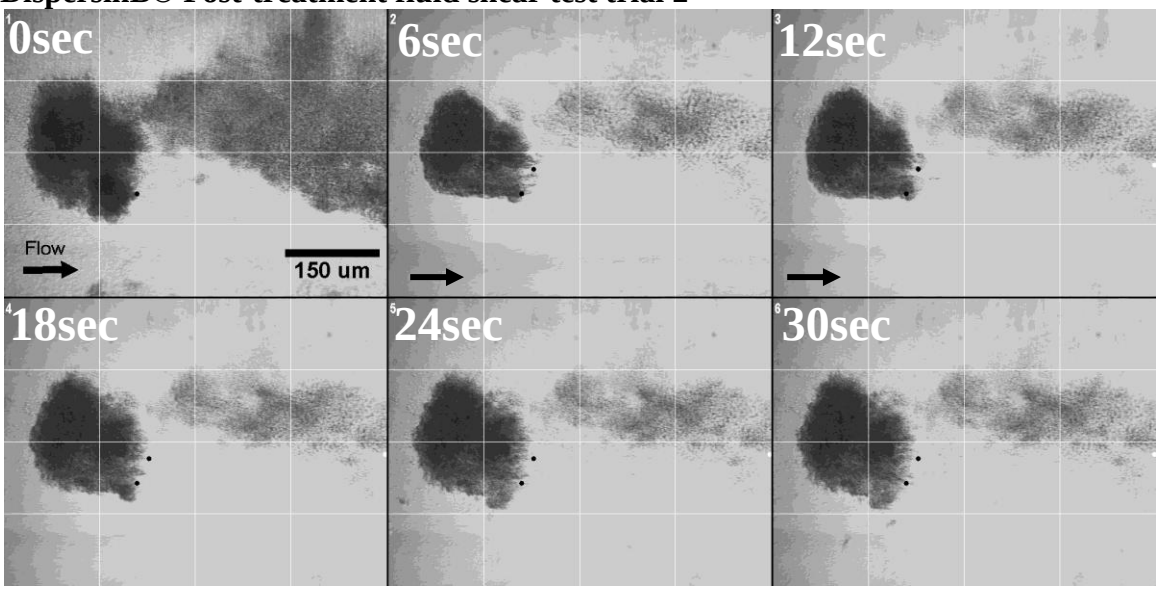

Figure 120) Post-treatment fluid shear creep relaxation test for a *S. epidermidis* biofilm cluster treated with 40 μg/mL of Dispersin B ® and 15sec fluid shear and 15 sec relaxation period. 0sec frame is the initial configuration of the biofilm and 30sec is the final configuration after the fluid shear test. (Black dots follow displacement through elongation of a single point and white dots follow displacement through relaxation of that single point)

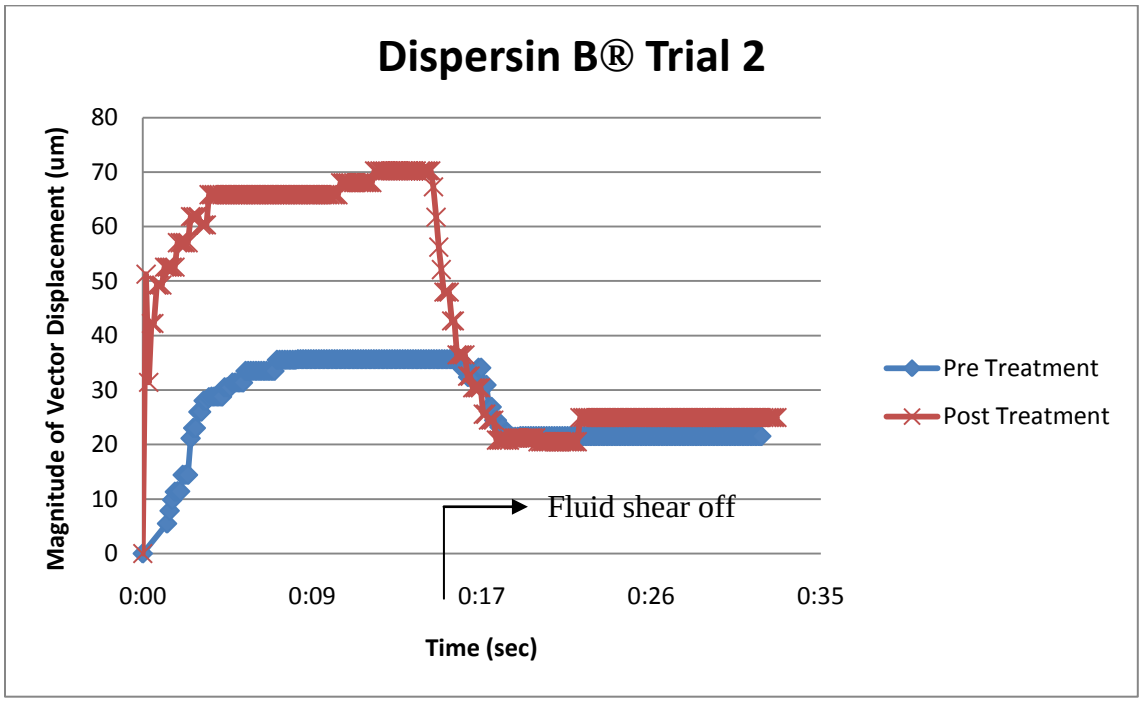

Figure 121) DispersinB® treatment of average of vector displacements for specified spots on the biofilm cluster

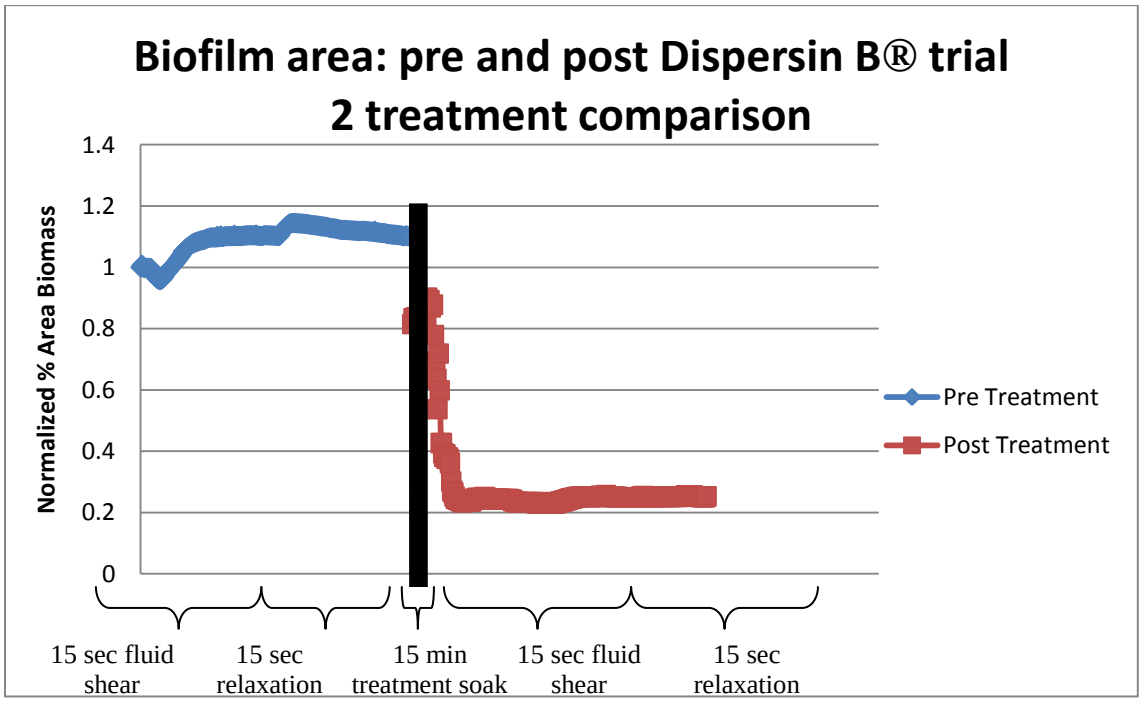

Figure 122) Pre and post-treatment measurement of biomass % area during fluid shear test for DispersinB®

DispersinB® Trial 3

DispersinB® Pre-treatment fluid shear test trial 3

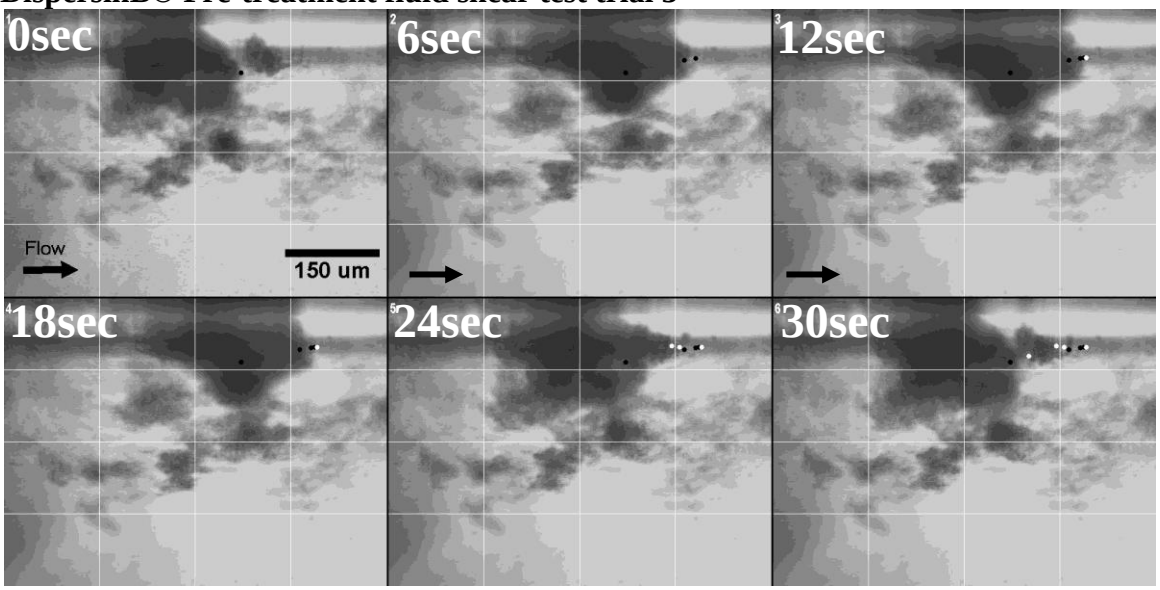

Figure 123) Pre-treatment fluid shear creep relaxation test for a *S. epidermidis* biofilm cluster with 15sec fluid shear and 15 sec relaxation period. 0sec frame is the initial configuration of the biofilm and 30sec is the final configuration after the fluid shear test. (Black dots follow displacement through elongation of a single point and white dots follow displacement through relaxation of that single point)

DispersinB® Post-treatment fluid shear test trial 3

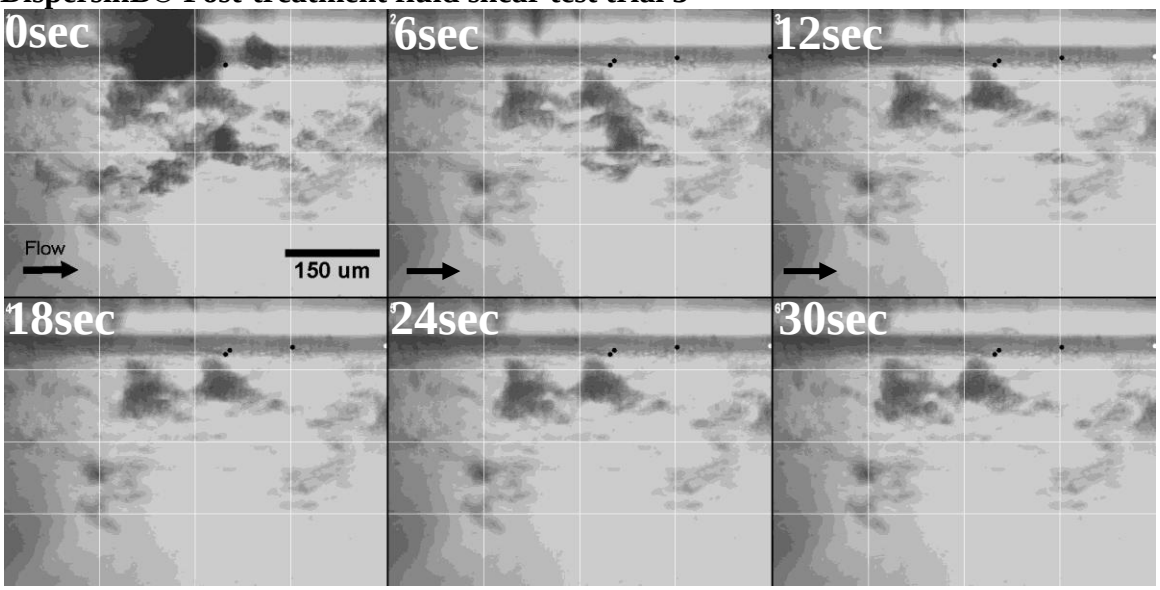

Figure 124) Post-treatment fluid shear creep relaxation test for a *S. epidermidis* biofilm cluster treated with 40 μg/mL of Dispersin B ® and 15sec fluid shear and 15 sec relaxation period. 0sec frame is the initial configuration of the biofilm and 30sec is the final configuration after the fluid shear test. (Black dots follow displacement through elongation of a single point and white dots follow displacement through relaxation of that single point)

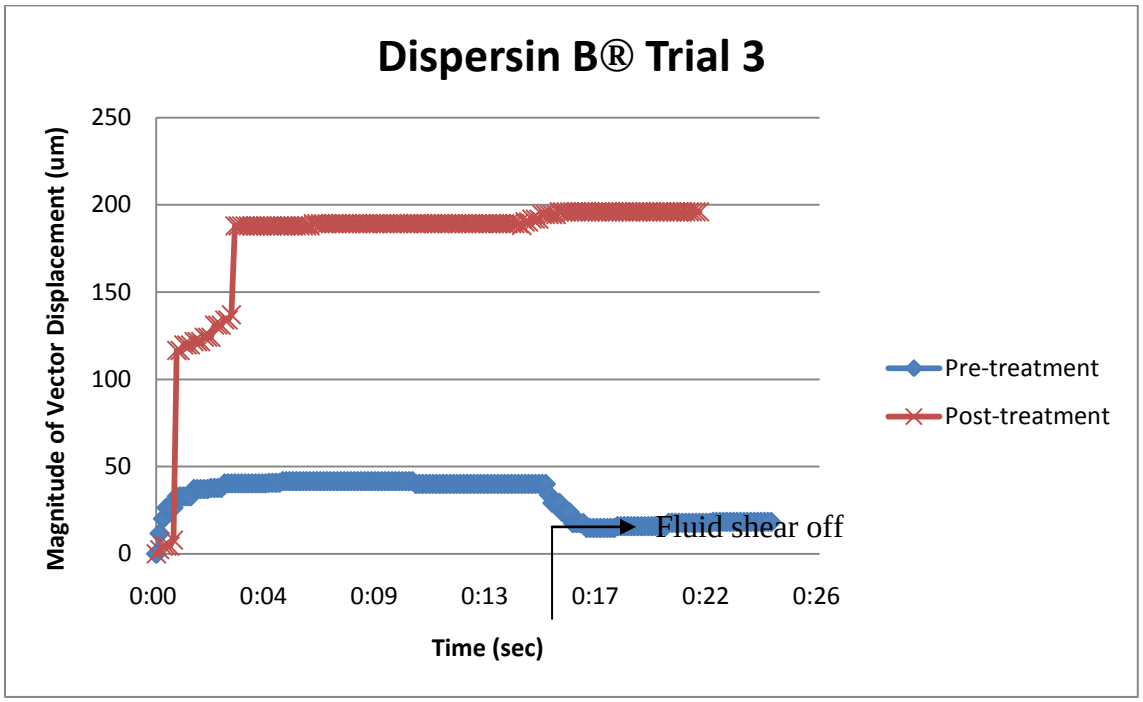

Figure 125) DispersinB® treatment of average of vector displacements for specified spots on the biofilm cluster

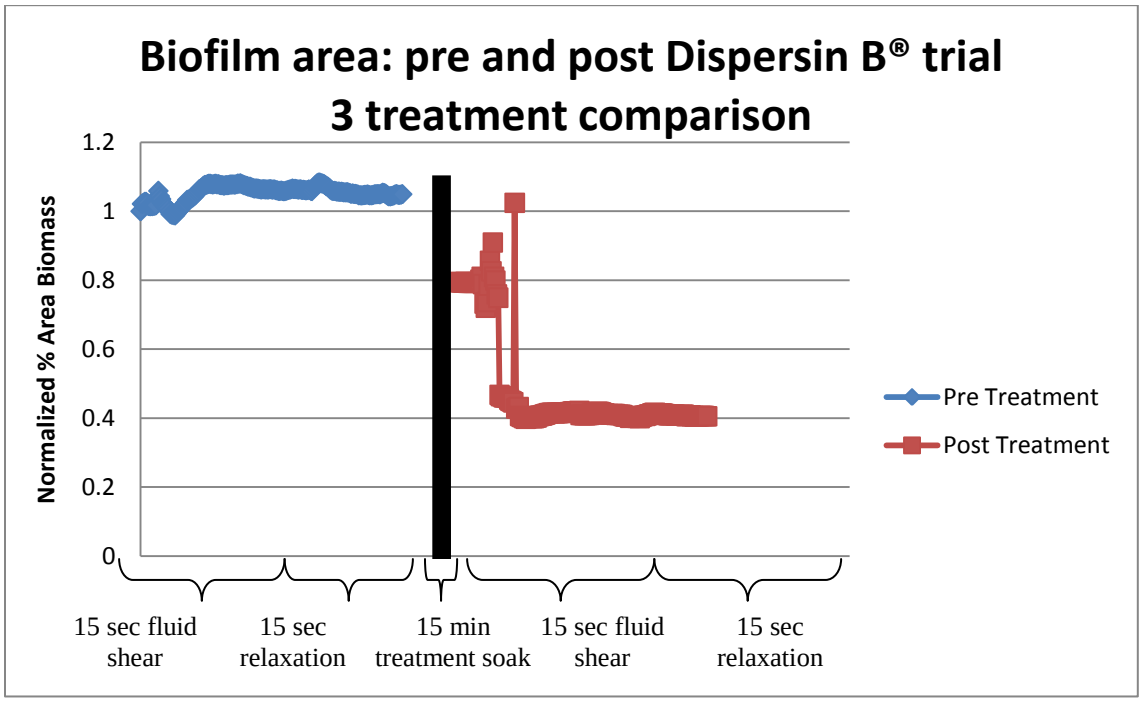

Figure 126) Pre and post-treatment measurement of biomass % area during fluid shear test for DispersinB®

APPENDIX B

AFM MICRO-INDENTATION TRIALS

Iron Chloride Trial #2

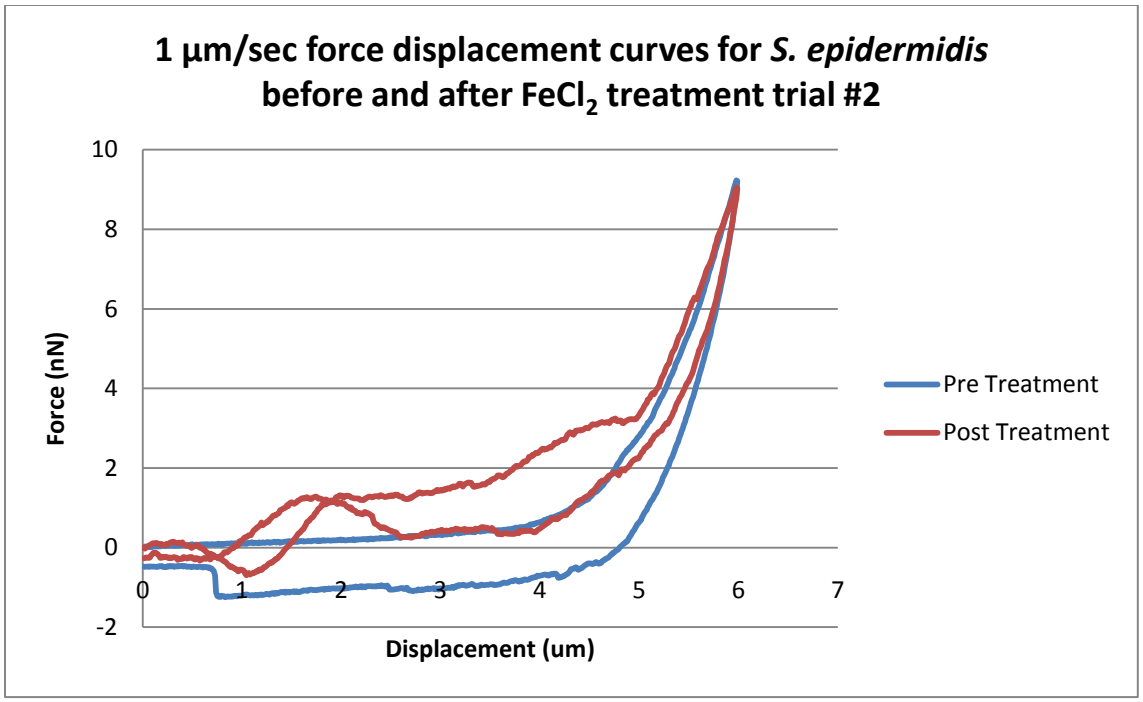

Figure 127) Force displacement curves for 1µm/sec loading rate for pre and post-treatment of iron chloride on *S. epidermidis* biofilm

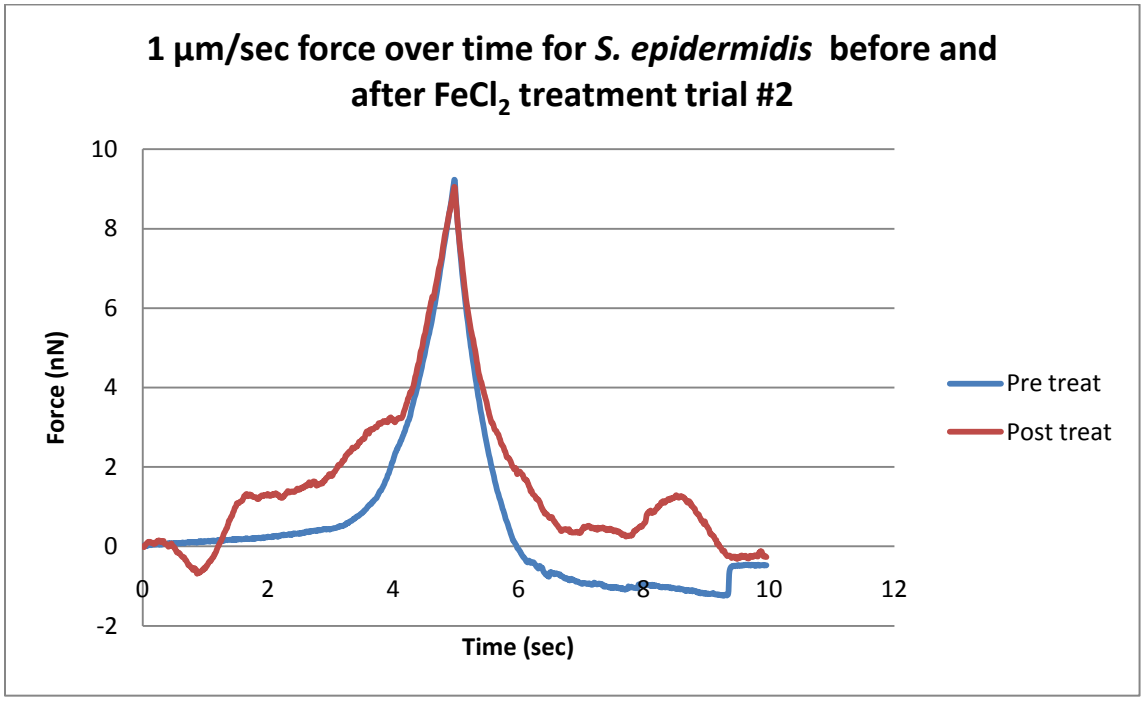

Figure 128) Force applied to *S. epidermidis* biofilm over loading time for pre and post-treatment of iron chloride using 1µm/sec loading rate

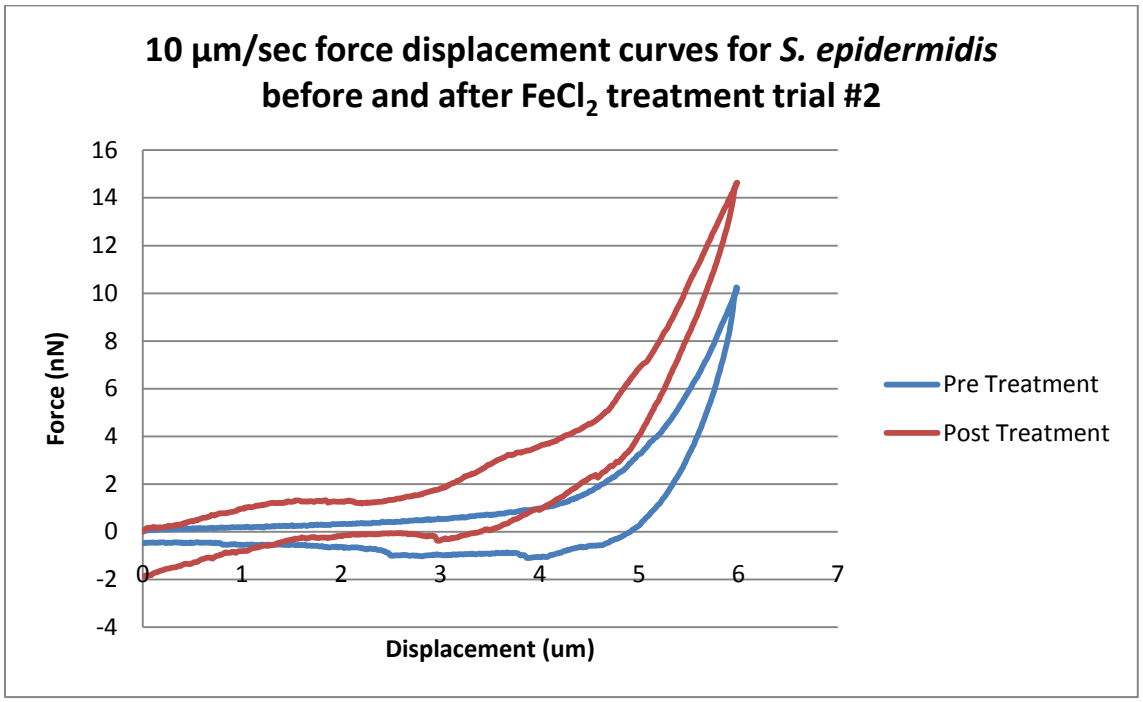

Figure 129) Force displacement curves for 10µm/sec loading rate for pre and post-treatment of iron chloride on *S. epidermidis* biofilm

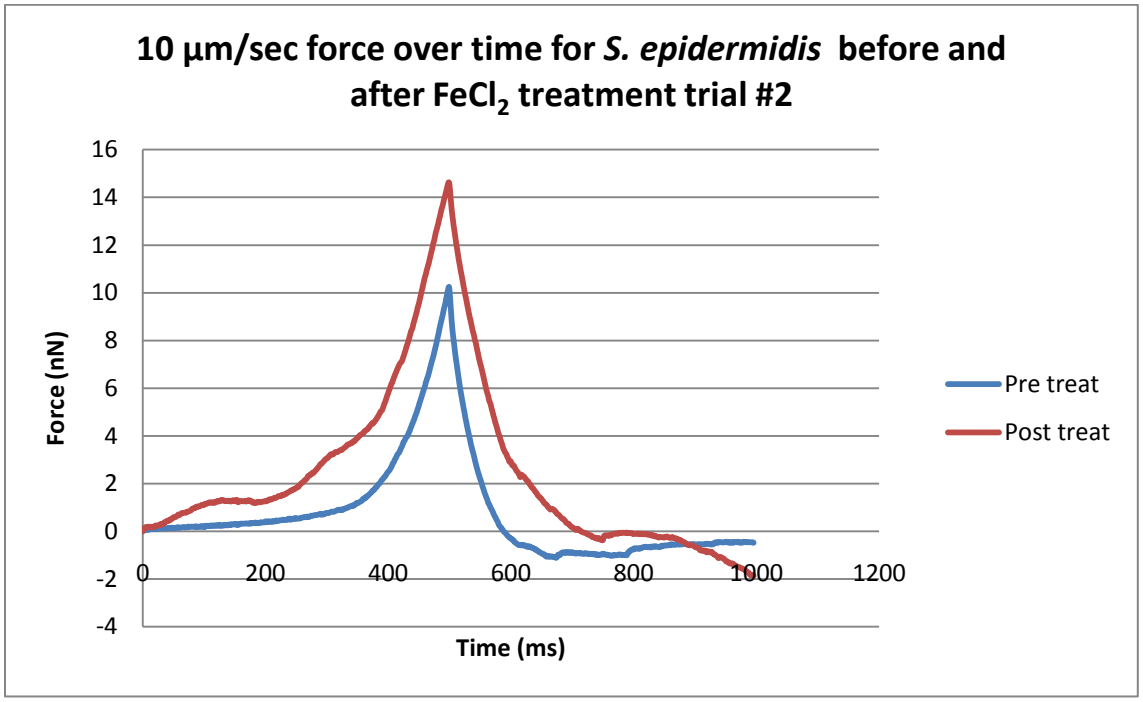

Figure 130) Force applied to *S. epidermidis* biofilm over loading time for pre and post-treatment of iron chloride using 1µm/sec loading rate

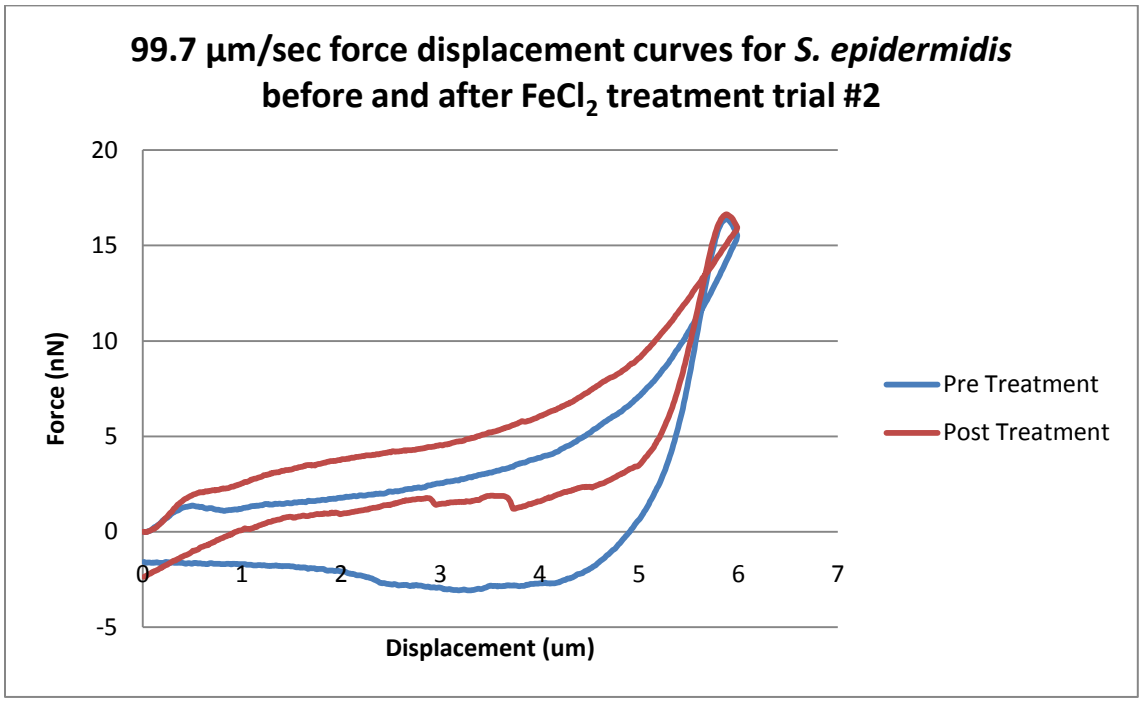

Figure 131) Force displacement curves for 99.7µm/sec loading rate for pre and post-treatment of iron chloride on *S. epidermidis* biofilm

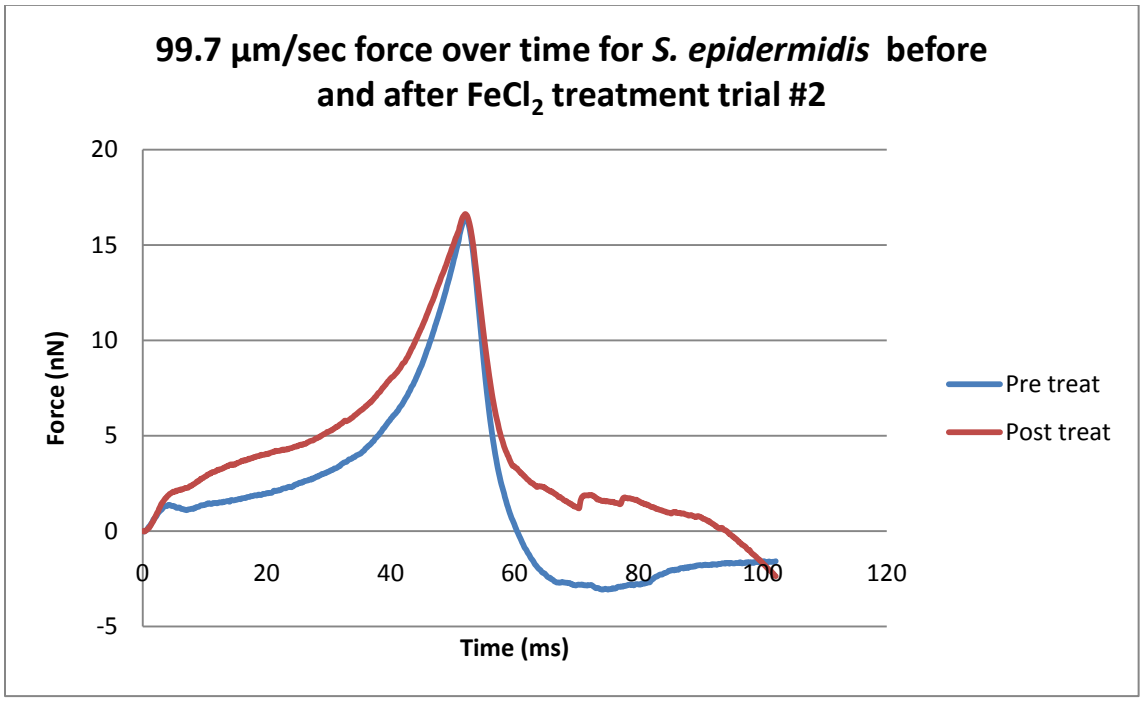

Figure 132) Force applied to *S. epidermidis* biofilm over loading time for pre and post-treatment of iron chloride using 99.7µm/sec loading rate

Iron Chloride Trial #2

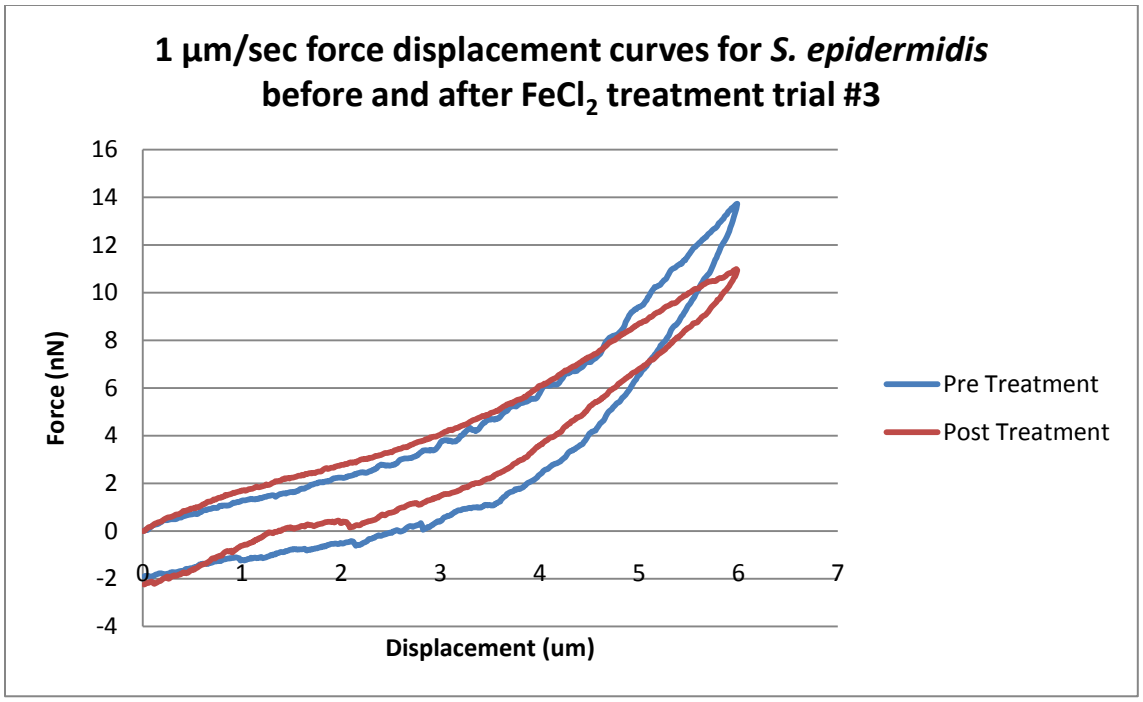

Figure 133) Force displacement curves for 1µm/sec loading rate for pre and post-treatment of iron chloride on *S. epidermidis* biofilm

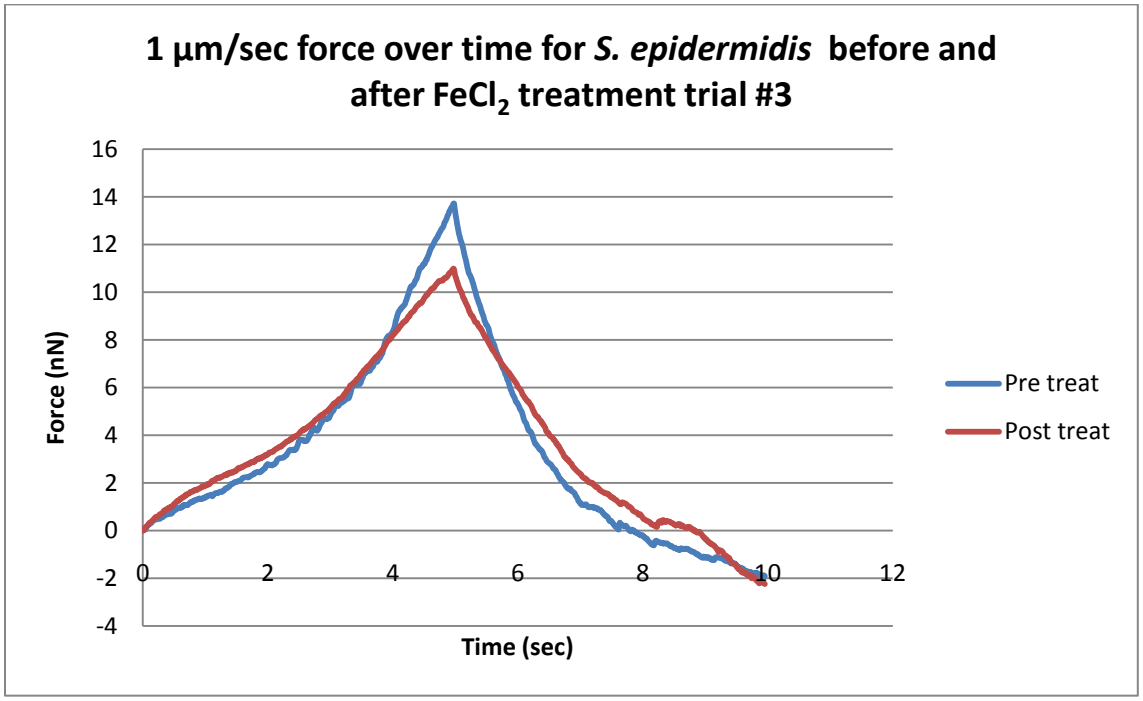

Figure 134) Force applied to *S. epidermidis* biofilm over loading time for pre and post-treatment of iron chloride using 1µm/sec loading rate

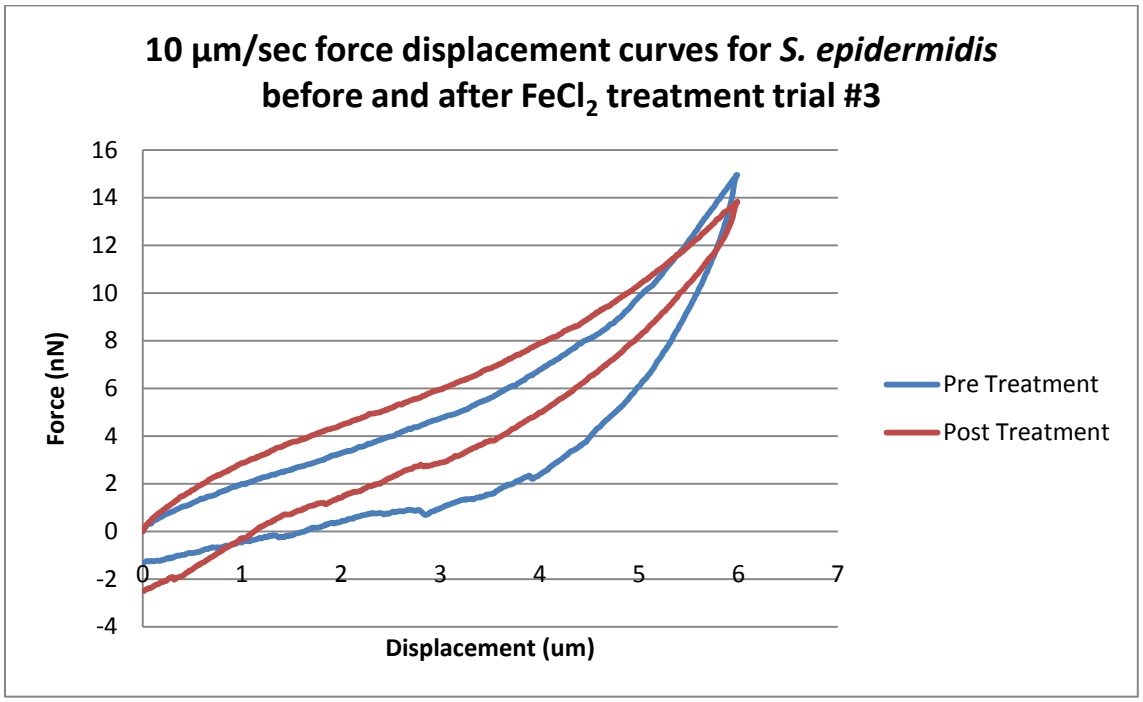

Figure 135) Force displacement curves for 10µm/sec loading rate for pre and post-treatment of iron chloride on *S. epidermidis* biofilm

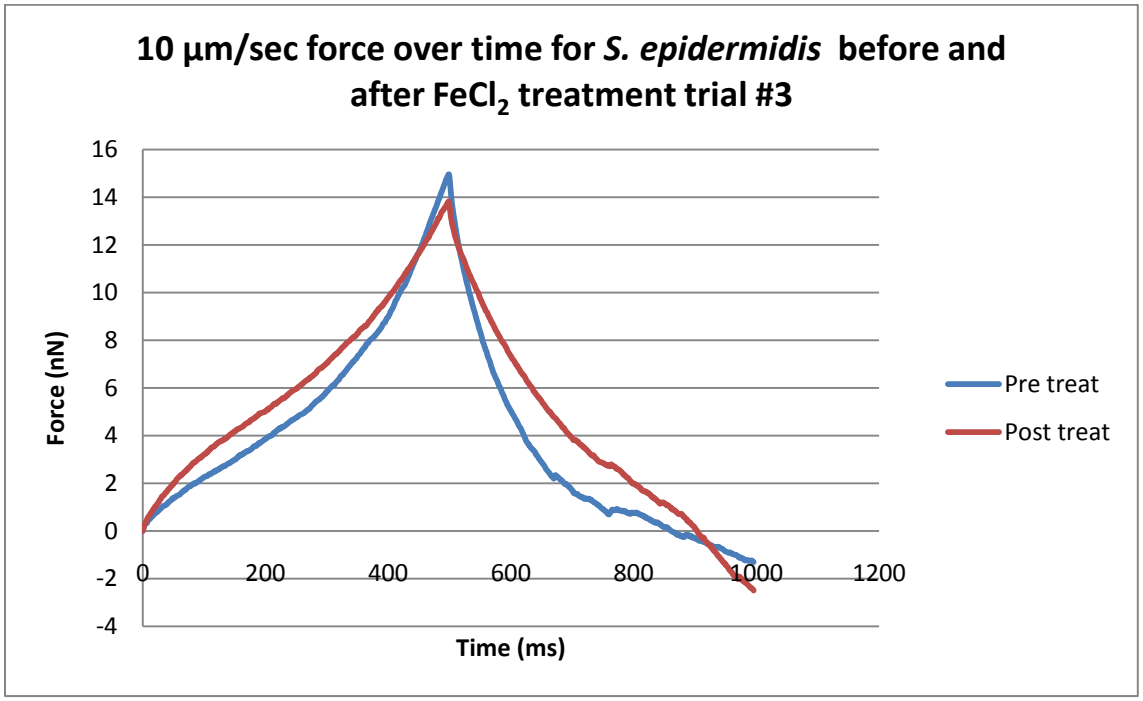

Figure 136) Force applied to *S. epidermidis* biofilm over loading time for pre and post-treatment of iron chloride using 10µm/sec loading rate

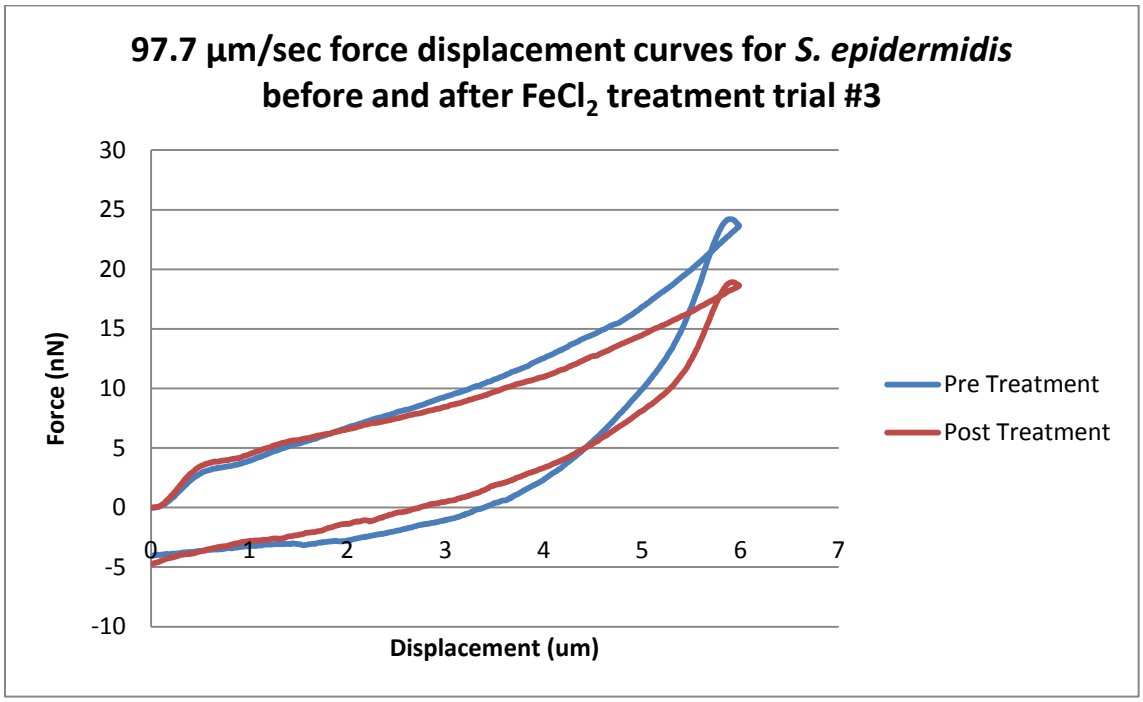

Figure 137) Force displacement curves for 97.7µm/sec loading rate for pre and post-treatment of iron chloride on *S. epidermidis* biofilm

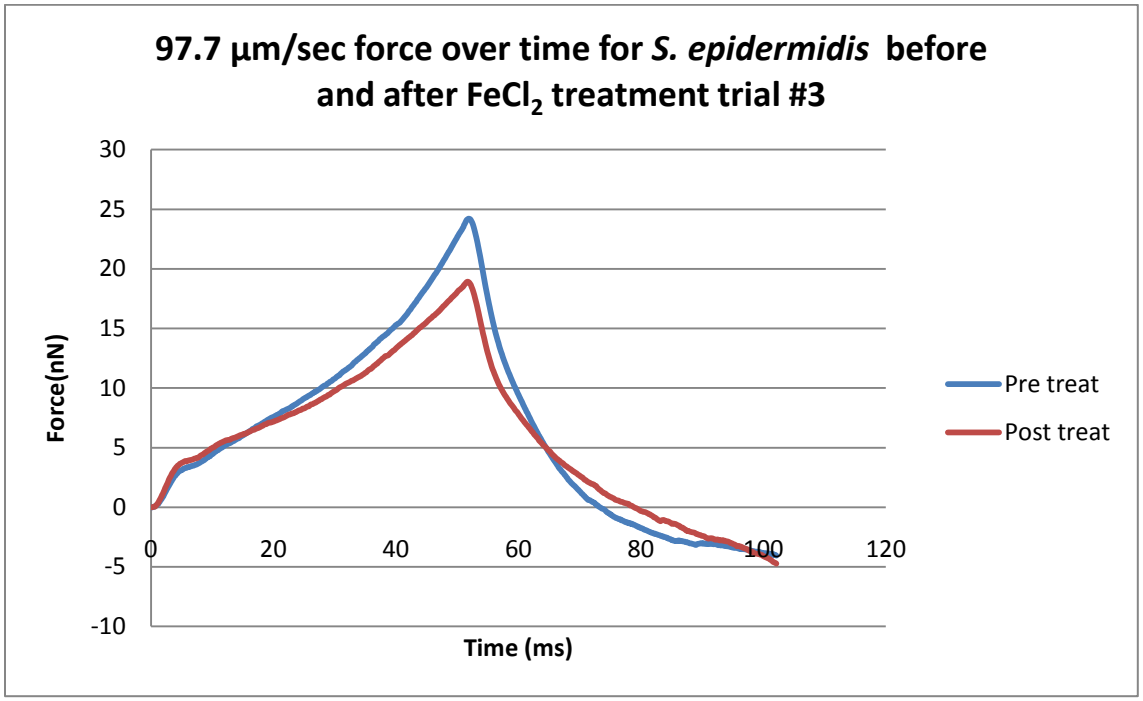

Figure 138) Force applied to *S. epidermidis* biofilm over loading time for pre and post-treatment of iron chloride using 97.7µm/sec loading rate

Chlorhexidine Trial #2

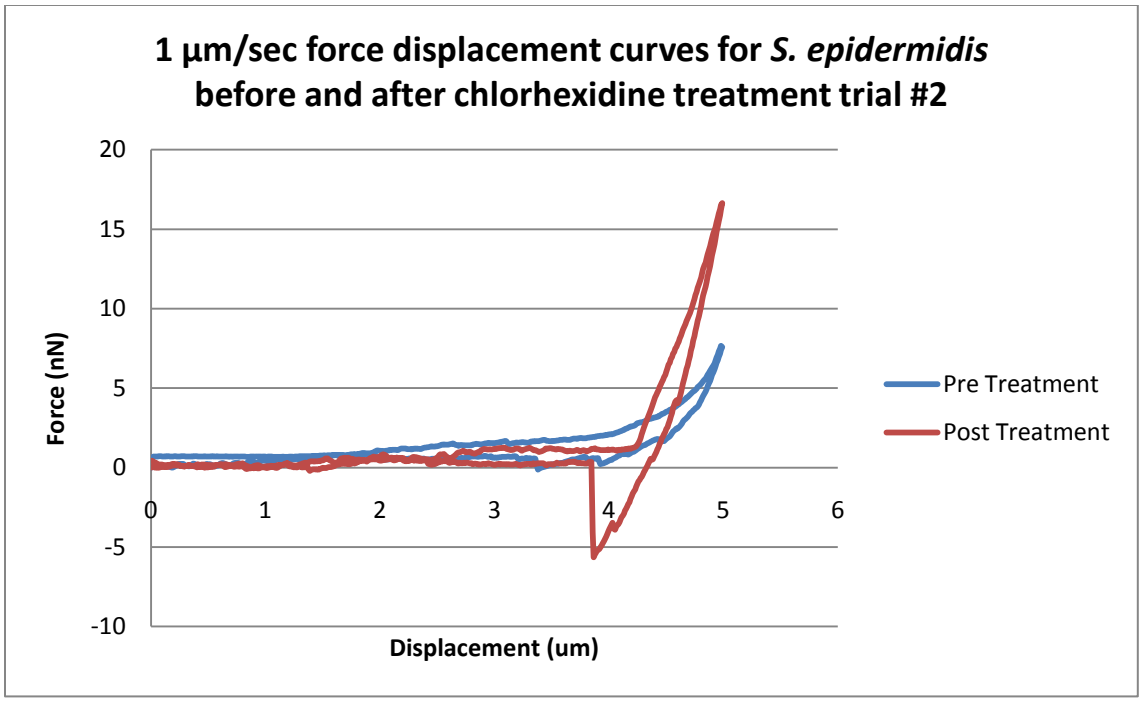

Figure 139) Force displacement curves for 1µm/sec loading rate for pre and post-treatment of chlorhexidine on *S. epidermidis* biofilm

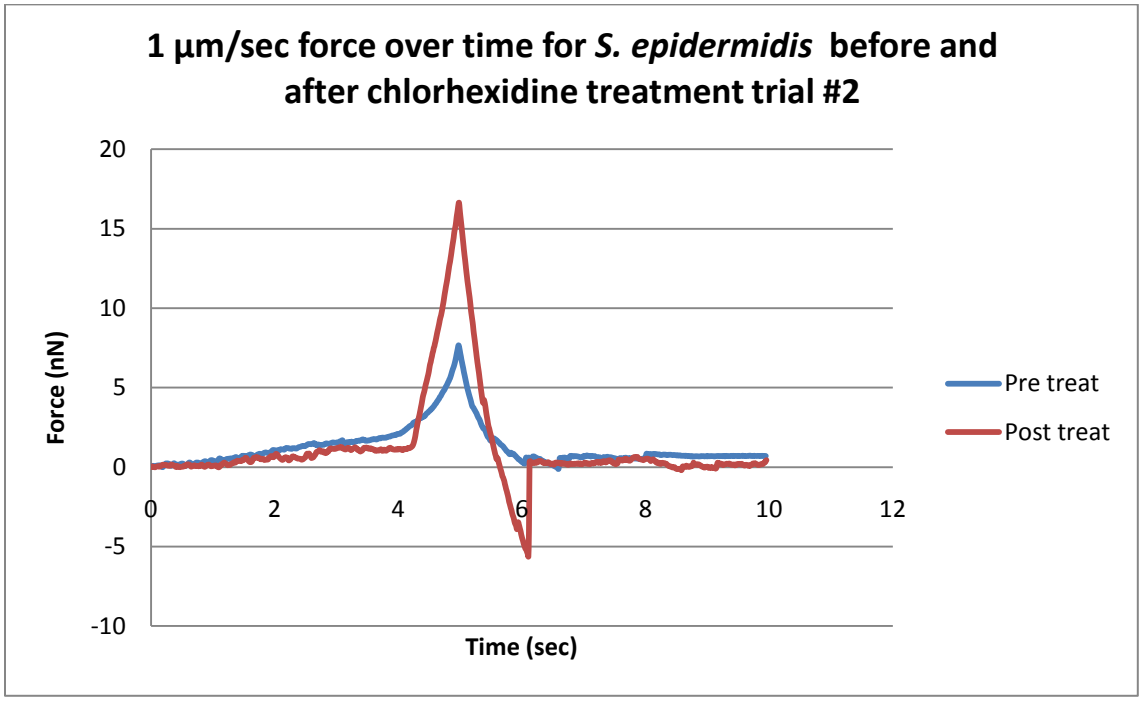

Figure 140) Force applied to *S. epidermidis* biofilm over loading time for pre and post-treatment of chlorhexidine using 1µm/sec loading rate

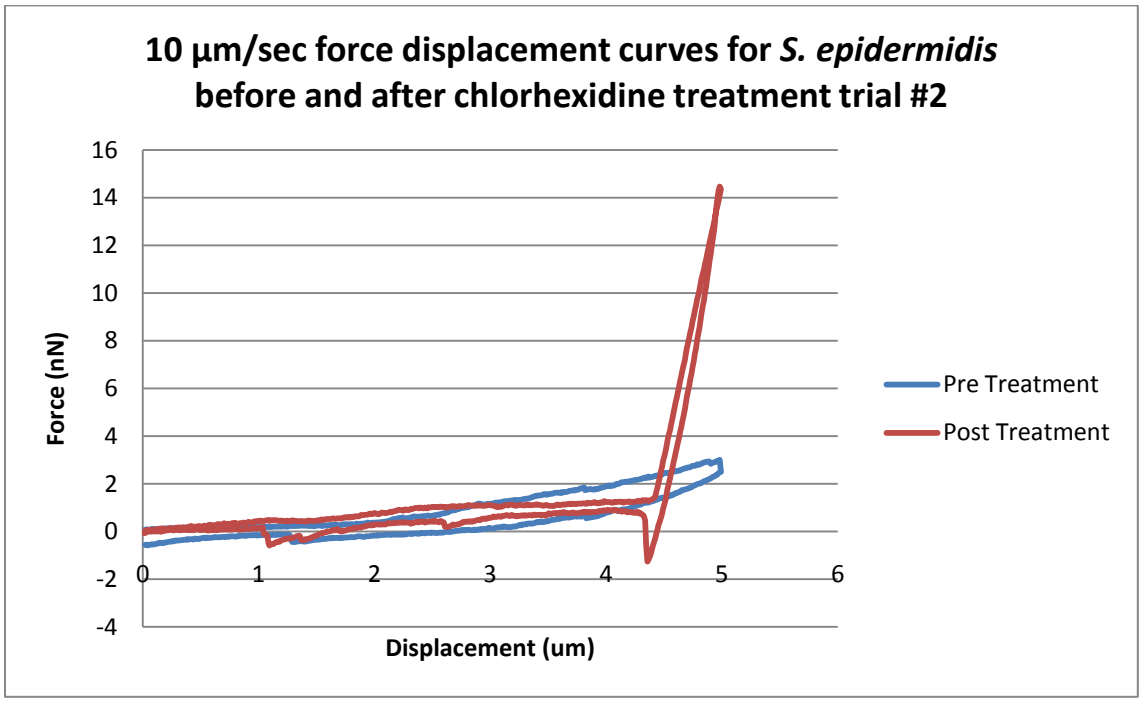

Figure 141) Force displacement curves for 10µm/sec loading rate for pre and post-treatment of chlorhexidine on *S. epidermidis* biofilm

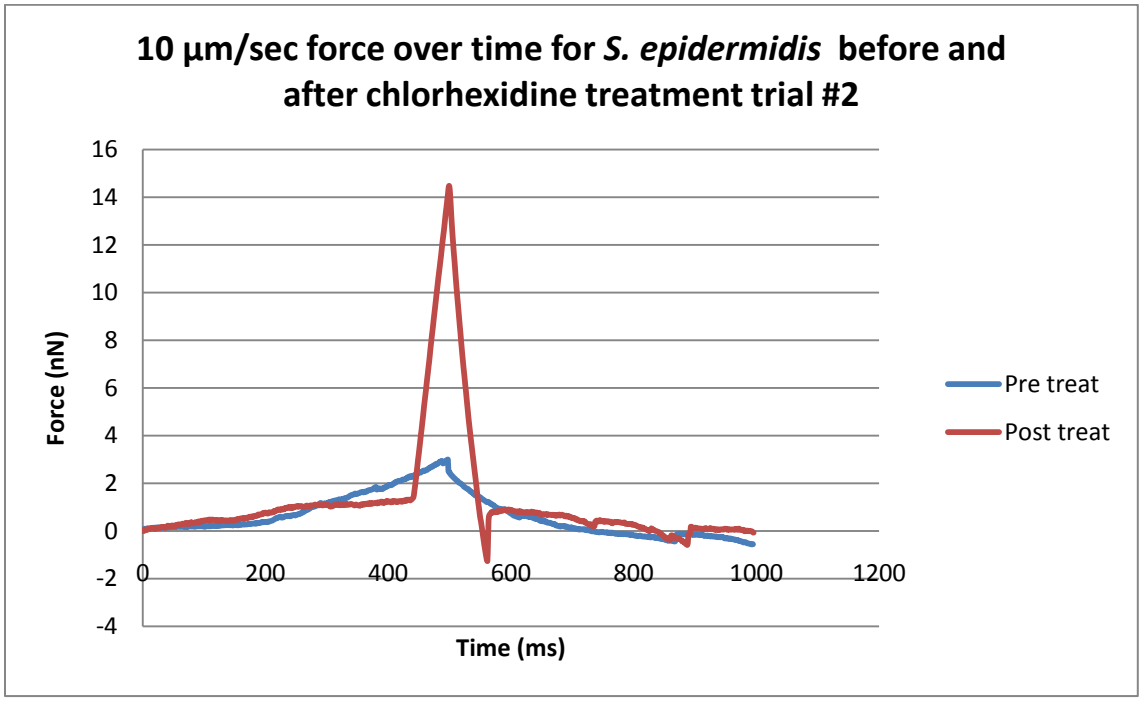

Figure 142) Force applied to *S. epidermidis* biofilm over loading time for pre and post-treatment of chlorhexidine using 10µm/sec loading rate

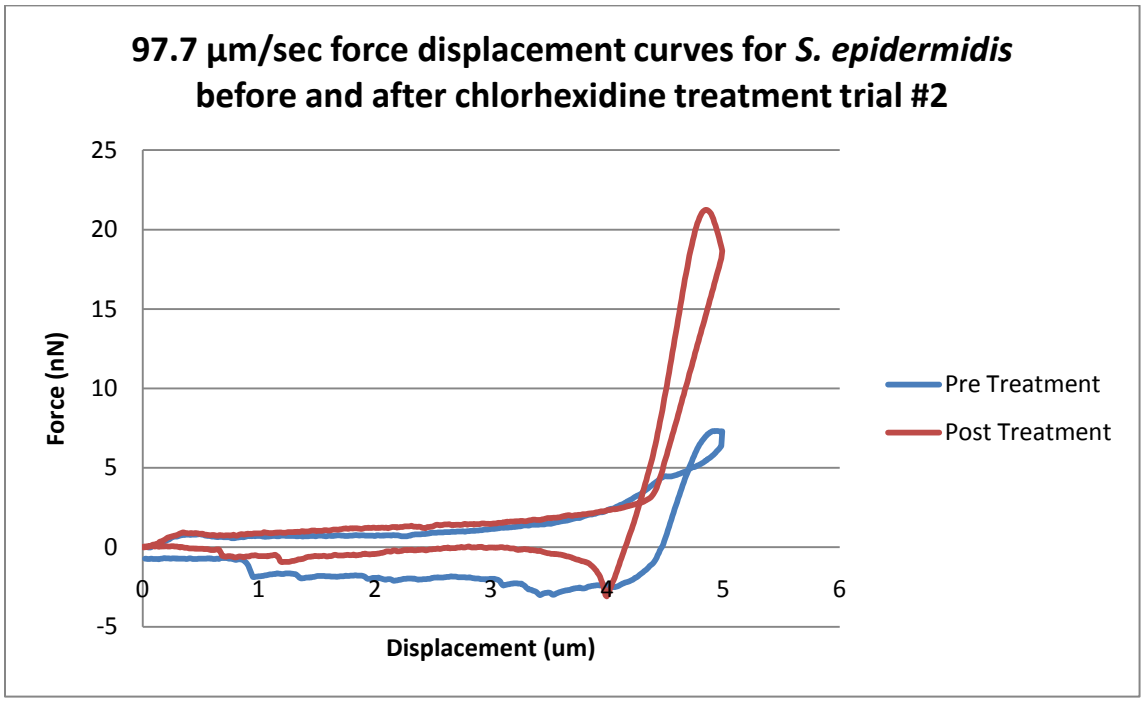

Figure 143) Force displacement curves for 97.7µm/sec loading rate for pre and post-treatment of chlorhexidine on *S. epidermidis* biofilm

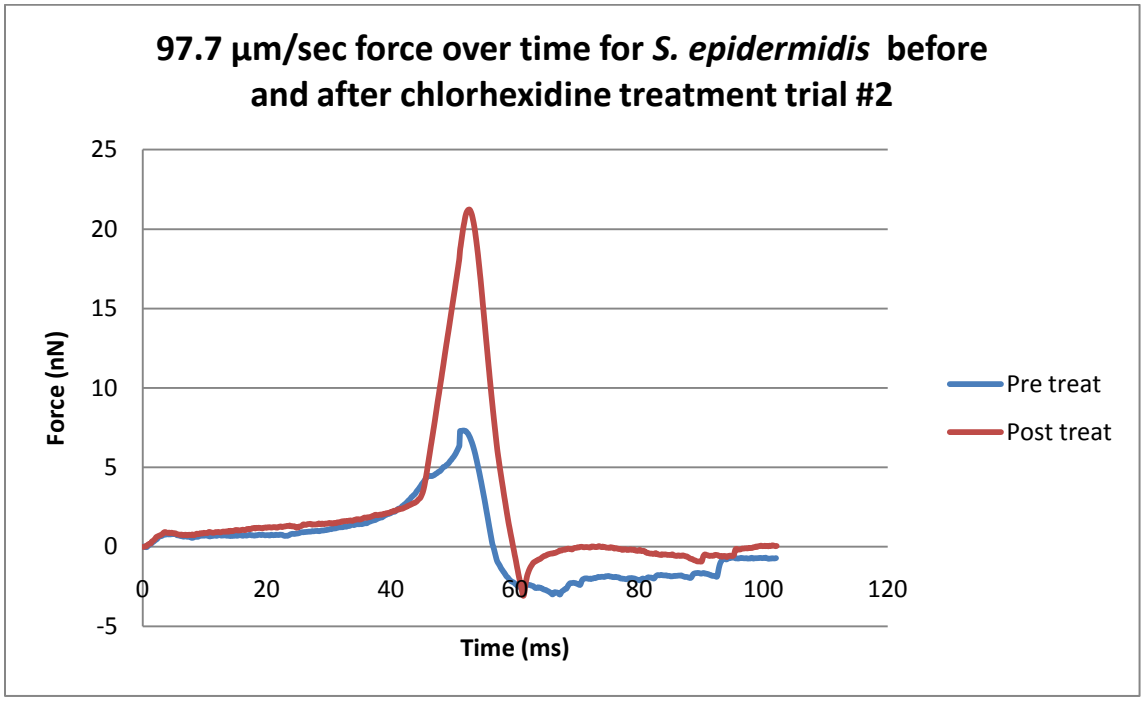

Figure 144) Force applied to *S. epidermidis* biofilm over loading time for pre and post-treatment of chlorhexidine using 97.7µm/sec loading rate

Chlorhexidine Trial #3

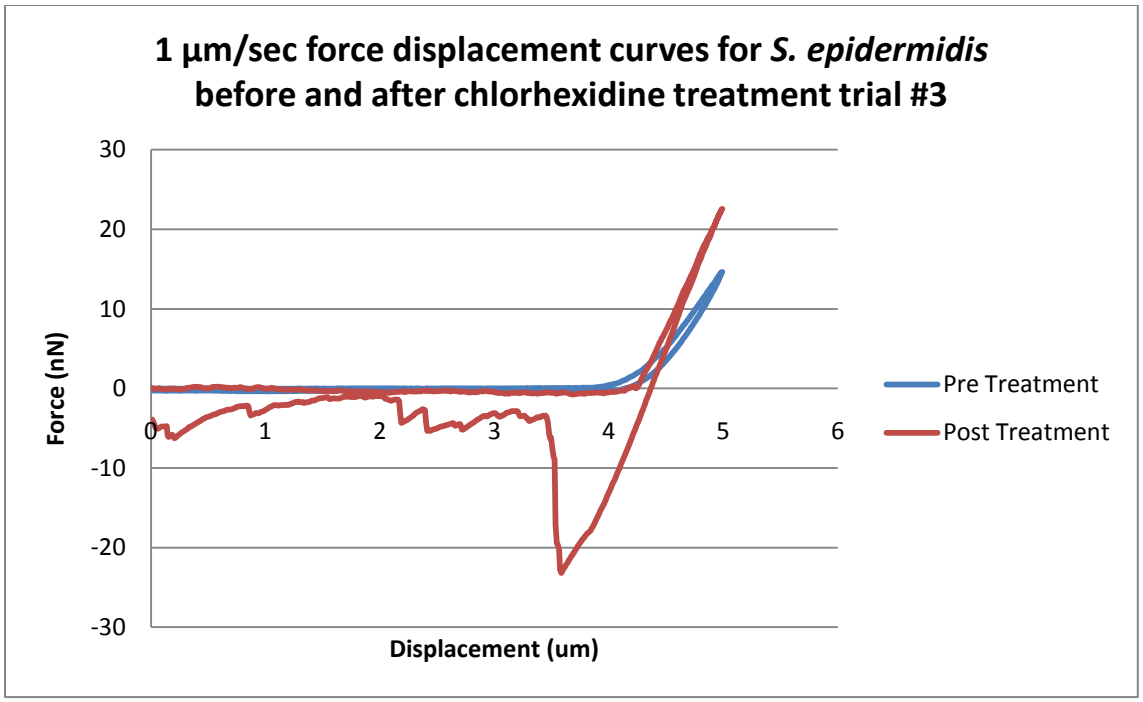

Figure 145) Force displacement curves for 1µm/sec loading rate for pre and post-treatment of chlorhexidine on *S. epidermidis* biofilm

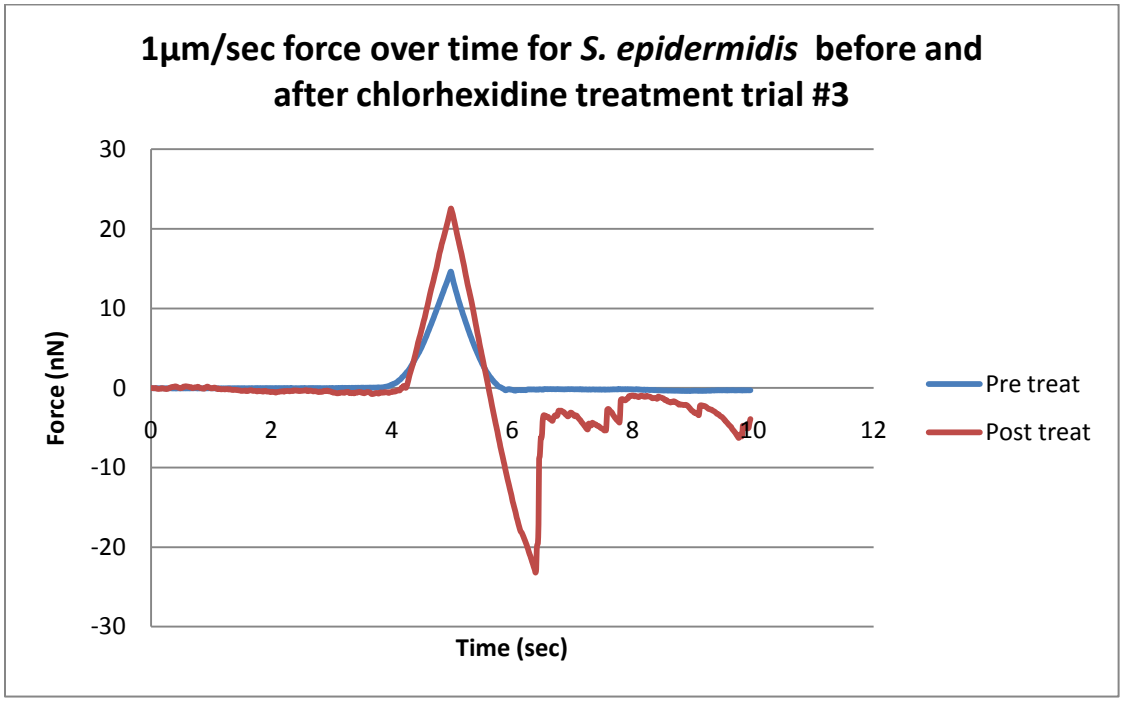

Figure 146) Force applied to *S. epidermidis* biofilm over loading time for pre and post-treatment of chlorhexidine using 1µm/sec loading rate

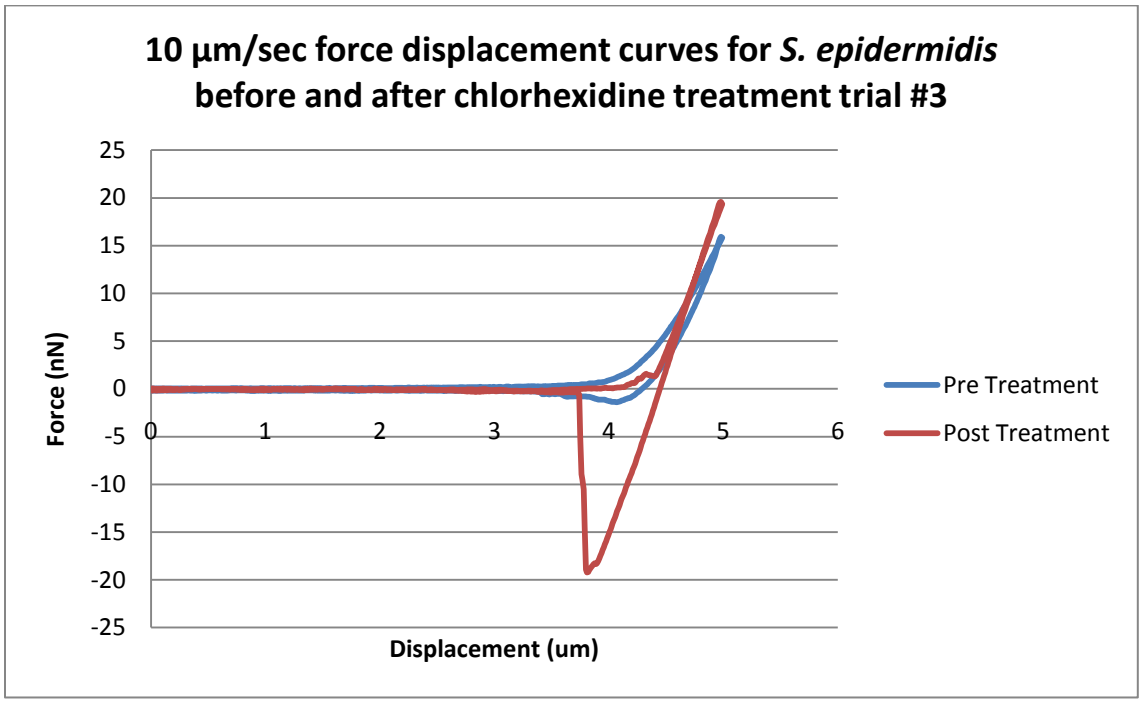

Figure 147) Force displacement curves for 10µm/sec loading rate for pre and post-treatment of chlorhexidine on *S. epidermidis* biofilm

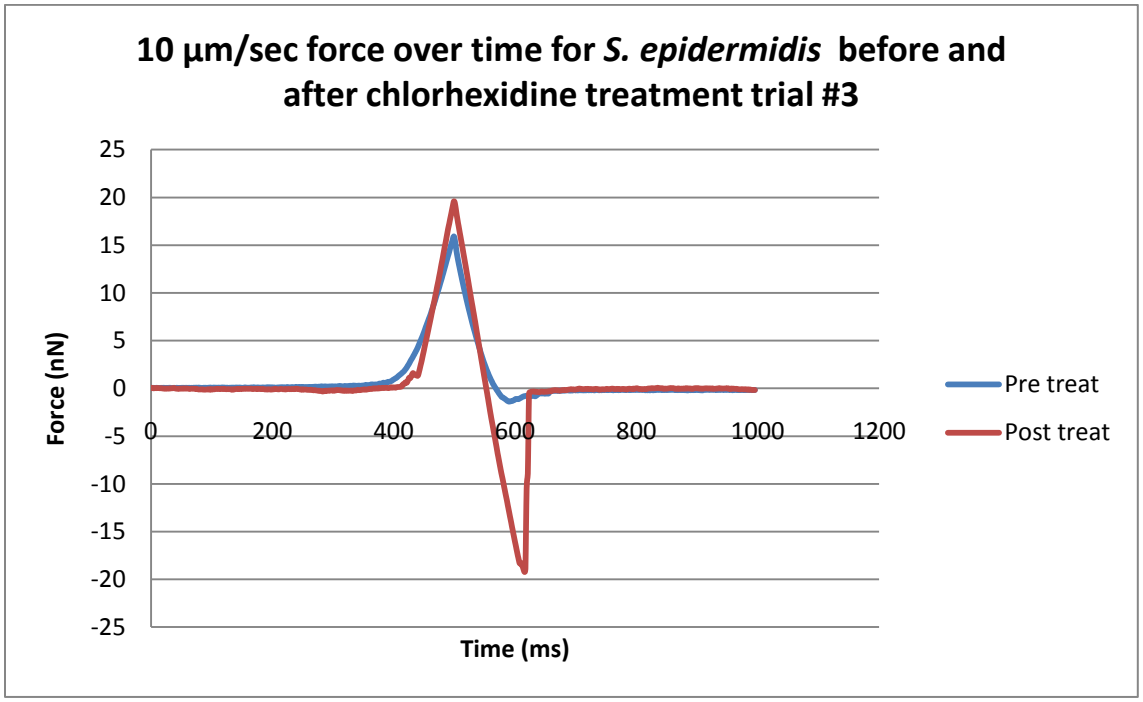

Figure 148) Force applied to *S. epidermidis* biofilm over loading time for pre and post-treatment of chlorhexidine using 10µm/sec loading rate

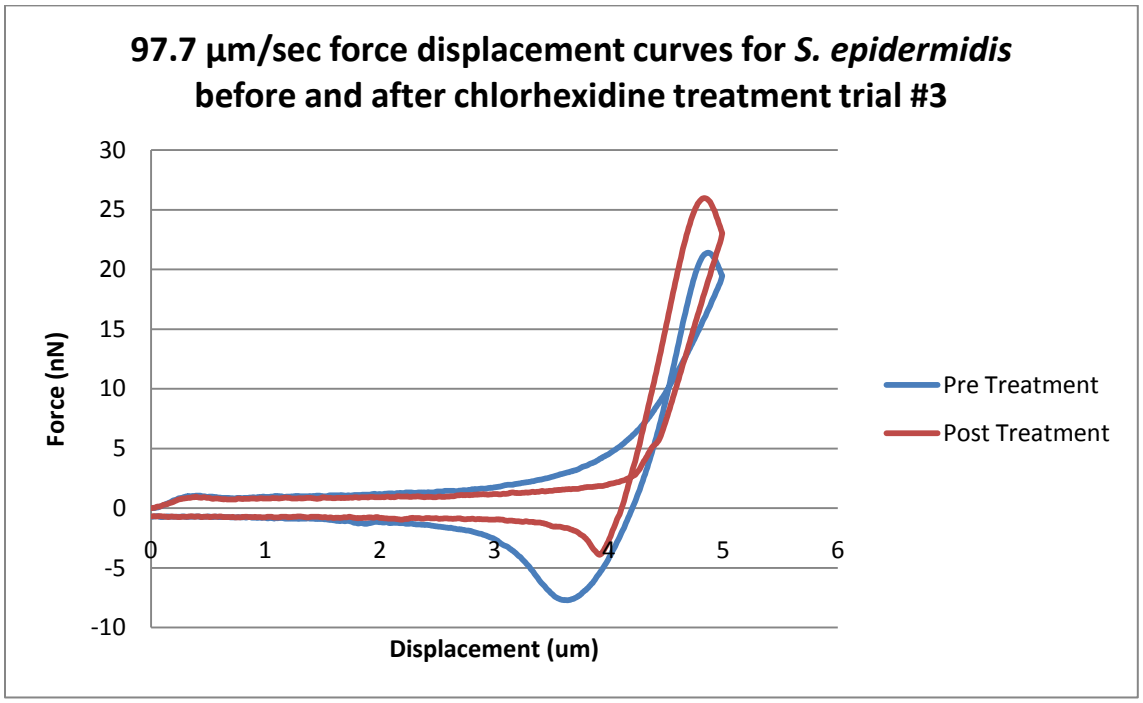

Figure 149) Force displacement curves for 97.7µm/sec loading rate for pre and post-treatment of chlorhexidine on *S. epidermidis* biofilm

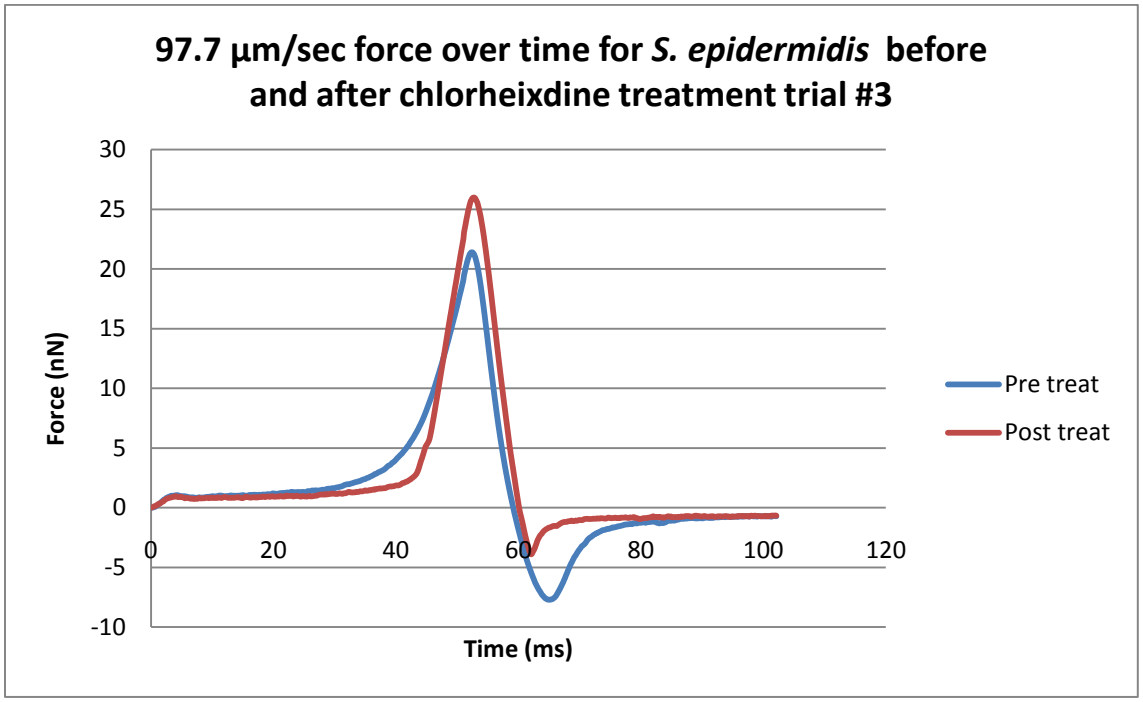

Figure 150) Force applied to *S. epidermidis* biofilm over loading time for pre and post-treatment of chlorhexidine using 97.7µm/sec loading rate

Urea Trial #2

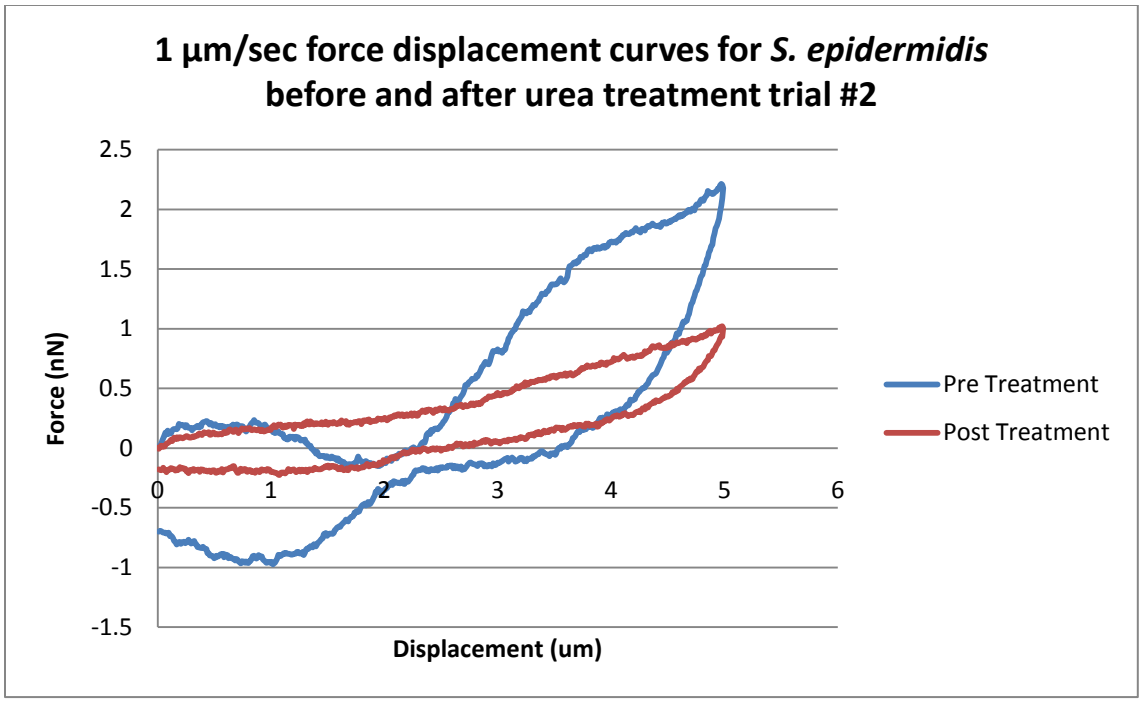

Figure 151) Force displacement curves for 1µm/sec loading rate for pre and post-treatment of urea on *S. epidermidis* biofilm

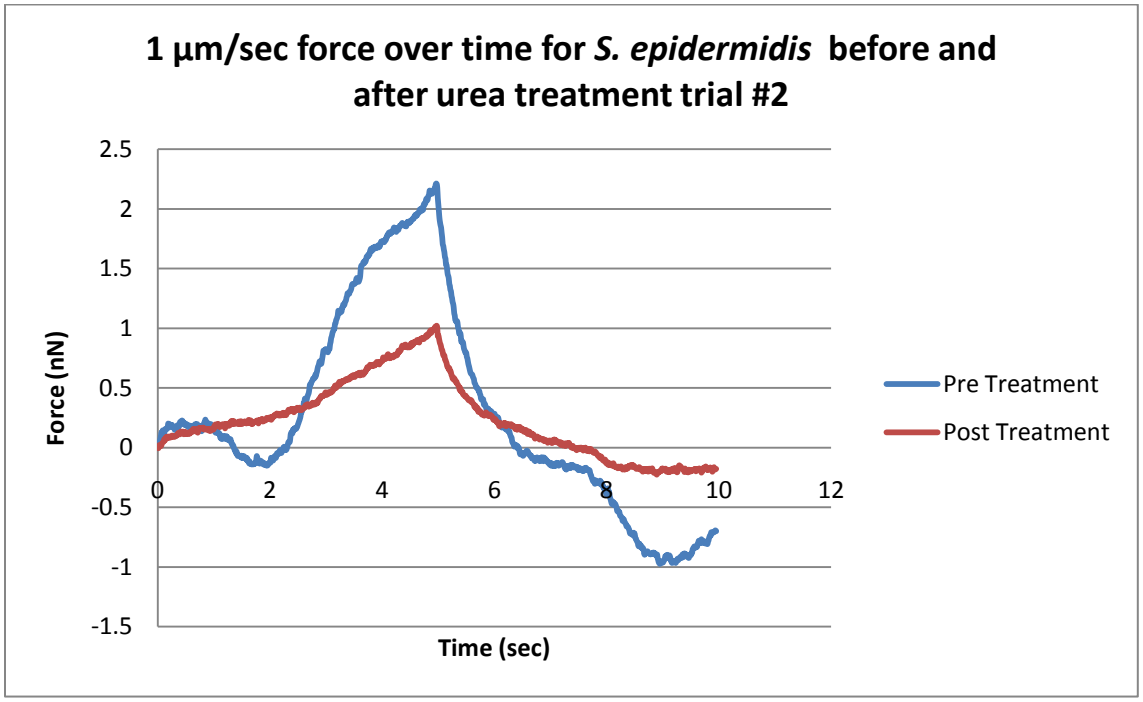

Figure 152) Force applied to *S. epidermidis* biofilm over loading time for pre and post-treatment of urea using 1µm/sec loading rate

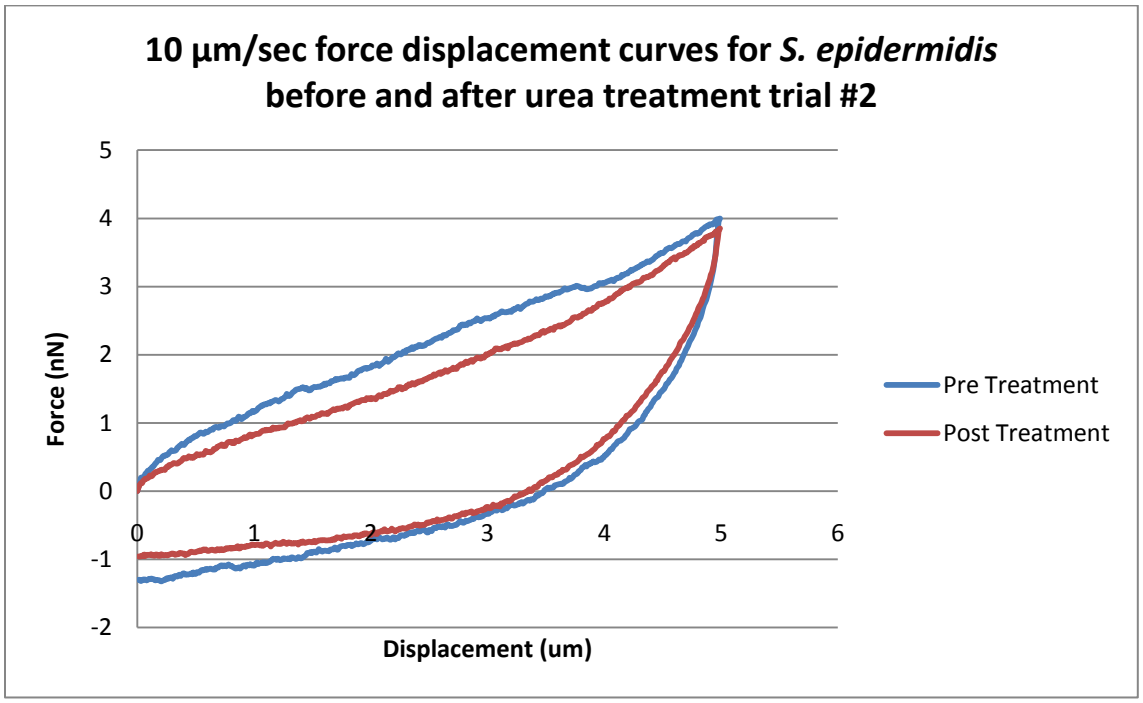

Figure 153) Force displacement curves for 10µm/sec loading rate for pre and post-treatment of urea on *S. epidermidis* biofilm

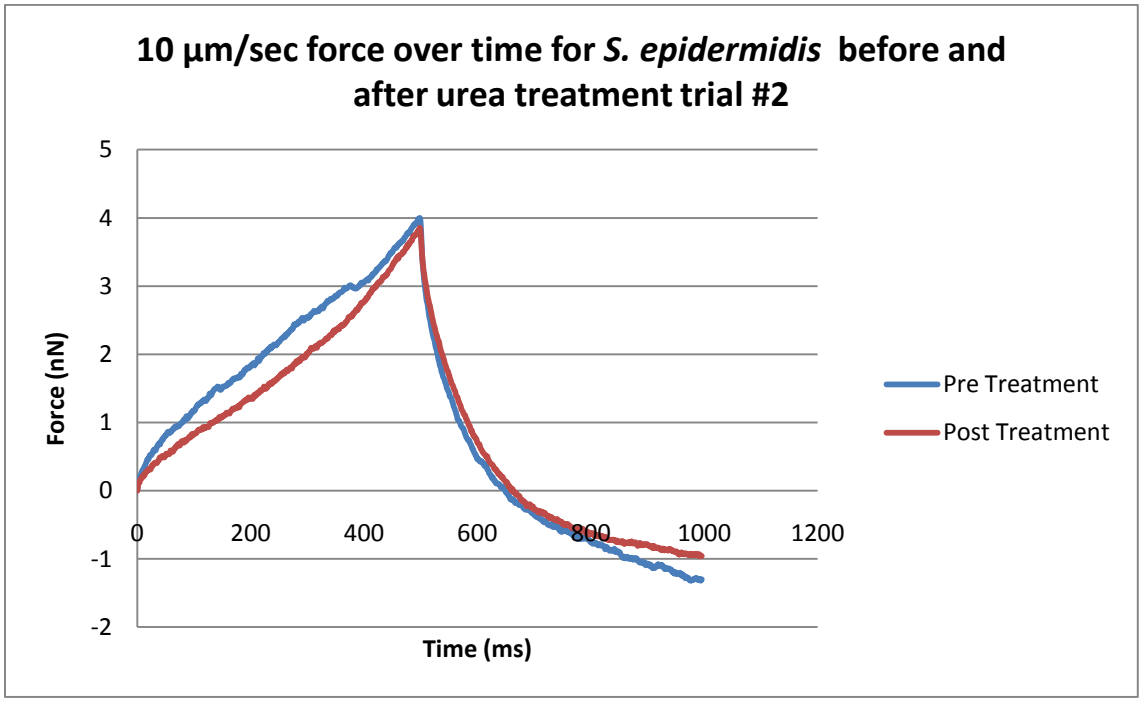

Figure 154) Force applied to *S. epidermidis* biofilm over loading time for pre and post-treatment of urea using 10µm/sec loading rate

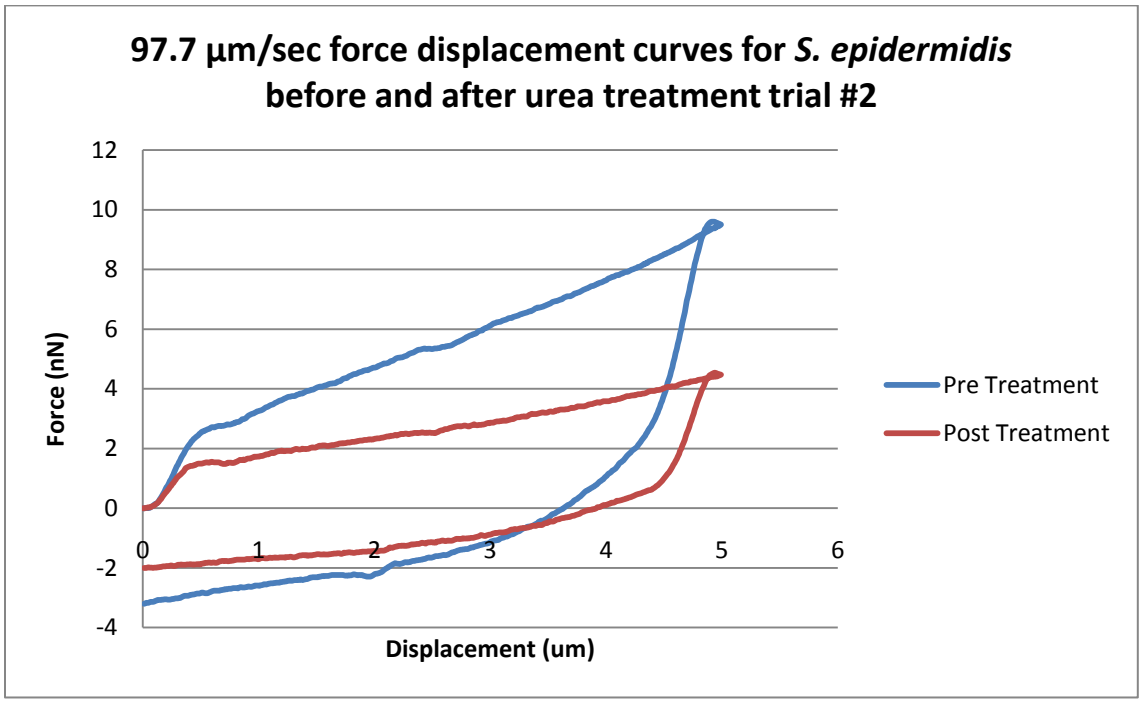

Figure 155) Force displacement curves for 97.7µm/sec loading rate for pre and post-treatment of urea on *S. epidermidis* biofilm

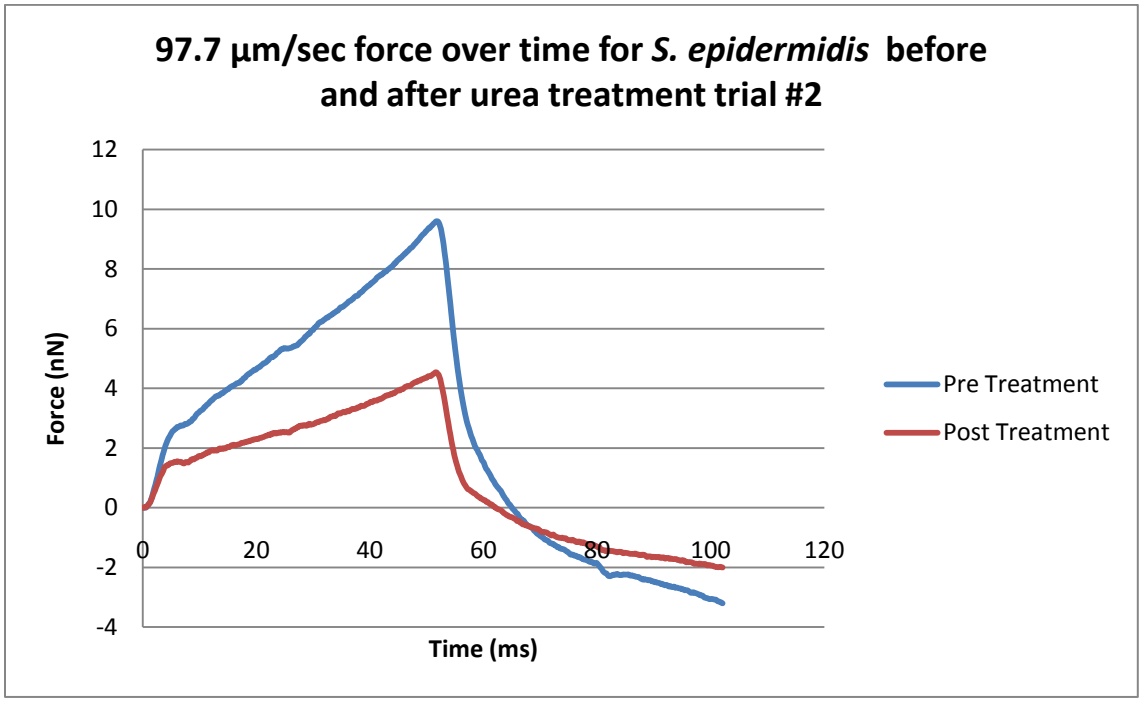

Figure 156) Force applied to *S. epidermidis* biofilm over loading time for pre and post-treatment of urea using 97.7µm/sec loading rate

Urea Trial #3

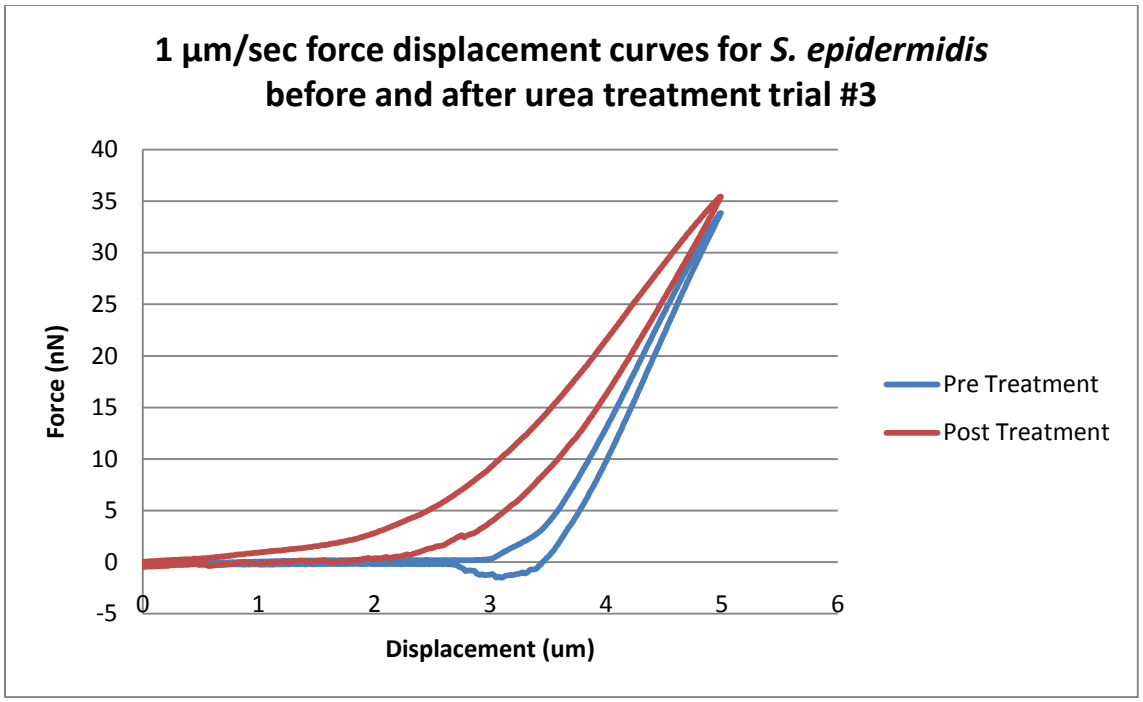

Figure 157) Force displacement curves for 1µm/sec loading rate for pre and post-treatment of urea on *S. epidermidis* biofilm

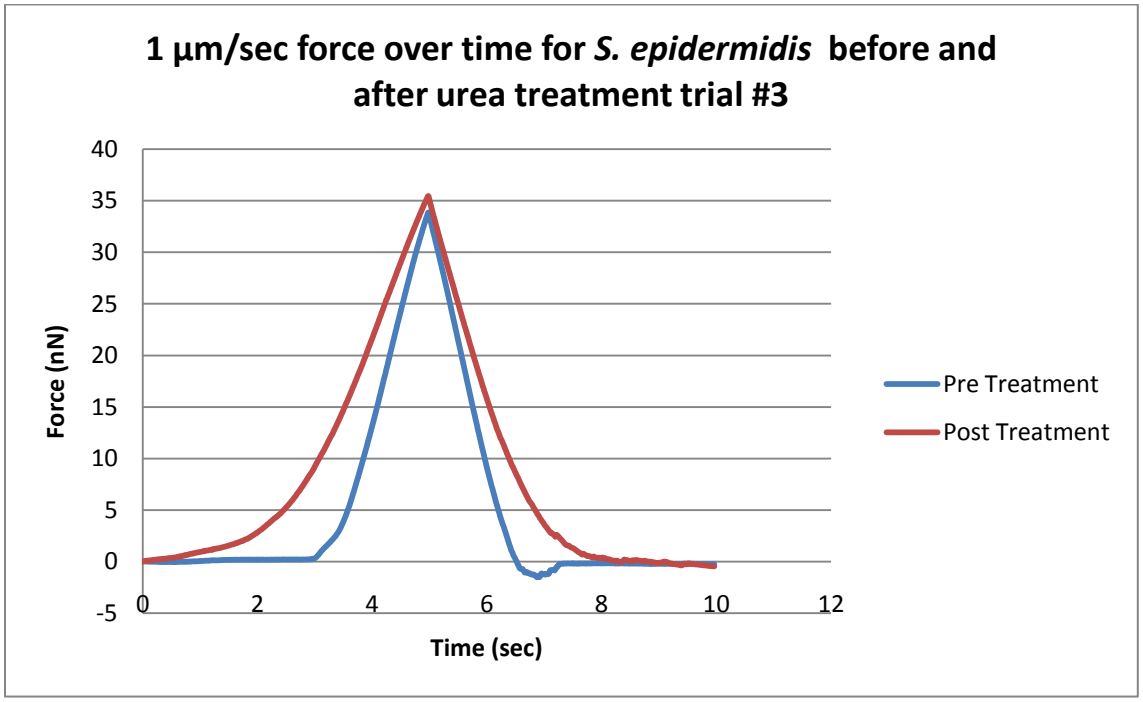

Figure 158) Force applied to *S. epidermidis* biofilm over loading time for pre and post-treatment of urea using 1µm/sec loading rate

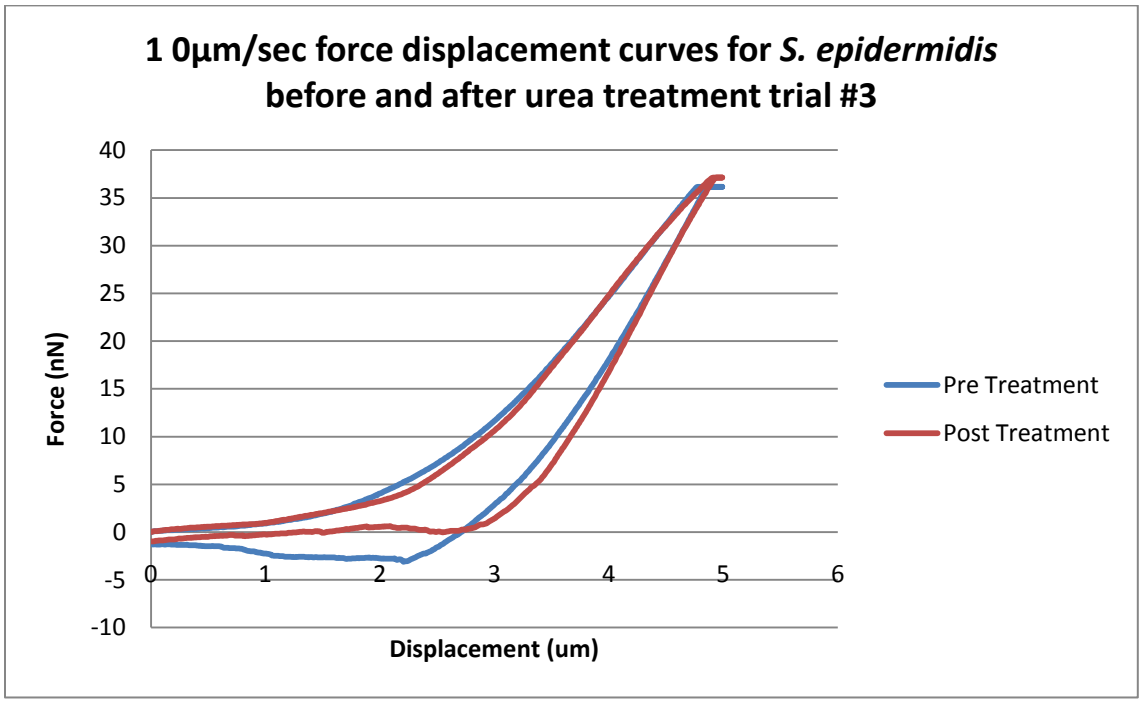

Figure 159) Force displacement curves for 10µm/sec loading rate for pre and post-treatment of urea on *S. epidermidis* biofilm

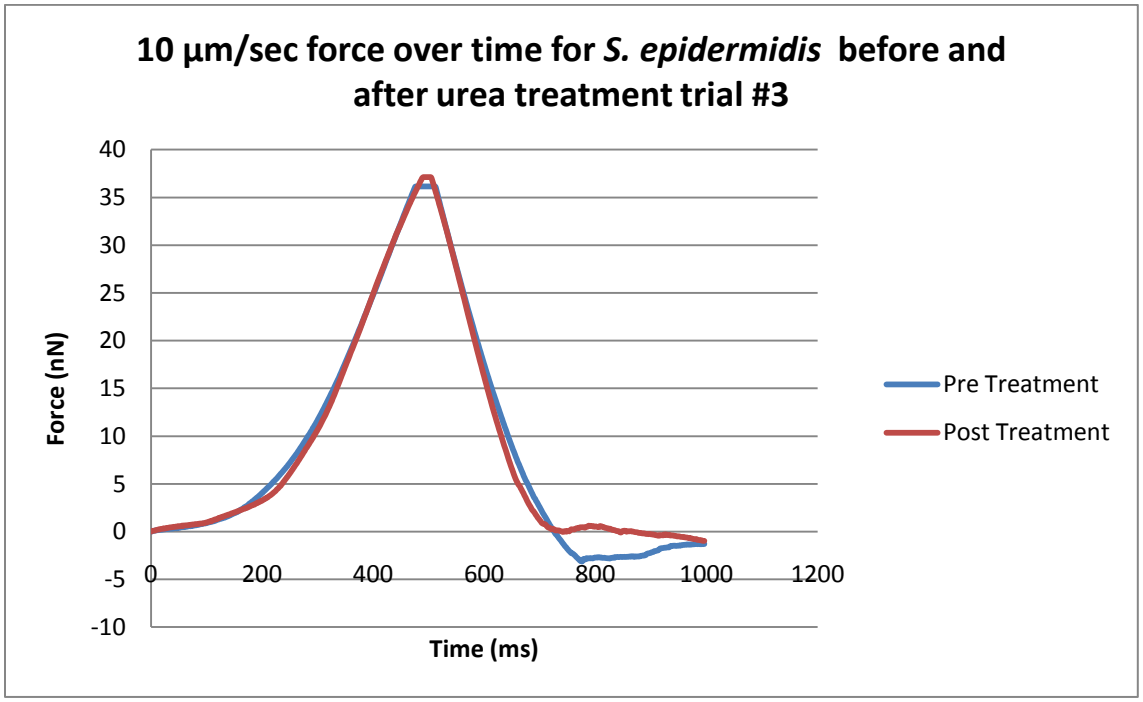

Figure 160) Force applied to *S. epidermidis* biofilm over loading time for pre and post-treatment of urea using 10µm/sec loading rate

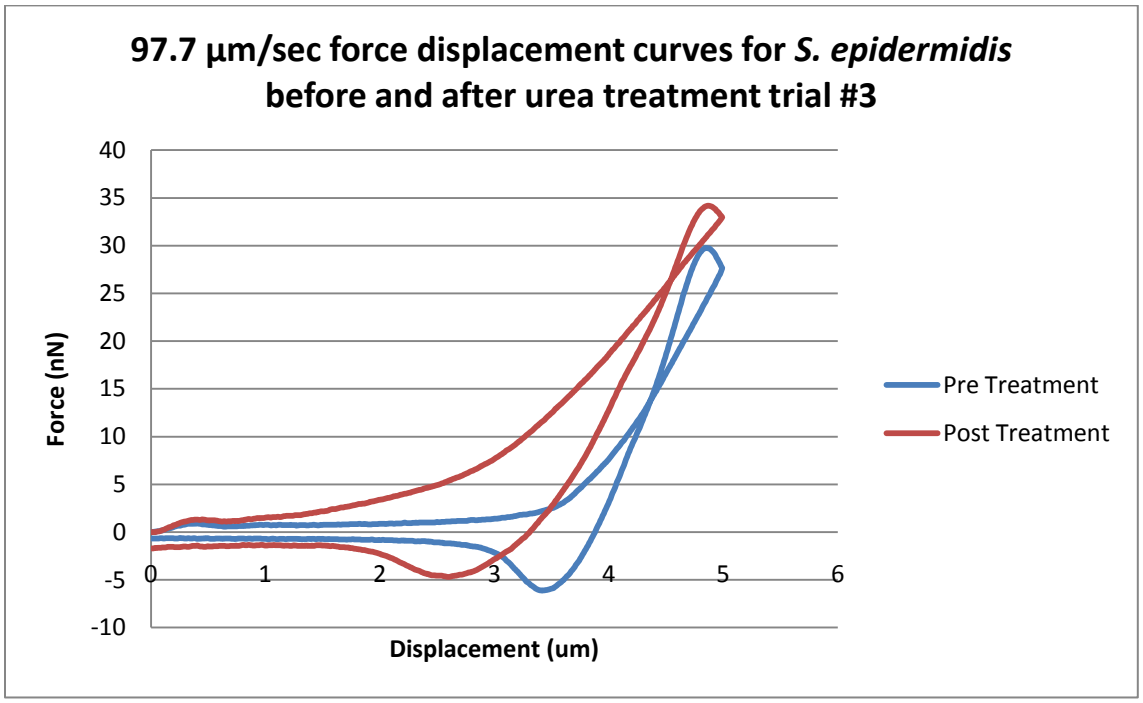

Figure 161) Force displacement curves for 97.7µm/sec loading rate for pre and post-treatment of urea on *S. epidermidis* biofilm

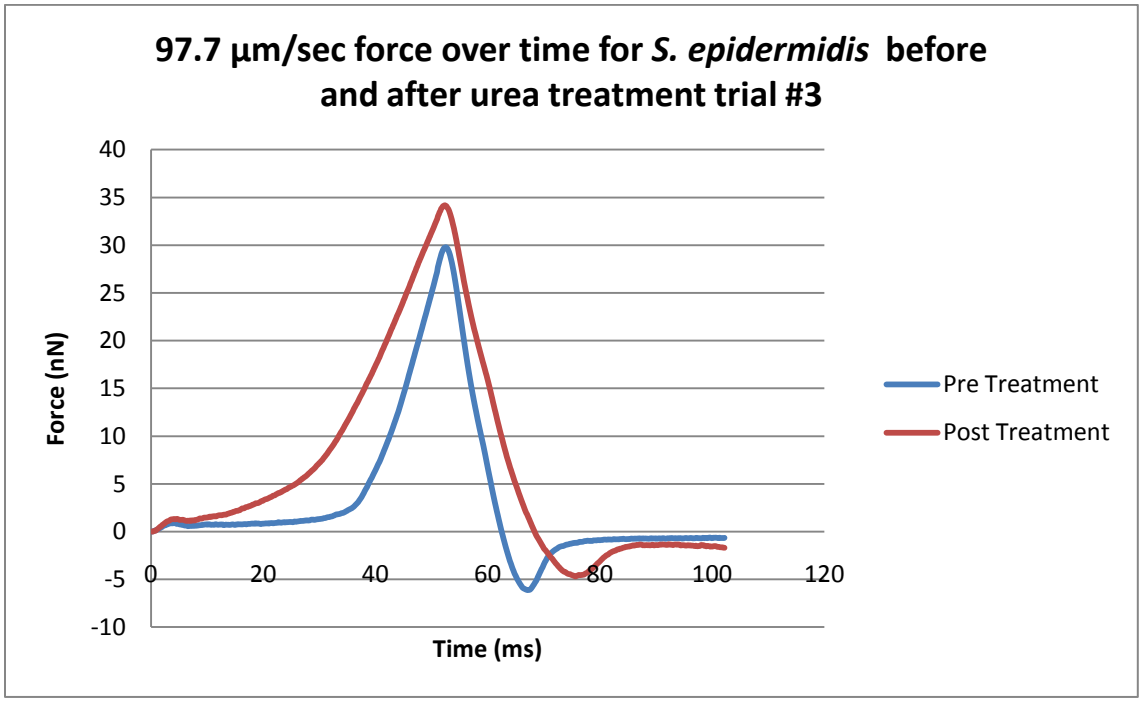

Figure 162) Force applied to *S. epidermidis* biofilm over loading time for pre and post-treatment of urea using 97.7µm/sec loading rate

DispersinB® Trial #2

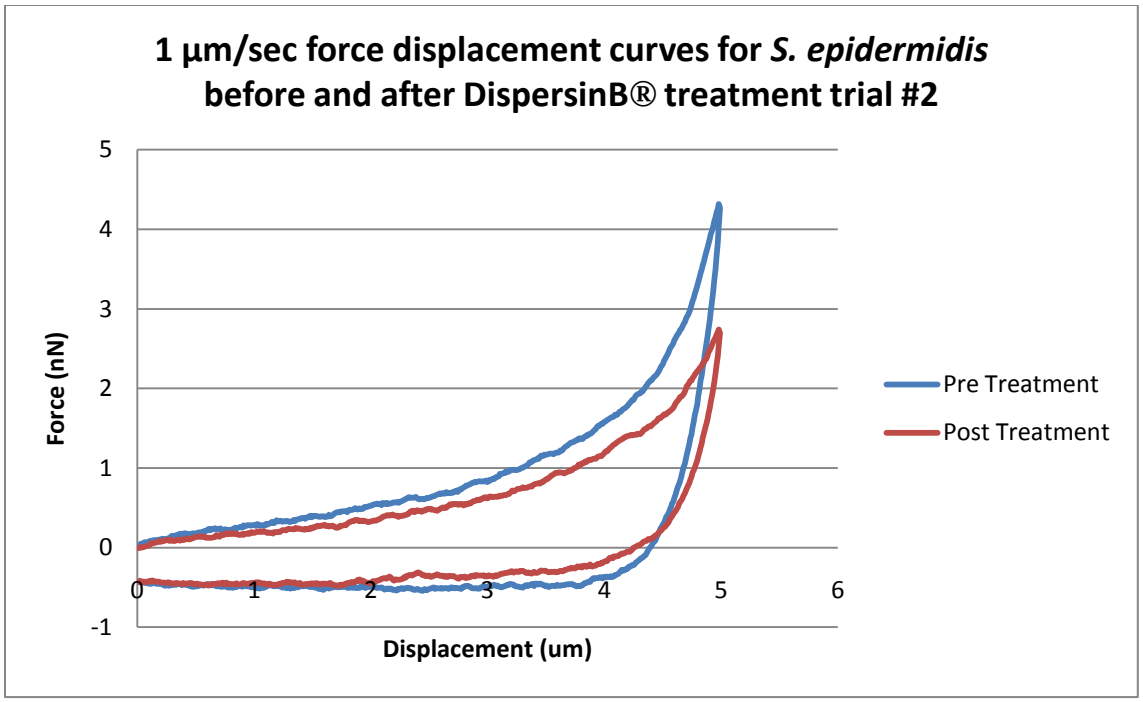

Figure 163) Force displacement curves for 1µm/sec loading rate for pre and post-treatment of DispersinB® on *S. epidermidis* biofilm

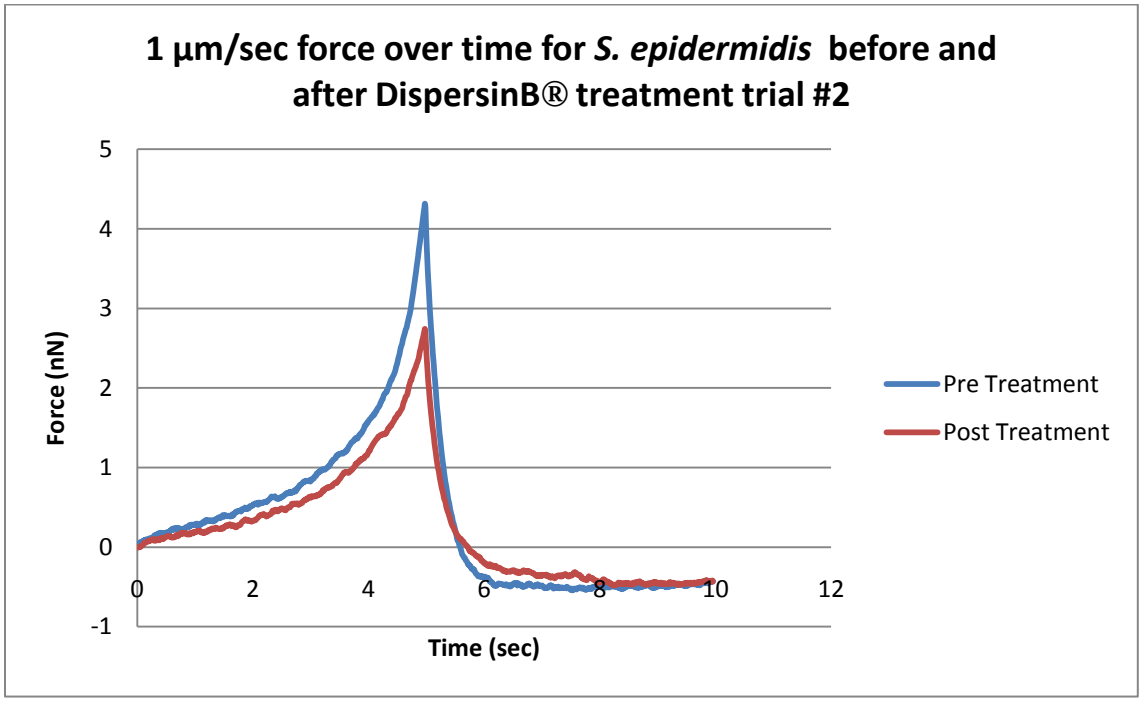

Figure 164) Force applied to *S. epidermidis* biofilm over loading time for pre and post-treatment of DispersinB® using 1µm/sec loading rate

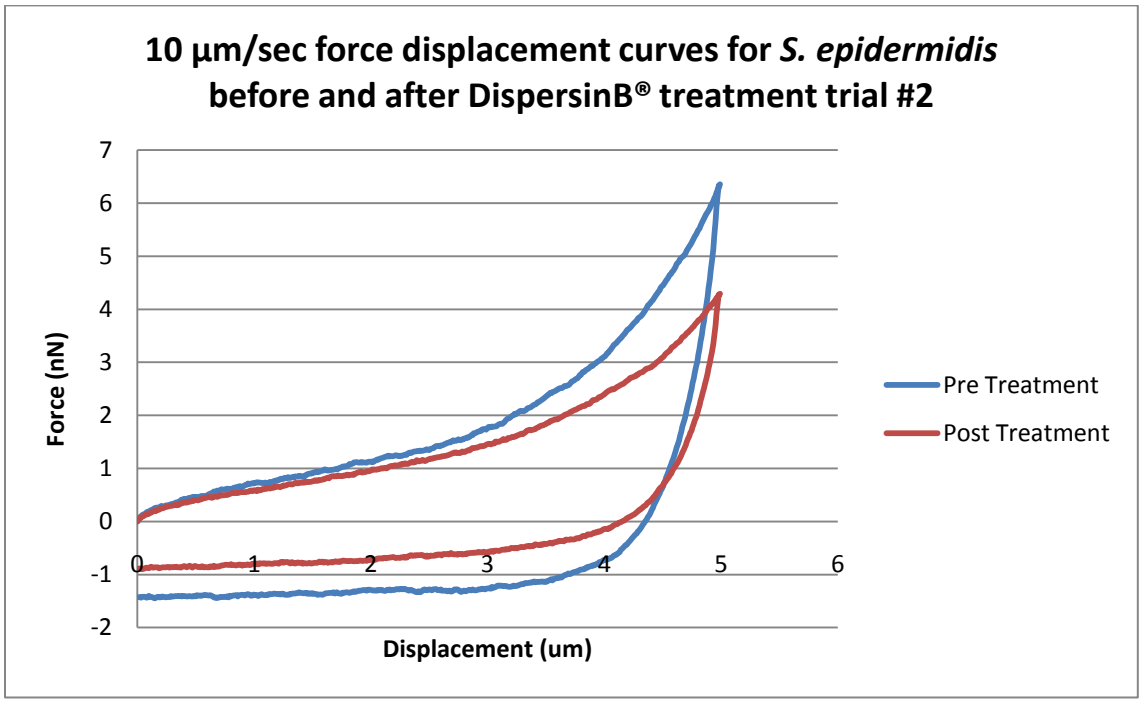

Figure 165) Force displacement curves for 10µm/sec loading rate for pre and post-treatment of DispersinB® on *S. epidermidis* biofilm

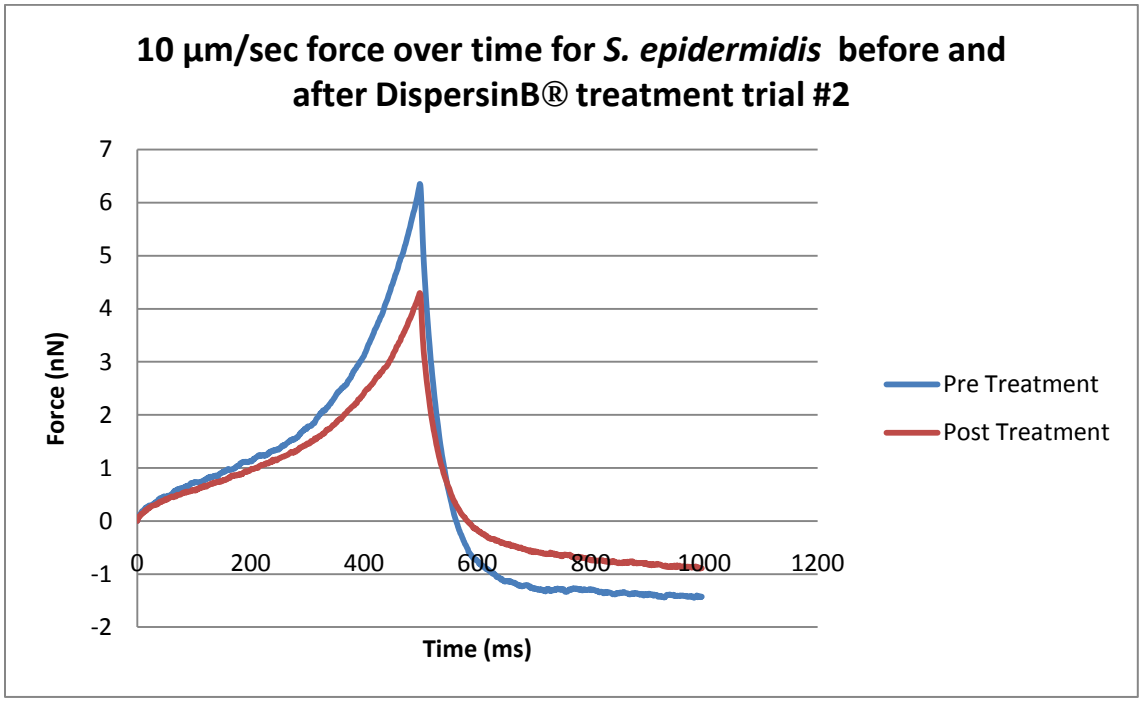

Figure 166) Force applied to *S. epidermidis* biofilm over loading time for pre and post-treatment of DispersinB® using 10µm/sec loading rate

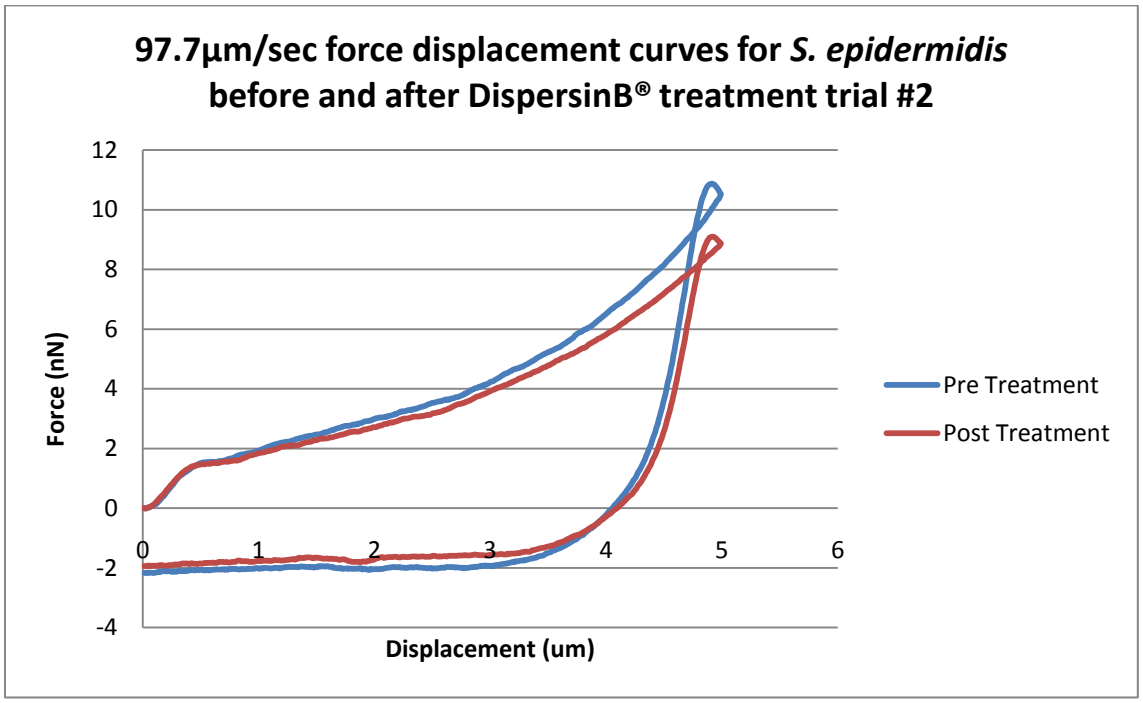

Figure 167) Force displacement curves for 97.7µm/sec loading rate for pre and post-treatment of DispersinB® on *S. epidermidis* biofilm

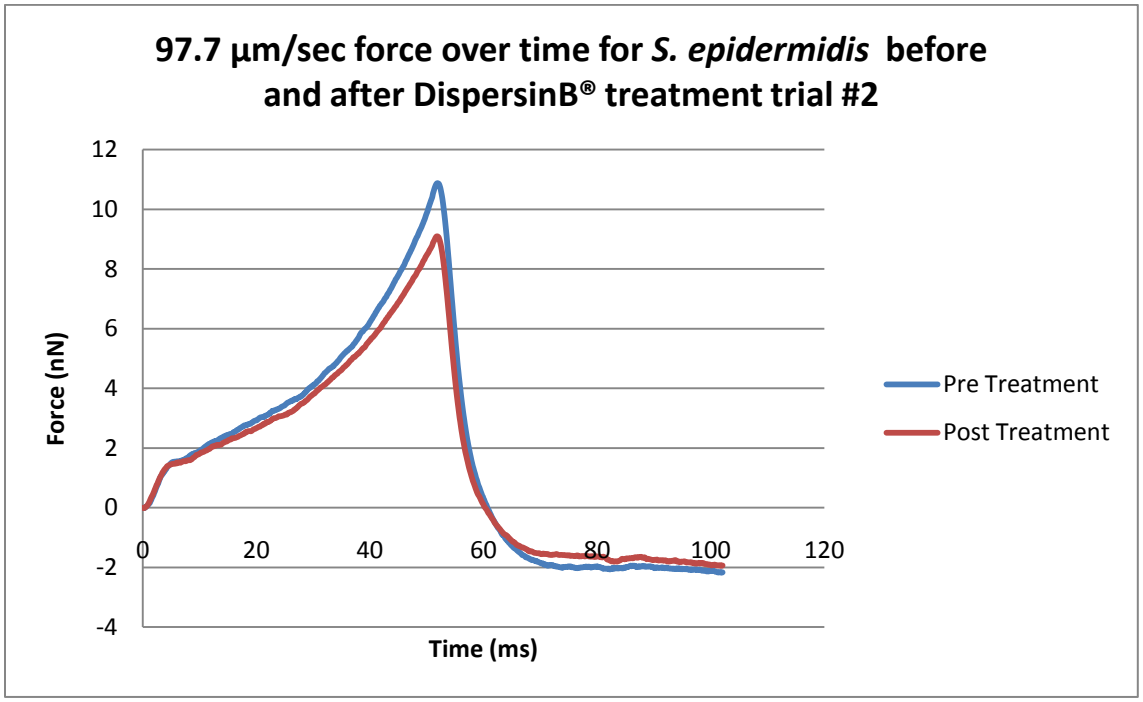

Figure 168) Force applied to *S. epidermidis* biofilm over loading time for pre and post-treatment of DispersinB® using 97.7µm/sec loading rate

DispersinB® Trial #3

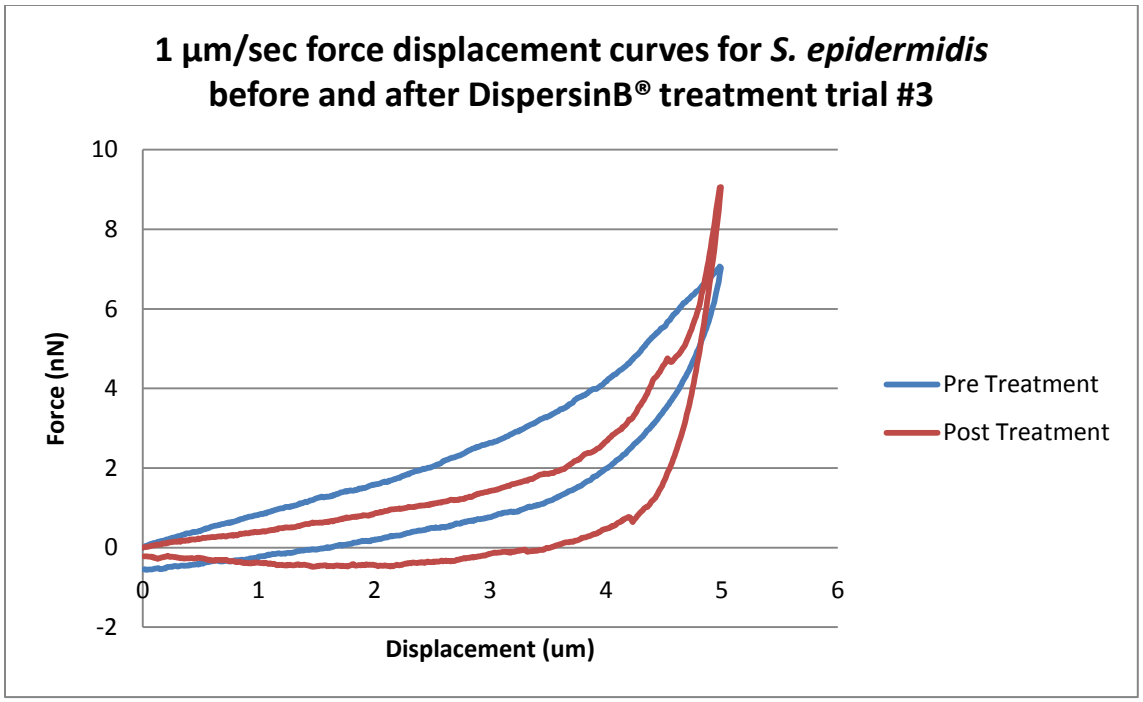

Figure 169) Force displacement curves for 1µm/sec loading rate for pre and post-treatment of DispersinB® on *S. epidermidis* biofilm

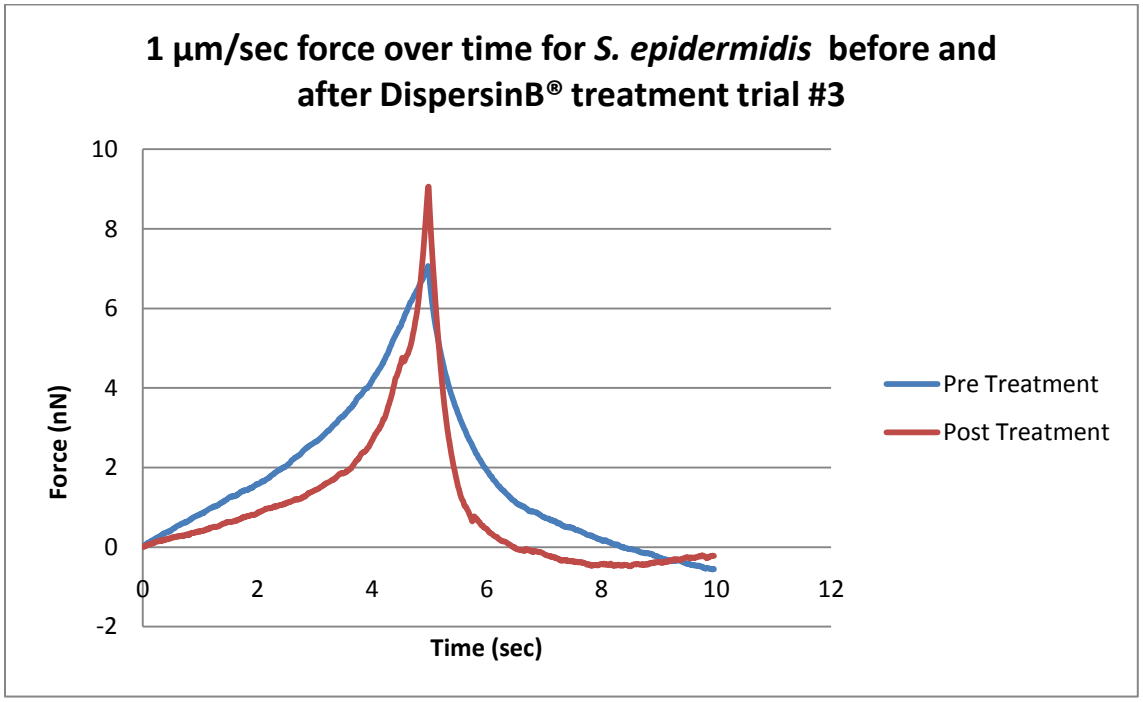

Figure 170) Force applied to *S. epidermidis* biofilm over loading time for pre and post-treatment of DispersinB® using 1µm/sec loading rate

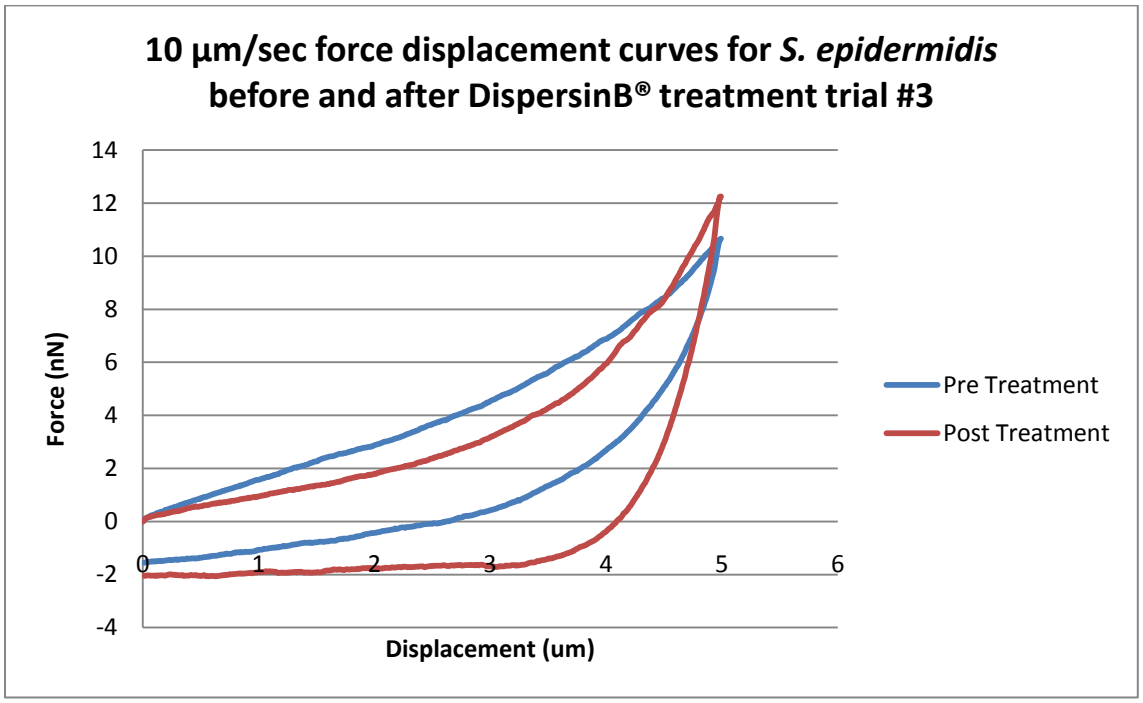

Figure 171) Force displacement curves for 10µm/sec loading rate for pre and post-treatment of DispersinB® on *S. epidermidis* biofilm

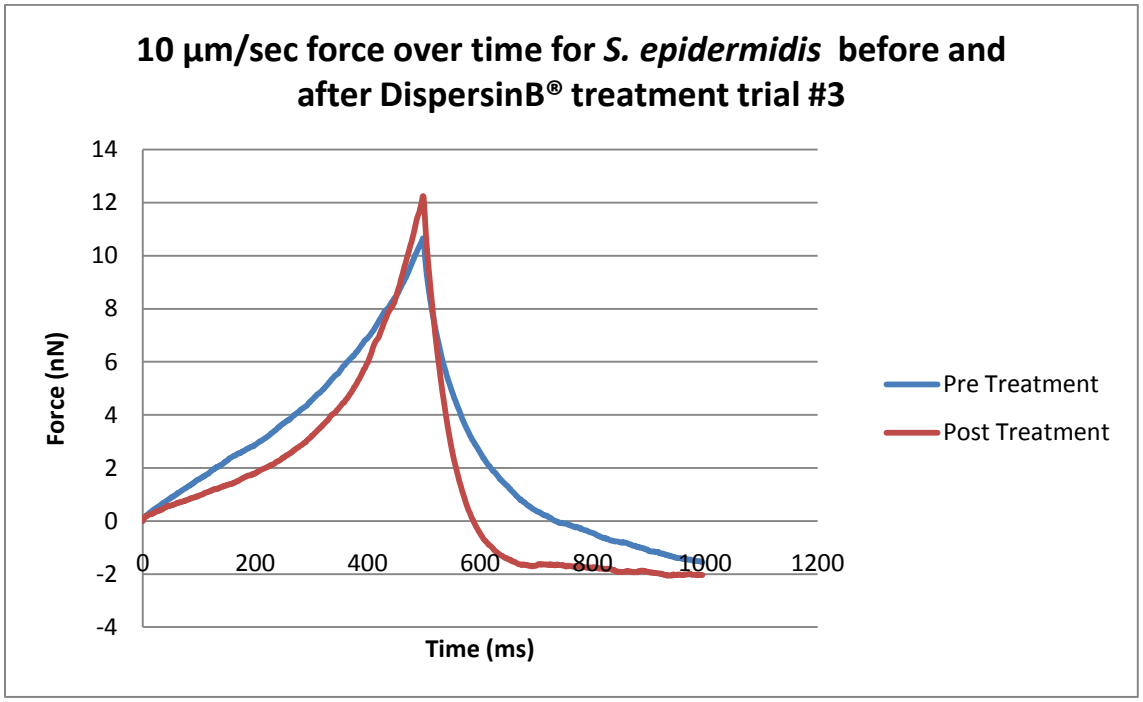

Figure 172) Force applied to *S. epidermidis* biofilm over loading time for pre and post-treatment of DispersinB® using 10µm/sec loading rate

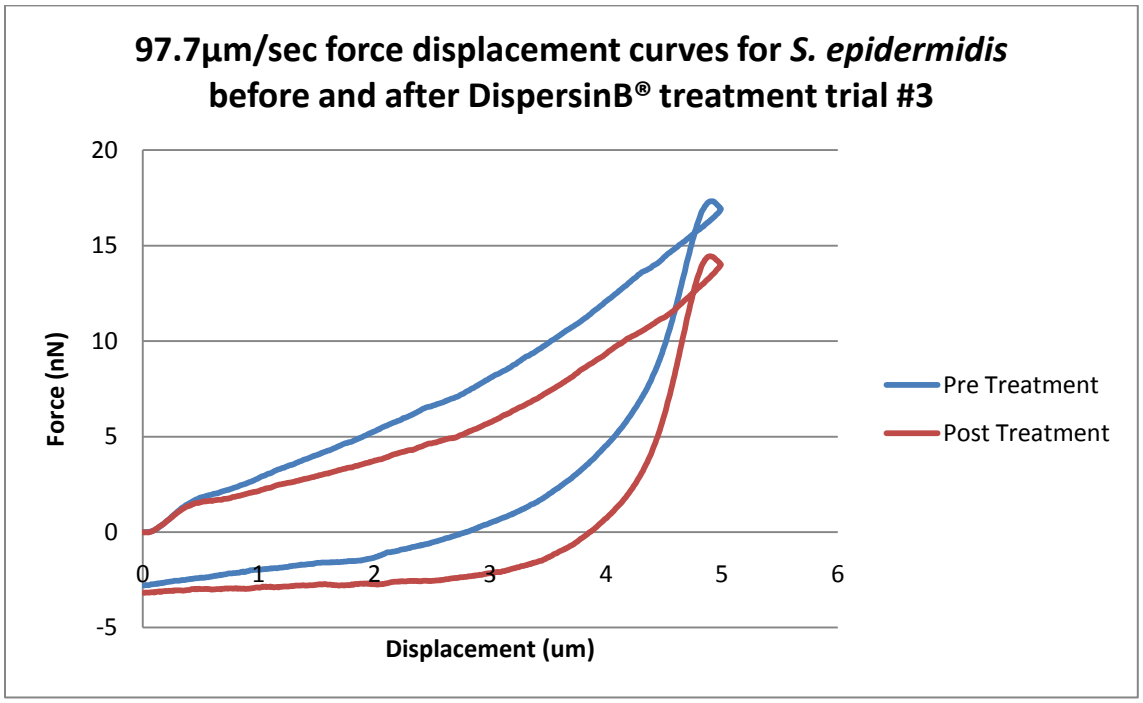

Figure 173) Force displacement curves for 97.7µm/sec loading rate for pre and post-treatment of DispersinB® on *S. epidermidis* biofilm

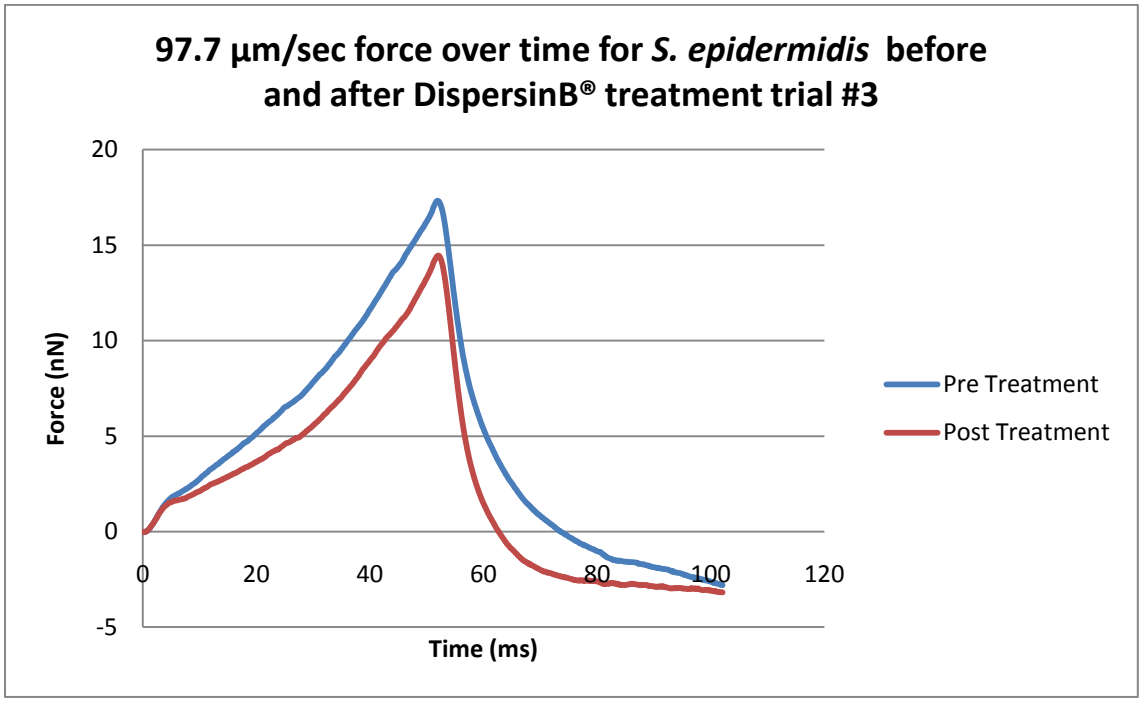

Figure 174) Force applied to *S. epidermidis* biofilm over loading time for pre and post-treatment of DispersinB® using 97.7µm/sec loading rate